THE BIOGEOCHEMICAL SOURCE AND ROLE OF SOLUBLE ORGANIC-FE(III) COMPLEXES IN CONTINENTAL MARGIN SEDIMENTS

A Dissertation
Presented to
The Academic Faculty

by

Jordon S. Beckler

In Partial Fulfillment
of the Requirements for the Degree
Doctor of Philosophy in the
School of Earth and Atmospheric Sciences

Georgia Institute of Technology

December 2014

THE BIOGEOCHEMICAL SOURCE AND ROLE OF SOLUBLE ORGANIC-FE(III) COMPLEXES IN CONTINENTAL MARGIN SEDIMENTS

Approved by:

Dr. Martial Taillefert, Advisor
School of Earth and Atmospheric Sciences
Georgia Institute of Technology

Dr. Thomas DiChristina
School of Biology
Georgia Institute of Technology

Dr. Mike Perdue
Department of Chemistry
Ball State University
Adjunct, School of Earth and Atmospheric Sciences
Georgia Institute of Technology

Dr. George W. Luther, III
College of Earth, Ocean, and Environment
University of Delaware

Dr. Jennifer Glass
School of Earth and Atmospheric Sciences
Georgia Institute of Technology

Date Approved: July 25th, 2014

ACKNOWLEDGMENTS

This dissertation would not have been possible without the support from colleagues, friends, and family.

I would first like to thank my committee members for their guidance over the years, and some great ideas in revising this work. Mike's enthusiasm in geochem 101 was my first exposure to rocks and water and reason I chose geochemistry as a career. In a similar way, Tom is one of the most stimulating lecturers and can make microscopic organisms almost "come to life" before your eyes. I am proud to have George as my academic grandfather, and he produced the foundation for much of the work in this thesis. Thanks also for the ALVIN dive. Jen is new but is already a rock star in our department, and it was a great organizing the SBS symposium with her.

Martial has been the best advisor and friend someone could ask for. He gave me the opportunity to join his lab as an undergraduate, and I immediately fell in love with oceanography after the first research cruise. Since then, he has given me opportunity to travel all over the world, mostly tropical environments with great port cities. I have learned so much from him – most importantly how to pack. I also appreciate the trust and freedom he gave me to test my own ideas in the lab.

Where would I be without my lab mates and other cohorts? Thanks to the present (Keaton, Eryn, Nicole, and Shannon) and past (Jennifer, Gwen, Steph, Melbeaze, Deidre, Mojo, Colin, Lin, Anna, Kate, and last but not least REU Meghan) group members. It was a really rough patch when we almost lost Morris, and I'm very thankful he pulled through in the end. Keaton you've been the only other guy in the group for some time, hang in there pal. Eryn you are super talented and have been a great office mate (Sid too!). Other colleagues and friends along the way: Justin Burns, Christine Fennessey, Becca, Seng, Ramanan, Darren, Jess Pruett. And finally folks who have enabled some of my research: Bill Savidge, Frank Stewart, Christophe Rabouille, and captains and crews of many research vessels.

Thanks mom and dad for being the most unconditionally loving people on the planet, and supporting my decisions and always being there for me no matter what.

TABLE OF CONTENTS

LIST OF TABLES

LIST OF FIGURES

LIST OF ABBREVIATIONS

ASWV	Anodic Square-Wave Voltammetry
AQDS	anthraquinone 2,6-disulfonate
BET	Brunauer–Emmett–Teller isotherm
CLE-ASV	Competitive-Ligand Exchange Adsorptive-Stripping Voltammetry
CoL	Congo River Fan (station designation)
CRF	Congo River Fan
CSWV	Cathodic Square-Wave voltammetry
DefB	Deferoxamine B
DIC	Dissolved Inorganic Carbon
DIR	Dissimilatory Iron-Reduction
DOM	Dissolved Organic Matter
DNRA	Dissimilatory Nitrate Reduction to Ammonium
DTPA	Diethylenetriaminepentaacetic Acid
EDTA	Ethylenediamenetetraacetic Acid
EPS	Extracellular Polymeric Substances
ETNP	Eastern Tropical North Pacific
FeRB	Dissimilatory Iron-Reducing Bacteria
GOM	Gulf Of Mexico (Station Designation)
HLB-SPE	Hydrophilic-Lipophilic Balanced Solid-Phase Extraction
HNLC	High-Nutrient Low-Chlorophyll
HOMO	Highest Occupied Molecular Orbital

HP-SEC	High-Pressure Size-Exclusion Chromatography
HPLC	High-Performance Liquid Chromatography
IC	Ion-Exchange Chromatography
ICP-MS	Inductively Coupled Plasma Mass-Spectrometer
IM	Inner Membrane
IMAC	Immobilized-Metal Affinity Chromatography
ISEA-IV-LC	In Situ Electrochemical Analyzer (IV) Liquid Chromatograph
ISLC	In-Situ Liquid Chromatograph
LAS	Louisiana Slope
LC/ESI-MS	Liquid Chromatography Electrospray-Ionization Mass Spectrometry
LSV	Linear Sweep Voltammetry
LUMO	Lowest Unoccupied Molecular Orbital
LOD	Limit Of Detection
MDL	Minimum Detection Limits
MTB	Methylthymol Blue
MW	Molecular Weight
NOM	Natural Organic Matter
NTA	Nitrilotriacetic Acid
OM	Outer Membrane
OMZ	Oxygen-Minimum Zone
PDA	Photo Diode Array
PEEK	Polyetheretherketone

PES	Polyethersulfone
PSS	Polystyrene sulfonate
RiOMar	River-dominanted Ocean Margin
SAT	Satilla River (station designation)
SERF	Salt marsh Ecosystem Research Facility
SGD	Submarine Groundwater Discharge
SRHA	Suwanee River Humic Acid
SIC	Single-Ion Chromatogram
HLB-SPE	Hydrophilic-Lipophilic Balanced Solid Phase Extraction
SWI	Sediment-Water Interface
TEA	Terminal Electron Acceptor
TIC	Total-Ion Chromatogram
TMAO	Trimethylamine-N-oxide
TRIS	Tris(hydroxymethyl)aminomethane
UHP	Ultra-High Purity
XRD	X-ray Diffraction spectroscopy

SUMMARY

In the past couple of decades, the discovery that iron is a limiting nutrient in large regions of the ocean has spurred much research into characterizing the biogeochemical controls on iron cycling. While Fe(II) is soluble at circumneutral pH, it readily oxidizes to Fe(III) in the presence of oxygen. Fe(III) is highly insoluble at circumneutral pH, presenting organisms with a bioavailability paradox stemming from the physiological challenge of using a solid phase mineral for assimilatory or dissimilatory purposes. Interestingly, dissolved organic-Fe(III) complexes can be stable in seawater in the presence of oxygen, and an active flux of these complexes has recently been measured in estuarine sediments. Their sources and biogeochemical role, however, remain poorly understood. In this work, a suite of field and laboratory techniques were developed to quantify diagenetic processes involved in the remineralization of carbon in marine sediments *in situ*, investigate the role of these organic-Fe(III) complexes in sediment biogeochemistry, and characterize the composition of the ligands possibly involved in the solubilization of Fe(III) in marine sediments. The first-of-its-kind *in situ* electrochemical analyzer and HPLC was used to better constrain diagenetic processes that may lead to the formation of dissolved organic-Fe(III) complexes in the Altamaha estuary and Carolina slope. An intensive study of the Satilla River estuary reveals that dissimilatory iron-reduction contributes to the formation of sedimentary organic-Fe(III) complexes, which are demonstrated to serve as an electron acceptor in subsequent incubations with a model iron-reducing microorganism. Similar observations in deep-sea slope and abyssal plain sediments fed by the Mississippi and Congo Rivers suggest that dissimilatory iron

reduction may represent an important component of carbon remineralization in river-dominated ocean margin sediments that may be currently underestimated globally. To confirm that these organic-Fe(III) complexes are produced during microbial iron reduction, novel separation schemes were developed to extract and identify Fe(III)-binding ligands from sediment pore waters. Preliminary results reveal the presence of a few select low-molecular weight compounds in all pore waters extracted, suggesting they might be endogenous ligands secreted by iron-reducing bacteria to non-reductively dissolve Fe(III) minerals prior to reduction.

CHAPTER 1

INTRODUCTION

1.1. Fe Chemistry in Natural Aquatic Systems

Fe is crucial to microbial life for its use as metal centers in proteins and enzymes (e.g. Fe-S proteins, c-type cytochromes), redox indicator for $O_{2(aq)}$ and NO (e.g. rubredoxin), hydroxylation (i.e. hydroxylases), hydrolysis of phosphate groups (i.e. acid phosphatases), and gene regulation (e.g. FUR, FNR) (Bannister 1992). Fe is typically observed in the +II, and +III valence states, the partitioning of which is largely determined by the environmental redox conditions. Fe(III) is highly insoluble at circumneutral pH, presenting organisms with a bioavailability paradox stemming from the physiological challenge of using a solid phase mineral for assimilatory or dissimilatory purposes (Boukhalfa and Crumbliss 2002a; Dichristina 2005). The small ionic radius of Fe(III) (0.65 Å) and positive charges allow a large affinity for Lewis bases, the most non-polarizable and electronegative ligands (e.g. $F^- > O^{2-} > N = Cl^- > Br^- > I^- > S^{2-} > OH^-$), resulting in the most ionic of bonds (Cotton 2007). In aqueous solutions at circumneutral pH, water-derived hydroxo species readily coordinate Fe(III) in various stoichiometries, forming the aqueous species $Fe(OH)^{2+}$, $Fe(OH)_2^+$, $Fe(OH)_4^-$, and the postulated neutral mononuclear complex $Fe(OH)_{3,aq}$. The more negative hydroxo species are favored to polymerize as dimers above at high OH/Fe ratios. The rate that the monomers and dimers are then fed to the nuclei determines the type of mineral formed (e.g. rapid consumption: ferrihydrite, slow growth: goethite/hematite) (Cornell and

Schwertmann 1996) which has important implications for bioavailability to microorganisms (Hyacinthe et al. 2006). Fe(II), on the other hand, is highly soluble over a wide range of pH; however, rapid oxidation to Fe(III) occurs at circumneutral pH in the presence of dissolved $O_{2(aq)}$ (Davison and Seed 1983; King et al. 1995; Sung and Morgan 1980). Fe(II) is a borderline soft acid that binds to soft bases (S>I>Br>Cl=N>O>F) which are larger and more polarizable (Cotton 2007). Fe(II) remains soluble in anoxic circumneutral pH water because, unlike Fe(III), hard bases such as OH^- do not have such an affinity for the larger Fe^{2+} ion (Stumm and Morgan 1996).

Fe chemistry in natural systems is also strongly influenced by organic ligands. Fe(III) remains in solution at circumneutral pH if bound to organic ligands, and organic complexation of Fe(III) is known to control the solubility of Fe in most marine environments (Rue and Bruland 1995; Witter and Luther 1998; Wu and Luther 1995). Moreover, ligand stabilization can alter the redox potential of the Fe center (Rose and Waite 2003). Stable Fe(III) complexes display a more negative reduction potential than unstable complexes, as it is more difficult to reduce Fe(III) which is stable in its oxidized form (Boukhalfa and Crumbliss 2002b). Conversely, Fe(II) complexes are stabilized at higher redox potential. Some ligands also have a polarizing character that can cause the gap between the t_{2g} and e_g orbital energies in an octahedral binding environment to change due to charge interactions. Weak field ligands, i.e. those with two or more lone pairs of electrons (e.g. Cl^-, OH^-, H_2O, oxalate, S^{-2}, HS^-) may decrease this energy gap, allowing Fe(III) to exist in the high spin state with an electron in all five hybridized orbitals (Boukhalfa and Crumbliss 2002a; Luther et al. 1992). Fe(II) is more stable in low spin state and therefore has a stronger tendency to bind strong field ligands (e.g.

those containing R-NH_2 groups). While not as strong as the ionic bonding contribution, an additional covalent component results from electron sharing across metal π Lewis base molecular orbitals (Luther et al. 1992). These fundamental properties govern the behavior of Fe-containing biomolecules and explain the importance of the steric and electronic effects of the binding environment on electron transfers mediated by Fe(II) and Fe(III).

1.2. Fe Solubilization

The importance of Fe limitations on oceanic primary productivity has been recognized since a few pioneering studies in which Fe fertilization of otherwise nutrient-rich waters stimulated plankton blooms (Boyd et al. 2000; Martin and Fitzwater 1988). Until this point, it was unknown why these high-nutrient low-chlorophyl (HNLC) regions had low rates of primary production. To date, the sources of Fe to the ocean as well as the mechanisms by which Fe remains bioavailable in the water column given its low solubility in oxygenated seawater remain poorly constrained (Sarmiento and Gruber 2006). While terrestrial dust is an important source of Fe(Jickells et al. 2005), Fe in dust is largely in the particulate form and not immediately soluble (Buck et al. 2010). Iceberg melt can deliver nano-particulate Fe to higher latitude open-ocean waters (Raiswell et al. 2008). Hydrothermal sources may provide Fe to the deep ocean (Bennett et al. 2008; Saito et al. 2013), and recent studies have demonstrated that nano-particulate Fe-sulfide minerals may be transported away from vent sources (Gartman et al. 2014; Yucel et al. 2011). Rivers may deliver Fe in particulate or dissolved form, but it is often assumed that it is rapidly removed by flocculation upon mixing with seawater (Boyle et al. 1977),

though some Fe may in fact remain in solution if stabilized by organic ligands (Buck et al. 2007; Laglera and Van Den Berg 2009). Finally, volcanic margin sediments (Lam and Bishop 2008), sediments underlying hypoxic basins (Elrod et al. 2004), and estuarine sediments (Jones et al. 2011) have recently been established to represent significant sources of Fe to the oceans. However, only a few studies have considered the oxidation state and speciation of Fe fluxing from sediments (Jones et al. 2011), and much work remains in determining its long-term stability.

If Fe solubility in natural waters was regulated by hydrolysis only, concentrations of dissolved Fe on the order of 10 pM would be expected in oxygenated ocean water (Liu and Millero 2002). Reported filterable (200 nm) Fe concentrations, however, are frequently several orders of magnitude higher in rivers and oceans (Beck et al. 1974; Powell and Wilson-Finelli 2003; Rue and Bruland 1995), and whether dissolved Fe is colloidal (~20 – 200 nm) or in the form of truly soluble complexes (< ~20 nm) is under debate (Wu et al. 2001). Size fractionation studies demonstrate Fe in a continuum of sizes, from larger colloids of nanoparticulate Fe(III)-oxyhydroxides stabilized by associated natural organic matter, to soluble Fe(III) complexes < 1,000 Da (Breitbarth et al. 2010). The exact nature of the soluble Fe(III) complexes is unknown, but Fe may be stabilized in solution by soil fulvic and humic acids or cell exudates (Beck et al. 1974; Chen et al. 2004; Krachler et al. 2010; Perdue et al. 1976). Several studies have demonstrated the existence of primarily two types of Fe-binding ligands (L_1 and L_2) based upon complex strength (Gerringa et al. 2007; Gledhill and Buck 2012). Strong-complex forming L_1 ligands have been observed from estuaries to the pelagic ocean, have binding constants consistent with soil fulvic acids or siderophores ($\log K^{cond} > 12$), and

tend to positively correlate with dissolved Fe concentrations (Buck and Bruland 2007; Buck et al. 2007; Laglera and Van Den Berg 2009). The weaker L_2 ligands (log $K^{cond} \approx$ 11 - 12), on the other hand, are not found in lower salinity waters, and while not well-understood, do not appear to exert a primary control on Fe solubility (Buck et al. 2007; Gledhill and Buck 2012).

As a result of the generally poor solubility of Fe in aquatic environments, organisms have developed special mechanisms to access Fe from insoluble minerals and other sources (e.g. ferric complexes, lyzing cells, humic-bound Fe). Siderophores are organic molecules with highly electronegative functional groups, typically of low molecular weight, that target Fe(III) by attaching to surface functional groups and promoting its non-reductive dissolution (Vraspir and Butler 2009). Most siderophore functional groups can align with and form hexadentate configurations with Fe(III), resulting in very strong complexes (Boukhalfa and Crumbliss 2002b). The catecholate, hydroxamate, and α-hydroxy carboxylate functional groups in siderophores are hard donors, with a high charge and small size allowing the ligand to act almost as a point charge. These properties are reflected in the highly negative redox potential of the siderophore-Fe(III) complex (-350 mV to -750 mV) (Boukhalfa and Crumbliss 2002a) that stabilizes the trivalent oxidation state and prevents incidental reduction/dissociation while returning to the cell. For 1:1 siderophore-Fe(III) complexes, the stability constants display log K values of 23 to 52 (compared to 20 for EDTA-Fe(III)) (Kraemer 2004). Interestingly, while a low redox potential enhances the stability of the siderophore complex in the environment (as it is unlikely to be outcompeted for the coordinating

Fe(III)), the complex has to be reduced or hydrolyzed upon eventual return to the cell for intracellular mobility (Brickman and Mcintosh 1992; Miethke et al. 2011).

1.3. The role of Fe(III) solubilization and reduction in sediment diagenesis

While solubilization of Fe oxides is well known to play an important role in the supply of this important micronutrient in surface marine waters, the existence of soluble Fe(III) complexes in marine sediments has only been recently demonstrated, and its importance in diagenetic processes remains poorly understood. Dissolved organic-Fe(III) complexes have been detected in harbor (Brendel and Luther 1995), salt marsh (Bull and Taillefert 2001; Koretsky et al. 2008; Luther et al. 1996; Taillefert et al. 2007b; Taillefert et al. 2002b), estuarine (Meiggs and Taillefert 2011; Taillefert et al. 2002a), and continental shelf (Taillefert et al. 2000) sediments. The accumulation of high concentrations of soluble Fe(III), however, is limited to suboxic ($O_{2(aq)}$ < 200 nM) sediments, as $\sum H_2S$ produced by SO_4^{2-} reduction rapidly reduces organic-Fe(III) complexes in anoxic sediments and precipitates Fe(II) as FeS minerals (Carey and Taillefert 2005; Taillefert et al. 2000). Indeed, seasonal measurements revealed that the production of soluble organic-Fe(III) complexes in estuarine sediments is strongly anti-correlated with the seasonal production of $\sum H_2S$ (Taillefert et al. 2002b). These complexes have also been demonstrated to oxidize pyrite in salt marsh sediments when dissolved sulfide concentrations are low (Luther et al. 1996), while sediment incubations in sulfate-reducing conditions demonstrated that pyritization was accelerated in the presence of organic-Fe(III) complexes (Carey and Taillefert 2005). Recently, a few studies have demonstrated that organically complexed Fe(III) (Jones et al. 2011) or

dissolved Fe(III) with an isotopic signature consistent with the non-reductive dissolution of Fe(III) oxides (Homoky et al. 2013) also flux from shelf sediments and are stable in oxic seawater. These complexes may eventually be transported to continental shelves and provide a significant source of Fe for primary productivity.

The production of organic-Fe(III) complexes is apparently controlled by the delivery of natural organic matter and Fe to sediments (Meiggs and Taillefert 2011) and may occur via a variety of processes in sediments. First, oxidation of Fe(II) by dissolved oxygen in the presence of organic ligands (Taillefert et al. 2000) or oxidation of organic-Fe(II) complexes by Fe(III) minerals (Luther et al. 1992) may generate these complexes near the surface of marine sediments. Second, the biotic oxidation of Fe(II) by aerobic Fe oxidizing bacteria in the presence of endogenous ligands (Roden et al. 2004; Sobolev and Roden 2001) could produce these complexes near the sediment-water interface to avoid mineral encrustation, a process similar to Fe mineralization on organic extracellular stalks (Miot et al. 2009). Third, the non-reductive dissolution of Fe(III) oxides (e.g. by reaction with bidentate or tridentate oxygen-containing ligands or NOM) (Biber et al. 1994; Bondietti et al. 1993; Deng and Stumm 1994; Homoky et al. 2009; Nowack and Sigg 1997; Radic et al. 2011; Santana-Casiano et al. 2000; Zinder et al. 1986) may generate organic-Fe(III) complexes. Finally, soluble organic-Fe(III) complexes may form as intermediates during the reductive dissolution of Fe(III) minerals by several Fe-reducing bacteria (FeRB) (Jones et al. 2010; Nevin and Lovley 2002a; Taillefert et al. 2007a) . Interestingly, another well-studied FeRB, *Geobacter metallireducens* is not capable of reducing Fe(III) oxides from a distance (Nevin and Lovley 2002b), suggesting different species of FeRB may use different biochemical pathways for metal respiration.

Sediments host a diverse group of organisms capable of coupling the oxidation of organic carbon to the reduction of terminal electron acceptors (TEAs; Berner 1975), in order of decreasing energy yield: $O_{2(aq)}$, NO_3^-, NO_2^-, Mn(IV)/Mn(III), Fe(III), SO_4^{2-}/$S_2O_3^{2-}$/S(0), acetate, and CO_2, for energy generation (Canfield and Thamdrup 1994; Froelich et al. 1979; Jorgensen and Bak 1991; Lin et al. 2012; Lovley and Phillips 1988; Madison et al. 2013). Although a multitude of chemical and biological reactions between reduced and oxidized products complicates the interpretation of sediment profiles (Berner 1975; Boudreau 1997; Rabouille and Gaillard 1991; Wang and VanCappellen 1996), sediment pore waters are generally chemically stratified with the most oxidized TEAs consumed near the sediment surface and the least oxidized TEAs consumed deeper in the sediments (Froelich et al. 1979). SO_4^{2-} reduction is generally considered to dominate anaerobic organic C remineralization in organic-rich sediments because of its ubiquity in seawater (~28 mM) and because one mole of SO_4^{2}- can oxidize 8 moles of C. However, the discovery of organisms capable of coupling the reduction of Fe(III) to organic C oxidation (Arnold et al. 1988; Lovley and Phillips 1988) spurred researchers to consider dissimilatory Fe reduction (DIR) as an important process in C remineralization in marine sediments for two reasons. First this reaction displays a relatively high free energy yield compared to SO_4^{2}- reduction:

$$CH_3COOH + 8Fe(OH)_3 + 14H^+ \rightarrow 8Fe^{2+} + 2HCO_3^- + 20H_2O \qquad \text{(Eq. 1.1)}$$

ΔG^0_{rxn}=-515.6 kJ mol^{-1}

$$CH_3COOH + SO_4^{2-} \rightarrow HS^- + 2HCO_3^- + H^+ \qquad \text{(Eq. 1.2)}$$

ΔG^0_{rxn}=-27.0 kJ mol^{-1}

Second, the fast recycling of reduced Fe to inorganic Fe(III) colloids or particles by abiotic reaction with $O_{2(aq)}$ transported into sediments by diffusion or advection during tidal fluctuations (Taillefert et al. 2007b), wave action (Precht et al. 2004), and bioturbation (Kristensen 2000), or by abiotic reaction with Mn(IV) oxides (Postma 1985) and chemoautotrophic oxidation by $O_{2(aq)}$ (Mcbeth et al. 2013; Saini and Chan 2013; Sobolev and Roden 2001) or NO_3^- (Sorokina et al. 2012) suggests that DIR may be ubiquitous in suboxic sediments. Indeed, multiple field studies (reviewed in Thamdrup 2000) were able to demonstrate the dominance of DIR activity in C remineralization in coastal ecosystems displaying high organic C sedimentation and exposed to physical mixing processes (e.g. up to 75% in bioturbated subtidal marine sediments (Jensen et al. 2003)).

Only a few studies have evaluated the role of microbial metal reduction relative to other anaerobic processes in C_{org} remineralization in deep-sea sediments (Haese et al. 2000; Law et al. 2009; Nedelec et al. 2007; Thamdrup and Canfield 1996; Van Der Zee et al. 2002). Interestingly, relatively high rates of C_{org} deposition have been observed in the deep ocean in regions underlying continental slope sediments (Haese et al. 2000; Law et al. 2009; Rabouille et al. 2009; Schulz et al. 1994), in areas where local circulation features may stimulate primary production such as the Benguelan, Peruvian, and Chilean upwelling regions and semi-enclosed basins (Ferdelman et al. 1999; Haeckel et al. 2001; Lee et al. 2008; Thamdrup and Canfield 1996), and even in the deepest trench on earth (Glud et al. 2013). However, metal reduction is generally disregarded, even though some of these deep areas may simultaneously receive large fluxes of oxidized terrigenous

minerals, especially around river-dominated ocean margins (RiOMars) (Mckee et al. 2004).

Finally, the effects of climate change on the C cycle remain poorly understood. While some studies demonstrated that seawater level rise might increase C_{org} remineralization by shifting respiration processes to SO_4^{2-} reduction (Weston et al. 2006), other studies demonstrate that Fe reduction might in fact be enhanced when salinity increases during drought events (Meiggs and Taillefert 2011). Because increases in global temperatures are likely to increase erosional processes and riverine discharge (Goudie 2006; Hamilton 2010), RiOMars may become increasingly important locations for DIR. Deep marine waters in contact with these sediments may be enriched in sediment-derived dissolved Fe, and their eventual upwelling could increase the supply of this limiting micronutrient to the photic zone.

1.4. Production of soluble organic-Fe(III) complexes by Fe(III)-reducing bacteria

Efforts to determine the biomolecular pathway of dissimilatory Fe reduction have focused on the model FeRB species of *Shewanella* and *Geobacter*. Early studies with *Geobacter* demonstrated the metabolic diversity and environmental implications of FeRBs capable of coupling Fe or Mn reduction to the oxidation of natural organic matter or organic contaminants (Lovley et al. 1989; Lovley and Phillips 1988), Fe mineral transformation (Lovley et al. 1987), and heavy metal reduction (Lovley 1993; Lovley et al. 1991). At the same time, extensive kinetic and genetic studies began with *Shewanella* sp. (formerly classified as a *Pseudomonas* species) for their possible role in ore extraction and corrosion removal (Arnold et al. 1988). Originally isolated from an oil pipeline in

1980 (Obuekwe et al. 1981), *Shewanella* species are perhaps better suited than *Geobacter* species for laboratory studies because they are facultative anaerobes, i.e. they use $O_{2(aq)}$ as a TEA when present but Fe(III) reduction activity is not directly inhibited by $O_{2(aq)}$ respiration (Arnold et al. 1990).

As most other TEAs are dissolved and can diffuse through cell membranes to intracellular components for reduction, the fundamental mystery of anaerobic Fe respiration lies in the mechanism by which bacteria are able to respire solid minerals. Several mechanisms have been proposed for electron transfer by *Shewanella* sp. from the electron donor through the electron transport chain to the TEA, including: direct physical contact between the Fe(III) mineral surface and outer membrane (OM) proteins (Figure 1.1a) or electrically conductive appendages (Figure 1.1b; El-Naggar et al. 2008; Gorby et al. 2006; Reguera et al. 2005); electron shuttling by endogenous or exogenous redox active molecules (Figure 1.1c; Hernandez et al. 2004; Lies et al. 2005; Lovley et al. 1996; Marsili et al. 2008; Newman and Kolter 2000; Shyu et al. 2002; Von Canstein et al. 2008); or solubilization of Fe(III) prior to reduction (Figure 1.1d; Jones et al. 2010; Taillefert et al. 2007a). Given the high metabolic flexibility of *Shewanella*, however, it is likely that multiple mechanisms may be employed depending on environmental conditions (Schicklberger et al. 2013). For reduction of Fe(III), the biomolecular branchpoint of the different mechanisms is proposed to begin on the inner membrane (IM) protein CymA (Marritt et al. 2012). With the direct contact mechanisms, it is hypothesized that electrons are transferred from CymA in a cascade-like manner to several cytochromes with overlapping redox potential inside the periplasm (Firer-Sherwood et al. 2008) until they are deposited onto MtrA, a decaheme c-type cytochrome

predicted to be localized to the inside face of the outer membrane (Firer-Sherwood et al. 2011). An additional ß-barrel, transmembrane protein MtrB has been demonstrated to link and serve as an electron conduit from MtrA (Firer-Sherwood et al. 2011) to outer membrane cytochromes MtrC and its homologue OmcA (Hartshorne et al. 2009; Ross et al. 2007; Shi et al. 2006; White et al. 2013) which are deployed to the outer membrane (Figure 1.1a) or surface pili (Figure 1.1b) by a Type II secretion system (DiChristina and DeLong 1994; DiChristina et al. 2002; Okamoto et al. 2012; Shi et al. 2008). Because of their location on the OM and Fe(III) reduction activity in purified form, these proteins have been proposed to form the terminal reductase complex for Fe(III) (Beliaev and Saffarini 1998; Edwards et al. 2012; Myers and Myers 1992; Myers and Myers 2003). However, cells incapable of attachment to solid Fe(III) still display wild-type reduction rates, suggesting reduction may occur at a distance via alternate biochemical pathways (Burns et al. 2010).

Simultaneously, electron shuttling between *Shewanella* and TEAs has been demonstrated with quinones, humic acids, and flavins (e.g. Figure 1.1c; Brutinel and Gralnick 2012; Hernandez et al. 2004; Kappler et al. 2004; Lovley et al. 1999; Newman and Kolter 2000). Flavins secreted by *Shewanella* in the presence of outer-membrane cytochromes are more easily reduced (Okamoto et al. 2013) relative to flavins with no cytochromes, and the presence of flavins in bioreactors increased electron transfer to insoluble Fe(III) oxides, suggesting they may represent endogenic compounds excreted to shuttle electrons to Fe(III) oxides (Kotloski and Gralnick 2013). Interestingly, however, exogenous flavins are typically added to pure cultures, and it remains unknown if they are deliberately released by *Shewanella* to reduce Fe oxides or if instead they are a

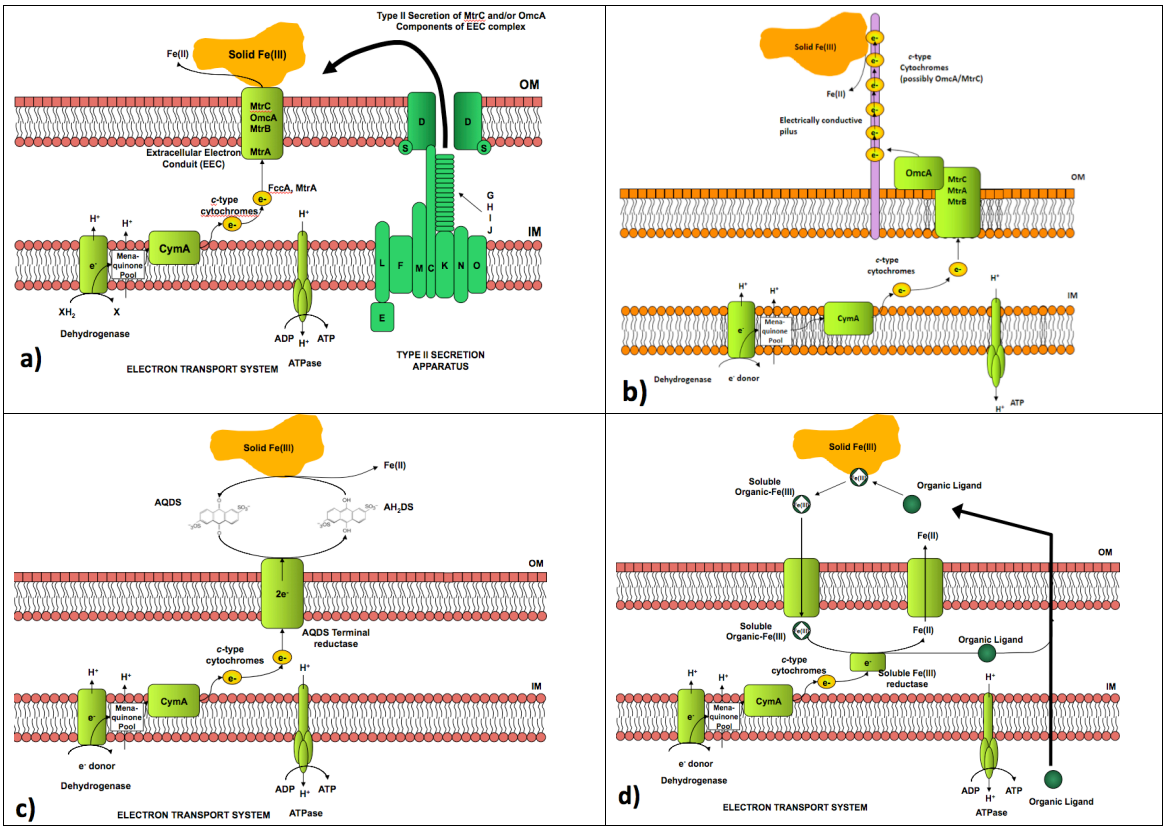
Type II Secretion of MtrC and/or OmcA
Components of EEC complex
Fe(II)
Solid Fe(III)
OM
MtrC
OmcA
MtrB
MtrA
Extracellular Electron
Conduit (EEC)
D
D
S
S
G
H
I
J
FccA, MtrA
c-type
cytochromes
IM
CymA
Mena-
quinone
Pool
L
F
M
C
K
N
O
E
XH2
X
Dehydrogenase
ADP
ATP
ATPase
a)
ELECTRON TRANSPORT SYSTEM
TYPE II SECRETION
APPARATUS
Solid Fe(III)
c-type
Cytochromes
(possibly OmcA/MtrC)
Fe(II)
Electrically conductive
pilus
OmcA
MtrC
MtrA
MtrB
OM
c-type
cytochromes
IM
CymA
Mena-
quinone
Pool
Dehydrogenase
e- donor
ATP
b)
Solid Fe(III)
Fe(II)
AQDS
AH2DS
OM
2e-
AQDS Terminal
reductase
c-type
cytochromes
IM
CymA
Mena-
quinone
Pool
e- donor
Dehydrogenase
ADP
ATP
ATPase
c)
ELECTRON TRANSPORT SYSTEM
Solid Fe(III)
Soluble
Organic-Fe(III)
Organic Ligand
Fe(II)
OM
Soluble
Organic-Fe(III)
Fe(II)
Organic Ligand
c-type
cytochromes
Soluble Fe(III)
reductase
IM
CymA
Mena-
quinone
Pool
e- donor
Dehydrogenase
ADP
ATP
ATPase
Organic Ligand
d)
ELECTRON TRANSPORT SYSTEM

Figure 1.1 – Proposed mechanisms for electron transfer from Shewanella sp. to solid Fe(III) oxides include: a) direct contact between cells and OM proteins; b) direct contact between cells and extracellular appendages (i.e. "nanowires"); c) electron shuttling via redox active molecules (AQDS shown as example); and d) solubilization of Fe(III) prior to reduction of the organic-Fe(III) complex. Figure modified with permission from Cooper et al, 2014.

byproduct of other cellular functions. Finally, a flavin-deficient mutant that does not reduce iron oxides has yet to be designed.

Another proposed mechanism involved in the anaerobic respiration of Fe(III) oxides by FeRB includes solubilization of Fe(III) oxides prior to reduction (Figure 1.1d). *Shewanella* species reduce soluble org-Fe(III) complexes faster and more efficiently than solid Fe(III) minerals (Arnold et al. 1988; Dollhopf et al. 2000), and an inverse relationship exists between the strength of the organic-Fe(III) complexes and rates of Fe(III) reduction (Haas and DiChristina 2002; Liu et al. 2002). In addition, exogenous Fe(III) chelators stimulate the activity of *Geobacter* (Lovley and Woodward 1996), and dissolved Fe(III) accumulates in *Geobacter* and *Shewanella* cultures physically separated from Fe(III) minerals (Nevin and Lovley 2002a; 2002b), though not when biofilm formation is promoted, suggesting that soluble Fe(III) may remain localized within the microbe/solid interface (Lies et al. 2005). Finally, voltammetric organic-Fe(III) signals are produced in sediment microcosms (Carey and Taillefert 2005) and in incubations of *Shewanella* with synthetic Fe(III) (oxy)hydroxides (Jones et al. 2010; Taillefert et al. 2007a) when the redox potential of cultures was less than 0.15 V (Jones et al. 2010), suggesting that FeRB may be required to solubilize Fe(III) prior to reduction. These org-Fe(III) complexes are not associated with siderophore biosynthesis pathways, and

siderophore-reductase deletion mutants can in fact still reduce synthetic org-Fe(III) complexes for respiration.

1.5. *In situ* study of diagenetic processes

It is necessary to fully characterize the geochemistry of sediments to determine the environmental controls and the impacts of Fe(III) reduction in the context of other diagenetic processes. *In situ* chemical analysis offers several advantages over traditional sampling and subsequent laboratory measurements. First, analyses are accelerated and simplified by eliminating sample collection and processing steps, such as sediment core extrusion and separation of interstitial waters. Second, chemical artifacts associated with sample mixing, oxidation, and changes in temperature and pressure are alleviated by *in situ* measurements. Finally, sampling logistics may be improved as: (i) automation may allow the user to perform additional work while data is collected; (ii) real-time data collection may help guiding the sampling for ancillary analyses or parallel experiments; and (iii) *in situ* analysis may accelerate data collection and improve temporal resolution.

Many analytical chemistry techniques have been adapted for *in situ* use, including mass spectrometry (Bell et al. 2012; Wankel et al. 2013), Raman spectroscopy (White et al. 2006), fluorometry (Desiderio et al. 1997), spectrophotometry (Adornato et al. 2007), and electrochemistry (Luther et al. 2008; Reimers 2007; Tercier-Waeber and Taillefert 2008). Voltammetric measurements using solid-state electrodes are particularly well-suited for *in situ* deployments in aquatic systems. While potentiometric or amperometric techniques have been employed *in situ* to measure individual species such as pH, dissolved $O_{2(aq)}$, H_2S, and NO_x (NO_3^- + NO_2^-) using separate sensors (e.g. De beer et al.

1997; Glud 2008; Luther et al. 1999; Rabouille et al. 2009; Reimers 2007), voltammetry with Au/Hg microelectrodes offers the unique ability to measure several redox analytes simultaneously (Brendel and Luther 1995). Accordingly, *in situ* voltammetric analyzers have been used to probe hydrothermal vent environments (Glazer and Rouxel 2009; Luther et al. 2001), surface marine waters (Moore et al. 2007), water columns (Glazer et al. 2006; Lewis et al. 2007), deep-subsurface wells (Cowen et al. 2012), and mounted to benthic landers to analyze interstitial water chemistry in marine sediments (Meiggs and Taillefert 2011; Tercier-Waeber and Taillefert 2008). In addition, longer-term studies using stationary moorings and renewable power sources have been implemented to monitor Chesapeake Bay (Moore et al. 2007) and salt-marsh (Meiggs 2010) ecosystem health.

Unfortunately, voltammetric techniques cannot measure important redox active species, including NO_3^-, NO_2^-, SO_4^{2-}, DIC, or NH_4^+, such that a complete characterization of diagenetic processes in sediments is impossible to obtain without processing sediment cores after collection. Developing new *in situ* techniques that complement the use of voltammetric microelectrodes in these environments may significantly advance our understanding of diagenetic processes by providing more geochemical information, increasing data collection frequency, and at the same time increasing the number of sites visited during research cruises. Surprisingly, one of the most commonly used and versatile analytical techniques in chemical oceanography, high-performance liquid chromatography (HPLC), has not been adapted for *in situ* use. HPLC can be used to measure inorganic ions (Ito et al. 2012; Smee et al. 1978), carbohydrates (Gremm and Kaplan 1997), algal pigments for taxonomic identities of phytoplankton communities

(Bidigare et al. 2005), amino acids (Mopper and Lindroth 1982), and sulfide oxidation intermediates (Bak et al. 1993) with conductivity, fluorescence, or UV detection. Ion-exchange chromatography (IC) is particularly useful for the measurement of the major marine ions Na^+, Mg^{2+}, Ca^{2+}, K^+, NH_4^+, Cl^-, SO_4^{2-}, Br^-, NO_3^-, NO_2^-, and I^-, which may, in combination with voltammetry, be able to provide concentrations of all soluble inorganic redox species in natural aquatic environments. Typical IC techniques require complicated chemical-suppression systems involving toxic chemicals that would be difficult to implement *in situ*. The design of an *in situ* liquid chromatograph therefore requires the development of simple, yet robust and sensitive analytical techniques that can be adapted to a deployable instrument.

1.6 Research Scope and Objectives

The mechanism by which carbon is transformed in coastal and deep ocean sediments has important implications for the carbon budget, yet the global contribution of Fe reduction to carbon oxidation remains poorly constrained because the speciation of Fe is difficult to quantify, molecular techniques to identify FeRB activity are lacking, and the biogeochemical processes regulating the transformation of Fe are not completely understood. In addition, the simultaneous characterization of all diagenetic processes involved in the remineralization of natural organic matter is generally not conducted, as these measurements are tedious, expensive, and sometimes prone to artifacts that may skew results. Finally, techniques to measure all TEAs or their reduced metabolites *in situ* do currently not exist. In this dissertation, both laboratory and field approaches were developed and used to determine the role of Fe(III) reduction in a variety of marine

environments, characterize the environmental controls on DIR, and evaluate the possible use of organic-Fe(III) complexes as indicators of DIR in marine sediments. Three main hypothesis were tested in this dissertation:

1. **Natural organic matter promotes the formation of organic-Fe(III) complexes**
2. **Deep continental margin sediments can be hotbeds for organic-Fe(III) production if sufficient terrigenous material is deposited**
3. **Dissimilatory iron-reducing bacteria produce and respire organic-Fe(III)**

Chapter 2 of this thesis presents a review of the analytical techniques used in this dissertation as well as a description and assessment of the newly developed oceanographic benthic landers equipped with new *in situ* instrumentation. Traditional analytical techniques used include colorimetry (Fe(II), total dissolved Fe, $\sum PO_4^{3-}$), flow-injection analysis with conductivity detection (DIC), voltammetric microelectrode measurements (dissolved $O_{2(aq)}$, Mn(II), Fe(II), ΣH_2S (= H_2S + HS^- + S(0) + S_x^{2-}), soluble organic-Fe(III) complexes, and $FeS_{(aq)}$), chromatography (size-exclusion chromatography and ion exchange chromatography), mass spectrometry (characterization of organic-Fe(III) complexes), and inductively-coupled mass spectrometry (total dissolved Fe). An immobilized metal-affinity chromatographic (IMAC) method was developed to extract natural Fe-reactive ligands from sediment pore waters for subsequent identification by liquid chromatography / electrospray ionization mass spectrometry (LC-ESI-MS). Novel applications of voltammetry and HPLC were also developed for use *in situ* on benthic landers, and in Chapter 3, a novel method is presented for the determination of the major anions Cl^-, SO_4^{2-}, Br^-, NO_3^-, and NO_2^- in marine waters. The development of this method

was motivated by the need for a HPLC technique that could measure all of these anions in a single step while remaining simple and practical enough for application in an *in situ* instrument. Coupled with voltammetric measurements, the ability to measure these anions *in situ* in sediment pore waters using benthic landers provides the capability to quantify the full suite of TEAs involved in early diagenesis for the first time.

As peat-draining blackwater rivers are rich in organic carbon and dissolved Fe (e.g. Beck et al. 1974), a complementary pool of these species likely exists in estuarine sediments fed by blackwater rivers. If accurate, these environments may be opportune locations to unravel the environmental factors regulating the extent of DIR and mechanisms for soluble Fe(III) production in sediments. A seasonal study of sediment diagenetic pathways along the Satilla River estuary in southeast Georgia is presented in Chapter 4. The objectives of this study were to elucidate the origin, composition, and reactivity of dissolved Fe(III) in estuarine sediments. Bulk estuarine sediments and pore waters were sampled and a suite of respiratory chemical species were measured seasonally and spatially along the estuary to determine the environmental processes responsible for the accumulation of dissolved Fe(III) in sediment pore waters. In addition, incubations were conducted with natural sediments to identify biogeochemical pathways potentially responsible for dissolved Fe(III) production and consumption.

In select regions of the deep sea, relatively higher rates of carbon deposition have been observed in trenches (Glud et al. 2013), underlying continental slope sediments (Law et al. 2009; Rabouille et al. 2009), oxygen-minimum zones (Law et al. 2009), and upwelling regions. Generally, the concentration of poorly crystalline Fe required to observe significant Fe(III) reduction (30 μmol cm^{-3}, Thamdrup 2000) is much higher than

that found in deep ocean sediments, and sediment bioirrigation is usually much less efficient at such great depths (Middelburg et al. 1997), limiting Fe recycling and the use of Fe as a TEA in carbon remineralization processes. Some river-dominated continental margin slopes, however, are subject to massive turbidite flow deposits that have the potential to deliver terrigenous particles rich in Fe(III) to abyssal plain sediments. The northern Gulf of Mexico slope is subject to frequent mass slumping of spillover mud discharged from the Mississippi River that accumulates unconsolidated mud mid-slope (Coleman et al. 1998; Dixon and Weimer 1998; Konyukhov 2008). On the other hand, the Congo River is directly connected to the deep-sea abyssal plain (5,000 m water depth) through a submarine canyon and discharges Fe-rich particles via turbidite flows (Rabouille et al. 2009). Using traditional voltammetric microelectrode profiling and measurement of other TEAs, nutrients, and DIC in sediment cores obtained from these deep sites, the potential for DIR to play an important role in sediment diagenesis, even in these deep sites, was investigated in Chapter 5.

The molecular mechanism by which FeRB respire solid Fe(III) remains poorly understood, which is surprising considering the implications for Fe transport in aquatic sediments. For example, if solubilization of Fe is required prior to reduction, this process may explain the observed distributions of dissolved Fe(III) in sediments, and have important implications for Fe flux from sediments. The paucity of mechanistic details on microbial Fe(III) reduction is due in part to a lack of analytical techniques that can accurately determine the complex chemical speciation of Fe during its dissimilatory reduction. By simulating reactions occurring in natural aquatic systems with well-defined mineral phases and pure microbial cultures, the proposed mechanisms of

formation of soluble organic-Fe(III) complexes in sediments can be verified in the laboratory. The two main objectives of Chapter 6 were to determine if *S. putrefaciens* strain 200 produces a Fe(III)-solubilizing chelator during anaerobic Fe(III) respiration and to examine the effects of crystallinity of the solid Fe(III) substrates on Fe(III) solubilization rates.

To determine the ultimate source of soluble organic-Fe(III) complexes in sediment pore waters, it is necessary to characterize the chemical composition of these complexes. If these complexes are produced by FeRB in marine sediments, the ligands involved are likely of biogenic origin and should have distinct chemical composition compared to exogenous organic-Fe(III) complexes. The main objective of Chapter 7 was to separate and characterize organic-Fe(III) complexes produced in natural sediments. A new technique was developed to isolate specific Fe(III)-binding ligands from natural waters and characterize their chemical composition by mass spectrometry.

Finally, Chapter 8 synthesizes the new findings generated in this dissertation and provides additional recommendations for future work.

CHAPTER 2

ANALYTICAL TECHNIQUES AND DEVELOPMENT OF *IN SITU* INSTRUMENTATION

2.1. Colorimetry

2.1.1. Iron

Dissolved Fe(II) was measured in cultures and natural samples using the Ferrozine technique (Stookey, 1970). Ferrozine forms a 3:1 ligand/Fe(II) complex with Fe(II) which obeys Beer's law to concentrations at least as high as 40 μM, and is strong enough to outcompete organic ligands for Fe(II) (Viollier et al., 2000). The final Ferrozine matrix consisted of sample and 2.5 mM of Ferrozine in 250 mM Na-acetate buffered to pH 5 with HCl. Total dissolved Fe was measured by the Ferrozine technique after Fe(III) in filtered samples was reduced by 20 mM NH_2-OH•HCl in 10 mM HCl (pH ~1). Dissolved Fe(III) was calculated from the difference of total dissolved Fe and dissolved Fe(II). This method is not expected to distinguish between truly soluble and colloidal Fe(III), as the acid is expected to dissolve any Fe(III) (oxy)hydroxide species. In incubations with *Shewanella* sp., Fe(II) in both the dissolved and solid phases was used as a measure of the total extent of reduction. In this case, samples were extracted in either 0.5 M HCl or 3 M HCl prior to measurement by the Ferrozine technique. The lower acid concentration was used to avoid dissolving more crystalline magnetite minerals (Zachara et al., 1998).

2.1.2. Phosphate

Soluble orthophosphates were measured in natural samples using the molybdate-blue method (Murphy and Riley, 1962). Seawater samples and a reagent composed of 2.5 M H_2SO_4, 4.8 mM $(NH_4)_6Mo_7O_{24}\cdot 4H_2O$, 30 mM ascorbic acid, and 205 μM potassium antimonyl tartrate were mixed in a 5:1 ratio. The molybdenum-antimony-phosphate complex that forms from the reaction displays an absorption maximum at 882 nm. Standards were prepared from Na_2HPO_4 in concentrations ranging from 1 to 20 μM. The intereferences of ΣH_4SiO_4 were accounted for by subtracting the absorbances of samples prepared without added ascorbic acid from those with ascorbic acid (Murphy and Riley, 1962).

2.2. Dissolved inorganic carbon

Dissolved inorganic carbon (DIC) was measured by flow-injection analysis (Hall and Aller, 1992). Both 30 mM HCl as carrier eluent and 10 mM NaOH as receiving eluent were pumped at approximately 1 mL/min with a peristaltic pump through two channels in a plastic manifold separated by a membrane made of Teflon tape. In this technique, samples are injected into the HCl carrier stream to convert DIC to H_2CO_3. which seeps through the gas permeable membrane and is trapped in the NaOH receiver stream to convert it back to HCO_3^-. The increase in conductivity of the effluent flow stream as the sample plug passes through a conductivity flow cell is recorded as a function of time using an integrator (LCC-100, Analytical Instrument Systems, Inc.). The entire procedure takes approximately 90 seconds per sample. Peak areas of the samples conductivity were integrated using a home-made MATLAB program.

2.3. Voltammetry

2.3.1. Theory

Voltammetry is a useful analytical technique in environmental analytical chemistry because it is non-destructive and allows for the analysis of multiple redox-active species simultaneously (Buffle and Horvai, 2000; Taillefert and Rozan, 2002; Tercier-Waeber and Taillefert, 2008). In voltammetry, the current of a redox reactive analyte is recorded at a counter electrode as a function of time as the potential at a working electrode in contact with an electrolyte is varied relative to the potential of a reference electrode. The development of solid-state Au microelectrodes with Hg amalgam (Brendel and Luther, 1995) offers a particularly useful window for environmental chemistry as numerous redox active species, including dissolved $O_{2(aq)}$, H_2O_2, Fe^{2+}, Mn^{2+}, $S_2O_3^{2-}$, and total dissolved sulfide ($\Sigma H_2S = H_2S + HS^- + S^0 + S_x^{2-}$) can be quantified simultaneously (Table 2.1). In addition, the qualitative detection of organic complexes of Fe(III) (org-Fe(III)) (Taillefert et al., 2000) and Fe sulfide clusters ($FeS_{(aq)}$) which are precursors involved in the precipitation of $FeS_{(s)}$ (Theberge and Luther, 1997), is particularly useful to evaluate the redox cycling of Fe in sediments. Dissolved $O_{2(aq)}$ is typically measured by scanning the potential linearly at a constant rate using linear sweep voltammetry (LSV), ideal for non-reversible reactions (Brendel and Luther, 1995). At the half-wave potential ($E_{1/2}$) of $O_{2(aq)}$, electrons from the working electrode are transferred to $O_{2(aq)}$ to form $H_2O_{2(aq)}$ and result in an increase in current. At great overpotentials (i.e. > ~100 mV), the rate of diffusion of the analyte to the electrode's surface becomes rate limiting, and the current stabilizes at this limiting current (Figure 2.1a). As $H_2O_{2(aq)}$ is formed at the electrode surface, it is further reduced to H_2O

Table 2.1 - Description of the reactions occurring at the Hg/Au amalgam electrodes used for sediment profiling and details of the analytical procedure adopted for each measurement.

Reaction	Scan type	Deposition time (s)	Deposition Potential (V)	Scan potential (V)	$E_{1/2}$ (V)	LOD (µM)
$O_2 + 2H^+ + 2e^- \rightarrow H_2O_2$	LSV	10	-0.1	-0.1 to -1.85	-0.33	5
$H_2O_2 + 2H^+ + 2e^- \rightarrow H_2O$					-1.23	5
$Mn^{2+} + Hg + 2e^- \leftrightarrow Mn(Hg)$	CSWV	10	-0.1	-0.1 to -1.75	-1.55	15
$Fe^{2+} + Hg + 2e^- \leftrightarrow Fe(Hg)$	CSWV	10	-0.1	-0.1 to -1.75	-1.44	25
$L - Fe^{3+} + e^- \leftrightarrow L - Fe^{2+}$	CSWV	10	-0.1	-0.1 to -1.75	-0.3 to -0.6	?
$HS^- + Hg \rightarrow HgS + H^+ + 2e^-$	CSWV	10	-0.1	-0.1 to -1.75	<-0.6	0.2
$HgS + H^+ + 2e^- \leftrightarrow HS^- + Hg$	ASWV	0	N/A	-1.75 to -0.1	-0.5	10
$FeS_{(aq)} + 2e^- + H^+ \rightarrow Fe(Hg) + HS^-$	CSWV	10	-0.1	-0.1 to -1.75	-1.1	na
$2S_2O_3^{2-} + Hg \rightarrow Hg(S_2O_3)_2^{2-}$	CSWV	10	-0.1	-0.1 to -1.75	-0.15	20

($E_{1/2}$ = -1.2 V) in a redox reaction that produces a second limiting current. As the height of the limiting current is proportional to the concentration of analyte, and the concentration of $H_2O_{2(aq)}$ is equivalent to the concentration of $O_{2(aq)}$ reduced, both limiting current intensities should be equivalent. Other redox species are typically detected by square-wave voltammetry (SWV), as good detection limits and high selectivity allow for the measurement of a variety of redox species simultaneously using this technique (Luther et al., 2008). In cathodic square-wave voltammetry (CSWV) (Figure 2.1b), the potential at the working electrode is scanned from more positive to more negative values with an oscillating staircase wave function to first reduce then immediately oxidize the analyte of interest in the next phase. The current measured at the end of the forward oscillation (reducing current) and that measured at the end of the backward oscillation (oxidizing current) are measured at each potential and recorded as a function of time

during the potential scan. As the forward and reverse currents for reversible electrochemical reactions should have the same intensities but reverse polarities, the resulting current obtained by the difference of forward and backward currents should be twice as large as the forward current alone, and thus the sensitivity for reversible reactions should be enhanced by a factor of two (Bard and Faulkner, 2000). Most electrochemical reactions, however, are not truly reversible, and typically backward response represents a fraction of the forward response (Figure 2.1b). In anodic square-wave voltammetry (ASWV), the method is the same except that the potential applied to the working electrode is scanned negatively as a function of time, and thus the forward current is issued from oxidation of the analyte while the backward reaction is produced by reduction of the analyte.

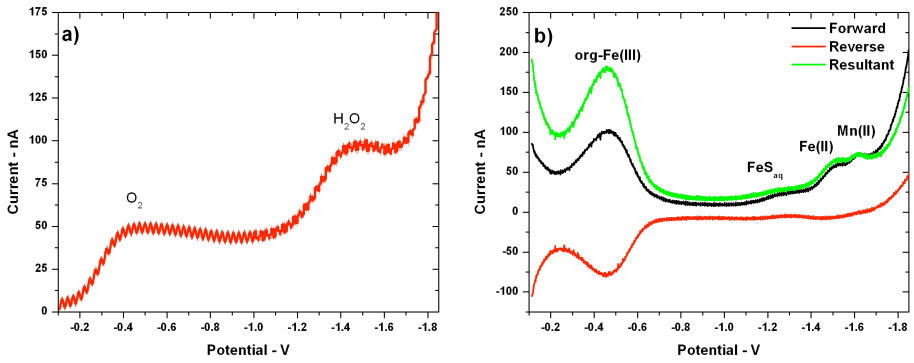

Figure 2.1 – Examples of voltammograms obtained with Au/Hg voltammetric microelectrodes by a) LSV and b) CSWV. To avoid memory effects between replicate measurements at Au/Hg microelectrodes, a potential at -0.1 V is applied for 10 s before each measurement. This step ensures that any $O_{2(aq)}$, $H_2O_{2(aq)}$, Fe^{2+}, or Mn^{2+} reduced during the previous measurement is reoxidized before the next analysis. As org-Fe(III) complexes adsorb at potentials > -0.4 to -0.6 V and as sulfide species (ΣH_2S) oxidize Hg(0) at potentials > -0.6 V, however, an initial conditioning step of 10 s at -0.9 V is added to this procedure if these species are detected to clean the electrode surface between subsequent analyses (Taillefert et al., 2000a).

2.3.2. Au/Hg microelectrode construction and calibration

Solid-state Hg/Au working voltammetric microelectrodes encased in polyether ether ketone (PEEK) and epoxy were constructed as previously reported (Luther et al. 2008) and used as part of a 3-electrode system consisting of Ag/AgCl reference and Pt counter electrodes with a DLK-60 or DLK-100 (Analytical Instrument Systems, Inc.) for discrete measurements of solutions. The AgCl coating was formed on the reference electrode by applying +9V between the Ag wire and a Pt electrode (Brendel and Luther, 1995). Electrodes were calibrated in a $MnCl_2$ solution (0 to 400 μM) and the pilot ion method (Brendel and Luther, 1995; Luther et al., 2008) was used to infer concentrations of Mn^{2+}, Fe^{2+}, and ΣH_2S in samples. $O_{2(aq)}$ calibration details are given in the next section. As the voltammetric response of organic-Fe(III) complexes and $FeS_{(aq)}$ cannot be quantified because their exact chemical composition is unknown, their response is directly reported in current intensities (Taillefert et al., 2000b). To compare the signal intensities of these species measured at different electrodes, each electrode's response to Mn^{2+} was normalized to a typical Mn^{2+} response (0.12 nA/μM), and this ratio was used to adjust the current response of the unquantifiable analytes. Peak heights were determined using a semi-automated VOLTINT software package (Bristow and Taillefert, 2008).

2.3.3. Sediment profiling

Ex situ voltammetric profiling of sediments was performed in a similar way to measurements in discrete samples, except that solid-state Au/Hg working microelectrodes encased in glass with a tip diameter < 1 mm (Brendel and Luther, 1995) were affixed to an Analytical Instrument Systems, Inc. (AIS) micromanipulator capable of sub-

millimeter increments, while the Ag/AgCl reference and Pt counter electrodes were kept in the overlying waters. When overlying waters were safely assumed to be fully oxygenated, $O_{2(aq)}$ was calibrated *in situ* by measuring the salinity and temperature of the overlying waters and calculating $O_{2(aq)}$ saturation from Henry's law. Because some sediments were from hypoxic zones ($O_{2(aq)}$ < ~80 μM), $O_{2(aq)}$ was calibrated externally by

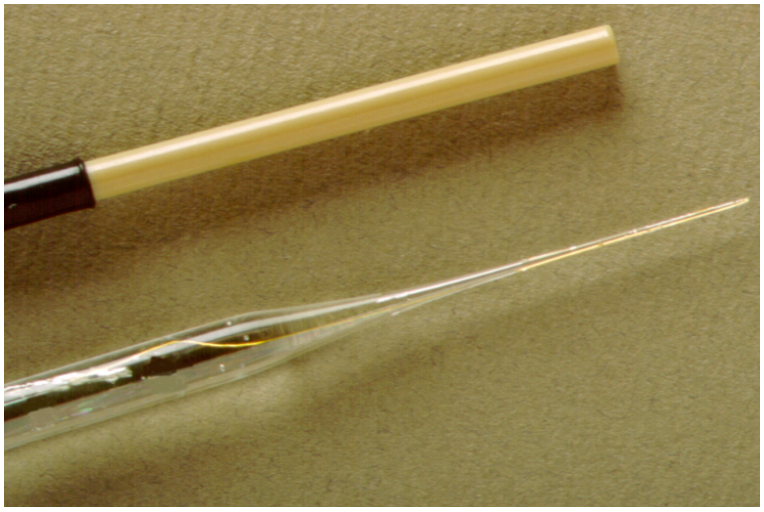

Figure 2.2 - Voltammetric microelectrodes in PEEK™ housing for discrete and long-term stationary measurements in batch reactors, sample vials, or benthic chambers, and in a glass housing for sediment profiling.

performing LSV in known-temperature, air-equilibrated, filtered estuarine or seawater from the site of interest, and relating the $O_{2(aq)}$ current response to the $O_{2(aq)}$ saturation concentration of this solution. Then, $O_{2(aq)}$ responses in sediments could be converted to concentrations by multiplying the ratio of the observed current to the calibrated current by the $O_{2(aq)}$ saturation value of the calibration.

2.4. Chromatography

2.4.1. Size-exclusion chromatography

High-pressure size-exclusion chromatography (HP-SEC) was used to separate dissolved Fe(III) and Fe(II) complexes from the bulk of the natural organic matter (NOM) and to provide size distribution information on the DOM in pore water samples. With HP-SEC, molecules are separated primarily by size, as smaller molecules take a longer path through a porous gel stationary phase and therefore elute later than larger molecules. Separations were performed with a Waters 1525 high-pressure pump, Waters 2487 dual-absorbance detector, Waters WFC fraction collector, and the Waters Empower software suite, with a Superdex PC 3.2/30 analytical column (100 to 30,000 Da size-exclusion limits, Amersham GE Biosciences)

A series of standards including synthetic humic-like compounds, Suwannee River Humic Acid (SRHA), and inorganic Fe^{2+} (as $Fe(NH_4)_2SO_4$ was injected onto the column (Figure 2.3a) using the manufacturers recommended pH 6.8 phosphate buffered eluent. Absorbance was monitored between 200 and 300 nm to determine the exclusion and permeation volume (i.e. the volumes at which molecules larger than 30,000 or smaller than 100 Da elute) and calibrate the separations for ranges of molecular weights (MWs). Unfortunately, while the expected correlation between the log(MW) and retention time (or volume eluted) was observed with the standards (Figure 2.3b), Fe^{2+} controls oxidized on the column (not shown), even with thorough sparging of the eluent and additional in-line eluent-degassing with UHP N_2. For pore water separations, the pH of the mobile phase was therefore buffered to a sufficiently low value to prevent oxidation of Fe(II)

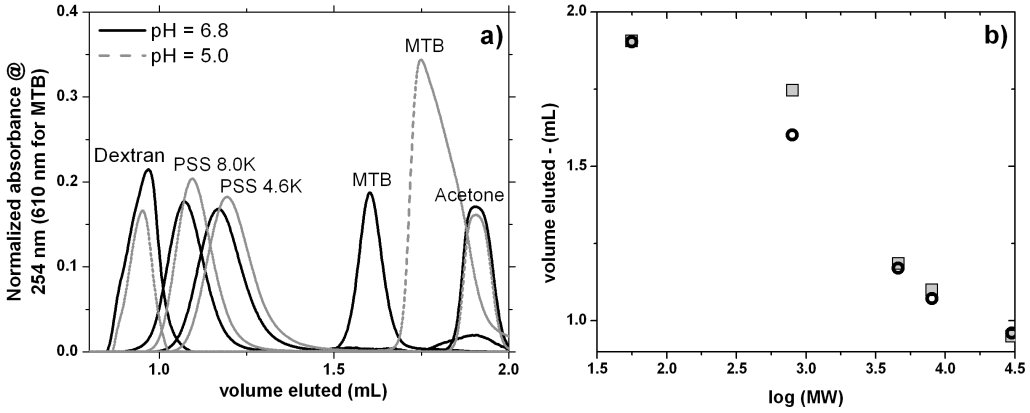

Figure 2.3 - a) Superdex PC 30 column calibration chromatograms obtained using the pH 6.8 or the pH 5 eluent and humic-type molecules. Dextran and acetone defined the exclusion and permeation volume, respectively. Polystyrene sulfonate (PSS) polymers with MW of 8,000 and 4,600, and MTB are used as intermediate molecular weight standards; b) Calibration curves for the pH 6.8 eluent (black circles) and pH 5.0 eluent (gray squares).

during the separation. Control HP-SEC separation experiments demonstrated that with a mobile phase consisting of 150 mM NaCl and 30 mM Na-acetate buffer (adjusted to pH 5 with acetic acid), less than 5% of a 1 mM Fe(II) solution in a 0.54 M NaCl sample matrix (pH 7.2) was oxidized (Figure 2.4).

To determine if the column could successfully determine molecular weights with this pH 5 eluent, the same synthetic humic-like molecules were separated (Figure 2.3a). A linear correlation between the log(MW) of the calibration standards and retention time (except with methyl thymol blue (MTB) at pH = 5 eluent) was observed with both eluents (Figure 2.3b), but the standards took slightly longer to elute with the lower pH eluent, suggesting that non-ideal charge interactions between the stationary phase and the

standards were occuring. Subsequently, 50 µL volumes of 4 mg L^{-1} SRHA (compliments of the Perdue lab at Georgia Tech) were separated in the recommended pH 6.8 eluent

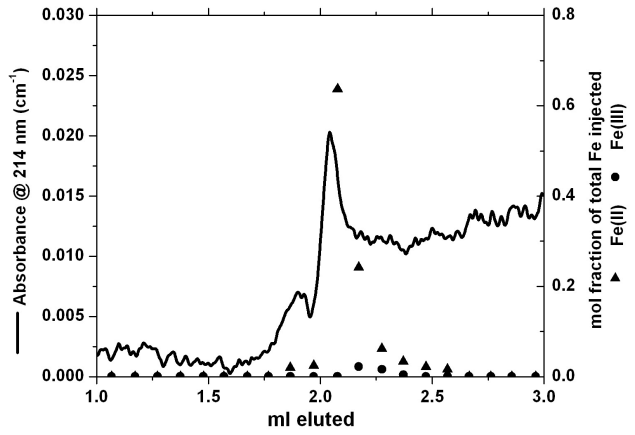

Figure 2.4 - A size exclusion chromatogram from a 50 µL injection of 1 mM $Fe(NH_4)_2(SO_4)_2$ with the pH 5 eluent. Black lines represents the UV trace at 214 nm obtained as a function of elution volume. Fe in each collected 100 µL fraction is represented as the mole fraction of the total Fe injected and symbols (triangles, circles) correspond to Fe(II) and Fe(III), respectively. The elution volume of each Fe fraction was shifted back by 750 µL to account for the dead volume between the flow-through UV detector and the fraction collector.

(Chin et al., 1994) and in the pH 5 eluent, and absorbance at 254 nm was monitored as a function of time in the column effluents (Figure 2.5). Weight average molecular weights (M_w) were determined according to the formula (Chin et al., 1994):

$$M_w = \sum_{i=1}^{n} (h_i * m_i^2) / \sum_{i=1}^{n} h_i * m_i \qquad \text{(Eq. 2.1)}$$

where *n* is the number of time/absorbance data points *i* within the column exclusion volumes, *h* is height of the absorbance signal at *i* (assumed to be proportional to the number of moles of *i*), and *m* is the calibrated MW corresponding to the time of the data point taken from the observed log(MW) – retention time correlation (Figure 2.3b) for

either of the two eluents (MTB was omitted from the pH 5 eluent calibration). The SRHA chromatograms reveal that eluent composition does have an effect on elution

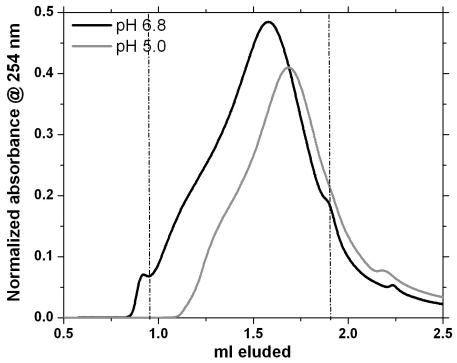

Figure 2.5 - Chromatograms of injections of 4 mg L^{-1} SRHA separated using a Superdex PC 30 column and the pH 6.8 or the pH 5 eluent. Vertical lines represent the void and permeation volumes as defined by dextran and acetone.

behavior (Figure 2.5). The calculated M_w values for an SRHA standard using each eluent's individual calibration were calculated to be 2038 Da and 635 Da with the pH 6.8 and pH 5 eluents. Although the pH 5 eluent severly underestimates the M_w (O'Loughlin and Chin, 2001), retention times of the calibration standards did not change upon repeated injections throughout the lifetime of the column, ensuring that the data obtained with the pH 5 eluent could be comparable even without normalization to calibrated molecular weights. For analysis of pore water samples, injections of a 50 µL sample at a flow rate of 100 µL/min in the pH 5.0 eluent offered a good peak resolution while maintaining the desired Fe detection limits in effluent samples. Samples were mixed in a 9:1 ratio with a 10x eluent solution (1.5 M NaCl, 300 mM Na-acetate adjusted to pH 5.0 with acetic acid) prior to injection to minimize matrix effects on UV absorbance and stabilize the Fe complexes against any oxidation that might occur before mixing with the

eluent. Absorbance at 254 nm was monitored in the column effluent, and 100 μL fractions (~ 2 column volumes) were collected for Fe speciation measured spectrophotometrically (section 2.1.1). To determine separation recoveries, mass balance calculations for Fe were performed using the following equation:

$$\sum_{i=1}^{m} C_f V_f + \sum_{i=1}^{n} C_r V_r = (1 - df)\, C_{inj} V_{inj} \qquad \text{(Eq. 2.2)}$$

where C and V represent the concentration of Fe (in mole L^{-1}) and the volume of each fraction (f), rinse (r), and pore water injected (inj), m and n represent the number of fractions and rinses eluted, and df is the dilution factor from matrix-matching with eluent prior to injection. The average concentration of Fe in the fractions collected prior to the predicted void volume of the column was subtracted from the concentrations of each individual fraction to remove the contribution of the baseline to the mass balance calculations. Three aliquots of EDTA (100 mM, in Na-acetate eluent) were injected at the end of each pore water injection to elute any residual Fe and quantify recoveries. Fe in the rinse fractions was measured with an Agilent 7500a inductively coupled plasma-mass spectrometer (ICP-MS), because EDTA prevents determination of Fe by the Ferrozine technique (details in section 2.5).

2.4.2 Metal-affinity chromatography and electrospray ionization mass spectrometry

Fe-binding ligands were extracted from sediment pore waters using immobilized-metal affinity chromatography (IMAC) according to the following strategy (Figure 2.6). Ligands presenting affinity for Fe(III) were first isolated on a Chelex-100 resin equilibrated with Fe^{3+} ions. The column retentate was then eluted and the natural ligands

simultaneously decomplexed from Fe^{3+} using EDTA as competitive ligand. The samples were then loaded on a C-18 solid-phase extraction cartridge to extract the natural organic ligands and eluted with methanol for Liquid Chromatography-Electron Spray Ionization-Mass Spectrometry (LC-ESI-MS) analysis.

All chemicals were purchased from Sigma-Aldrich and prepared with HPLC-grade deionized H_2O (Fisher Scientific). The Fe(III) solid sorbent was first prepared by packing 1 g of Chelex-100 resin (Sigma, sodium form) in a low-pressure column (Kontes, Flex-column 0.7 mm ID x 4 mm). The resin was converted to its Fe form by flushing in sequence 4 mL HCl, 10 mL dionized H_2O, 4 mL 100 mM $FeCl_3$ adjusted to pH 2.2 with NaOH, and 10 mL dionized H_2O with a peristaltic pump (Ismatec) at a flow rate of 1 mL/min. The column was subsequently conditioned for natural saline samples with 4 mL of 0.54 M NaCl containing 2.3 mM $NaHCO_3$ (pH 7.5). Between 10 and 50 mL of pore water samples or standards were loaded onto the Fe-Chelex, and excess salts then rinsed with 4 mL deionized H_2O. Ligands bound to the Fe-Chelex were then extracted with 4 mL of 20 mM EDTA adjusted to pH 8.5 with NaOH and allowed to equilibrate with the column overnight. Solid-phase extraction (SPE) cartridges (Supelco, Select HLB SPE tube 60 mg or Supelclean C-18 3 mL tubes) were conditioned with 2 mL of 80% methanol and then 2 mL of dionized water. The EDTA extracts were syringe-loaded onto the SPE tubes, and retained ligands were subsequently eluted with 2 mL of 80% methanol. These samples were then concentrated ~10 fold by evaporation under vacuum overnight in the presence of desiccant (Drierite).

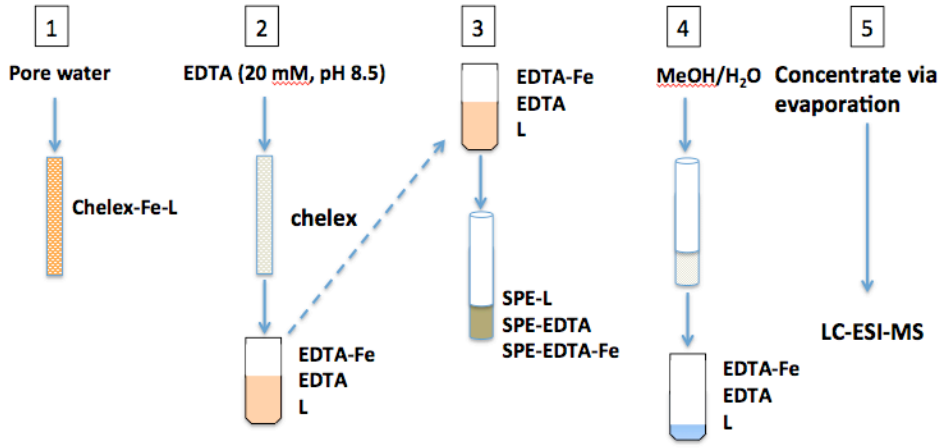

Figure 2.6 – Sequence of steps performed in the IMAC procedure to extract ligands from standards and pore waters.

Ligands were identified by LC-ESI-MS by introducing extracted samples into a triple quadropole mass spectrometer (Micromass Quattro LC) using electrospray after chromatographic separation on a reversed phase C-18 column (Phenomenex Gemeni C-18, 150 x 2 mm, 5 um). A linear gradient from 5% acetonitrile to 100% acetonitrile (both water and acetonitrile solutions contained 0.2% formic acid) was provided by a binary HPLC system (Agilent 1100). NaI and RbI standards from 20 to 3,000 Da were used to calibrate the instrument, and data was collected in both positive and negative ionization modes.

2.4.3 Anion-exchange chromatography

The major marine anions Cl^-, SO_4^{2-}, Br^-, NO_3^-, and NO_2^- as well as the tracer I^- were measured by anion-chromatography with UV detection. The method used was developed specifically for *in situ* applications and is described in detail in Chapter 3 of this thesis.

2.5. Inductively coupled plasma mass spectrometry

Total dissolved Fe in EDTA-rinse fractions was measured with an Agilent 7500a by inductively coupled plasma-mass spectrometer (ICP-MS), as control tests revealed that Ferrozine cannot quantitatively outcompete EDTA for Fe and therefore renders the Ferrozine Fe measurement technique invalid (data not shown). Samples were diluted with 2% nitric acid (trace metal grade, Fisher) diluted in Nanopure water (Barnstead). Fe standards and samples contained yttrium (10 ppb) as internal standards. For the HP-SEC measurements, EDTA was added to standards and did not affect counts relative to standards with no EDTA. Blanks, calibration check standards (95-105% recovery), and River Water Certified Reference Material for Trace Metals (SLRS-4, National Research Council Canada, Ottawa, Canada) were analyzed as quality controls.

2.6. Benthic landers

A pair of benthic landers were constructed and used to monitor diagenesis and sediment fluxes in sediments offshore of Cape Lookout, NC.

2.6.1. Development of a benthic lander rated for full ocean depth deployments

A pair of benthic landers were constructed and used to monitor diagenesis and sediment fluxes in sediments offshore of Cape Lookout, NC. For *in situ* analysis of deep environments (<1000 m), an autonomous deep-sea benthic lander (courtesy of R.A. Jahnke (Jahnke and Christiansen, 1989; Jahnke and Jahnke, 2000)) was outfitted with new instrumentation to collect benthic flux data from a single square titanium benthic chamber (30 x 30 cm) and sediment pore water profiles completely autonomously (Figure

2.7). Detailed mechanical specifications regarding the lander frame construction, release mechanisms, and ballast systems are provided in the original paper (Jahnke and Christiansen 1989). Briefly, the autonomous deep-sea benthic lander is equipped with eight glass flotation spheres (Teledyne-Benthos, Inc.), but is initially ballasted with 3 buckets of scrap metal of 48 kg each to allow descent to the seafloor. An AIS SMC-1 (Smart Motor Controller, Analytical Instrument Systems, Inc.) is programmed prior to deployment to close the benthic chamber lid after a settling period on the seafloor, inject a chemical tracer into the chamber for volume determination, operate a benthic chamber water sampling system, and activate a hydraulic shovel to seal the bottom of the benthic chamber to retrieve sediments at the end of the deployment. The tracer injecting and water sampling system uses a spring-loaded mechanism triggered by a traveling pin itself activated by a 12 V DC motor that can be programmed via the AIS SMC-1, to collect approximately 30 mL of water in a series of 18 x 60 mL syringes at discrete time intervals (typically ~ 1.5 hours) for subsequent *ex situ* analyses. At the end of the deployments, two newly-designed redundant burn-wire systems housed in separate pressure housings are used to drop the extra ballast and release the lander from the seafloor. An additional backup mechanism consisting of a Mg rod of specific diameter that dissolves in seawater at a known rate is also mounted in line with the burn-wire systems in case a catastrophic failure of the microcontroller. An AIS ISEA-IV, (*In Situ* Electrochemical Analyzer, Analytical Instrument Systems, Inc.) mounted on the lander frame controls up to four microelectrodes individually with a built-in multiplexer. The AIS ISEA-IV is encased in a titanium housing of 30 cm long by 20 cm in diameter,

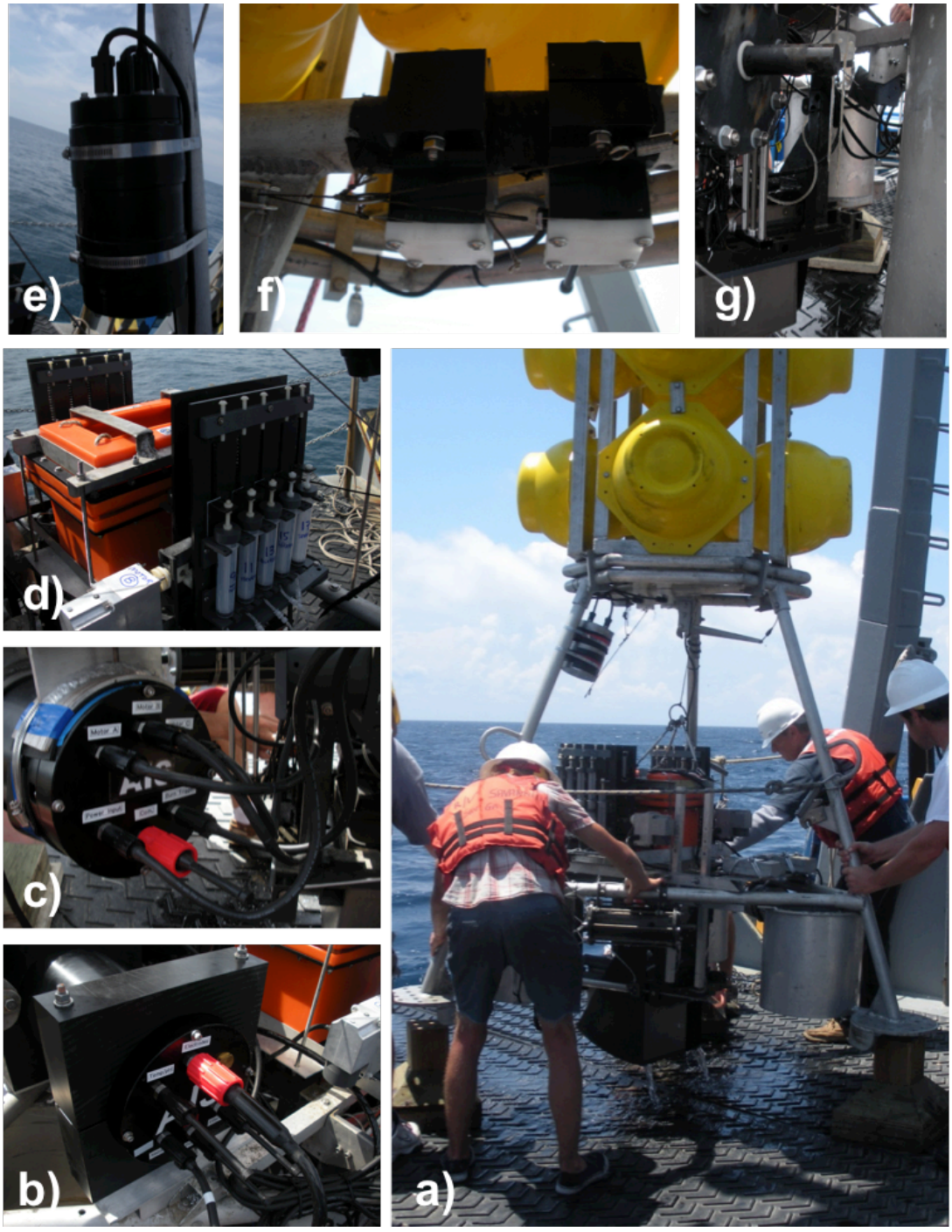

Figure 2.7 - Clockwise from bottom right: a) the deep benthic lander during deployment; b) the ISEA-IV potentiostat (AIS, Inc.); c) the AIS SMC-1 Smart Motor Controller; d) syringe racks and controlling motors, and deep-sea battery; e) the backup burn wire release controller; f) redundant burn wire release mechanisms; g) and the microelectrode manifold and hydraulic shovel.

pressure-proofed to full ocean depth, and is powered by a 12 V DC SeaBattery™ power module (Deep-Sea Power and Light). The ISEA-IV controls all analytical aspects of the electrochemical system. It can be programmed to start sequences of electrochemical experiments at any time during the deployments and controls an *in situ* micromanipulator (UN-MAN-1, AIS) to obtain depth profiles of geochemical constituents in pore waters. Au/Hg glass or PEEK voltammetric microelectrodes were constructed as previously reported (Figure 2.2, Luther et al., 2008) and used as part of a 3-electrode system consisting of Ag/AgCl reference and Pt counter electrodes. With this system, $O_{2(aq)}$, H_2O_2, Fe^{2+}, Mn^{2+}, $S_2O_3^{2-}$, total dissolved sulfide ($\Sigma H_2S = H_2S + HS^- + S^0 + S_x^{2-}$), as well as the qualitative detection of organic complexes of Fe(III) (org-Fe(III)) and Fe sulfide clusters ($FeS_{(aq)}$) (Tercier-Waeber and Taillefert, 2008) could be quantified in sediments as a function of depth by mounting two glass Hg/Au voltammetric microelectrodes positioned within 1.5 cm from each other on the *in situ* micromanipulator. The two profiling electrodes were positioned at a known depth interval from one another (typically 5 cm) to determine the position of the sediment-water interface more accurately (within 2 mm) (Meiggs and Taillefert, 2011). Simultaneously, two PEEK Hg/Au voltammetric microelectrodes were affixed across the benthic chamber lid with high-pressure fittings (IDEX) to monitor benthic fluxes over time.

The micromanipulator is controlled by the AIS ISEA-IV and the resolution step increment can be changed during a single deployment to more efficiently capture the sediment-water interface (typically 0.6 mm) or for rapid progression through larger sediment intervals (typically 2 or 4 mm). The AIS ISEA-IV was preprogrammed prior to

Table 2.2 – Sequence of voltammetric experiments preprogrammed in the AIS ISEA-IV *in situ* potentiostat for collection of sediment profiles and benthic chamber data at two different electrodes each. The first sequence of 12 scans (top) is performed for each profiling electrode, and the sequence of 8 scans (bottom) is performed for the benthic chamber or water column electrodes.

Scan count	Wave form	Scan Rate (mV/s)	Sensitivity, Current Range nA	Conditioning
4	ASW	200	±100 nA ± 800 nA	none
4	CSW	200	±100 nA ± 800 nA	-0.9 V, 10 s -0.1 V, 10 s
4	LSV	2000	±100 nA ± 800 nA	-0.1 V, 10 s
4	CSW	200	±100 nA ± 800 nA	-0.9 V, 10 s -0.1 V, 10 s
4	LSV	2000	±100 nA ± 800 nA	-0.1 V, 10 s

deployment with a voltammetric sequence optimized previously (Meiggs, 2010) capable of measuring all redox species, including I^- used as chemical tracer in the benthic chamber, without memory effects (Table 2.2).Deployments usually lasted between 30 and 35 hours, and a series of steps operated independently by the AIS SMC-1 microcontroller operated all lander features (Table 2.3). While a pinger system (Teledyne-Benthos, Inc.) was used to confirm location of the lander on the seafloor, pressure-activated radio beacon and strobe light were positioned on the top of the floats to locate the lander once at the surface.

2.6.2 Shallow lander and AIS ISEA-IV-LC optimization

To collect benthic fluxes and depth profiles of the main redox species in sediments underlying shallow waters (< 70 m), a tethered lander (courtesy R.A. Jahnke, Jahnke et al., 2000), was outfitted with new instrumentation (Figure 2.8) and

Table 2.3 – Sequence of steps programmed in the AIS SMC-1 microcontroller to operate the deep-sea benthic lander during a typical 35 hour deployment. The AIS SMC-1 operated the water sampling system (motors A and B), which also controlled the injection of a tracer in the benthic chamber and the hydraulics used to close the benthic chamber lid at the beginning of the deployments, as well as the benthic chamber shovel at the end of each deployment. The AIS SMC-1 also operated the primary burn wire system at the end of each deployment to drop the extra ballast before recovery. Typically, motors A and B were turned on for 10 seconds each time, enough to turn each traveling screw an appropriate amount to trigger hydraulics or fire a syringe on one of two syringe-holding racks.

Step	Step duration (seconds)	Description	Time after deployment (min)
Deploy		*Release lander from A-frame*	0
Pause	1200	Descent time	0
Motor A	10	Close lid	20
Motor B	10	Inject tracer	21
Motor C	1	Toggle stirrer ON	22
[1]Motor A	10	Collect 17 syringe samples alternating between racks A & B (Repeat 8 x *steps 1 through 4*, then 1 x *step 1*)	23
[2]Pause	7200		
[3]Motor B	10		
[4]Pause	7200		
Motor C	1	Toggle stirrer OFF	2065
Motor B	10	Trigger shovel close	2066
Pause	600	10 minutes for shovel to close	
Burn Wire	180	Release ballast	2077
Retrieve		*Lander surfaces*	2080

simultaneously deployed with the free lander on the same research cruises. The shallow lander is also equipped with an AIS UN-MAN-1 micromanipulator for depth profiles,both an opaque and translucent benthic chamber, to evaluate the effect of natural light on benthic fluxes, and two syringe racks to collect water samples as a function of time. The lander also includes a sediment coring device to recover a sediment core within 50 cm from the profiling electrodes at the end of the deployments.

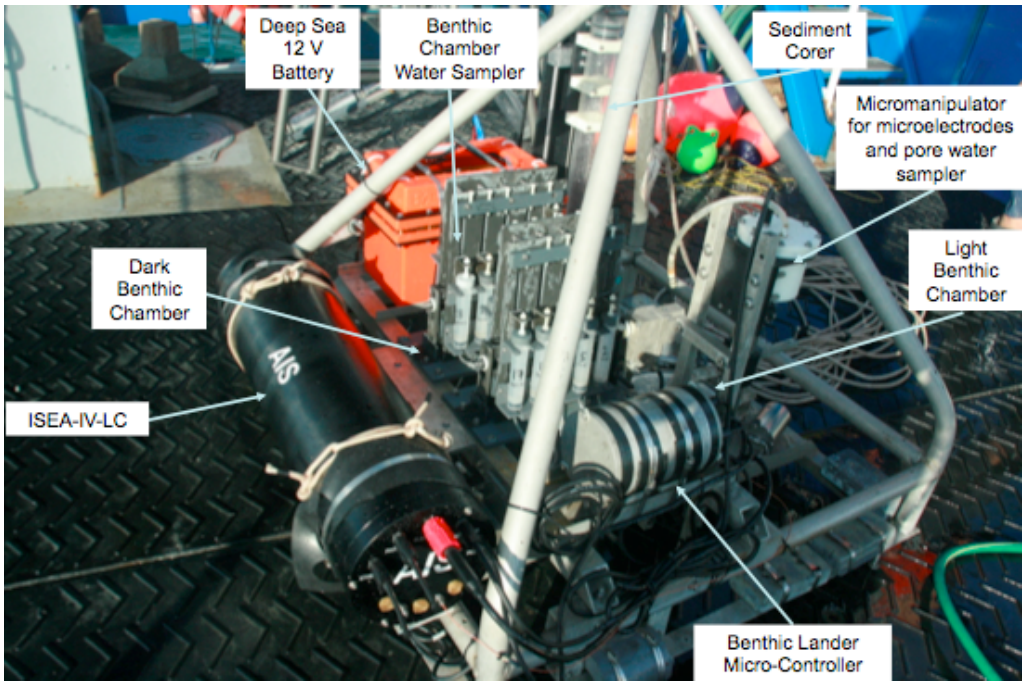

Figure 2.8 - The shallow lander is tethered and is equipped with the AIS ISEA-IV-LC, which contains both an electrochemical analyzer as well as a new *in situ* HPLC. From this lander, up to 18 syringe samples can be taken alternately from two benthic chambers (9 samples from each chamber). In this design, a PEEK Au/Hg voltammetric microelectrode can be deployed in each chamber and typically two glass Au/Hg voltammetric microelectrodes are deployed on the AIS UN-MAN-1 micromanipulator for depth profile measurements.

The shallow lander is equipped with an Analytical Instrument Systems, Inc. *in situ* electrochemical analyzer coupled to a high performance liquid chromatograph (AIS ISEA-IV-LC) to perform voltammetric and potentiometric analyses along with chromatographic separations of either overlying water from one of the benthic chambersfor flux measurements or pore water using the micromanipulator for sediment depth profiles. The HPLC method optimized for these applications targeted the analysis of Cl^-, SO_4^{2-}, Br^-, NO_3^-, but various types of HPLC analyses could be adapted depending on the needs. The ISEA-IV-LC, developed by Analytical Instrument Systems, Inc., is to

our knowledge the first *in situ* electrochemical analyzer / HPLC ever to be constructed and deployed on benthic landers. It consists of two independent liquid handling systems. The sampling system to collect samples from the outside environment includes a low pressure sample pump that turns on when a sample is collected, an inlet valve on the bulk head of the instrument to open and close the system to the outside environment, a sampling sipping probe, and an electronic Rheodyne, Model Titan-HP™ injection valve to inject a constant volume of sample into the HPLC system (Figure 2.9). The AIS ISEA-IV-LC as configured for anion measurements consists of a 6-way injection valve with fixed injection loop that allows the sample to mix with the eluent, a low voltage HPLC pump from SSI, Inc. able to handle pressures up to 2,000 psi (a higher pressure pump (10,000 psi) is available for UHPLC separations) and flow rates from 0.7 to 1.2 ml min^{-1}, pulse dampeners, four inline filters of decreasing pore size (10, 5, 2, and 0.5 μm; A-722, OC-813, A-706, A-707; IDEX), a Metrohm A Supp 5 150.0/x 4.0 mm anion exchange column with a Metrohm A Supp 4/5 10.0/4.0 mm guard column and a Photo Diode Array Spectrometer, Model USB 2000+ from Ocean Optics, capable of monitoring dual wavelengths from 190 to 700 nm. The mobile phase is supplied to the system via a solvent bag and the waste is collected in a similar manner. The AIS ISEA-IV-LC uses a modified AIS DLK-70/HPLC Webpstat™ that allows control of the pumps and spectrometer (Figure 2.9) and controls every aspect of the electrochemical (i.e. pH and Au/Hg voltammetric microelectrodes) and chromatographic analyses. The data collected during separation are stored on a Secure Digital (SD) memory card with a minimum of 8 Gb of memory. After the same sequence of electrochemical measurements as that used for the deep lander is performed with the AIS ISEA-IV-LC (Table 2.2), the inlet valve is

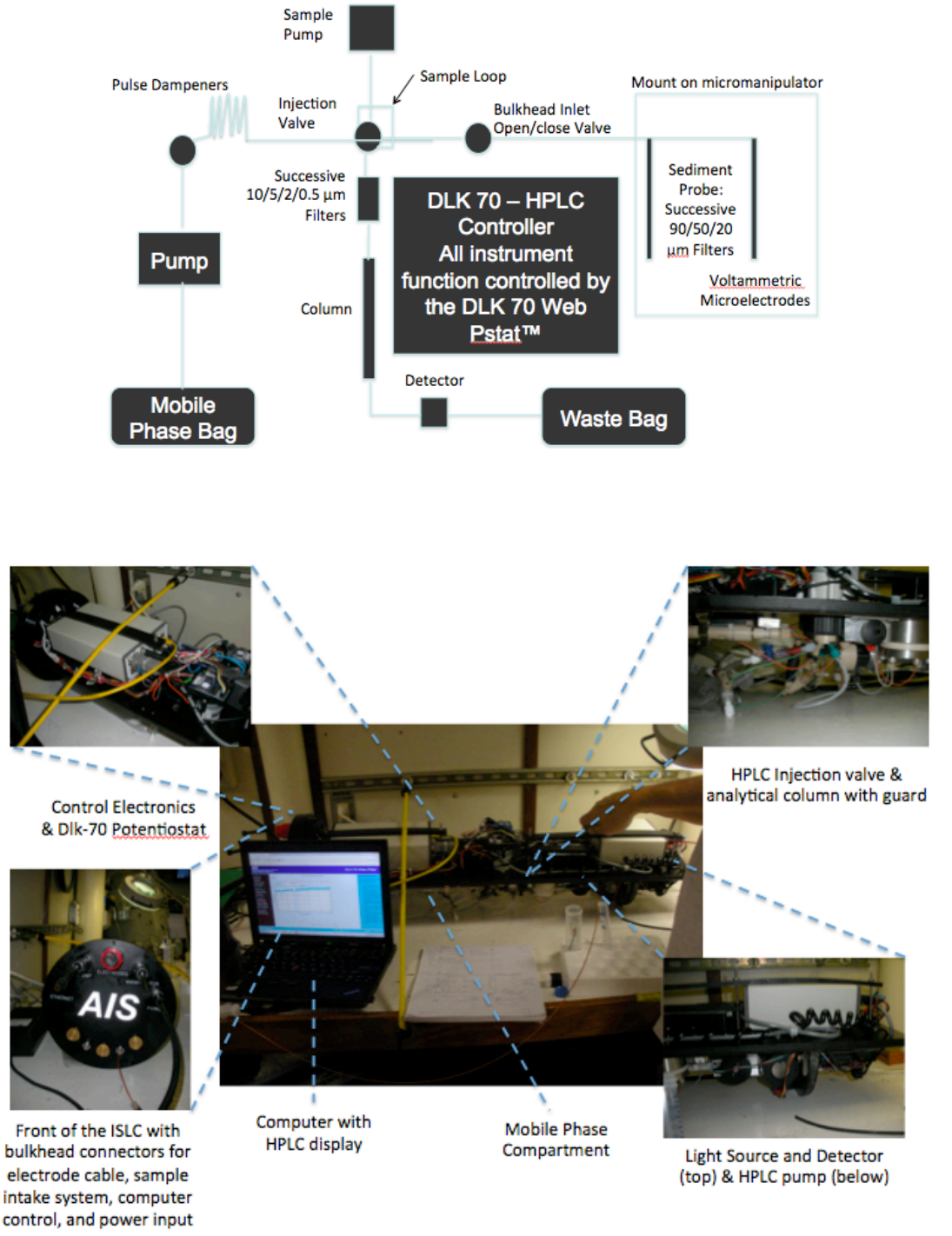

Figure 2.9 - Flow chart of the ISEA-IV-LC instrument, electrodes, and sampling probes (top). Photographs of the ISEA-IV-LC instrument and its individual components (bottom)

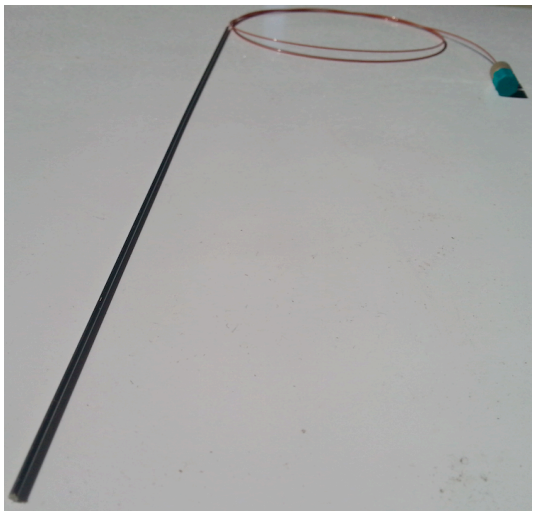

Figure 2.10 – Photograph of the sediment sipping probe. The probe is 1.5 mm in diameter and 20 cm in length. The stainless steel housing is lined with PEEK tubing, and filters embedded in the tip filter samples from 160 μm to 50 μm.

opened, pore water and/or benthic water samples are pumped into the HPLC from the external water column, benthic chamber, or sediment, through the sample sipping probe, loaded onto the sample loop, and injected into the column to initiate the chromatographic separation. After sample injection, the inlet valve is closed and the sampling pump turned off. After chromatographic separation, the micromanipulator assembly descends a preset increment and the HPLC pump turns off to save power and eluent. Voltammetric scans are run immediately after each micromanipulator move and prior to HPLC separations because a longer equilibration time is likely required for pore waters to readjust near the larger-bore sample sipping probe. Approximately 14 minutes elapse during the sequence of electrochemical experiments at four electrodes, likely ample time for pore waters to equilibrate prior to sampling for HPLC analysis.

The sediment sipping apparatus was constructed from 30 cm long, 17-gauge stainless steel tubing lined with 1/32" OD / 0.020" ID (794 μm / 508 μm) PEEK™ tubing (IDEX) with a series of filters embedded in the tip (90-160 μm / 50-90 μm / 20-40 μm pore sizes, each 1/16" (1.59 mm) thick (Interstate Specialty Products) to prevent clogging of the sampling probe (Figure 2.10). Samples were pulled using a peristaltic pump positioned in-line behind the injection valve at a rate of 40 μL/min for 5 minutes along a flow path of the same 0.020" ID tubing of length 90 cm to fill a 25 μL sample loop. Only ~200 μL of pore water sample is typically withdrawn from sediments at a time to avoid contamination between sediment layers and maximize the vertical resolution of the depth profiles, while collecting enough sample to wash the sampling system and avoid memory effects during measurements. The probe is typically mounted on the micromanipulator at a depth equal to the deeper of the two voltammetric microelectrodes. As small volumes of samples are not necessarily required from overlying waters, the benthic chamber sipping apparatus was constructed with sturdier 1/16" OD / 0.030" ID (1.59 mm / 762 μm) PEEK™ tubing (IDEX) with a single, 1/8" (3.18 mm) wide, 20-40 μm porex plastic filter attached to the tip with heat-shrink tubing, and sampling pump flow rates were increased to 300 μL/min for 5 minutes. Regardless of the configuration of the HPLC sample sipping probe, samples are then injected into the HPLC system using a sequence of steps controlled by the AIS DLK-70/HPLC Webpstat™ and optimized for these applications (Table 2.4).

The HPLC method used was developed specifically for this work and depended on the analytes of interest (Chapter 3 of this thesis). Absorbance was acquired by the detector at 215 nm using a sampling rate of 200 mV/sec for HPLC runs between 8 and 20

minutes, depending on the eluent used. This data acquisition frequency provided the best peak resolution and sensitivity for that method. The detector internal parameters optimized by repeated injection of a mixture of standards used a pixel number of 65, equivalent to 214 nm, a boxcar integration pixel number of 15 (the number of pixels averaged around this wavelength), and an integration time of the absorbance signal of 10. The HPLC pump was turned on approximately 5 minutes prior to sample injection to ensure the flow equilibrated before chromatographic separation, but turned off during electrochemical measurements to conserve both eluent and battery power (Table 2.4). Finally, all electrochemical data and chromatographic data for a single micromanipulator increment and/or a benthic chamber time point are archived together (Table 2.4). The AIS ISEA-IV-LC is rapidly calibrated to well-established and environmentally relevant ranges (Chapter 3 of this thesis) prior to deployments using a similar sequence as in Table 2.3 modified to remove data archiving between HPLC runs.

2.6.3. Assessment

2.6.3.1. Shallow and deep lander comparative in situ voltammetry

The landers were deployed with voltammetric profiling electrodes on the Cape Hatteras shelf and slope to measure respiratory metabolites *in situ* (Figure 2.11). As measurements over a total depth of around 15-20 cm are usually preferred, the spatial resolution achieved depends on the total time the lander is deployed. While typical profile

Table 2.4 – Sequence of steps preprogrammed in the ISEA-IV-LC to collect and analyze a single sample by HPLC. This sequence is called immediately after the electrochemical sequence shown in Table 2.2. An additional experiment called "HPLC" was created that monitors the absorbance at a specific wavelength for a predetermined amount of time consistent with the HPLC method used in Chapter 3 of this thesis.

Step	Description	Parameter
HPLC pump on	Flow rate set to 0.70 mL min^{-1}	0
Outside sample valve open	Open bulkhead inlet valve	0
Sample loop load position	Set sample loop to load position	0
Sample pump on	Turn sampling pump on	0
Pause	Load sample from sipping probe into loop at 40 µL/min for 300 seconds	300
Sample pump off	Turn sampling pump off	0
Outside sample valve close	Close bulkhead inlet/safety valve	0
Sample loop inject position	Inject sample	0
Run experiment "HPLC"	Collect HPLC chromatogram (Details Chapter 3 in this thesis)	0
HPLC pump off	Flow rate set to 0.0 mL min^{-1} to conserve eluent.	0
Archive	Archive all of the voltammetry scans from the 4 electrodes and the HPLC run from a single depth in one compressed file	0
Micromanipulator preset	Parameter X corresponds to a pre-defined increment between 0.6 and 4 mm in micromanipulator window	*X*

measurements should not take more than 5-6 hours, the instrument is currently not able to run both benthic chamber and profiling microelectrodes independently of each other, such that depth profiles are acquired continuously during lander deployments. As measurements are obtained at each depth right after the benthic chamber measurements (Table 2.4) and as benthic chamber measurements are performed with a relatively low frequency (i.e. every 1-2 hours depending on the length of the deployment), the electrodes are maintained at a holding potentials of -0.9 V between measurements to prevent their degradation between electrochemical runs. While using this procedure may pose some risk for the profiling electrodes exposed to sulfidic environments,

voltammograms obtained during such deployments were generally reproducible with flat baselines, indicative of their good quality. The measurements conducted on the shelf and slope of Cape Hatteras revealed two very separate geochemical provinces, with SO_4^{-2} reduction dominating on the shelf (Figure 2.11a), but concurrent metal reduction dominating on the slope (Figure 2.11b), which is a deposition center for organic carbon. The production of $FeS_{(aq)}$, however, suggests that SO_4^{2-} reduction is taking over metal reduction.

2.6.3.2. Sediment profiling with the AIS ISEA-IV-LC

Control tests with a dye in the laboratory demonstrated that the sipping probe is able to resolve depth gradients in highly porous sand (Figure 2.12). Further testing with natural sediments revealed the probe could withdraw pore water samples from sand, silty sediments, or sandy sediments with up to 50% added clay (not shown). The AIS ISEA-IV-LC was tested in silty sediments from the Altamaha River, and depth profiles of both redox metabolites (i.e. $O_{2(aq)}$, Mn^{2+}, Fe^{2+}, ΣH_2S) and anions (i.e. NO_3^-, NO_2^-, and Br^-) were simultaneously quantified in sediment pore waters using Au/Hg voltammetry and HPLC (Figure 2.13). Chromatogram baseline noise was high relative to the peak heights due to low analyte concentrations (Figure 2.13a). Profiles demonstrated an increase in salinity (by measurement of Br^-) from the overlying waters to the sediments, as the river was in a flood stage from recent precipitation events during the measurements. The traditional redox zonation as a result of the different aerobic and anaerobic respiration reactions observed in early diagenesis (Chapter 1.3 of this thesis; Froelich et al., 1979) is illustrated

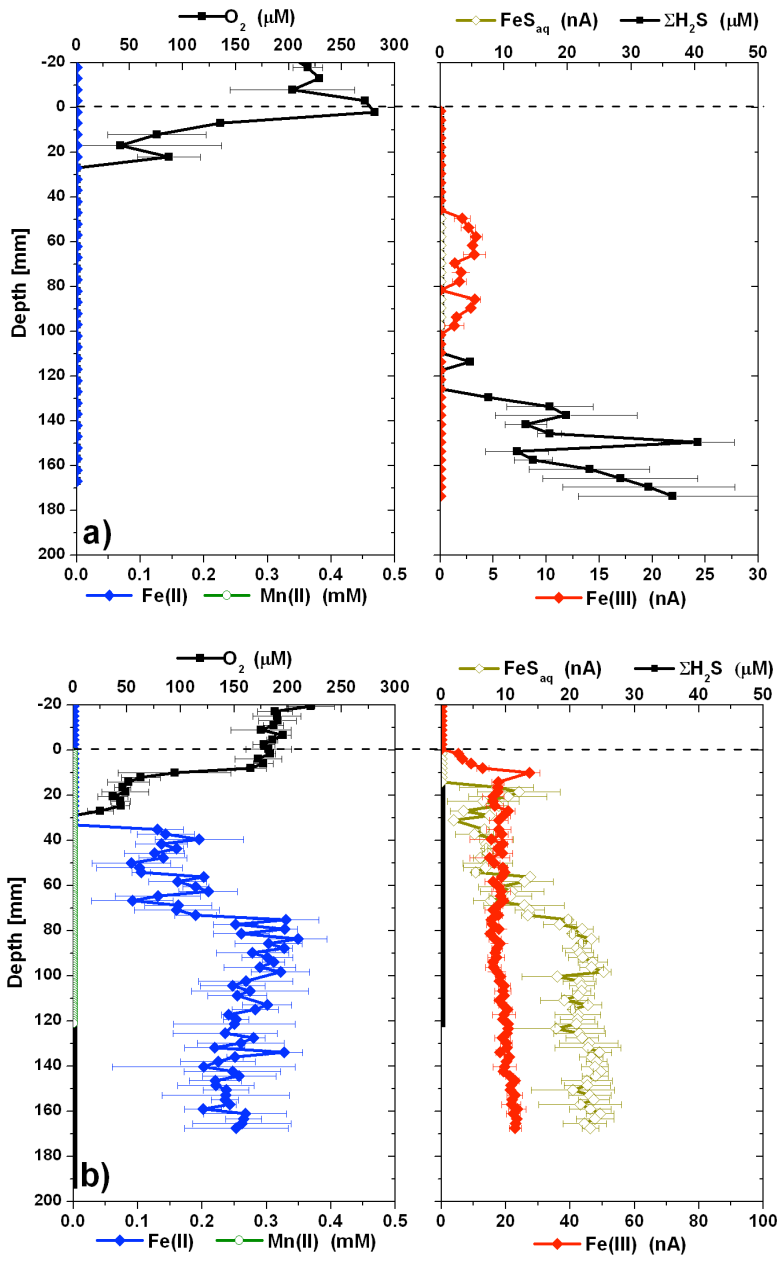

Figure 2.11 - Sediment profiles of redox species obtained with the *In Situ* Electrochemical Analyzer (ISEA IV) from a) the Cape Hatteras shelf (~40 m) and b) the Cape Hatteras slope (~200 m). The shelf is dominated by SO_4^{2-} reduction, but the slope is dominated by metal reduction, though it appears that SO_4^{2-} reduction may be taking over respiration processes at that time.

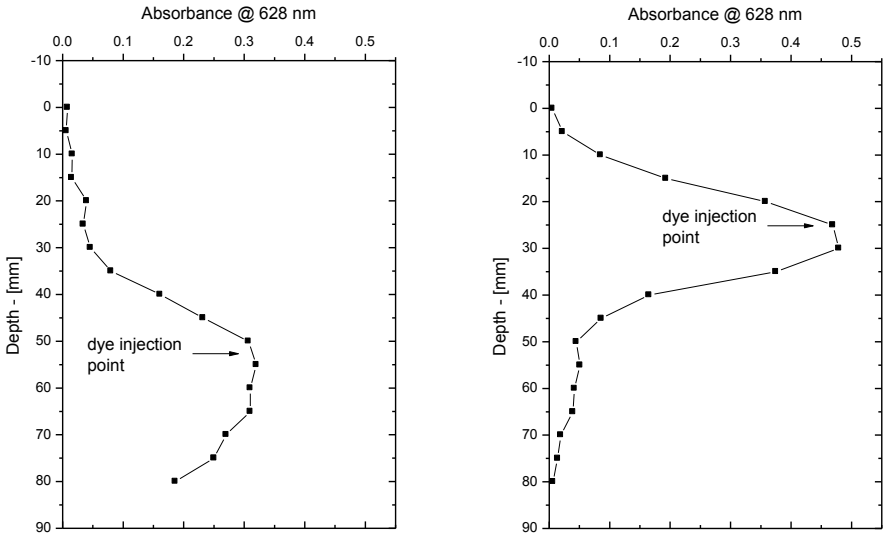

Figure 2.12 - Sampling of pore waters as a function of depth using the *in situ* pore water sampling probe designed in this study and in line spectrophotometric detection (absorbance at 628 nm) of the water sample collected at each depth. A food dye injected horizontally at 55 mm (left profile) and injected vertically at 25 mm (right profile) was used as chemical tracer. A spatial resolution of 5 mm was used with the sampling probe. Results show that the sampling probe is able to collect pore waters without contamination between layers.

for the first time as obtained from one measurement-platform. Below a zone of aerobic respiration (< 5 mm penetration depth, Figure 2.13b), NO_3^- was consumed as a function of depth through denitrification or dissimilatory nitrate reduction to ammonium (DNRA). In turn, NO_2^-, an intermediate product of NO_3^- reduction, remained below detection limit (< ~1 μM). The onset of Mn(IV) reduction, detected by the production of Mn^{2+}, occurred deeper in the pore waters, after NO_3^- was depleted. While Fe^{2+} concentrations remained under detection limit (< 10 μM) of the electrochemical analyzer, indirect evidence of Fe(III) reduction was observed through the accumulation of org-Fe(III) complexes at

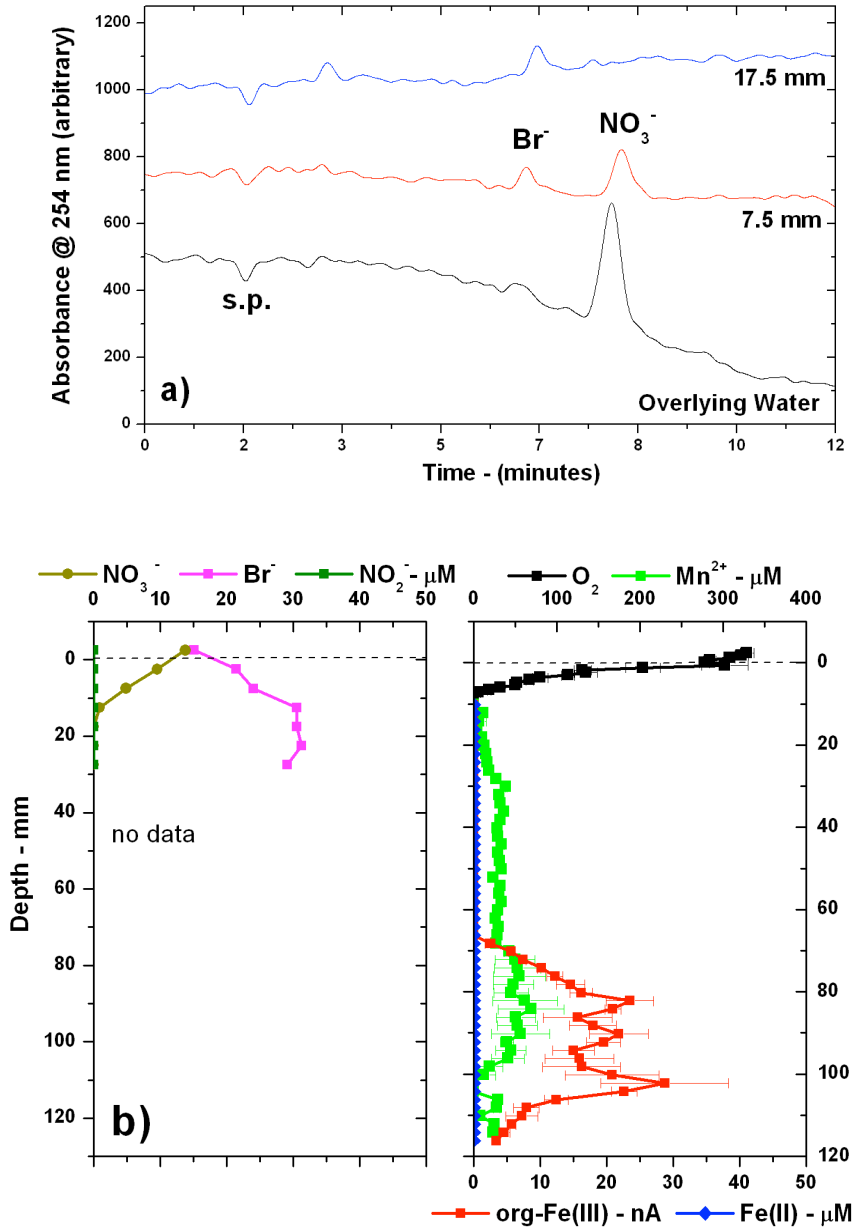

Figure 2.13 – a) An overlay of chromatograms obtained using the AIS ISEA-IV-LC when sipping pore waters from sediments using the sample sipping probe; b) A corresponding sediment profile from a station 9 km upstream (salinity 0.63) from the mouth of the Altamaha River demonstrate the AIS ISEA-IV-LC can resolve all discrete redox layers and salinity features using a combination of *in situ* voltammetry and HPLC.

depth (Figure 2.13b). Sulfate reduction was not observed, as no dissolved ΣH_2S (MDL < 0.1 μM) nor $FeS_{(aq)}$ were observed in these sediments.

2.6.3.3. Benthic chamber testing with the AIS ISEA-IV-LC

Flux studies conducted in shallow sediments using the AIS ISEA-IV-LC demonstrate the successful *in situ* determination of the nutrients NO_3^- and NO_2^- and the tracers Br^- and I^- in an experiment in which all 4 anions were injected simultaneously into the benthic chamber to examine nitrification/denitrification processes and advection/diffusion across the sediment-water interface. An overlay of chromatograms reveals decreasing concentrations of all of the anions as a function of time (Figure 2.14), either as a result of transport across the sediment-water interface (i.e. Br^- and I^-) or transport and consumption by reduction (i.e. NO_3^-). In another deployment of the shallow lander with the AIS ISEA-IV-LC, I^-, used as chemical tracer, decreased as a function of time until concentrations were no longer detectable after 15 hours, while ever-present seawater Br^- behaved conservatively, i.e. remaining within 10% of seawater values during the deployment (Figure 2.15). These findings provide another piece of evidence that the *in situ* HPLC method developed is accurate and precise. These measurements also revealed that NO_3^- was consumed by the sediment, likely during denitrification, while ΣPO_4^{3-} and possibly DIC, measured in discrete water samples collected with the syringe sampler, were produced simultaneously in the overlying waters as a result of respiration processes (Figure 2.15). These findings confirm that the AIS ISEA-IV-LC instrument is capable of collecting water samples from the outside environment, injecting

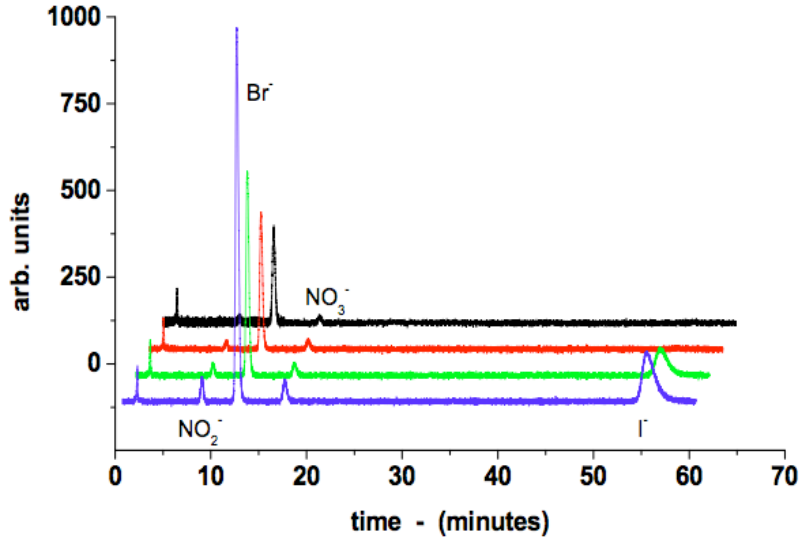

Figure 2.14 – Overlay of raw chromatograms reveal the concentrations of the nutrients NO_3^- and NO_2^- and the tracers Br^- and I^- as a function of time in a benthic chamber during deployment of the shallow lander on the continental shelf off the Cape Hatteras.

them in the HPLC, and reliably and accurately quantifying the major and minor anions in seawater multiple times over a 24 hour period.

2.6.4. Discussion

In this work, an instrument AIS ISEA-IV-LC instrument capable of performing simultaneous HPLC and electrochemical analyses *in situ* in marine sediments was constructed and tested. The ISEA-IV-LC was deployed on a benthic lander platform complete with a micromanipulator for the analysis of sediment chemistry as a function of depth, and benthic chambers for measurements of sediment fluxes as a function of time. The instrument is pre-programmed to collect data autonomously prior to deployments typically lasting between 18 and 24 hours. Voltammetric microelectrodes are positioned

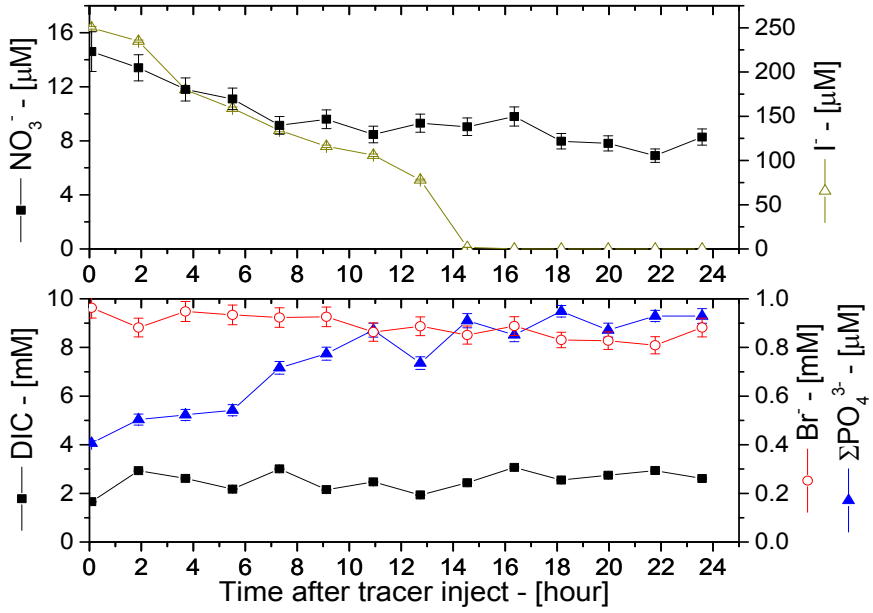

Figure 2.15 – Concentrations of NO_3^-, I^-, Br^-, ΣPO_4^{3-}, and DIC as a function of time during a benthic chamber deployment of the AIS ISEA-IV-LC on the shallow lander on the continental shelf off Cape Hatteras. While NO_3^-, Br^-, and, I^- were measured *in situ* by the AIS ISEA-IV-LC, ΣPO_4^{3-} and DIC were measured after lander retrieval in discrete benthic chamber samples collected by the syringe sampling system. The decrease in both NO_3^- and I^- as a function of time suggests that active transport across the SWI along with denitrification are responsible for the removal of NO_3^- from the benthic chamber. The relatively constant behavior of Br^- over time is another indicator that the AIS ISEA-IV-LC provides reliable measurements of major and minor anions in seawater.

in an electrode holder that protrudes from the micromanipulator by 12 cm and through the lid of the chambers at about 2 cm from the top of the chambers. They continuously measure concentrations of $O_{2(aq)}$, H_2O_2, Fe^{2+}, Mn^{2+}, $S_2O_3^{2-}$, and ΣH_2S, as well as qualitative measurements of org-Fe(III) and $FeS_{(aq)}$ species during deployments. A syringe system collects up to 18 benthic chamber samples from the benthic chamber for wet chemical analyses after retrieval. The ISEA-IV-LC can be configured to sample from sediments or from one of the benthic chambers by simply attaching the tail-end of the appropriate probe to the bulkhead using standard HPLC fittings and placing the probe into the

electrode holder or into one of the chamber's lid. The stainless steel sediment-sampling probe penetrates sediments with a small footprint of only 1.5 mm and the sample flow path is lined with inert PEEK tubing. Five minutes are required to draw an appropriate sized sample (200 μL from sediments or 1.5 mL from chamber) in either configuration using an internal peristaltic pump. Samples are loaded into a sample loop and injected into an anion exchange column with a photo diode array detector for the detection of Br^-, NO_3^-, and NO_2^-, as well as Cl^- and SO_4^{2-} if desired with a small method modification (Chapter 3 of this thesis). Typically, a sequence to measure analytes at 2 profiling electrodes, 2 benthic chamber electrodes, and an HPLC run (either of a pore water or chamber sample) requires around 30 minutes. In this configuration, sediment profiles of the first ~15 cm of sediments are obtained with a 4 mm depth increment during an 18 hour deployment, and ~35 benthic chamber data points are collected.

Using this coupled electrochemical and HPLC system the majority of TEAs (i.e. $O_{2(aq)}$, NO_3^-, SO_4^{2-}) and/or their reduced metabolites (i.e. Mn^{2+}, Fe^{2+}, $\sum H_2S$) involved in diagenetic processes in both freshwater and marine environments can be determined simultaneously. The HPLC pumping system consumes low power and generates little pulsing (Figures 2.12a and 2.13), which, along with the PDA detector used, allows for good detection limits for most anions of interest. The detection limits of the *in situ* instrument for NO_3^- and NO_2^- are in the same range (100 - 200 nM) as those obtained with other instruments developed for *in situ* instruments, including an ultraviolet spectrophotometer for NO_3^- (~200 nM; Johnson and Coletti, 2002) and a double-beam spectrophotometer for NO_2^- (~100 nM; Gong et al., 2009). Because of its low power consumption (5 Ah under the current configuration), its relatively compact size (60 cm

long by 20 cm diameter), the system could easily be adapted to other platforms such as autonomous underwater vehicles (AUVs), remotely operated vehicles (ROVs), and surface or bottom moorings for measurements of major (Cl^-, Br^-, SO_4^{2-}) or minor (NO_3^- and NO_2^-) anions. While HPLC analyses may be relatively slow, this instrument can also be adapted to CTD rosettes as has been realized with the AIS ISEA-IV previously (Glazer et al., 2006; Lewis et al., 2007) to measure anions in the water column of marine and freshwater environments. To circumvent the frequency of analysis issue given the duration of the chromatographic separations, it may be possible to develop a procedure that relies on the injection of multiple samples with a relatively high frequency over time on the same column as long as the sampling frequency is slow enough to prevent overlapping between the last analyte of the previous sample and the first analyte of the next sample.

The existing system (i.e. PDA detector and single pump) could be easily adapted for the quantification of a few other analytes, including sulfide oxidation intermediates such as tetrathionate and thiosulfate (Bak et al. 1993). Although the system as described here is not currently optimized to measure cations, a method could be developed to analyze cations by UV. For example, no method currently exists to measure NH_4^+ *in situ* in marine environments. NH_4^+ is released during organic matter degradation, is a by-product of DNRA, and is involved in both aerobic and anaerobic nitrification and anammox (Brandes et al., 2007). Developing a HPLC method for major cations in marine waters may represent another significant progress that could be exploited by the present AIS ISEA-IV-LC. Further, it may also be possible to analyze both anions and cations in the same sample by running two columns in parallel during a run. Valves

controlled by the AIS ISEA-IV-LC instrument could easily be added to split the sample between two columns, and the UV detector could be programmed to alternate between data collection parameters required for either method. The sampling pump could also be used to constantly supply reagents to mix with samples post-column, allowing colorimetrically-determined species such as Fe(II) (Viollier et al., 2000) or colloidal Fe (Pullin and Cabaniss, 2001) to be separated by any HPLC technique (e.g. HP-SEC, Chapter 4 of this thesis) and then continuously quantified in the PDA detector. Supplementing the system with another HPLC pump and/or a switching valve would probably be the most versatile and cost-effective addition to the instrument, by allowing for gradient elution and preconcentration. A gradient pumping system would allow measurement of iodine, iodate, organic-iodine by UV detection with (Schwehr and Santschi, 2003). The addition of a fluorescence detector and valve to the existing system may also allow determination of hydroxyl radicals by isocratic fluorescence detection with on-line preconcentration (Takeda et al., 2004), or amino acids by fluorimetric detection with pre-column derivation (Mopper and Lindroth 1982). Other detectors may also be useful for carbohydrates, which can be measured isocratically by pulsed amperometric detection (Gremm and Kaplan 1997).

2.6.5. Comments and recommendations

The AIS ISEA-IV-LC has been successfully shown to collect natural waters from any marine environment to a depth of 60 m. While the AIS ISEA-IV-LC has for the first time measured all of the key TEAs or their reduced metabolites involved in early diagenesis (i.e. $O_{2(aq)}$, NO_3^-, NO_2^-, SO_4^{2-}, Mn^{2+}, Fe^{2+}, and ΣH_2S), these measurements have

revealed several key areas in which continued optimization should be undertaken. In sandy, coarse-grained sediments, it is currently possible to withdraw at least 100 samples of approximately 200 μL volume at low flow-rates (i.e. 40 μL min^{-1}) before the column is contaminated enough to increase retention times and back pressure to unreasonable values. As the finer filtration (i.e. < 10 μm and as fine as < 0.5 μm) is performed through a series of pre-column filters, the total system back pressure has been observed to increase from ~1,000 psi to 2,000 psi during runs, pressures at which the system is programmed to terminate for safety reasons. Cleaning the pre-column filters and analytical column by flushing with a 1 M Na_2CO_3 solution reduces backpressure and restores elution times, and accordingly, an independent cleaning system may be required for long-term monitoring efforts. Similarly, salts may accumulate on the column and require high concentrations of a divalent anion to be eluted through the column to regenerate it. To increase the life of the column and allow for long-term deployments, a procedure that switches the eluent upstream of the column to a cleaning solution every ~80 samples could easily be implemented using the existing system. Alternatively, if organic contaminations are responsible for the pressure increase, a black-carbon pre-column filter may be an appropriate solution for longer term *in situ* deployments.

In silty or slightly muddy sediments, it is only possible to withdraw between 10 and 20 samples at the same flow rate before clogging the sipping probe. Again, pre-column filters are also prone to clogging as evidenced by increased system back pressure and it is recommended they are changed prior to each deployment. At a somewhat elevated cost of around $30 for the 4 successive filters, however, alternative options should be explored. The sampling pump currently used is limited to flow rates as low as

40 μL min^{-1}, which may still be too rapid to prevent cavitation. If a stronger pump with a lower possible flow rate is used (i.e. a syringe pump), it may be possible to use tubing of a narrower bore, therefore requiring less pore water volumes. A stronger pump might also be capable of performing finer filtration at the tip of the sample sipping probe directly, avoiding use of some of the in-line filters and preventing the system backpressure from increasing. Finally, tests with thick clay sediments revealed that pore water could not be collected with the sampling probe irrespective of flow rate, likely because a thick layer of impermeable clay accumulated onto the tip of the sampling probe filter during micromanipulator descent. Drilling new slotted ports in the side of the sampling probe a few mm from the tip and repositioning the coarse filters to pull laterally and from a larger surface area may prevent immediate encrustation of the bottom of the probe. Dimensions, however, must be carefully considered so as to not adversely affect spatial resolution.

CHAPTER 3

DEVELOPMENT OF SINGLE-STEP LIQUID CHROMATOGRAPHY METHODS WITH ULTRAVIOLET DETECTION FOR THE MEASUREMENT OF MAJOR ANIONS IN MARINE WATERS

This is a copy of an article currently in press in *Limnology and Oceanography Methods*, authored by Jordon S. Beckler, Donald B. Nuzzio, and Martial Taillefert entitled "Development of single-step liquid chromatography methods with ultraviolet detection for the measurement of major anions in marine waters."

Abstract

While a number of techniques exist to measure major anions Cl^-, NO_2^-, Br^-, NO_3^-, or SO_4^{2-} in marine waters and sediment pore waters, a single method that can quantify all five anions in a single step with a sufficiently low detection limit has yet to be developed. In this work, a novel ion-chromatographic separation procedure was developed that exploits the UV-absorbing properties of Br^-, NO_3^-, and NO_2^- as well as the suppression of eluent absorbance by high concentrations of Cl^- and SO_4^{2-} to quantify all these anions in a single step in marine waters. If additional sensitivity for the minor anions Br^-, NO_3^-, and NO_2^- is needed, NaCl can be used as eluent in a matrix elimination method that no longer allow for Cl^- and SO_4^{2-} determination. These methods are isocratic, require no chemical or electronic suppression, are not subject to interferences, and can resolve the anions in less than 18 minutes. The decrease in analysis time and the number of analyses required

compared to conventional methods lowers the costs associated with laboratory analysis of marine samples. Lastly, the simplicity and good limits of detection make this separation method suitable for *in situ* deployments in marine waters and pore waters.

3.1. Introduction

Oceanographic chemical measurements are essential to study, preserve, and manage the oceans. Despite the rapid advances in oceanographic technology, the number of chemical measurements obtained in these environments relies largely on sampling and *ex situ* analyses of water and sediment samples using a variety of techniques (Dickey and Bidigare 2005). To continuously improve our understanding of the biogeochemical processes regulating the distribution and flux of elements between the sediment, water column, and the atmosphere, it is necessary to monitor the geochemical composition of marine environments continuously with high spatial and temporal resolution. The recent technological advances in electronics, power consumption, and communication have boosted the development of *in situ* monitoring systems (Delaney and Chave 2000; Jannasch et al. 2008; Luther et al. 2008; Meiggs and Taillefert 2011). For such applications, versatile techniques are needed, including chromatographic techniques to measure the concentration of major anions Cl^-, Br^-, NO_3^-, NO_2^-, and SO_4^{2-} in a variety of marine environments.

Cl^- measurements may offer insights into biogeochemical and hydrological processes in estuaries, sediments, and hydrothermal systems. In estuaries, Cl^- concentrations are used as indicators of mixing processes between fresh and marine waters (Grace et al. 2008). Cl^- depth profiles in sediments can also be used to trace brine

inputs (Castellini et al. 2006; Lapham et al. 2008; Wallmann et al. 2006) or submarine groundwater discharge (SGD) to the seafloor (Martin et al. 2006; Schlüter et al. 2004). Simultaneously, Cl^- concentrations may offer insights into deep subsurface high-temperature phase separation processes in hydrothermal systems (Butterfield and Massoth 1994; Pester et al. 2011). The marine chemistry of Br^- is similar to Cl^-, and because of its low reactivity Br^- is often used as a tracer of mixing processes (Berg et al. 2001; Leblanc et al. 1991). SO_4^{2-} is mainly used as terminal electron acceptor by dissimilatory sulfate-reducing bacteria in anoxic sediments, and depletion of SO_4^{2-} can be observed in a variety of highly active cold seeps and coastal environments (Hoehler et al. 2001; Lapham et al. 2008; Metzger et al. 2007; Schmidt et al. 2005). *In situ* depth profiles of SO_4^{2-} may be useful in environments where pressure changes may mix the sediment upon recovery or where a high spatial resolution is needed (e.g., sediments with strong pore water gradients). In addition, SO_4^{2-} removal may occur abiotically by reaction with basalt or by precipitation with Ca^{2+} as anhydrite, thus the extent of removal of SO_4^{2-} from hydrothermal fluids may provide information on hydrothermal circulation (Janecky and Seyfried 1984; Sleep 1991). Finally, nitrogen is an essential element for life on Earth, yet the cycling of nitrogen in marine environments is complex and poorly characterized (Galloway et al. 2004) mainly because the concentration of fixed nitrogen remains relatively low and nitrogen intermediates are either transformed efficiently (i.e. NO_2^-) or escape in the gas phase (i.e. NO, N_2O, N_2). Conventional analytical techniques for nitrogen species typically suffer from matrix effects that prevent their determination in seawater (Debeer and Sweerts 1989; Gros et al. 2008b; Muller et al. 1998), though a spectrophotometric technique has been successfully developed to quantify NO_3^- in marine

waters (Johnson and Coletti 2002), and this method has been adapted to various platforms for *in situ* measurements (Johnson 2010; Johnson et al. 2013). In addition, conventional centrifugation techniques used to extract pore waters from sediment cores may create artifacts as intracellular NO_3^- may be released by cell lysis (Larsen et al. 2013). Similarly, squeezing methods developed to minimize these types of issues (Bender et al. 1987) present other disadvantages, including mixing between layers and over pressurization of pore waters that may create similar artifacts, while passive sampling systems, e.g. dialysers or 'peepers' (Hesslein 1976) and diffusive gradients in thin films (Davison et al. 1994) require long deployments that may not be practical in oceanographic expeditions.

The simultaneous analysis of these major anions in natural waters may be performed by ion chromatography with conductivity detection (Small et al. 1975; Smee et al. 1978; Tabatabai and Dick 1983). In seawater, however, dilution is necessary to prevent the major anions from oversaturating the analytical column, maintain separation efficiency, and gain sensitivity for the analysis of some of the minor anions (Connolly and Paull 2002; Hu et al. 1999; Tirumalesh 2008). As a result, the ability to resolve low concentrated anions (i.e. NO_2^- and NO_3^-) in natural marine waters are lost, and these techniques are typically only used to quantify Cl^- and SO_4^{2-}. Various methods have been developed to resolve this issue, including changing the detector output range during separation (Gros et al. 2008b), using dual columns to separate and concentrate minor anions (Wang et al. 2012), or using matrix elimination to prevent interferences from Cl^- and SO_4^{2-} on minor anions (Evenhuis et al. 2008; Hu et al. 1999; Ito et al. 2005). While these methods are able to detect minor anions, they in turn prevent the determination of Cl^- and SO_4^{2-}. In addition, some of these methods may not be easily applied to *in situ*

instrumentation as they may require complex software or liquid handling systems. Simultaneously, different types of columns have been used with equal success for the analysis of seawater anions, including high capacity anion exchange columns (Evenhuis et al. 2008; Gros et al. 2008a; Rozan and Luther 2002; Wang et al. 2012) and reverse phase C-18 (octadecyl-silica, ODS) columns using permanent coating with anion exchangers (typically quaternary amines; Connolly and Paull 2002; Hu et al. 1999; Ito et al. 2012; Ito et al. 2005). Finally, conventional ion chromatography techniques using conductivity detection require eluent suppression which is typically achieved with a strong acid (Small et al. 1975; Smee et al. 1978; Tabatabai and Dick 1983). Such systems not only require an additional, caustic reagent with all its safety implications, but also require additional liquid handling systems that will increase the complexity of *in situ* measurements. Non-suppressed liquid chromatography may represent a good alternative to the detection of major and minor anions in *in situ* instruments, and the majority of non-suppressed techniques either use low-conductivity eluents (Gjerde et al. 1979; Gjerde et al. 1980), exploit the UV absorbance properties of NO_3^-, NO_2^-, Br^-, and iodide to analyze these anions in natural waters directly (Hu et al. 1999; Ito et al. 2012; Ito et al. 2005; Rozan and Luther 2002; Tirumalesh 2008), or use a UV-absorbing eluent to indirectly detect F^-, Cl^-, carbonates, orthophosphates, BrO_3^-, NO_2^-, SO_4^{2-}, Br^-, and NO_3^- in natural waters (Connolly and Paull 2002; Ohta et al. 1996). To our knowledge, however, an isocratic method with no suppression that allows the simultaneous quantification of Cl^-, Br^-, NO_2^-, NO_3^-, and SO_4^{2-} with suitable detection limits in seawater has yet to be developed. In this work, a technique coupling UV detection to anion chromatography was developed for the measurement of most seawater anions in a single step. The

development of this method was motivated by the need for a simple procedure for the *in-situ* analysis of anions in marine waters and pore waters. This technique, however, can also be used in the laboratory to limit the number of analyses of seawater samples and thus lower analysis costs. The method is isocratic, eliminates the need for chemical suppression, and separates Cl^-, SO_4^{2-}, Br^-, NO_3^-, and NO_2^- rapidly enough to resolve most dynamic processes if deployed in situ in aquatic systems.

3.2. Materials and Procedures

3.2.1. Chemicals

All chemicals were ACS certified or of higher purity and were dissolved in milli-Q water (>18.2 MΩ). The eluent used consisted either of 3.2 mM $NaCO_3$ and 1.0 mM $NaHCO_3$ (high absorbance eluent) or 54 mM NaCl (matrix elimination) in deionized water. Artificial seawater consisted of the following salts dissolved in 1 liter: 24.99 g NaCl (0.428 M), 4.15 g Na_2SO_4 (29.27 mM), 11.13 g $MgCl_2.6H_2O$ (54.74 mM), 0.789 g KCl (10.58 mM), 1.58 g $CaCl_2.2H_2O$ (10.75 mM), 0.196 g $NaHCO_3$ (2.33 mM). The minor anions (i.e. NO_3^-, NO_2^-, and Br^-) were omitted from the general artificial seawater recipe and instead added from stock solutions prepared daily using sodium salts. Potential interferences of inorganic and organic anions as well as natural organic matter (NOM) were tested with $NaIO_3$, NaI, Na_2S, $Na_2S_2O_3$, $NaSiO_3$, $NaHCO_3^-$, $NaHPO_4^-$, Na-oxalate, Na-pyruvate, Na-citrate, malic acid, Na-acetate Na-lactate, and Suwanee River Humic Acid (SRHA) solutions in diluted or full-strength artificial seawater.

3.2.2. Instrumentation

A Beckman Coulter DU 720 detector was used to measure the UV absorbance properties of the eluents, anions of interest, and potential interferences between 190 and 350 nm and determine the optimal wavelength to adopt for the chromatographic runs. The HPLC assembly consisted of a Waters 1525 binary high-pressure pump with a Rheodyne 7725i manual injection valve capable of electronically signaling the start of runs to the Empower software data collection suite (Waters, Inc.) to ensure maximum reproducibility of retention times between runs. Samples of 20 μL volumes were injected onto a Metrohm A Supp 5 150.0/x 4.0 mm anion exchange column with a Metrohm A Supp 4/5 10.0/4.0 mm guard column at a flow rate of 0.7 mL/min. A Waters in-line degasser and ultra-high purity (UHP) grade nitrogen were used to ensure complete degassing of the eluents. Ultraviolet absorbance was monitored as a function of time using a Waters 2487 dual wavelength absorbance detector at wavelengths between 210 and 230 nm. Peak heights, areas, and retention times were determined using peak analysis features of the Empower software suite as part of the Waters chromatography system. Calibrations were obtained by representing peak heights or peak areas as a function of the concentration of each anion in seawater over the range of concentrations typically found in natural environments. As blanks did not provide signals, detection limits were calculated as 3 times the standard deviation of the intercept of a linear regression fitted through the individual standard deviations of replicate standards (n=6). Minimum detection limits (MDL) were extrapolated to undiluted seawater by multiplying the detection limits obtained at each dilution by the dilution factor.

3.2.3. Sediment core profiling and pore water chemistry

Cores (10 x 70 cm) were collected from continental-slope sediments underlying the oxygen-minimum zone in the Eastern Tropical North Pacific (ETNP-OMZ) at ~2500 m (18.6°N, -104.5°W) with a gravity corer (MC-800, Ocean Instruments) during a cruise of opportunity on the R/V *New Horizon* (Scripps Institute of Oceanography, California) in June 2013. Depth profiles of major redox chemical species $O_{2(aq)}$, Mn^{2+}, Fe^{2+}, SH_2S ($=H_2S+HS^-+S^{(0)}+S_x^{2-}$) (Brendel and Luther 1995) as well as $FeS_{(aq)}$ clusters (Theberge and Luther 1997) and organic-Fe(III) complexes (Taillefert et al. 2000) were determined in intact cores immediately after sampling using voltammetric Au/Hg microelectrodes (Meiggs and Taillefert 2011) to illustrate distinct diagenetic zones, thus providing a context for anion measurements. The sediment core was sectioned into 7 mm thick slices in a UHP N_2-filled glove bag (Sigma Aldrich, Inc.) immediately after the electrode profiles were completed. Each slice was stored in 50 ml 'Falcon' tubes, and pore waters were extracted by centrifuging (IEC Centra CL2, Thermo Scientific, Inc.) these tubes for at least 10 minutes at 3,000 rpm in the same N_2-filled glove bag. Pore waters were then pipetted directly into 10 mL disposable plastic syringes (HSW Norm-Ject), filtered through 0.2 mm PES membrane filters (Whatman Puradisc), and preserved at -20°C until chromatographic analyses.

3.3. Assessment

3.3.1. Wavelength choice

To simultaneously use direct and indirect detections, it is imperative to select an appropriate eluent and optimum wavelength. The eluent must display some background

absorbance at the wavelength chosen to monitor the column effluent during separations to ensure major anions without significant UV absorption properties (i.e. Cl^- and SO_4^{2-}) suppress the absorbance of the eluent and appear as negative peaks. If the eluent exhibits too high a background absorbance at the chosen wavelength, detection of anions with significant UV absorbance (NO_3^-, NO_2^-, and Br^-) will be less efficient. To select a wavelength capable of detecting all analytes simultaneously, the UV absorption properties of the eluents and analytes were first examined by measuring their absorbance as a function of wavelength relative to a water blank (Figure 3.1).

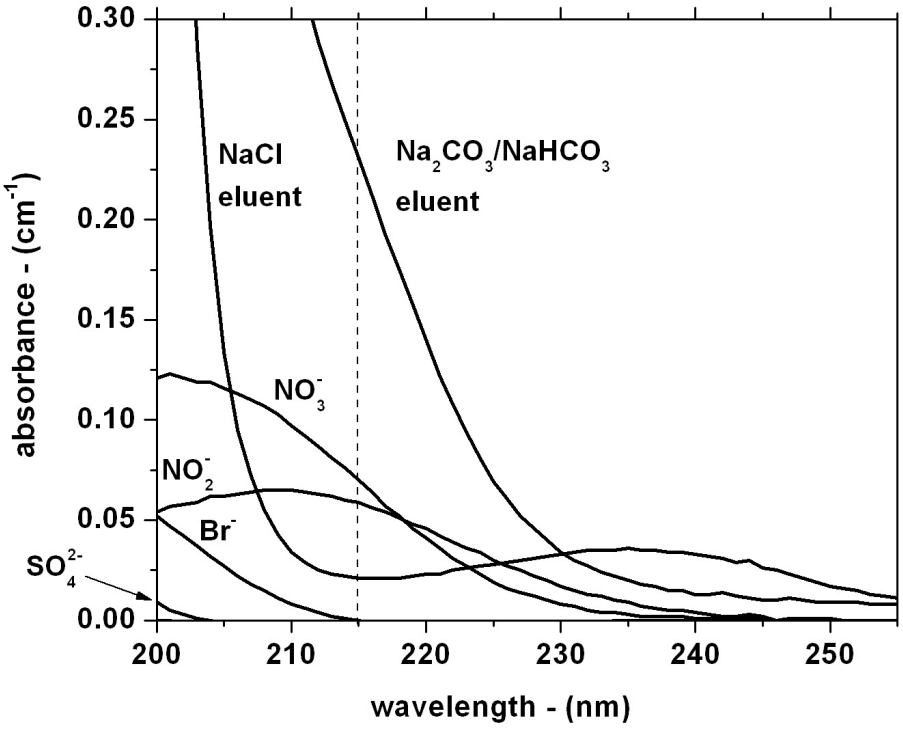

Figure 3.1 - Absorbance of both eluents and the anions of interest as a function of wavelength. The concentrations of Cl^- (54 mM) and SO_4^{2-} (2.8 mM) used for these measurements reflected their proportion in diluted seawater (10x), while the concentrations of Br^- (8.4 μM), and NO_3^- and NO_2^- (15 μM) were selected to match the same range of absorbances as Cl^- and SO_4^{2-}.

The Na_2CO_3/$NaHCO_3$ eluent absorbed significantly at all wavelengths between 190 and 230 nm, though its absorption properties decreased as the wavelength increased. In turn, SO_4^{2-} only absorbed below 200 nm and Cl^- absorbed minimally between 210 and 230 nm, suggesting that the Na_2CO_3/$NaHCO_3$ eluent may be suitable for the measurement of the major anions Cl^- and SO_4^{2-} by UV signal suppression (indirect UV detection) at wavelengths between 210 and 230 nm. As the NaCl eluent displayed a much lower absorbance in this region, it may be better suited for the direct detection of minor anions. The absorbance of anions generally decreased as wavelength increased, but Br^-, NO_3^-, NO_2^- and I^- exhibited relative absorbance maximums at wavelengths greater than 190 nm, suggesting they could be detected directly in the column effluent. Indeed, such an approach has been adopted successfully for the analysis of these anions in seawater (Ito et al., 2012).

While absorbance overlays are useful in choosing an appropriate detection wavelength (Figure 3.1), the wavelength with the highest molar extinction coefficient (or absorbance for the same concentration of anion) may not offer the highest detection limit upon separation. As the background absorbance of the eluent decreases more than the absorbance of a particular anion at a seemingly more optimal wavelength, the actual detection limit is lowered as the difference between the absorptions of the eluent and analytes are greater. To optimize the sensitivity of the UV detection, samples consisting of 5 μM NO_3^- and NO_2^- and 100 μM Br^- were then prepared in both undiluted seawater and seawater diluted 30x (salinity of 1.2) for separation using the NaCl and Na_2CO_3/$NaHCO_3$ eluent respectively, while monitoring absorbance at several wavelengths between 215 and 225 nm. Generally, the shorter wavelengths produced

larger peaks (Table 1), and while the appropriate wavelength depends on the anions of interest, a wavelength of 215 nm was chosen for subsequent method development as it represents the best compromise between sensitivity and selectivity of multiple anions.

Table 3.1 - Peak areas of Cl^- and SO_4^{2-} in a seawater sample diluted 30x (salinity of 1.2) and peak heights of 5 mM NO_2^-, 100 mM Br^-, and 5 mM NO_3^- spiked in the same diluted seawater sample expressed as a percentage of the area or height of their respective absorbance at 215 nm.

anion	215 nm	220 nm	225 nm
Cl^-	100	59	31
NO_2^-	100	82	50
Br^-	100	21	3
NO_3^-	100	64	33
SO_4^{2-}	100	58	29

3.3.2. Optimizing dilutions with the $Na_2CO_3/NaHCO_3$ eluent

A 20 μL sample loop was chosen for convenience with the benchtop HPLC system. Saline samples were diluted when necessary to ensure the column integrity was not compromised due to sample overloading. Cl^- is of greatest concern as its concentration in seawater is much higher than in samples typically injected onto HPLC columns (< 1 mM). Artificial seawater samples spiked with NO_3^-, NO_2^-, and Br^- were therefore diluted from 10x to 60x with the eluent to examine the sensitivity of the technique for major and minor anions in seawater samples. With the $Na_2CO_3/NaHCO_3$ eluent, the major anions Cl^- and SO_4^{2-} eluted first and last and, as expected, suppressed the background UV absorbance of the eluent to generate negative peaks in the chromatograms (Figure 3.2a). In turn, NO_2^-, Br^- and NO_3^- eluted in this order and displayed positive absorbance peaks with respect to the eluent (Figure 3.2b).

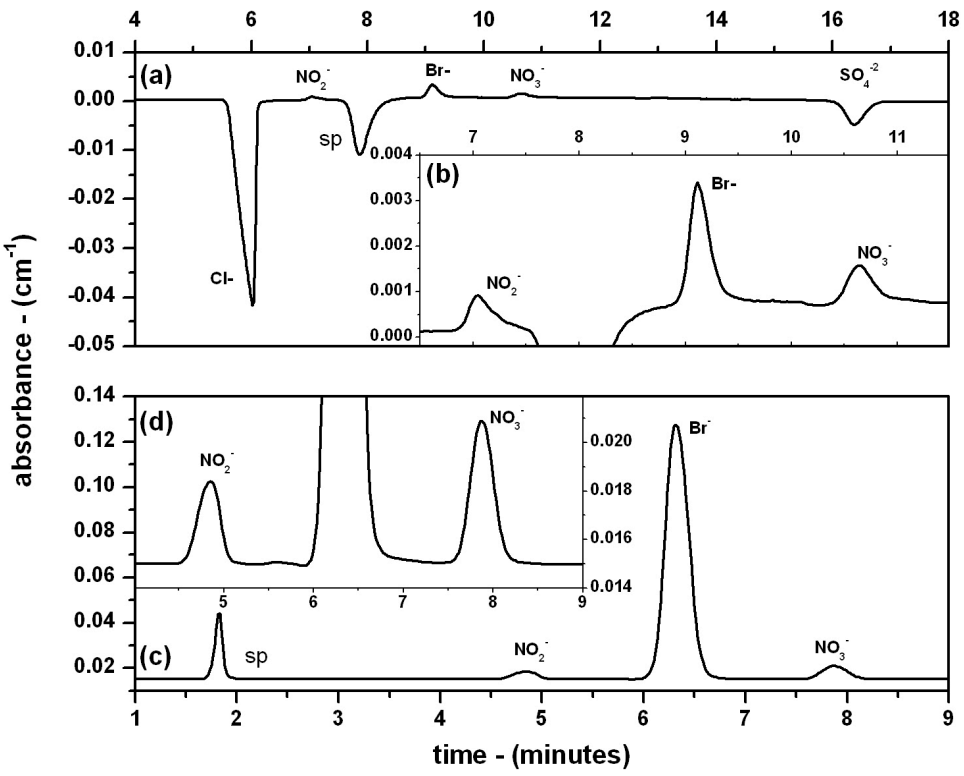

Figure 3.2 - Chromatograms generated by monitoring absorbance at 215 nm during the separation of an artificial seawater standard containing a) 30 μM of NO_3^- and NO_2^- and 1 mM of Br^- using the Na_2CO_3/$NaHCO_3$ eluent, b) a close up of the same chromatogram to identify the minor anions, c) 10 μM of NO_3^- and NO_2^- and 1 mM of Br^- using the NaCl eluent, and d) a close up of the same chromatogram to identify the minor anions. The seawater sample separated with the Na_2CO_3/$NaHCO_3$ eluent was diluted 30x to a salinity of 1.2 prior to separation, while the sample separated with the NaCl eluent was not diluted. SP identifies the position of the system peak observed in each chromatogram.

The Cl^- peak became asymmetrical and shifted towards longer retention times at increasing salinity (data not shown). At salinities greater than ~3.5, it co-eluted with the system peak which prevented accurate determination of peak area or height and thus accurate quantification. Despite the asymmetric response of the Cl^- signal and the indirect measurements of both Cl^- and SO_4^{2-} in the Na_2CO_3/$NaHCO_3$ eluent, calibration curves constructed from peak areas remained linear over an order of magnitude between

5 and 55 mM for Cl^- and between 0.3 and 3 mM for SO_4^{2-} (Figure 3.3 a and b). When seawater samples were diluted 30x (salinity 1.2) before measurements, the detection of SO_4^{2-}, Br^-, NO_2^-, and NO_3^- was possible (Figure 3.2b). Simultaneously, calibrations obtained with Br^-, NO_2^-, and NO_3^- in the same eluent were linear over an order of magnitude between 5 and 50 mM for Br^- and between 0.2 and 5 mM for NO_2^- and NO_3^-, though with a higher sensitivity for NO_3^- (Figure 3.3 c and d). The required dilution with this method, however, indicates that it can only accurately determine concentrations greater than 422 mM Cl^-, 218 mM SO_4^{2-}, 114 mM Br^-, 6 mM NO_2^-, and 3 mM NO_3^- in undiluted seawater samples (Table 3.2).

Table 3.2 - Retention time (t_R), sensitivities, and the minimum detection limits (MDL) of anions Cl^-, SO_4^{2-}, Br^-, NO_3^-, and NO_2^- in artificial seawater when using a 20 μL sample loop. Because artificial seawater blanks did not yield a signal for all analytes of interest, MDLs were calculated by using the standard deviation of the intercept of a linear regression fitted through the individual standard deviations of six replicate standards. While the sensitivities presented for the anions separated with the Na_2CO_3/$NaHCO_3$ eluent were obtained in 30x-diluted artificial seawater, minimum detection limits (MDL) were extrapolated to full salinity conditions by multiplying detection limits by the dilution factor. No dilution was required with the NaCl eluent such that both sensitivities and MDL represent full salinity samples.
[a]For both eluents, units are: *min* mM^{-1} cm^{-1} for Cl^- and SO_4^{2-} (peak areas) and cm^{-1} μM^{-1} for NO_2^-, NO_3^-, and Br^- (peak heights).

	$NaHCO_3/Na_2CO_3$ eluent			NaCl eluent		
anion	t_R (min)	sensitivity[a]	MDL (μM)	t_R (min)	sensitivity[a]	MDL (μM)
Cl^-	6	4.05	422	-	-	-
NO_2^-	7	3.5×10^{-4}	6.2	4.8	6.9×10^{-4}	0.12
Br^-	9.5	9.7×10^{-5}	114	6.4	9.6×10^{-5}	0.558
NO_3^-	10.5	7.3×10^{-4}	2.5	7.9	7.7×10^{-4}	0.112
SO_4^{2-}	16	11.8	218	-	-	-

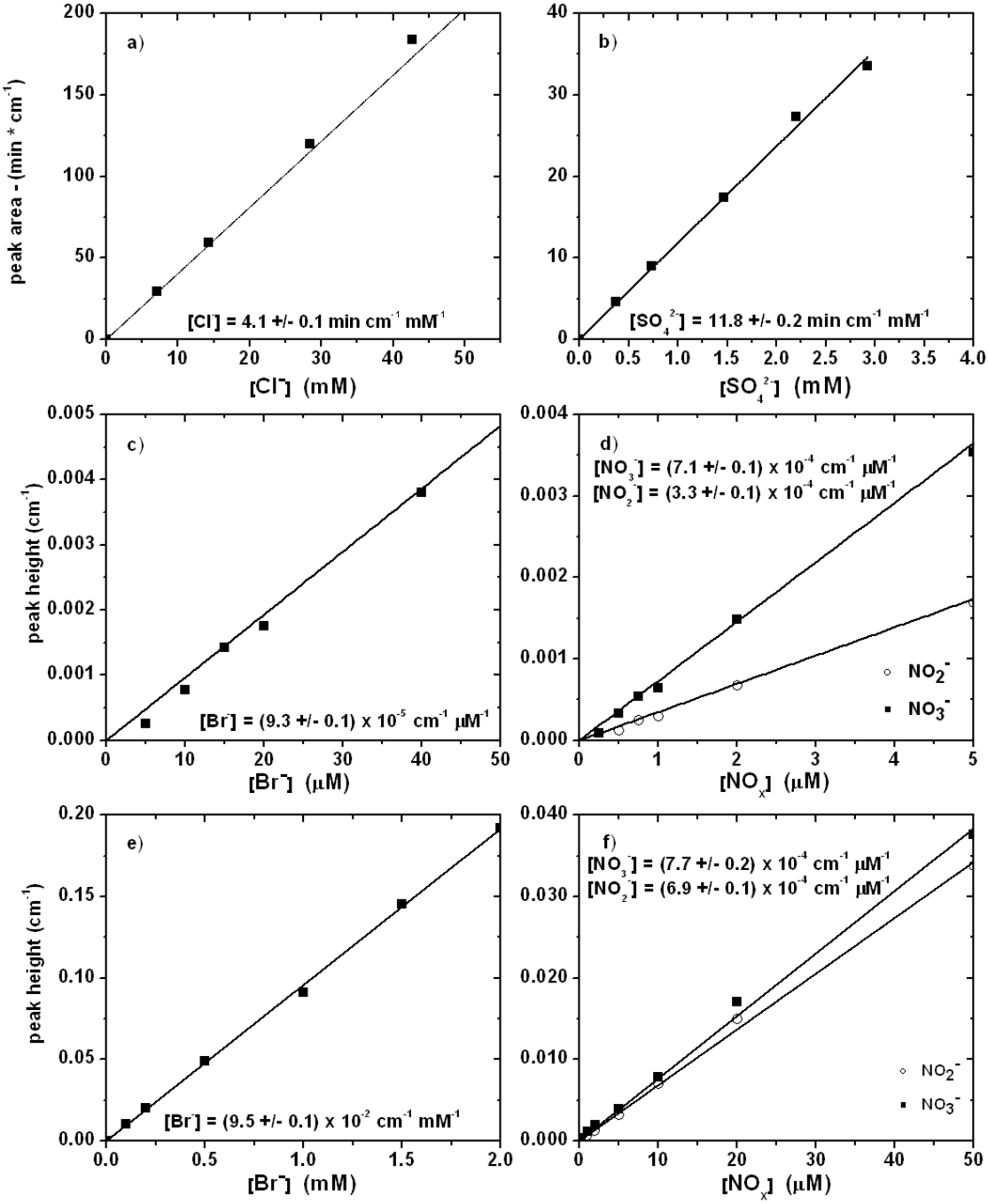

Figure 3.3 - Calibration curves for a) Cl^-, b) SO_4^{2-}, c) Br^-, and d) NO_2^- and NO_3^- obtained with the Na_2CO_3/$NaHCO_3$ eluent, and e) Br^- and f) NO_2^- and NO_3^- with the NaCl eluent. The standards analyzed with the Na_2CO_3/$NaHCO_3$ eluent were diluted 30x to a salinity of 1.2 while those using the NaCl eluent were not diluted. The slope and standard deviation of the slope of each calibration is included in the figure.

Calibrations were also performed at variable sample salinities to optimize the sensitivities of the methods to the minor anions Br^-, NO_2^-, and NO_3^- in seawater or brackish samples (Figure 3.4). Calibration curves with the $Na_2CO_3/NaHCO_3$ eluent demonstrated that the sensitivity of the method to NO_2^- decreased as salinity increased, while NO_3^- and Br^- sensitivities were not affected by salinity (Figure 3.4a & b). As Cl^- and NO_2^- display similar retention times, high Cl^- concentrations in the sample plug

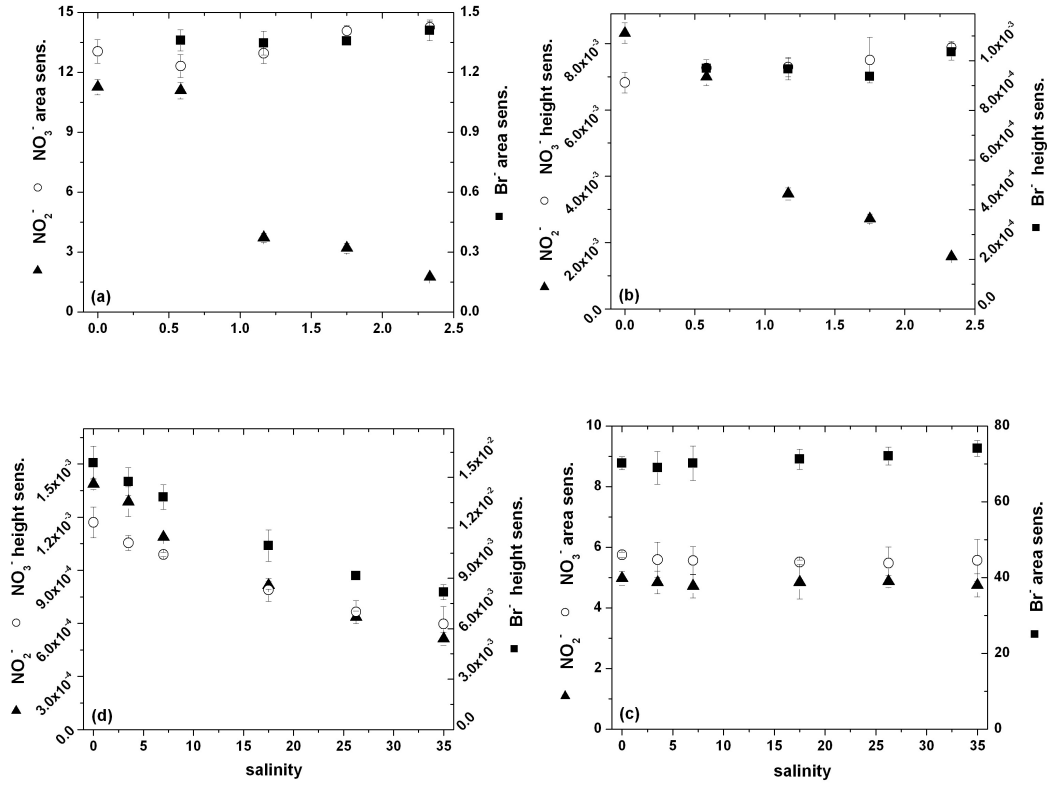

Figure 3.4 - Sensitivities of NO_2^-, Br^-, and NO_3^- calculated from calibration curves using both peak areas (a, c; min cm^{-1} μM^{-1}) and peak heights (b, d; cm^{-1} μM^{-1}) as a function of the salinity of the samples using the $NaH_2CO_3/NaHCO_3$ eluent (a,b) and the NaCl eluent (c,d). With the $NaH_2CO_3/NaHCO_3$ eluent, Br^- and NO_3^- peak area and height sensitivities were independent of salinity, but NO_2^- areas and heights decreased with increasing salinity. With the NaCl eluent, the peak areas of all three anions were independent of salinity, while peak heights decreased with increasing salinities as peaks grew wider.

may outcompete NO_2^- for interaction with the functional groups of the stationary phase and thus prevent separation and quantification of NO_2^-. Sample dilution was therefore optimized when using the Na_2CO_3/$NaHCO_3$ eluent to quantify NO_2^- in marine waters, and the optimal chromatographic conditions were determined to be a simulated salinity of 1.2, or a dilution factor of 30 times (Table 3.2). To maximize the sensitivity of the method with the Na_2CO_3/$NaHCO_3$ eluent while minimizing dilution, a 30x dilution factor was used in all measurements conducted with full salinity seawater samples.

3.3.3. Evaluation of the NaCl eluent

A NaCl eluent may be used in place of the Na_2CO_3/$NaHCO_3$ eluent to increase detection limits of NO_2^-, Br^- and NO_3^- in environments that require extremely low MDL (e.g. marine water columns). This modification, however, prevents determination of both Cl^- by matrix elimination and SO_4^{2-} as the eluent absorbance is too low to be suppressed by SO_4^{2-}. Several eluent concentrations between 27 and 108 mM NaCl were tested (data not shown), and a concentration of 54 mM offered the best combination of resolution of NO_2^-, Br^-, and NO_3^- while maintaining short elution times (Figure 3.2c and d). While calibrations of Br^- using the NaCl eluent also remained linear over at least an order of magnitude (between 0.2 and 2 mM), NO_3^- and NO_2^- calibrations covered at least three orders of magnitude (between 0.05 and 100 mM) (Figure 3.3 e and f). As this method does not require dilution of the original seawater sample, its sensitivity is much higher than with the Na_2CO_3/$NaHCO_3$ eluent, and MDLs of less than 600 nM in undiluted seawater samples were obtained for Br^-, NO_2^-, and NO_3^- in the chromatographic

conditions used in the present study (Table 3.2). With the NaCl eluent, sensitivities determined using peak areas for Br^-, NO_2^-, and NO_3^- remained constant as a function of sample salinity, while sensitivities determined using peak heights decreased with increasing salinity. These findings suggest that peak areas should be used in samples of varying salinity (e.g. from estuarine environments) with this eluent to avoid possible artifacts.

3.3.4. Interferences

The methods were evaluated for their ability to resolve the anions of interest even in the presence of possible interferences that may be found in natural environments (IO_3^-, HS^-, $H_3SiO_4^-$, ΣPO_4^{3-}, HCO_3^-, oxalate, pyruvate, citrate, maleate, acetate, lactate, and NOM) or I^- sometimes used as chemical tracer in oceanographic experiments (Reimers et al. 2004; Tercier-Waeber and Taillefert 2008). UV spectra indicated that besides pyruvate, and oxalate, organic acids did not absorb significantly at 215 nm (Figure 3.5). Similarly, HCO_3^-, ΣPO_4^{3-}, and ΣH_4SiO_4 contributed little to the absorbance at 215 nm. In turn, $S_2O_3^{2-}$, IO_3^-, HS^-, and I^- presented, in decreasing intensity, significant absorption at 215 nm. UV spectra were not obtained for the NOM solution, but is well known to absorb significantly in the UV wavelength range (Helms et al. 2013).

Upon injection of 100 μM of each analyte (or 1.7 mg/L SRHA) in a seawater sample diluted 60x, however, only IO_3^-, ΣH_4SiO_4, ΣH_2S, and pyruvate produced detectable peaks on the chromatograms using the $Na_2CO_3/NaHCO_3$ eluent (Figure 3.6a). Note that a sample containing 100 mM of analytes in 60x diluted seawater corresponds to 6 mM, well above concentrations of organic acids, IO_3^- (Sugawara and Terada 1958), I^-

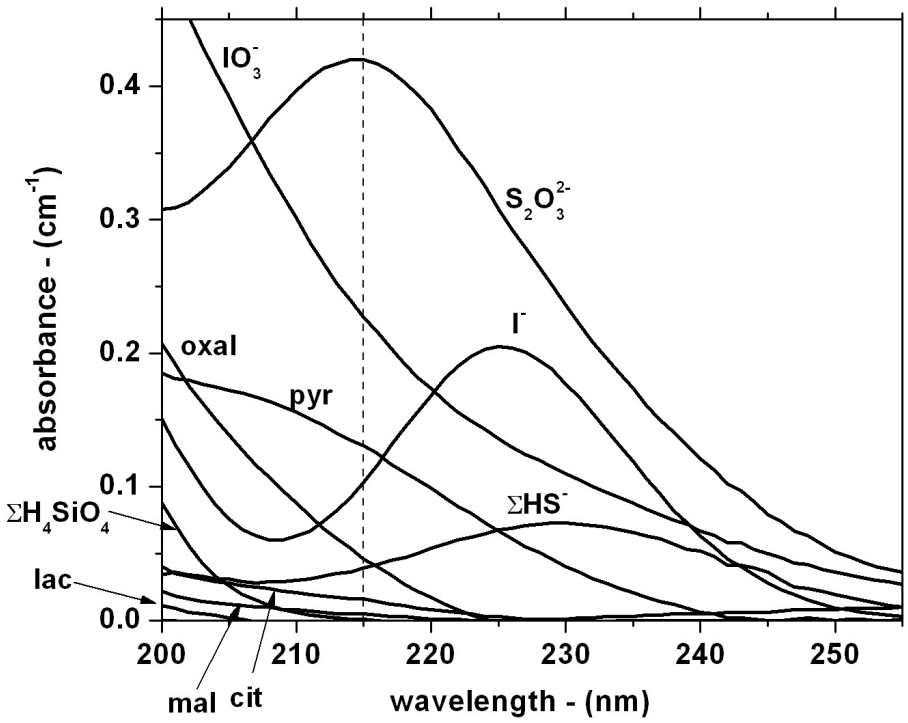

Figure 3.5 - The absorbance of inorganic and organic anions potentially interfering with the measurement of Cl^-, NO_2^-, Br^-, NO_3^-, and SO_4^{2-} as a function of wavelength. All concentrations of potentially interfering anions were fixed at 100 mM in deionized H_2O. Acetate, ΣCO_3^{-2}, and ΣPO_4^{3-} absorbance spectra were measured but were at or below the water blank. The vertical dash line represents the wavelength monitored during all chromatographic measurements displayed in this study.

(Chapman and Truesdale 2011), $S_2O_3^{2-}$ (Luther et al. 1991), ΣH_4SiO_4 (Treguer et al. 1995), $\Sigma H_3PO_4^{-3}$ (Froelich et al. 1982), or ΣH_2S in sedimentary environments where the concentrations of these anions may be the highest. Similarly, 1.7 mg/L SRHA in 60x diluted seawater corresponds to 100 mg/L humics in full seawater, much higher than DOM concentrations reported in marine pore waters (Burdige et al. 1992). As the carbonate ion is likely responsible for the UV response of the $Na_2CO_3/NaHCO_3$ eluent (Figure 3.1), the lack of interference by HCO_3^- is not surprising and makes this method

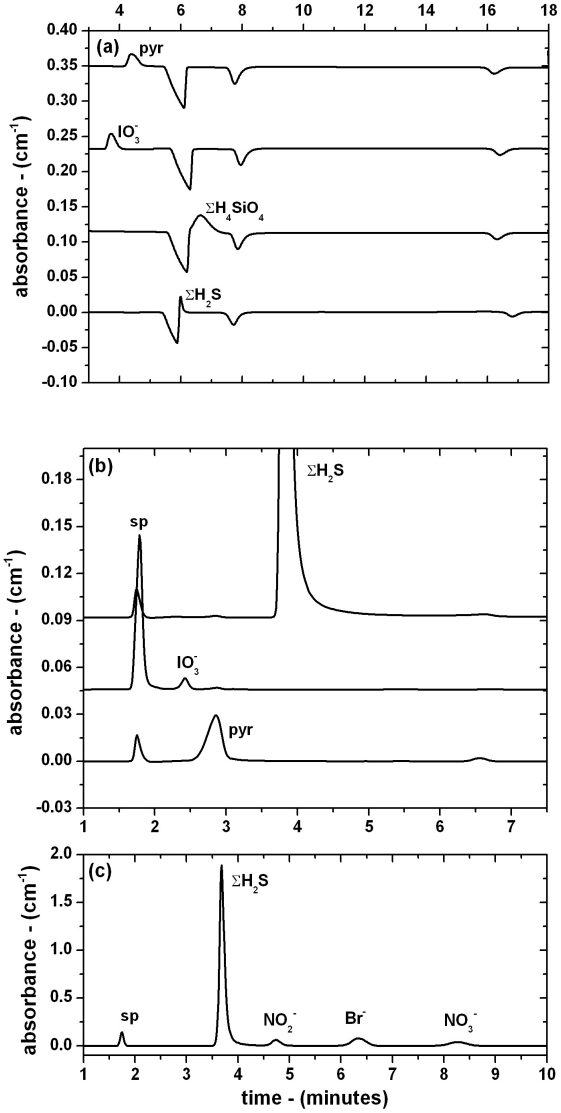

Figure 3.6 - Overlays of chromatograms generated by monitoring absorbace at 215 nm during the separation of a) 100 mM ΣH_4SiO_4, IO_3^-, and pyruvate (pyr), and ΣH_2S in an artificial seawater matrix separated using the $Na_2CO_3/NaHCO_3$ eluent after a 60x dilution (salinity of 0.58), b) the same potential interferences separated using the NaCl eluent without dilution, and c) 2 mM ΣH_2S , 100 mM NO_2^- and NO_3^-, and 1 mM Br^- in undiluted artificial seawater using the NaCl eluent at pH 3 (adjusted with HCl). Other anions tested (i.e. HPO_4^{-2}, oxalate, pyruvate, citrate, malate, acetate and lactate) did not generate chromatographic responses. SP identifies the position of the system peak observed in each chromatogram.

perfectly suitable at the pH of most marine environments. In addition, IO_3^- and pyruvate elute earlier than Cl^-, preventing eventual artifacts from their presence in natural samples. Finally, while ΣH_2S and ΣH_4SiO_4 elute at intermediate retention times, between 6.5 and 8 minutes, ΣH_2S elutes before NO_2^- and is therefore not problematic at concentrations at least as high as 6 mM. In turn, ΣH_4SiO_4 could potentially interfere with the determination of NO_2^-, but the much higher molar absorptivity of NO_2^- at 215 nm (Figure 3.1) indicates this interference should not be problematic at typical ΣH_4SiO_4 concentrations of 1 mM in sediments (Dixit et al. 2001). With the NaCl eluent, pyruvate, IO_3^-, and ΣH_4SiO_4 generated peaks prior to 3 minutes (Figure 3.6b) while I^- eluted after ~15 minutes (data not shown), indicating these anions do not interfere with Br^-, NO_2^-, or NO_3^- determination. In turn, ΣH_2S eluted at a very similar retention time to NO_2^- (Figure 3.6b) and may represent a significant interference for NO_2^- measurements in reduced pore waters. In such conditions, it is recommended to buffer the pH of the NaCl eluent to 3 using HCl to offer sufficient separation (Figure 3.6c); however, the total elution time is extended by approximately 20%.

3.3.5. Lifetime of the columns

The lifetime of the columns should be carefully monitored as species resolution and sensitivity decreased over time, likely due to their exposure to relatively high salt concentrations. After approximately 100 injections of seawater, column backpressure increased by ~200 psi, and peak retention times increased by 1 or 2 minutes (data not shown). The original backpressure and retention times could be restored, however, by following the cleaning procedure recommended by the manufacturer. Flushing with 20

column volumes of a 32 mM Na_2CO_3 solution and then heating in an oven at 40 to 50ºC for 24 hours was enough to be able to regenerate the columns. These columns could be used for more than 1,000 analyses using this cleaning procedure.

3.3.6. Analysis of marine sediment pore waters and method precision and accuracy

To provide an example of the usefulness of these methods, a typical depth profile of these anions was obtained from a marine sediment collected in the ETNP (Figure 3.7). NO_3^- and NO_2^- concentrations were measured using both methods, and NO_3^- data for the overlying water are comparable (relative difference < 3.6%±0.8%) thus validating both methods. In turn, NO_2^- concentrations lay just below the quantification limit with the carbonate eluent method, and the NO_2^- data obtained with the NaCl eluent is presented only. High NO_3^- concentrations of 49±1.6 μM (using the NaCl eluent) were observed in the overlying water with a progressive decrease deeper in the sediments, except for a small excursion to 44±1.4 μM at 3.5 cm that would require a higher spatial resolution to be confirmed. NO_2^- reached 5 μM at a depth of ~1 cm but was detectable to depths of 6 cm. These profiles are consistent with those expected from traditional nitrification/ denitrification processes, i.e. NO_3^- is produced by the oxidation of NH_4^+ and is simultaneously consumed immediately below the sediment-water interface (SWI) by dissimilatory reduction to NO_2^- (Froelich et al. 1979). Below this zone of active N cycling, metal reduction and SO_4^{2-} reduction processes dominate the redox chemistry (depths of the different zones are shown in Figure 3.7). Interestingly, dissolved Fe(II) was observed simultaneously in the layers occupied by NO_2^- and NO_3^-, while a sulfidic zone was observed below 4 cm, consistent with diagenetic expectations (Froelich

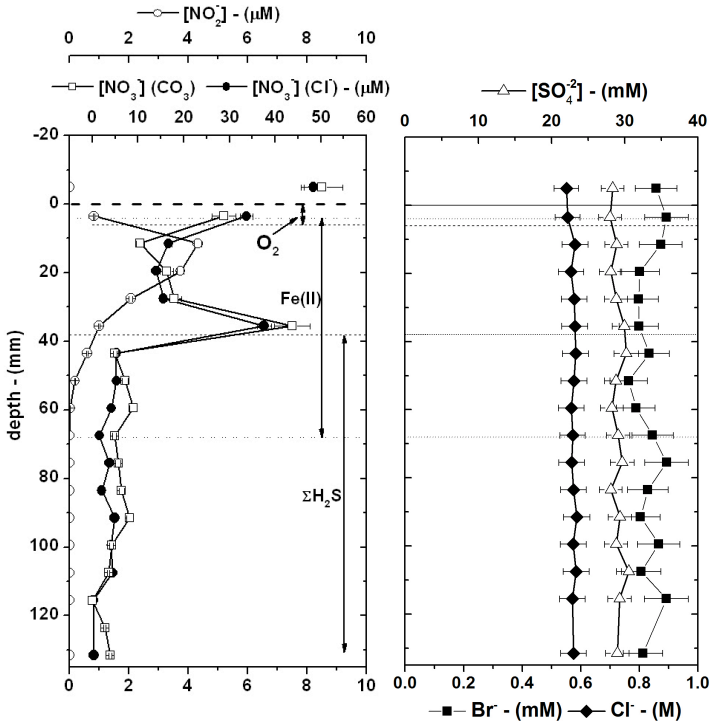

Figure 3.7 - Profiles of major anions measured in pore waters extracted from a sediment core extruded from sediment underlying the Eastern Tropical North Pacific (ETNP) oxygen minimum zone (Mexico). Br^-, NO_3^-, and NO_2^- were measured using the single-step liquid chromatography technique with the NaCl eluent, and Cl^-, SO_4^{2-}, and Br^- (and NO_3^-, duplicate measurement) were measured with the $NaHCO_3/Na_2CO_3$ eluent (b). The zones of aerobic respiration, Fe reduction, and SO_4^{2-} reduction were determined by Au/Hg voltammetric profiling in the same intact core prior to pore water extractions (data not shown).

et al. 1979). The concentrations of Cl^-, SO_4^{2-}, and Br^- were 551 mM, 28.4 mM, and 858 μM in the overlying water and showed no discernable trends with depth. Both SO_4^{2-} and Br^-, however, were more variable than Cl^- as a function of depth. These anions are not expected to vary to any great extent in marine sediments over such a short depth interval unless SO_4^{2-} reduction is intensive, which was not the case.

The two methods were evaluated for precision by conducting replicate analyses of the pore water sample from 2.7 cm (Table 3). Relative standard deviations of six

injections of the same sample were lower than 2% for all analytes with both eluents. The sample was then spiked with a standard containing each analyte and analyzed in replicates to test the accuracy of the measurements. Recoveries of six injections of the same sample after standard addition were at least 93% and no more than 108% for all analytes with both eluents (Table 3). Comparison of both methods revealed less than 3% relative deviation between methods suggesting that the methods are accurate.

3.4. Discussion

While major and minor inorganic anions play an important role in a variety of biogeochemical processes in marine environments, their measurement often requires multiple analyses given the disparity between the range of concentrations of each anion, from hundreds of millimolar to submicromolar. Liquid chromatography provides a

Table 3.3 - Average concentration of Cl^-, NO_2^-, Br^-, NO_3^-, and NO_2^- in the same pore water sample from ETNP sediments quantified using both methods in six subsequent injections before and after spiking the same sample with a standard. The agreement between both tests was calculated relative to the natural sample, and the standard deviation includes error propagation from each method. Samples were diluted 30x with the Na_2CO_3/$NaHCO_3$ eluent, but the concentrations reported were extrapolated to full salinity seawater. No dilutions were made with the NaCl eluent.

anion	$NaHCO_3/Na_2CO_3$ eluent					NaCl eluent				
	sample		standard addition		agreement	sample		standard addition		agreement
	conc.	$\sigma_{n=6}$	conc.	σ	(%)	conc.	$\sigma_{n=6}$	conc.	σ	(%)
	(mM)		(mM)			(mM)		(mM)		
Cl^-	577.6	3.9	574.3	7.6	99.4 ± 1.5	-	-	-	-	-
SO_4^{2-}	28.7	0.2	28.1	0.3	98.2 ± 1.3	-	-	-	-	-
	(μM)		(μM)			(μM)		(μM)		
Br^-	792.4	7.2	783.2	5.7	98.8 ± 1.1	804.3	5.5	799.2	7.4	99.3 ± 1.1
NO_3^-	18.1	0.3	16.9	0.5	93.3 ± 3.0	17.6	0.2	17.4	0.2	98.9 ± 1.4
NO_2^-	< MDL	-	-	-	-	2.07	0.01	2.23	0.01	107.8 ± 0.8

relatively simple way to analyze these anions in water samples, but several analytical challenges have prevented its use in seawater matrices. In this study, a simple isocratic liquid chromatography technique was developed to quantify the major anions Cl^-, Br^-, and SO_4^{2-} as well as the minor anions NO_2^- and NO_3^- in seawater using a single injection after dilution of the original seawater sample. Another matrix elimination technique was developed to quantify NO_2^- and NO_3^- with submicromolar detection limits while simultaneously analyzing Br^-, if the measurements of Cl^- and SO_4^{2-} are not required (e.g. in water column samples).

The UV absorption properties of Br^-, NO_2^-, and NO_3^- have already been used extensively in separation methods (Hu et al. 1999; Ito et al. 2012; Ito et al. 2005; Rozan and Luther 2002; Tirumalesh 2008) and the suppression of the background absorbance of the eluent has been exploited before to measure a variety of ions in natural samples (Connolly and Paull 2002; Ohta et al. 1996). In this study, the simultaneous quantification of the minor seawater anions NO_3^- and NO_2^- and the major seawater anions Cl^-, Br^-, and SO_4^{2-} was facilitated by using a $Na_2CO_3/NaHCO_3$ eluent as the absorbance properties of NO_2^- and NO_3^- or the concentration of Br^- in seawater are high enough to contribute to the total absorbance measured even in the presence of the eluent, and the high concentrations of Cl^- and SO_4^{2-} chemically suppress the background absorbance of the eluent (Figure 3.2a). When the Cl^- and SO_4^{2-} anions from the samples encounter the stationary phase, their high concentration displaces the mobile phase HCO_3^-/CO_3^{2-} anions from the column. As they eventually elute from the column at different retention times, Cl^- or SO_4^{2-} are released in separate sample plugs that are deficient in HCO_3^-/CO_3^{2-} anions and generate negative peaks on the chromatogram due to their lower molar absorptivity

than the HCO_3^-/CO_3^{2-} eluent (Figure 3.1). Although the peaks are asymmetrical and indicative of column overloading, the Cl^- and SO_4^{2-} measurements are not compromised as long as peak areas are used instead of heights to calibrate and analyze seawater samples (Figure 3.3). The method allows for the determination of all five anions with the $Na_2CO_3/NaHCO_3$ eluent in about 17 minutes with detection limits as low as 1.8 and 5.8 μM for the minor anions NO_3^- and NO_2^- in full salinity seawater and 422, 114, and 218 μM for the major anions Cl^-, Br^-, and SO_4^{2-} respectively (Table 2).

If better detection limits are needed for NO_3^-, NO_2^-, and Br^- in seawater, a NaCl eluent can be used to condition the column (Evenhuis et al. 2008; Hu et al. 1999; Ito et al. 2005) and detect these ions in nanomolar range in seawater (Ito et al., 2012). In this matrix elimination method, the stationary phase functional groups are saturated with Cl^-, such that any additional seawater Cl^- injected onto the column is not retained and elutes in the void volume of the column. As a result, seawater Cl^- from the sample does not compete as much with the minor anions for retention on the column, and minimum detection limits of the absorbing anions are enhanced by one or two orders of magnitude (0.07, 0.137, and 0.307 μM for NO_2^-, NO_3^-, and Br^- respectively in Table 2). As SO_4^{2-} is not detectable using this method, the total analysis time is simultaneously shortened to about 9 minutes (Figure 3.2). Both techniques are precise (<2% relative variations between replicate measurements of each analyte) and appear accurate as determined by standard addition and comparison to each other (< 3% relative difference). They also provide much better detection limits for the minor anions in seawater compared to suppression techniques which lose the ability to resolve lower concentrations of NO_2^- and NO_3^- after the sample dilution step required to prevent overloading the column with Cl^-

and SO_4^{2-}. For example, Cl^-, SO_4^{2-}, and Br^- concentrations in seawater were accurately resolved in a study that used chemical suppression ion chromatography, but the detection limits of NO_3^- (~50 μM) and NO_2^- (~70 μM) extrapolated to full salinity were too high to detect these anions in most marine waters (Gros et al. 2008b). The present method with the Na_2CO_3/$NaHCO_3$ eluent offers more than one order of magnitude lower detection limits, while maintaining the ability to measure the major anions Cl^-, SO_4^{2-}, and Br^-. The method with the NaCl eluent presents more than two-orders of magnitude lower detection limits for NO_3^- and NO_2^-. Finally, both methods do not suffer from interferences by relevant concentrations of other inorganic and organic anions present in marine environments, except for high ΣH_2S concentrations, which interfere with NO_2^- measurements by the matrix elimination method. In this case, however, it was found that acidifying the NaCl eluent increased the resolution between chromatographic peaks and provided sufficient separation for NO_2^- determination. While beyond the scope of this study, ΣH_2S and I^- calibrations performed with the NaCl eluent were linear, which may be of interest to some researchers.

These methods resolve all anions of interest in less than 18 minutes or NO_x species in less than 9 minutes. They also simplify the quantification of major and minor anions in marine environments greatly, limiting labor and analysis costs, while improving detection limits for marine applications. They differ from traditional ion chromatographic techniques, as they do not require chemical or electronic suppression, thereby simplifying the required instrumentation. By eliminating chemical suppression systems required with traditional ion chromatography, these techniques ease liquid volume requirements and eliminate additional mechanical/electronic components. These properties make them

suitable for in-situ deployments on manned or unmanned underwater vehicles, including submarines, remotely operated vehicles, AUVs, gliders, and benthic landers.

3.5. Comments and recommendations

In this work, two chromatography techniques were developed to simultaneously quantify multiple major and minor anions in marine waters in a single step. These methods provide several benefits. First, they limit the number of analyses performed on the same sample to quantify major and minor anions and therefore minimize labor and costs associated with these analyses. Second, they decrease the sample volume that would be required to characterize the same anions using conventional techniques, which may be helpful when working with pore waters or other small samples. Finally, their detection limits are good enough for applications in most marine environments, including water columns, sediment pore waters, and hydrothermal systems across a wide range of salinities. The choice of the appropriate method depends on the type of marine environment investigated. For example, for sediment pore waters and hydrothermal waters, the Na_2CO_3/$NaHCO_3$ eluent may be preferred to monitor Cl^- and SO_4^{2-} as well as eventual NO_3^- and NO_2^- concentrations and seek insight into subsurface mixing and SO_4^{2-} reduction processes in addition to diagenetic processes involving nitrogen species. The required dilution for the analysis of anions in seawater with the Na_2CO_3/$NaHCO_3$ eluent also implies that the determination of anions in brackish waters may be realized without dilution, though the exact salinity of the samples has to be known to quantify NO_2^- concentrations accurately. If the dilution step is undesired (e.g. for *in situ* applications), a smaller sample loop on the order of 1 μL can be used for full strength seawater. In turn,

the NaCl eluent provides much better detection limits for NO_3^-, NO_2^-, and Br^- (Table 2), as samples do not have to be diluted, and the background absorbance of the eluent is much lower than that of the Na_2CO_3/$NaHCO_3$ eluent at 215 nm, allowing for a greater signal to noise ratio and therefore a higher sensitivity and precision. Thus, the NaCl eluent may be ideal for overlying waters and water column samples, where Cl^- and SO_4^{2-} concentrations are not expected to vary to a great extent and NO_3^- and NO_2^- species tend to display lower concentrations than in sediments. Finally, when using this eluent in environments with strong salinity gradients, peak areas should be used to quantify NO_3^-, NO_2^-, and Br^- concentrations, as sensitivities determined using peak areas remained constant as a function of salinity.

These methods are currently tested for *in situ* measurements with an underwater liquid chromatograph rated to 1,000 meters water depth deployed on a benthic lander. The *In Situ* Electrochemical Analyzer / Liquid Chromatograph (AIS ISEA-IV-LC, AIS Inc.) is equipped with a high-pressure pump, a capillary flow cell with absorbance detector tunable to wavelengths between 190 and 700 nm, an open/close valve to allow samples through the bulkhead, an injection valve, and a pump to draw samples through both valves. The sample collector may be affixed inside a benthic chamber to monitor analytes fluxing in and out of the underlying sediment as a function of time. Alternately, the sample collector may be inserted in a custom-built probe mounted on a micromanipulator capable of sipping pore waters from sandy or silty sediments. The system is programmed prior to deployments to run a sequence of voltammetric and chromatographic analyses autonomously, and deployments on the order of 48 hours are possible.

3.6. Acknowledgements

This work was supported by the Ocean Technology and Interdisciplinary Coordination (OTIC) program of the National Science Foundation (Grant #OCE 0928331). The authors would like to thank Eryn Eitel of the Taillefert laboratory for help with core profiling and Frank Stewart at Georgia Tech's School of Biology as well as the captain and crew of the R/V *New Horizon* for the opportunity to obtain sediment cores for this research. Finally, the authors would like to thank two anonymous reviewers and the associate editor for their comments that improved an earlier version of the manuscript.

CHAPTER 4

SOURCES OF SOLUBLE IRON(III) COMPLEXES IN COASTAL ORGANIC-RICH SEDIMENTS

This is a copy of an article submitted to *Geochimica et Cosmochimica Acta* in April 2014, authored by Jordon S. Beckler, Morris E. Jones, and Martial Taillefert entitled "Sources Of Soluble Iron(III) Complexes In Coastal Organic-Rich Sediments".

Abstract

The redox chemistry and speciation of iron in both solid and dissolved phases were characterized in the organic-rich sediments of the Satilla River estuary in South-East Georgia (USA) on a series of four cruises between July 2007 and January 2008. Results indicate that dissolved iron is present in relatively high concentration in the overlying waters at the freshwater end of the estuary and flocculates along the river as the salinity increases downstream. Soluble organic-Fe(III) complexes comprise the majority of dissolved Fe (< 0.2 μm) in the suboxic pore waters of the upriver stations that are characterized by high concentrations of reactive solid-phase iron oxides. In contrast, sulfate reducing conditions downstream prevent the accumulation of soluble organic-Fe(III) in the pore waters by titrating iron from the sediment. Separation of dissolved Fe by size exclusion chromatography revealed that Fe(II) is complexed by organic ligands in the pore waters while the organic-Fe(III) complexes are either small or highly reactive with the column matrix. Finally, dissimilatory iron reduction, stimulated by inoculating

anaerobic sediments with an iron-reducing bacterium, *Shewanella putrefaciens* strain 200, increased production of soluble organic-Fe(III) complexes, and addition of reactive Fe(III) hydroxides accelerated the non-reductive dissolution of Fe(III) hydroxides irrespective of the presence of exogenous Fe(III)-reducing bacteria. These findings suggest soluble organic-Fe(III) complexes in suboxic pore waters are produced either as intermediates during the dissimilatory reduction of Fe(III) hydroxides by iron-reducing microorganisms or during the oxidation of organic-Fe(II) complexes by solid Fe(III) hydroxides. These soluble organic-Fe(III) complexes are stable in pore waters and may flux from the sediments to the continental shelf.

4.1. Introduction

As iron bioavailability controls phytoplankton blooms in marine environments (Boyd et al., 2000) it is important to characterize the different sources of Fe to the ocean to understand the effects of a changing climate on primary production (Boyd and Ellwood, 2010; Breitbarth et al., 2010). Dust deposition (Johansen et al., 2000), iceberg melt (Hawkings et al., 2014; Raiswell et al., 2008), and lateral flux from continental margin sediments (Lam and Bishop, 2008) have been identified as sources of Fe to the pelagic ocean, while vertical flux from sediments in upwelling regions (Elrod et al., 2004) or estuarine sediments (Jones et al., 2011) may provide Fe to coastal regions. Given the poor solubility of Fe(III) at circumneutral pH, it is often assumed that the majority of river-borne dissolved Fe flocculates in coastal areas upon mixing with seawater (Boyle et al., 1977). Several recent studies, however, have demonstrated that Fe(III) may remain in solution in estuarine waters even at high salinities if it is

complexed to dissolved organic matter (DOM; Buck et al., 2007; Gledhill and Buck, 2012; Jones et al., 2011; Krachler et al., 2010; Krachler et al., 2012; Laglera and van den Berg, 2009; Powell and Wilson-Finelli, 2003; Stolpe et al., 2010). Simultaneously, relatively large concentrations of dissolved Fe(III) have been identified in coastal sediments (Jones et al., 2011; Koretsky et al., 2008; Liang et al., 1993; Luther et al., 1996), and remobilization and eventual diffusive flux from pore waters has been demonstrated in at least one case (Jones et al., 2011). The source of these complexes in marine sediments, however, remains unknown.

Fe(II) in marine sediments may be oxidized to inorganic Fe(III) colloids or particles by abiotic reaction with $O_{2(aq)}$ transported into sediments by diffusion or advection during tidal fluctuations (Taillefert et al., 2007b), wave action (Precht et al., 2004), and bioturbation (Kristensen, 2000), or by abiotic reaction with Mn(IV) oxides (Postma, 1985). Chemoautotrophic oxidation of Fe(II) by $O_{2(aq)}$ (McBeth et al., 2013; Saini and Chan, 2013; Sobolev and Roden, 2001) or NO_3^- (Sorokina et al., 2012) are also potential reactions resulting in cell-associated solid Fe(III). The rapid coagulation of inorganic Fe(III) colloids, however, should eventually precipitate particulate Fe(III) (oxy)hydroxides (Lohan and Bruland, 2008; Severmann et al., 2010) unless organic ligands maintain Fe(III) under the form of soluble complexes in sediments. Indeed, organic-Fe(III) complexes with a size < 5000 Da (Taillefert et al., 2000) have been detected using Au/Hg voltammetric microelectrodes in harbor (Brendel and Luther, 1995), salt marsh (Bull and Taillefert, 2001; Luther et al., 1996; Taillefert et al., 2002a; Taillefert et al., 2007b), estuarine (Taillefert et al., 2002b; Meiggs and Taillefert, 2011), and continental shelf (Taillefert et al., 2000) sediments. The accumulation of high

concentrations of soluble Fe(III), however, is limited to suboxic sediments, as $\sum H_2S$ produced by SO_4^{2-} reduction reduces organic-Fe(III) complexes rapidly and subsequently precipitates Fe(II) as FeS minerals (Carey and Taillefert, 2005; Taillefert et al., 2000). Indeed, seasonal measurements revealed that the production of soluble organic-Fe(III) complexes in estuarine sediments is strongly anti-correlated with the seasonal production of $\sum H_2S$ (Taillefert et al., 2002b). Finally, these complexes have been demonstrated to oxidize pyrite in salt marsh sediments when dissolved sulfide concentrations are low (Luther et al., 1996), while sediment incubations in sulfate-reducing conditions demonstrated that pyritization was accelerated in the presence of organic-Fe(III) complexes (Carey and Taillefert, 2005).

The production of organic-Fe(III) complexes is controlled by the delivery of natural organic matter (NOM) and Fe to sediments (Meiggs and Taillefert, 2011) and may occur via a variety of processes in sediments. First, oxidation of Fe(II) by dissolved $O_{2(aq)}$ in the presence of organic ligands (Taillefert et al., 2000) or oxidation of organic-Fe(II) complexes by Fe(III) minerals (Luther et al., 1992) may generate these complexes near the surface of marine sediments. Second, the biotic oxidation of Fe(II) by aerobic iron oxidizing bacteria in the presence of endogenous ligands (Roden et al., 2004; Sobolev and Roden, 2001) could produce these complexes near the sediment-water interface to avoid mineral encrustation, a process similar to Fe mineralization on organic extracellular stalks (Miot et al., 2009). Third, the non-reductive dissolution of Fe(III) (oxy)hydroxides (e.g. by reaction with bidentate or tridentate oxygen-containing ligands or NOM) (Biber et al., 1994; Bondietti et al., 1993; Deng and Stumm, 1994; Homoky et al., 2009; Nowack and Sigg, 1997; Radic et al., 2011; Santana-Casiano et al., 2000;

Zinder et al., 1986) may generate organic-Fe(III) complexes. Finally, soluble organic-Fe(III) complexes may form as intermediates during the reductive dissolution of Fe(III) minerals by iron-reducing bacteria (FeRB; Jones et al., 2010; Nevin and Lovley, 2002; Taillefert et al., 2007a). To date, it has yet to be determined which of the above processes are responsible for soluble Fe(III) production in marine sediments.

The objectives of this study were to elucidate the origin, composition, and reactivity of dissolved Fe(III) in estuarine sediments. Bulk estuarine sediments and pore waters were sampled and the main redox species involved in the cycling of Fe were measured seasonally and spatially in a river-fed estuary to determine the environmental processes responsible for the accumulation of dissolved Fe(III) in sediment pore waters. In addition, dissolved Fe(II) and Fe(III) complexes were separated using size exclusion chromatography to gain insight into their composition. Finally, incubations were conducted with natural sediments to identify biogeochemical pathways potentially responsible for dissolved Fe(III) production and consumption.

4.2. Methods

The Satilla River is a pristine, blackwater river draining the coastal plain swamps of South East Georgia (USA). As a result of the acid leaching of surrounding soils by low pH, high NOM groundwater, dissolved Fe concentrations are high in this river (Beck et al., 1974). Sediment cores (10 cm diameter, 50 cm long) from five stations described previously (Jones et al., 2011; Meiggs and Taillefert, 2011) were collected using a gravity corer (Marinelli et al., 1998) during four cruises on the R/V *Savannah* (Skidaway Institute of Oceanography) in July, September, and November 2007, and January 2008.

The stations range from muddy and almost completely fresh at the upper end of the estuary (SAT1 and SAT2) to sandy and fully saline at the mouth of the estuary (SAT5). Immediately upon collection, the core overlying water was sampled and the first 12 cm of sediment were sectioned in 1 cm increments under a N_2 atmosphere. The overlying water and the sediments of each section were collected in 50 mL Falcon tubes and centrifuged at 3000 rpm for 10 minutes under N_2 atmosphere to separate pore waters. The pore waters were then filtered through 0.2 μm filters (Whatman, Puradisc PES) under the same N_2 atmosphere, and small aliquots immediately added to acetate-buffered Ferrozine (3-(2-Pyridyl)-5,6-di(4-phenylsulfonic acid)-1,2,4-triazine, Sigma-Aldrich) at pH 5 for measurement of dissolved Fe(II) (Stookey, 1970). For determination of dissolved Fe(III), including soluble and colloidal Fe(III), separate aliquots were reduced in 100 mM hydroxylamine (Sigma-Aldrich) in 50 mM HCl (pH < 2, Sigma-Aldrich) prior to addition of Ferrozine, and Fe(III) was quantified by the difference of acidified Fe and Fe(II) (Viollier et al., 2000). A third aliquot of pore water was used onboard ship for analysis of dissolved inorganic carbon (DIC) by flow-injection (Hall and Aller, 1992). Finally, a small aliquot was kept for voltammetric measurements using Au/Hg voltammetric microelectrodes and pH measurements using a MI-414B needle combination pH microelectrode (Microelectrodes, Inc.). The pH electrode was calibrated with a seawater-TRIS buffer (Dickson, 1993) if overlying water salinity was > 10 or with standard NIST pH buffers if the salinity was < 10.

Solid-state Hg/Au working voltammetric microelectrodes were constructed as previously reported (Luther et al., 2008) and used as part of a 3-electrode system with a DLK-100 (Analytical Instrument Systems, Inc.) potentiostat to measure dissolved $O_{2(aq)}$,

Mn(II), Fe(II), ΣH_2S (= H_2S + HS^- + S(0) + S_x^{2-}) (Brendel and Luther, 1995), soluble organic-Fe(III) complexes (Taillefert et al., 2000), and $FeS_{(aq)}$ (Theberge and Luther, 1997) in each filtered pore water sample in the anaerobic chamber. Linear sweep voltammetry (LSV) and cathodic square-wave voltammetry (CSWV) were used to measure dissolved $O_{2(aq)}$ and organic-Fe(III), Fe(II), Mn(II), ΣH_2S, and $FeS_{(aq)}$, with an applied potential between -0.1 V and -1.75 V at a scan rate of 200 mV/sec after a conditioning step of 10 s at -0.1 V when organic-Fe(III) and sulfides were not detected (Brendel and Luther, 1995). If these compounds were detected, an initial conditioning step of 10 s at -0.9 V was added to this procedure to clean the electrode surface between subsequent analyses (Taillefert et al., 2000). Unlike measurement of dissolved Fe(III) by difference using the Ferrozine technique, which measures both colloidal and truly dissolved Fe(III), voltammetry only measures the truly soluble Fe(III) fraction. Voltammograms were integrated using the semi-automated VOLTINT software package (Bristow and Taillefert, 2008). Electrodes were calibrated in a $MnCl_2$ solution (0 to 400 μM), and the pilot ion method (Brendel and Luther, 1995; Luther et al., 2008) was used to infer concentrations of Fe(II) and ΣH_2S in samples. Organic-Fe(III) complexes and $FeS_{(aq)}$ (Taillefert et al., 2000; Theberge and Luther, 1997) could be quantified because their exact chemical composition is unknown. To compare the signal intensities of these species, each electrode's response to Mn(II) was normalized to a typical Mn(II) response (0.12 nA μM^{-1}), and this ratio was used to adjust the current response of the unquantifiable analytes.

Another filtered aliquot was used to measure the absorbance of the pore waters at 254 nm with a Waters model 2487 spectrophotometer after eventual dilution. Leftover

filtered samples were frozen for analyses of anions at later date. Leftover wet sediments were also frozen until extraction in triplicate of poorly crystalline iron hydroxides (e.g. ferrihydrite) with ascorbate-citrate-bicarbonate at pH 7.5 (Kostka and Luther, 1994). Another sediment sample was weighed before and after drying at 40°C to measure porosity and normalize ascorbate-extractable iron to a mass of dry sediment.

Visual MINTEQ thermodynamic modeling software was used to simulate mixing between Satilla River water in equilibrium with atmospheric CO_2 (pH = 5.65 (fixed), Na^+ = 111 μM, K^+ = 16 μM, Mg^{+2} = 24 μM, Ca^{+2} = 27 μM, Cl^- = 175 μM, SO_4^{-2} = 13 μM; data from Beck et al., 1974) and seawater (pH = 8.1 (fixed), Na^+ = 0.468 M, K^+ = 10.2 mM, Mg^{+2} = 50.32 mM, Ca^{+2} = 10.2 mM, HCO_3^- = 2.38 mM, Cl^- = 0.545 M, SO_4^{-2} = 28.2 mM) to predict the pH values expected at a given salinity in the estuary in the absence of natural organic matter. The H^+ concentration required to obtain the pH at both of these end-members was determined from the MINTEQ results, and then added explicitly to additional runs simulating conservative mixing. Other simulations were conducted by adding 3.8 mM Fulvic DOM (Beck et al., 1974) and 18 μM Fe(III) (Jones et al., 2011) to the freshwater end member using the NICA-Donnan feature in Visual MINTEQ, to either predict the pH or determine the saturation state of Fe minerals at fixed pH and salinity.

The depth-normalized concentration, Z (mol m^{-3}), of each dissolved chemical species described above was calculated for each core according to Eq. 1 and compared seasonally along the estuary:

$$Z = \frac{\sum_{i=1}^{n} \varphi c_i v_i}{\sum_{i=1}^{n} v_i} \qquad \text{(Eq. 4.1)}$$

where i denotes the depth-interval of each core section, C_i is either the Fe_{asc} concentration (μmol gdw^{-1}) or the dissolved species concentration (mol L^{-1}) of section i, V_i is the volume of the sediment section i, and $\varphi = (1-\phi)\rho$ for solids, and $\varphi = \phi$ for solution species, where ϕ is the porosity and ρ is the solid phase density. The solid phase was assumed to have a density of 2.6 g cm^{-3} (Roychoudhury 2001).

High-pressure size-exclusion chromatography (HP-SEC) with a Superdex PC 3.2/30 column (100 to 30,000 Da, Amersham GE Biosciences) was used to separate dissolved Fe(III) and Fe(II) from the bulk of the NOM and to provide size distribution information of the DOM. Separations were performed with a Waters 1525 high-pressure pump, Waters 2487 dual-absorbance detector, Waters WFC fraction collector, and the Waters Empower software suite. The pH of the mobile phase was buffered to a sufficiently low value to prevent oxidation of Fe(II) during the separation. Control HP-SEC separation experiments demonstrated that less than 5% of Fe(II) was oxidized in a 0.54 M NaCl matrix (pH 7.2) with a mobile phase consisting of 150 mM NaCl and 30 mM Na-acetate buffer adjusted to pH 5 with acetic acid. Injections of 50 mL sample at a flow rate of 100 µL/min offered a good peak resolution while maintaining the desired Fe detection limits in effluent samples. Samples were mixed in a 9:1 ratio with a 10x eluent solution (1.5 M NaCl, 300 mM Na-acetate adjusted to pH 5 with acetic acid) prior to injection to minimize matrix effects on UV absorbance and stabilize the Fe complexes against any oxidation that might occur before mixing with the eluent. Absorbance at 254 nm was monitored in the column effluent as a proxy for DOM (Chin et al. 1998), and 100 mL fractions (~ 2 column volumes) were collected for Fe speciation measured spectrophotometrically as above. The column was periodically calibrated for size versus

retention time with organic molecules generally used for HP-SEC separation of NOM, including Dextran Blue, PSS MW 8000, PSS 4600, methylthymol blue (MTB), and acetone, by monitoring the absorbance of these complexes at wavelengths between 200-300 nm. Three aliquots of EDTA (100 mM, in Na-acetate eluent) were injected at the end of each pore water injection to elute any residual Fe and quantify recoveries. Fe in the rinse fractions was measured with an Agilent 7500a by inductively coupled plasma-mass spectrometer (ICP-MS). Samples and standards were diluted with 2% nitric acid (trace metal grade, Fisher) in Nanopure water (Barnstead) and spiked with yttrium (10 ppb) as internal standard to monitor instrument drift during analysis. Blanks, calibration check standards, and River Water Certified Reference Material for Trace Metals (SLRS-4, National Research Council Canada, Ottawa, Canada) were analyzed as quality controls (95-105% recovery). Mass balance calculations for Fe measured in eluted fractions were performed to determine the recovery of each separation:

$$\sum_{i=1}^{m} C_f V_f + \sum_{i=1}^{n} C_r V_r = (1 - df) C_{inj} V_{inj} \qquad \text{(Eq 4.2)}$$

where C and V represent the concentration of iron (in mole L^{-1}) and the volume of each fraction (f), rinse (r), and pore water injected (inj), m and n represent the number of fraction and rinse eluted, and df is the dilution factor from matrix-matching with eluent. The average concentration of iron in the fractions collected prior to the predicted void volume of the column was subtracted from the concentrations of each of the individual fractions to remove the contribution of the baseline to the mass balance calculations.

Sediment slurry incubations were performed with homogenized wet sediments collected from depths of 7 to 10 cm in the upper end of the estuary (SAT1) in July 2007 to elucidate interactions between sediments and the natural microbial population. The

sediment was subjected to four treatments including unamended sediments as controls, sediments amended with 10^7 cells/mL of *Shewanella putrefaciens* strain 200, a model Fe(III)-reducing bacterium grown anaerobically on fumarate as electron acceptor in LB medium (Taillefert et al., 2007a), sediments amended with Fe(III) hydroxides (10 mM 2-line ferrihydrite) to determine if Fe limitation affects the overall solubilization and reduction kinetics of Fe(III) oxides, and sediments amended with both *S. putrefaciens* and Fe(III) hydroxides. An additional incubation was conducted with both *S. putrefaciens* and Fe(III) hydroxides, but without sediments as live control. The 2-line ferrihydrite was prepared by titration of a 400 mM solution of $FeCl_3$ with NaOH to pH 7 and washing 3 times with sterile deionized H_2O. Four polyether ether ketone (PEEK) reactors that can accommodate gas lines, electrodes, and sampling ports (Taillefert et al., 2007a) were filled with 90 mL of defined minimal salts media (Myers and Nealson, 1988) (ionic strength = ~0.1; consistent with SAT2 sediment pore waters) modified to contain 50 μM of PO_4^{-3}. Approximately 10 g of wet sediment was added to the reactors for a final concentration of ascorbate-extractable natural Fe of 4.6 mM. The reactors were sealed, and a sparging line, a septum sampling bag port (Qosina), as well as working, reference, and counter electrodes (prepared as described above) were connected to the lid via gas-tight HPLC fittings. The reactors were degassed with UHP N_2 gas and stored in an anaerobic chamber while stirring at ~40 rpm using a magnetic stir bar. Voltammetry data (dissolved $O_{2(aq)}$, organic-Fe(III), Fe(II), Mn(II), ΣH_2S, and $FeS_{(aq)}$) were obtained approximately every 24 hours by connecting the electrodes to a DLK-100 potentiostat (Analytical Instrument Systems, Inc.) via connectors mounted on the wall of the anaerobic chamber, and samples were collected periodically with gas tight syringes under

N_2 atmosphere for analysis of Fe(II) and total dissolved Fe. After 150 hours, the contents of each of the four reactors were centrifuged in two 50 mL Falcon tubes and the supernatant was filtered through 0.2 μm filters (Whatman, Puradisc PES) inside the anaerobic chamber. The reactors were rinsed with sterile water and refilled with the filtrate. For *S. putrefaciens* amended treatments, the reactors were then inoculated again with 10^7 cells/mL to monitor the evolution of the speciation of the remaining dissolved Fe(III) in the absence of any solid phases.

4.3. Results

4.3.1. Estuarine chemistry

The sampling period corresponded with the end of the worst drought in recent record for the southeast region of North America (Campana et al., 2012). Accordingly, during periods of low discharge (e.g. July 2007) salinities at or above 20 were measured in core overlying waters along the entire estuary. Under non-drought conditions, however, salinities were typically less than 10 at SAT1 and SAT2, between 7 and 13 at SAT3, and greater than 22 at SAT4 and SAT5 (Figure 4.1). While dissolved Fe(II) concentrations ($Fe(II)_d$) were always below detection limit (< ~200 nM) in the overlying waters, dissolved Fe(III) ($Fe(III)_d$) concentrations generally decreased with increasing salinity along the estuary (Figure 4.1a), reaching up to 28.3 μM at the upriver stations SAT1, SAT2, and SAT3, but only 8.2 μM at the downriver stations SAT4 and SAT5. The pH in the overlying waters of each core generally increased non-linearly as a function of salinity (Figure 4.1b); the lowest pH (4.68) was measured at SAT2, the least saline (S = 2) station, while the highest pH (8.29) was observed at SAT4 (S = 32).

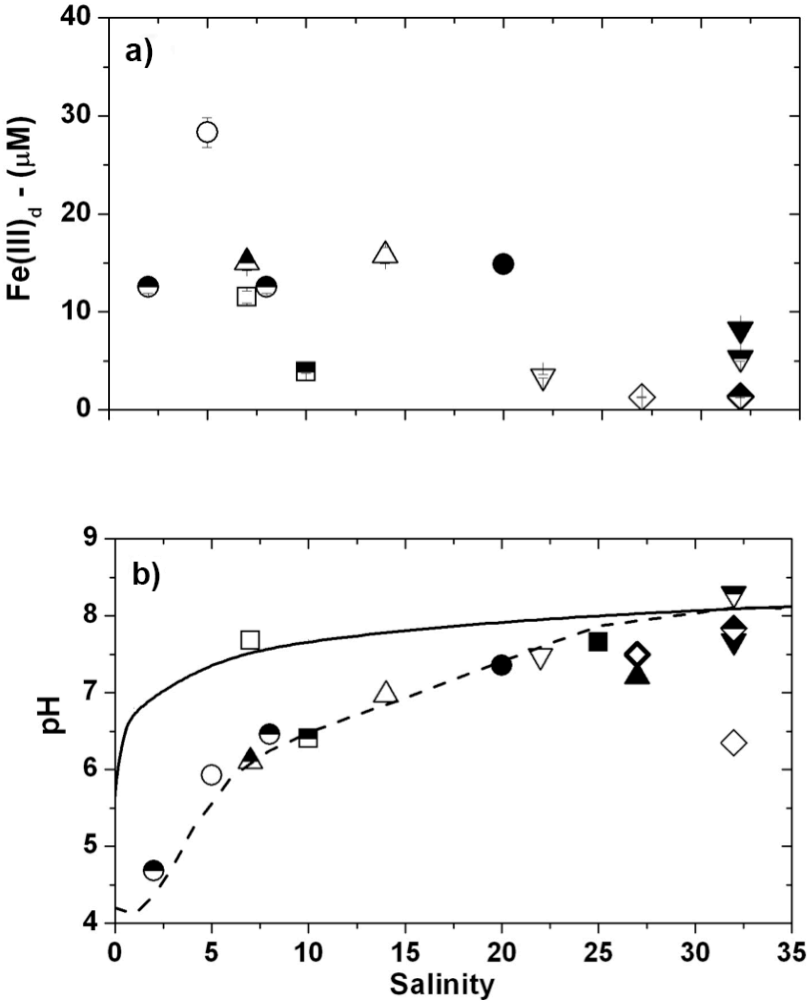

Figure 4.1 - a) Total dissolved Fe concentrations and b) pH of the overlying waters just above the sediment as a function of salinity in the Satilla River. Symbols represent stations as follows: SAT1 (circles), SAT2 (squares), SAT3 (triangles), SAT4 (upside-down triangles), and SAT5 (diamonds). Fill pattern indicates month: Jul. 2007 (solid), Nov. 2007 (open), Jan. 2008 (half-filled). The modeled lines simulate the pH calculated with MINEQL+ by mixing fresh and salt water end-members to the salinity of each station in the presence (dashed) or not (solid) of dissolved organic matter, as described in the methods section.

4.3.2. Sediment Fe speciation and distribution

Depth profiles obtained in January 2008 at the most active (SAT1, Figure 4.2a) and inactive (SAT4, Figure 4.2b) stations with respect to Fe cycling are shown as examples to demonstrate the variation in biogeochemical processes in surficial sediments along the estuary. At SAT1, Ferrozine-reactive Fe(II) species ($Fe(II)_d$), voltammetrically measured org-Fe(III) ($Fe(III)_{volt}$), and dissolved Mn(II) ($Mn(II)_d$) displayed large contrasts in concentration above and below a depth threshold of 8 cm, while ΣH_2S and $FeS_{(aq)}$ were never detected. Concentrations of $Fe(III)_d$ progressively increased from below detection limit at the sediment surface to a peak around 680 μM at 8.5 cm, then decreased slightly to around 500 μM at 11.5 cm. $Fe(II)_d$ remained low in the first 7.5 cm and increased below that to peak at 1 mM at 10.5 cm before decreasing to around 800 μM at 11.5 cm. Similarly, $Mn(II)_d$ remained low before 8 cm and reached a maximum around 300 μM only at 9.5 cm and stabilized around 200 μM deeper. Although representing a single point measurement at each depth compared to $Fe(III)_d$ integrated over the entire volume of each slice, soluble organic-Fe(III) complexes measured voltammetrically (org-Fe(III)) displayed a similar depth profile as $Fe(III)_d$, suggesting that these complexes are distributed homogenously in the sediments. Their current intensities were similarly low above 8 cm, increased up to 500 nA at 9.5 cm and remained relatively stable deeper. The increase in dissolved Fe with depth was mirrored by an increase in dissolved inorganic carbon (DIC) concentrations from 1.4 mM at the SWI to as high as 16.2 mM at 10.5 cm. Similarly, absorption at 254 nm of each pore water section at SAT1 mirrored that of $Fe(III)_d$, suggesting that soluble Fe(III) is in the form of organic-Fe(III) complexes

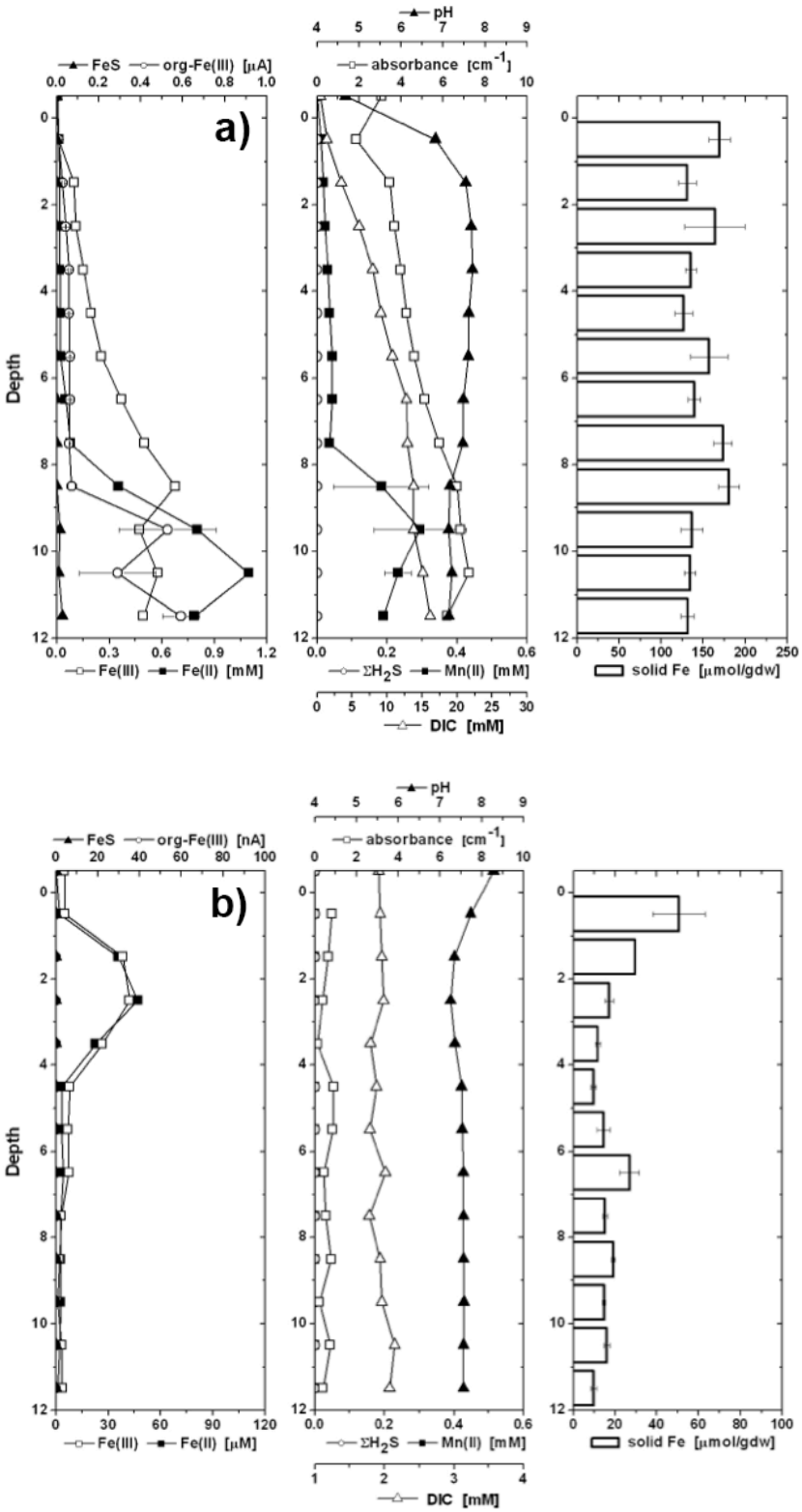
a)
b)
Depth
FeS
org-Fe(III) [µA]
org-Fe(III) [nA]
absorbance [cm^{-1}]
pH
Fe(III)
Fe(II) [mM]
Fe(II) [µM]
ΣH$_2$S
Mn(II) [mM]
DIC [mM]
solid Fe [µmol/gdw]

Figure 4.2 - Typical depth profiles of $Fe(III)_d$ and $Fe(II)_d$ measured by Ferrozine, $FeS_{(aq)}$, org-Fe(III), $\sum H_2S$, and Mn(II) measured by Au/Hg voltammetric microelectrodes, DIC measured by FIA, pH measured with potentiometric microelectrodes, absorbance at 254 nm, and amorphous Fe(III) oxides in Satilla River sediments. Sediment cores collected in January 2008 at (a) SAT1 and (b) SAT4 illustrate the variation in biogeochemical processes along the estuary. In the freshwater end-member (SAT1), the large input of Fe(III) oxides allows Fe reduction to dominate, while near the mouth of the estuary (SAT4), sulfate reduction controls the biogeochemical cycling of Fe. Data points represent measured values at the midpoint of 1 cm thick sections. $O_{2(aq)}$ penetration depths in all these sediments did not exceed 2 mm and was omitted for clarity. Error bars represent the analytical error for pore water measurements, and the standard deviation of triplicate extractions for solid phase analyses. Note the much lower concentration scales for the SAT4 profile.

(Figure 4.2a). While the acidic pH of the overlying river water at SAT1 was reflected in the surface pore waters, the pH increased rapidly as a function of depth and stabilized to ca. 7.2 in the zone of metal reduction. Finally, the content of poorly crystalline Fe oxide (Fe_{asc}) remained relatively constant around 125 to 175 μmol gdw^{-1} as a function of depth over the whole profile.

At the more saline station SAT4, both $Fe(II)_d$ and $Fe(III)_d$ formed peaks in much lower concentrations (< 50 mM) than at SAT1 (Figure 4.2b) immediately below the sediment surface (0-4 cm), while $Fe(III)_{volt}$, $Mn(II)_d$, ΣH_2S, and $FeS_{(aq)}$ were always below detection limit. Unlike SAT1, there were no discernable trends in absorbance values or DIC concentrations, which remained constant around seawater values, and the pH decreased from 8.2 in the more saline overlying waters to ca. 7.2 in the zone of Fe reduction, then stabilized around that value deeper. Finally, Fe_{asc} concentrations decreased rapidly with depth (~50 μmol gdw^{-1} between 0-1 cm to < 20 μmol gdw^{-1} below 2 cm).

The results of similar profiles obtained at each station during the four different cruises were integrated over the depth of each core to be compared. Generally, the Fe_{asc}

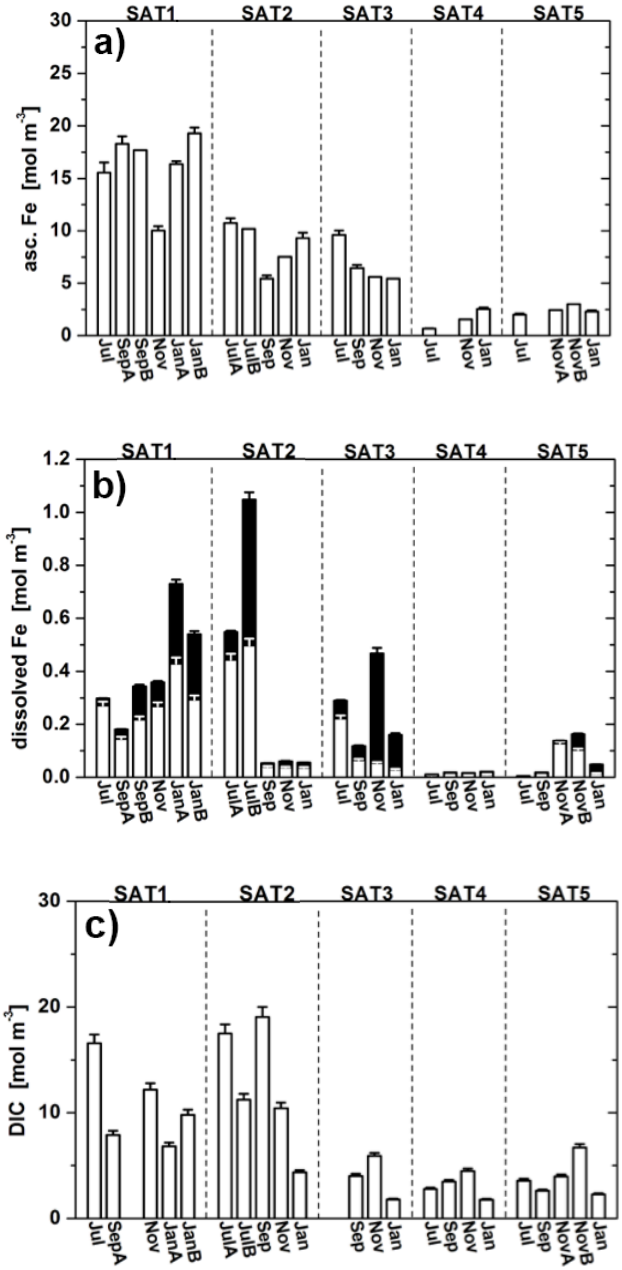

Figure 4.3 - Iron and carbon inventories of Satilla River sediments collected between Jul. 2007 and Jan. 2008 presented as volume normalized: a) ascorbate extractable Fe, b) dissolved Fe(III) (open bars) and dissolved Fe(II) (closed bars), and c) dissolved inorganic carbon found in the first 12 cm of the sediment cores. Duplicate cores at the same station are denoted with the suffix "A" and "B".

content of the sediment decreased towards the mouth of the estuary with increasing salinity, but varied little seasonally between stations (Figure 4.3a). Moving downstream from SAT1 to SAT5, average Fe_{asc} in the top centimeter of sediment was 146 (+/- 38), 75 (+/- 30), 68 (+/- 28), 30 (+/- 29), and 20 (+/- 3) μmol/gdw (errors represent standard deviations between seasons), much more variable than the entire sediment column sampled. Following a similar trend, the upriver stations (SAT1, SAT2, and SAT3) displayed higher Fe_d concentrations than the more permanently saline stations (SAT4 and SAT5, Figure 4.3b). In addition, depth-integrated concentrations of Fe_d in SAT1 sediments (300 – 950 mmol m^{-3}) generally increased from summer to winter, while high Fe_d was only found at SAT2 during the summer. In turn, Fe_d levels were more variable at SAT3 while Fe_d during the two fall/winter sampling events was not significant at SAT4 (< 20 mmol m^{-3}). Interestingly, more dissolved Fe (10 – 180 mmol m^{-3}) was typically found at SAT5, the mouth of the estuary, than at SAT4. Except at SAT2 in July (Core B) and at SAT3 in November, $Fe(III)_d$ concentrations almost always exceeded $Fe(II)_d$ concentrations across the estuary when Fe_d was detected, and $Fe(III)_d$ comprised a larger percentage of Fe_d at SAT1 during the summer months (91.5%) than the winter months (54.4%) (Figure 4.3b). Simultaneously, sediments displayed consistently higher DIC concentrations at the upriver stations SAT1 and SAT2 than all downriver stations (SAT3, SAT4, and SAT5) (Figure 4.3c). In turn, total dissolved sulfides were only observed at SAT4 in July, September, and November, and at SAT5 in July, September, and January (data not shown), while $FeS_{(aq)}$ was only observed in July in cores from SAT2 and SAT3. Finally, $Mn(II)_d$ was observed seasonally at each station except for SAT4, where it was only observed in November (data not shown). Interestingly, the pH of the pore waters

ranged between 7.5 and 8 when $Fe(II)_d$ was not a dominant species in the sediments but only ranged between 7 and 7.5 under strong Fe-reducing conditions (Figure 4.4). This trend was evident at all stations, irrespective of the pH of the overlying waters, except for SAT3 which displayed a consistently low pH of 6.4 throughout the study period (Figure 4.4).

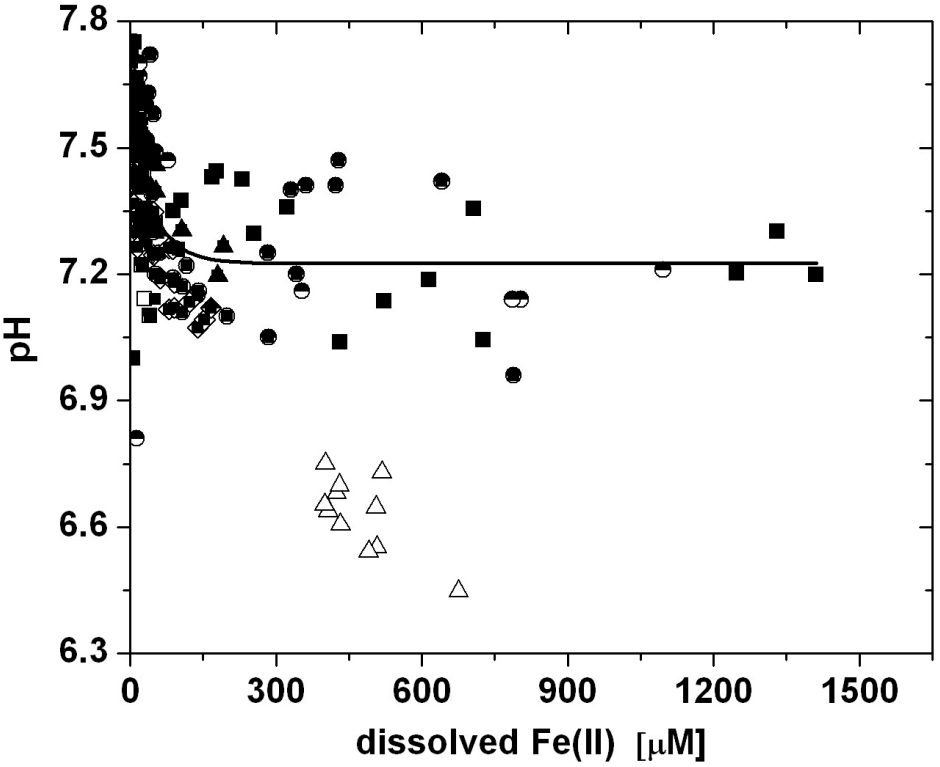

Figure 4.4 - pH as a function of $Fe(II)_d$ concentrations in individual pore water sections from the first 12 cm of Satilla River sediments. The solid line represents a sigmoidal fit through all of the pore water data and predicts the most probable pore water pH for a given $Fe(II)_d$ concentration. Symbols represent stations as follows: SAT1 (circles), SAT2 (squares), SAT3 (triangles), SAT4 (upside-down triangles), and SAT5 (diamonds). Filled patterns indicate month: Jul. 2007 (solid), Nov. 2007 (open), and Jan. 2008 (half-filled).

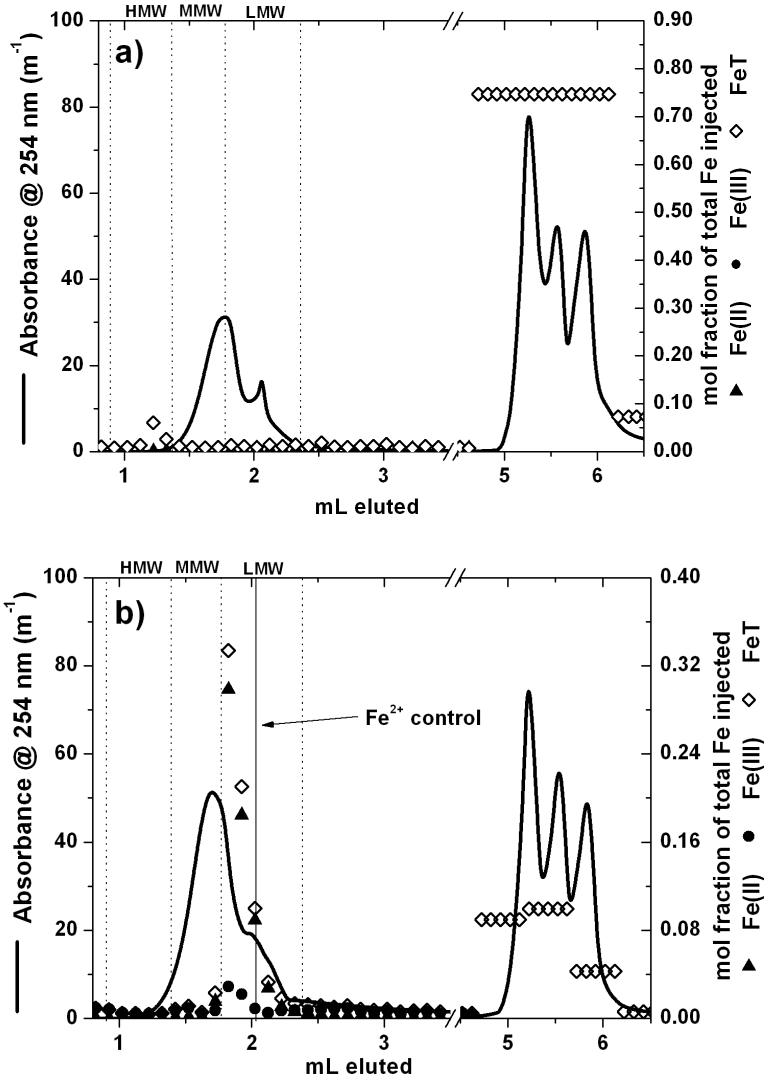

Figure 4.5 - Size exclusion chromatograms of pore waters isolated from SAT1 in January 2008 between (a) 6 to 7 cm and (b) 10 to 11 cm are presented as examples of samples from various depths and with different Fe speciation. Black lines represent absorption at 254 nm obtained as a function of elution volume and can serve as a proxy for DOM distribution in a humic –rich environment. Iron measured in each collected fraction is represented as the mol fraction of the total Fe injected and symbols (triangles, circles, diamonds) correspond to Fe(II), Fe(III), and the sum Fe_{total}. Dashed vertical lines represent size-fraction boundaries used to define the Fe recoveries in Table 1. The solid black line indicates the fraction in which inorganic Fe(II) control standards eluted. Three subsequent EDTA rinse injections eluted after 5 mL were collected for mass balance calculations.

Table 4.1 - Size distribution of DOM, total dissolved Fe (Fe_d), dissolved Fe(III) ($Fe(III)_d$), and dissolved Fe(II) ($Fe(II)_d$) in the pore waters of SAT1 obtained by HP-SEC compared to the composition of the bulk sample. DOM determined by monitoring absorbance at 254 nm as a function of time during separations always elutes after approximately 1.75 mL. The mole fractions (moles collected/moles injected) of Fe(III) and Fe(II) are categorized into High (> 2 kDa), Medium (2 kDa – 200 Da), and Low (< 200 Da) molecular weights as determined by column calibration and defined by the following elution volumes (in mL): H: 0.9 – 1.3; M: 1.4 – 1.7; L: 1.8 – 2.3. Fe_d recovery includes Fe measured in the different molecular weight fractions as well as Fe measured in the rinse steps by ICP-MS. Designations: NM - not measured; NA – not applicable because Fe(III) could not be calculated by difference as Fe(II) was not measured.

	Bulk sample composition				Molecular Weight Distribution										
					$Fe(II)_d$			$Fe(III)_d$			Fe_d				
Core	Depth	DOM height	Fe_d	$Fe(III)_d$	H	M	L	H	M	L	H	M	L	EDTA Rinse	Recovery
	(cm)	(cm^{-1})	(μM)	(mol $Fe(III)_d$/ mol Fe_d)	(mol $Fe(II)_d$/ mol $Fe(II)_d$)			(mol $Fe(III)_d$/ mol $Fe(III)_d$)			(mol Fe_d/ mol Fe_d)				
Sep2B	6 – 7	0.29	318.6	0.819	NM	NM	NM	NA	NA	NA	0	0	0.194	0.694	0.888
Sep2B	9 – 10	0.3	428.4	0.458	NM	NM	NM	NA	NA	NA	0.016	0.146	0.055	0.895	1.112
Jan2A	6 – 7	0.31	406.3	0.936	0.001	0	0.039	0.073	0.002	0.007	0.072	0.004	0.02	0.883	0.979
Jan2B	7 – 8	0.3	487.8	0.897	NM	NM	NM	NA	NA	NA	0.02	0.008	0	0.808	0.836
Jan2B	10 – 11	0.51	1423.2	0.31	0	0.021	0.923	0	0.003	0.135	0	0.011	0.652	0.213	0.876
Jan5A	1 - 2	0.1	181.4	0.163	0	0	0.755	0.434	0.012	0.012	0.065	0	0.642	0.695	1.402

4.3.3. Characterization of Satilla River organics & iron complexes by HP-SEC

Pore waters from a series of sediment cores collected in September 2007 and January 2008 at SAT1 were separated by HP-SEC to examine the molecular weight of the soluble organic-Fe(III) complexes and gain insights into their composition. Representative chromatograms (Figure 4.5) of pore waters from 6 - 7 cm that contained mostly Fe(III) (Jan2A in Table 4.1) and from 10 - 11 cm that contained a mixture of Fe(II) and Fe(III) (Jan2B in Table1) revealed asymmetrical signals for DOM at 254 nm in both the low (LMW) and medium (MMW) molecular weight fractions, indicating that chromophores of different molecular weight are present in these pore waters. Surprisingly, no $Fe(III)_d$ was observed in any of the fractions separated from these two samples (Figure 4.5), and 8.2% and 13.8% of $Fe(III)_d$ only eluted within the column exclusion limits (Table 4.1). In turn, while only a negligible fraction of $Fe(II)_d$ eluted from the 6 - 7 cm sample, which did not contain an appreciable amount of Fe(II), more than 90% of $Fe(II)_d$ from sample 10 – 11 cm, which contained a significant fraction of Fe(II), eluted in the LMW fraction (Figure 4.5b, Table 4.1). More importantly, the Fe(II) fractions eluted earlier than inorganic Fe(II) standards injected in control experiments (Figure 4.5b), indicating that Fe(II) is of a larger MW than inorganic Fe(II) and is therefore complexed by natural organic ligands or is in the form of FeS nanoparticles. The MW distribution of pore water DOM displayed at least two convoluted fractions of low to middle MWs which co-eluted with $Fe(II)_d$ in all the pore waters examined (e.g. Figure 4.6), further supporting the notion that the Fe(II) is complexed to DOM in these pore waters. Total recoveries for the six pore waters subject to the separation procedure ranged between 83.6% and 140.2% (Table 1) and were overestimated in samples with

small initial Fe_d concentrations. $Fe(II)_d$ typically eluted in the LMW fraction regardless of station or depth, while $Fe(III)_d$ was retained on the column and recoverable only in the EDTA rinse (Table 4.1). Of the $Fe(III)_d$ that did elute within the column exclusion limits (maximum 45.8 %), no trends in its distribution between high, middle, and low MW fractions were observed. Finally, while the separations demonstrated similar MW distributions of DOM between samples, absorption at 254 nm tended to increase with depth and distance from the mouth of the estuary (Table 1).

4.3.4. Incubation results

Fe(III) minerals were dissolved and reduced in slurry incubations performed with SAT1 sediments, irrespective of the addition of exogenous Fe(III)-reducing microorganisms and/or Fe(III) oxides (Figure 4.6). $Fe(II)_d$ was produced above baseline concentrations after ~2 days in the cell-amended treatments and after ~4 days in treatments with the natural sediment community only, suggesting *S. putrefaciens* stimulated Fe(III) reduction. While the addition of Fe(III) hydroxides generally doubled the extent of Fe(III) reduction, $Fe(II)_d$ in the treatments amended with cells reached concentrations approximately 5 times higher than in treatments without *S. putrefaciens* amendments regardless of the addition of exogenous Fe(III) hydroxides (Figure 4.6a). Although $Fe(III)_d$ background concentrations of approximately 100 μM were present in the original SAT1 sediment, $Fe(III)_d$ concentrations in 2-line ferrihydrite- and *S. putrefaciens*-amended treatments reached as high as 1.16 mM, approximately 4 times higher than in treatments containing no exogenous cells (Figure 4.6b). Similarly, current intensities of org-Fe(III) complexes were about 7 times greater in treatments amended

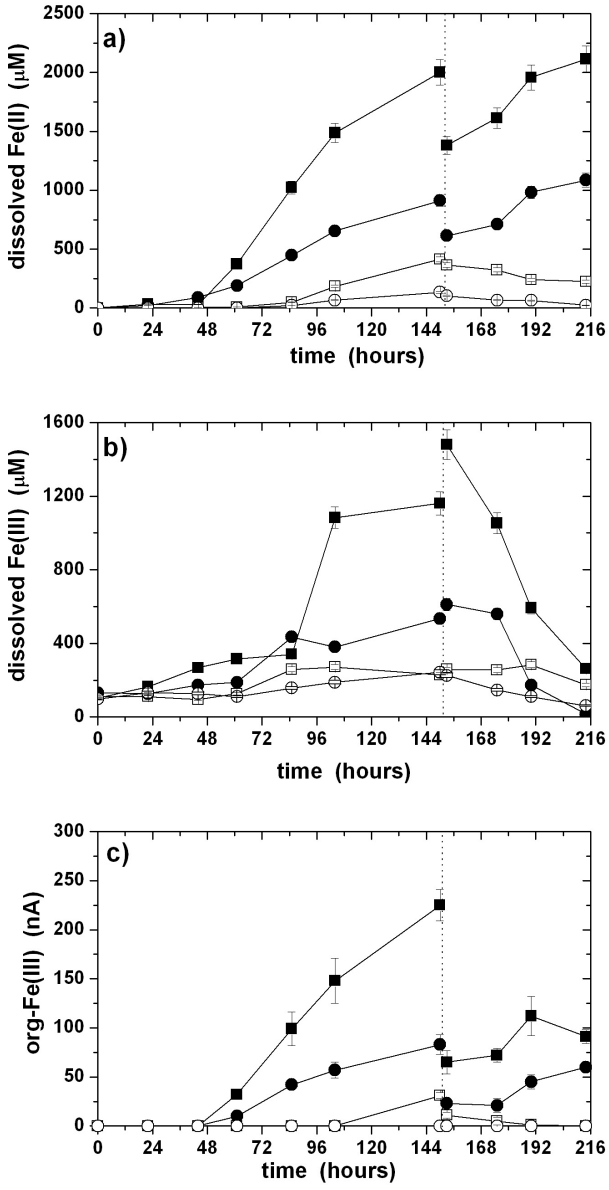

Figure 4.6 - Production of $Fe(II)_d$ (a), $Fe(III)_d$ (b), and $Fe(III)_{volt}$ (c) as a function of time in slurry incubations of SAT1 sediments amended (closed symbols) or not (open symbols) with *S. putrefaciens* in the presence (square symbols) or absence (circles) of 10 mM 2-line ferrihydrite. Solids were removed at 150 hours (dashed line), and live treatments were reinoculated with cells to monitor the potential for reduction of soluble Fe(III) by *S. putrefaciens*.

Table 4.2 - Net production (positive numbers) or consumption (negative numbers) rates of $Fe(II)_d$, $Fe(III)_d$, and $Fe(III)_{volt}$ in slurry incubations with SAT1 sediments amended or not with 2L ferrihydrite ($Fe(OH)_3$) and/or *S. putrefaciens* before (0-150 hours) and after removal of the solid phase by filtration (153-214 hours). Initial rates were calculated from the slope of the first ~24 hours of total Fe(II) accumulation, after accounting for any phase lags. The concentrations of $Fe(II)_d$ and $Fe(III)_d$ lost or gained during filtration (i.e. oxidized or precipitated) were quantified by difference of Fe_d and $Fe(II)_d$ before and immediately after removal of the solid phase by filtration. The last three columns include the net rates of $Fe(II)_d$, $Fe(III)_d$, and $Fe(III)_{volt}$ production or consumption after re-inoculation of the filtered supernatants.

		time: 0 - 150 hours			from filtration		time: 153 - 214 hours		
$Fe(OH)_3$	Cells	$Fe(II)_d$ rate ($\mu M /hr^{-1}$)	$Fe(III)_d$ rate ($\mu M\ hr^{-1}$)	org-Fe(III) rate ($nA\ hr^{-1}$)	$Fe(II)_d$ (μM)	$Fe(III)_d$ (μM)	$Fe(II)_d$ rate ($\mu M\ hr^{-1}$)	$Fe(III)_d$ rate ($\mu M\ hr^{-1}$)	org-Fe(III) rate (nA hr-1)
+	+	19.13 ± 2.19	12.03 ± 6.02	2.51 ± 0.12	-620 ± 131	318 ± 101	12.60 ± 1.97	-20.55 ± 2.08	0.54 ± 0.43
+	-	5.50 ± 0.49	3.30 ± 0.66	0.67 ± 0.00	-50 ± 30	29 ± 19	-2.47 ± 0.58	-1.19 ± 0.98	-0.18 ± 0.05
-	+	9.62 ± 0.74	3.38 ± 1.33	1.00 ± 0.10	-298 ± 59	77 ± 44	8.33 ± 1.71	-13.29 ± 5.16	0.67 ± 0.21
-	-	1.55 ± 0.14	1.24 ± 0.19	0 ± 0	-30 ± 9.0	-17 ± 18	-1.25 ± 0.18	-2.68 ± 0.28	0 ± 0

with *Shewanella* than in treatments without amended cells, regardless of the presence of exogenous Fe(III) hydroxides (Figure 4.6c). Initial production rates of $Fe(II)_d$ and $Fe(III)_d$ were determined by linear regression of their concentrations as a function of time after phase lag, while initial production rates of org-Fe(III) were determined by regression of their current intensities as a function of time (Table 4.2). Net production rates of $Fe(II)_d$ were highest in treatments containing both bacterial amendments and added Fe(III) oxides, but the addition of *S. putrefaciens* contributed more to the increase in the rate of Fe reduction than added Fe(III) hydroxides. Finally, relative changes in $Fe(III)_d$ and $Fe(III)_{volt}$ accumulation rates between the four treatments were approximately the same as the changes in $Fe(II)_d$ production rates (Table 2).

Up to 20% of $Fe(II)_d$ was removed during the filtration step at 150 hours and between 25 and 50% of it accumulated as $Fe(III)_d$ (Table 4.2), likely due to the oxidation of Fe(II) to colloidal or organic-Fe(III) complexes and partial precipitation of Fe(III) on the filters. Simultaneously, org-Fe(III) current intensities were reduced drastically, suggesting that electrochemically labile forms of Fe(III) may have a high affinity for the filters. Nonetheless, active reduction of the leftover dissolved Fe(III) after removal of the solid phase was evidenced by an increase in $Fe(II)_d$ concentrations at the expense of $Fe(III)_d$ in treatments reinoculated with *S. putrefaciens* (Figure 4.6a). Production rates of $Fe(II)_d$ in the presence of the cells after the filtration step represented between 66 and 87% of those obtained during the initial incubation period with solid phases (Table 4.2). Additionally, the phase lags between the addition of cells and the onset of Fe(III) reduction were lower than in the original incubations with the solid phase (Figure 4.6a). Finally, the rates of $Fe(II)_d$ accumulation in the presence of the cells were around 60%

lower than the rates of $Fe(III)_d$ loss in the same incubations, while both $Fe(II)_d$ and $Fe(III)_d$ were removed from solution (Figure 4.6) at similar rates (Table 4.2) in treatments with no added cells. More importantly, org-Fe(III) current production increased in treatments amended with live cells only (Figure 4.6c) despite the fact that $Fe(III)_d$ decreased over time during these incubations, as would be expected from the production of an endogenous ligand to destabilize $Fe(III)_d$ during microbial reduction (Taillefert et al., 2007). However, net rates of org-Fe(III) production were significantly lower after removal of the solid phase than when Fe(III) oxides were present (Table 4.2), indicating that org-Fe(III) is produced at higher rates when both solid Fe(III) sources and adsorbed DOM are present.

4.4. Discussion

Organic-Fe(III) complexes have been observed in a variety of coastal marine sediments, yet the processes responsible for their production and their chemical composition remain elusive. In this study, the speciation of dissolved and solid phase iron as well as redox species involved in the biogeochemical cycling of iron in these sediments were measured seasonally along the estuary of the Satilla River (GA), a blackwater river rich in iron and dissolved organic matter, to elucidate the main factors controlling the production of these complexes. Incubations with natural sediments and a model iron-reducing microorganism were subsequently conducted to determine whether the soluble organic-Fe(III) complexes may have a biogenic origin.

4.4.1. Delivery of Fe to estuarine sediments

To understand the sedimentary processes allowing for the formation of dissolved Fe(III) complexes in Satilla River sediments, the chemical composition of the solid Fe(III) precursor must be described. The composition of solid phase Fe is determined by the mechanism of precipitation, which is affected by the composition and concentration of DOM (Furukawa et al., 2014) and the concentration of Fe(III) undergoing hydrolysis in the water column and near the sediment-water interface. Blackwater rivers such as the Satilla River receive run-off from coastal plain sediments and contain much more DOM than most rivers (Otero et al., 2000) because sandy drainage basins display a low adsorption capacity for terrestrial carbon leached from vegetation (Meyer, 1986). Rising river water can leach both sandy soils and stagnant swampy floodplains, flushing high concentrations of soil fulvic acids into the headwaters (Beck et al., 1974). Indeed, the Satilla River headwater pH is approximately 1 unit lower than that of freshwater in equilibrium with atmospheric CO_2 (Figure 4.1b) because of the dominant control DOM exerts on the acidity of these waters (Beck et al., 1974). In similar systems, Fe(III) is maintained in the truly dissolved or nanoparticulate phases (< 3 nm), indicative of organic complexation (Ingri et al., 2006; Stolpe et al., 2013). Finally, the excellent correlation between DOC and the sum of dissolved Fe and Al revealed that all dissolved Fe (~18 μM) in the freshwater end-member of the Satilla River exists as truly dissolved complexes (Perdue et al., 1976).

Overlying waters along the estuary are also more acidic than predicted by conservative mixing of organic-depleted fresh water with seawater (solid line, Figure 4.1b) by approximately 0.5 pH units, even at salinities greater than 20. Such variations

are less likely to result from analytical errors (precision +/-0.02), suggesting that DOM is not completely removed by flocculation during mixing of freshwater with seawater and instead controls the pH even near the mouth of the estuary. Indeed, the addition of Suwanee River fulvic acid DOM to the freshwater end-member in the equilibrium model allows for accurate prediction of the pH at salinities less than 25. As fulvic DOM in size fractions < 3 nm is resistant to salt-induced flocculation (Stolpe and Hassellov, 2007) and prevents the aggregation of small Fe(III) colloids due to repulsion effects (Illes and Tombacz, 2006), Fe(III) complexes with stability constants consistent with those of fulvic acids (Laglera and van den Berg, 2009) are routinely detected in estuaries. Similarly, Satilla River particles are enriched in lignin (Hopkinson et al., 1998), suggesting Satilla DOM may also be composed of lignin-type molecules, which are resistant to flocculation in seawater and form complexes with Fe(III) (Krachler et al., 2012). These complexes may therefore play an important role in the transfer of Fe(III) to the oceans (Buck et al., 2007; Jones et al., 2011; Powell and Wilson-Finelli, 2003).

Nonetheless, as increasing concentrations of divalent seawater cations neutralize DOM, repulsive effects are diminished and flocculation of Fe eventually occurs (Boyle et al., 1977; Mylon et al., 2004; Sholkovitz, 1976). The fraction of colloidal Fe determined by difference of total dissolved Fe and soluble organic-Fe(III) complexes measured by Competitive-Ligand Exchange Adsorptive-Stripping Voltammetry (CLE-ASV) increases to 48% of total dissolved Fe by a salinity of 7 (Jones et al., 2011). Ultimately, Fe flocculation to sediments removes approximately 98% of total dissolved Fe by the mouth of the estuary (Figure 4.1a). Considering the high variability in salinity during the study

period, rates of Fe(III) deposition at a given station should be highly dependent on river discharge (Meiggs and Taillefert, 2011).

4.4.2. Estuarine sediment gradient

Removal of Fe(III) from the overlying waters is confirmed by the high concentrations of amorphous Fe(III) hydroxides (Fe_{asc}) in the top 12 cm of sediments in the upper estuary (Figure 4.2a), though concentrations decrease non-linearly with distance from the freshwater end-member to the mouth of the estuary. Upriver stations (SAT1, SAT2 & SAT3) are dominated by Fe(III) reduction with concentrations of Fe(II) as high as 1.4 mM (Figure 4.3a), rivaling other coastal sediments (Thamdrup, 2000), and metal reduction is the only anaerobic respiratory process observed at SAT1 and SAT2 (Meiggs and Taillefert, 2011). Despite the high Fe(III)-reducing capacity of these three stations, Fe_{asc} concentrations remain constant with depth in these sediments (e.g. Figure 4.2a), suggesting that delivery of Fe(III) hydroxides to SAT1 and, in a lesser extent, to SAT2 and SAT3 is high enough to compensate for the extensive reduction of Fe(III) in the first 12 cm of sediment. Conversely, Fe_{asc} concentrations at SAT4 (e.g. Figure 4.2b), and to a lesser extent at SAT3 (data not shown), decrease rapidly as a function of depth because these two stations both show periodic SO_4^{-2} reduction events, especially in the summer and early fall, which could rapidly reduce Fe(III) hydroxides and precipitate FeS minerals (Meiggs and Taillefert, 2011). Interestingly, SAT5 displayed low SO_4^{-2} reduction because of additional Fe inputs from nearby rivers (Meiggs and Taillefert, 2011).

Seasonally, temperature and river discharge affected both the nature and extent of the diagenetic processes in the Satilla River estuary (Meiggs and Taillefert, 2011). Examination of individual stations indicates more temporal stability in the solid phase (Figure 4.3a) than in the dissolved phase (Figure 4.3b) as sediments are gradually deposited and reworked over the course of several years. Generally, higher concentrations of $Fe(II)_d$ are found in the winter months at all stations except SAT2 (Figure 4.3b), suggesting either that $Fe(II)_d$ is titrated by sulfide along most of the estuary during periods of intense SO_4^{-2} reduction in the summertime or that respiration processes in these sediments alternate seasonally between Fe(III) and SO_4^{2-} reduction (Lowe et al., 2000). The non-linear decrease in pore water pH with increasing $Fe(II)_d$ concentrations along the estuary regardless of the seasons (Figure 4.4) provides further evidence of these processes. A decrease in pore water pH may indicate active siderite precipitation (Hunter et al., 1998), $FeS_{(am)}$ or mackinawite precipitation (Rickard and Morse, 2005), or $Fe(II)_d$ oxidation near the sediment-water interface (Wang and VanCappellen, 1996). As the low pH values were mostly found in the pore waters of SAT1 and SAT2, containing the highest concentrations of $Fe(II)_d$, the precipitation of Fe-S minerals was likely not significant, corroborating the hypothesis that SO_4^{2-} reduction was not intense in the upper estuary, even during the summer and fall periods. In fact, while $CaCO_3$ was undersaturated (S.I. = -0.27) and $FeCO_3$ and $MnCO_3$ were slightly oversaturated (S.I. = 0.225 and 0.343) in the upper portion of the sediment at SAT1 in January (Figure 4.2a), $CaCO_3$ was slightly oversaturated (S.I. = 0.27) and $FeCO_3$ and $MnCO_3$ were both supersaturated (S.I. = 1.74, and 1.94) deeper in the same sediments, suggesting that precipitation of carbonate phases controls the pH in the upper estuary. Interestingly, the

excessively low pH values measured at SAT3 in November (Figure 4.5) correspond to an intense period of Fe(III) reduction (Figure 4.3b), further supporting the hypothesis that the precipitation of carbonate minerals controls the pH of the pore waters. In turn, $CaCO_3$, $FeCO_3$, and $MnCO_3$ remained undersaturated in both the surface (S.I. = -0.41, -0.52, and -0.80) and deep sediments (S.I. = -0.08, -1.92, and -0.50) at SAT4, suggesting that carbonate precipitation was not significant in the lower estuary. Instead, the more significant increase in DIC, $Fe(II)_d$, and Mn(II) concentrations as a function of depth in the pore waters of SAT1 and SAT2 compared to SAT3, SAT4, and SAT5 suggest that SO_4^{-2} reduction is more likely responsible for removal of Fe(II) in the lower estuary. Overall, these findings suggest that the solid Fe(III) content of the upper estuary sediments is controlled by the high deposition of Fe(III) hydroxides flocculating from the water column while the solid Fe(III) content of the lower estuary is regulated by a combination of low deposition and high consumption, mainly by reduction with sulfides.

4.4.3. Composition of dissolved Fe(III) in the pore waters

While NOM/Fe colloids originating in the overlying estuarine waters may serve as the precursors to the Fe that eventually flocculates to the sediments, diagenetic processes must disturb the established equilibrium between the mineral aggregates and the pore waters, resulting in the accumulation of $Fe(III)_d$ either in the form of colloidal aggregates or true complexes. Several lines of experimental evidence suggest that dissolved Fe(III) in the pore waters consists of truly dissolved organic complexes. First, absorbance at 254 nm represents a good proxy for DOC measurements in systems with high humic content because of the dominance of UV absorbing aromatic chromophores

in DOM (Chin et al., 1994; Chin et al., 1998). Although the Ferrozine technique used to measure $Fe(III)_d$ cannot distinguish between truly dissolved and colloidal particles (Pullin and Cabaniss, 2001), the good correlation between UV absorbance and $Fe(III)_d$ (R^2 = 0.72) during the November 2007 and January 2008 cruises (Figure 4.7) supports the notion that organic matter controls dissolved sedimentary Fe(III) in Satilla estuarine sediments. The entire data set (Figure 4.7) can be fitted to the linear equation:

$$Abs(254nm) = 98\ (\pm 10)\ m^{-1} + 0.82\ (\pm 0.04)\ m^{-1}\ (\mu M\ Fe(III)_d)^{-1} \quad (4.3)$$

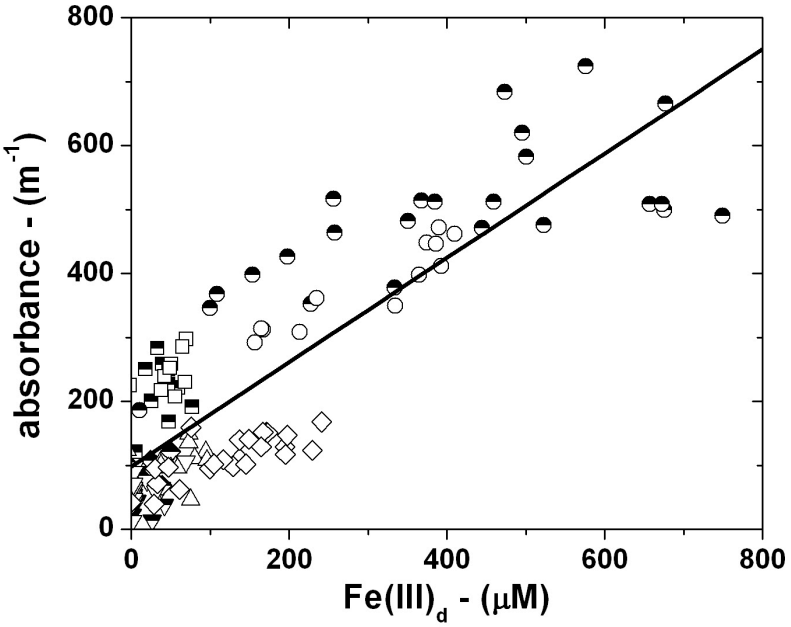

Figure 4.7 - Correlation between absorbance at 254 nm and $Fe(III)_d$ content of pore waters for the months of Nov. 2007 and Jan. 2008 provides evidence for the organic complexation of dissolved ferric iron. A linear fit through the data is also shown. Symbols represent stations as follows: SAT1 (circles), SAT2 (squares), SAT3 (triangles), SAT4 (upside-down triangles), and SAT5 (diamonds). Fill pattern indicates month: Nov. 2008 (open), Jan. 2008 (half-filled).

The non-zero intercept suggests some excess UV absorbing chromophores not bound to Fe at 254 nm exist in the pore waters. The intercept determined for each individual station decreases towards the mouth of the estuary (data not shown), consistent with the expectation that less DOM is delivered to the sediment downriver. Second, for Fe(III) to react at a voltammetric microelectrode at circumneutral pH, it must be small enough to diffuse to the electrode surface (less than a few nm; Buffle and Horvai, 2000; Taillefert et al., 2000). Indeed, CLE-ASV experiments previously conducted in Satilla River sediments demonstrated that the majority of dissolved Fe(III) in the pore waters is in fact truly dissolved and complexed to organic ligands (Jones et al., 2011). Finally, HP-SEC experiments (Figure 4.5, Table 4.1) indicate that Fe(III) complexes may carry net positive charges that may interfere with the slightly negatively charged Superdex resin. On the other hand, pore water Fe(II) elutes sooner than inorganic Fe(II) controls, as expected for higher molecular weight complexes, and simultaneously displays higher absorbance at 254 nm, suggesting that it is likely complexed to organic ligands in these pore waters (Figure 4.5b, Table 1).

4.4.4. Formation of soluble Fe(III) in Satilla estuarine sediments

Near millimolar levels of $Fe(III)_d$ are observed in Satilla River sediments, concentrations which exceed any previously measured concentrations for pristine, circumneutral pH environments (Table 3). The highest concentrations measured previously (Luther et al., 1996) were observed under highly saline, acidic conditions (pH 4.5). While relatively high concentrations (~700 μM) were measured in salt marsh creek sediments (Koretsky et al., 2008), where macrophytes provided organic ligands and/or dissolved $O_{2(aq)}$ for

Fe(II) oxidation and complexation of Fe(III), the Satilla River estuarine sediments harbor few plants and instead receive detritus primarily from upstream and surrounding marsh areas (Otero et al., 2000). As mixing with overlying waters cannot explain the distribution of these complexes in these sediments, the source of such high subsurface concentrations of $Fe(III)_d$ at depth must therefore have a biogeochemical origin within the sediment.

Table 4.3 - Previously observed Fe(III) concentrations in natural samples.

Reference	Environment	Maximum $Fe(III)_d$ conc (uM)	Max depth (cm)
Liang et al. 1993	Coastal plain aquifer	~40	~200
Luther et al. 1996	Vegetate mid-salt marsh	1255	6 - 8
Koretsky 2006	Lake	~250	10 - 20
Koretsky et al. 2007	Fen	~200	5 - 20
Koretsky et al. 2008	Salt marsh: vegetated creek	~700	15 - 45
Morrison & Aplin 2009	Artificial wetland	~300	0 - 6
This work	Blackwater estuary	996	7 - 8

In the presence of natural organic ligands, the oxidation of $Fe(II)_d$ by $O_{2(aq)}$ advectively transported into the sediments could explain the correlation between $Fe(III)_d$ and absorbance at 254 nm (Figure 4.7). The production of these complexes as deep as 10 cm in the sediment (e.g. Figure 4.2a), however, cannot be explained by oxygenation of organic-Fe(II) complexes, as dissolved $O_{2(aq)}$ is never detected below a few mm in Satilla estuarine sediments and $O_{2(aq)}$ uptake fluxes are far less than the outward fluxes of reduced metal species (Meiggs and Taillefert, 2011). Oxidation of Fe(II) by Mn(IV) would require surface contact, and the reduction of Mn(IV) coupled to $Fe(II)_d$ oxidation should produce $Mn(II)_d$ concentrations at least half as high as $Fe(III)_d$ concentrations.

Mn(II), however, is only detected sporadically (Meiggs and Taillefert, 2011) while $Fe(III)_d$ is ubiquitous in Satilla River sediments. Similarly, NO_3^- concentrations are not high enough in Satilla estuarine sediments to explain the production of such elevated $Fe(III)_d$ concentrations (Jahnke et al., 2003).

Interestingly, the formation of high concentrations of $Fe(III)_d$ in incubations and in sediments could result from the chelation pathway proposed to be used during DIR (Figure 1.1d). As production of endogenous organic ligands has been demonstrated with this organism in a process proposed to non-reductively dissolve Fe(III) to make it bioavailable for respiration (Chapter 6 of this thesis; Fennessey et al., 2010; Jones et al., 2010), it is possible that the organic-Fe(III) complexes detected in Satilla River sediments may be generated endogenously by Fe(III)-reducing microorganisms. This mechanism may assist Fe(III)-reducing microorganisms in destabilizing Fe(III) hydroxides (Chapter 7 of this thesis) or overcoming physical blocking by NOM coating the mineral aggregates (Borch et al., 2007). In turn, generation of microbial metabolites is likely costly to the organisms suggesting that the organic chelator should be recycled efficiently. Several pieces of evidence, however, indicate that the organic ligand complexing the $Fe(III)_d$ is not recycled nor of microbial origin. First, organic-Fe(III) complexes accumulate continuously during the sediment incubations in contrast to what is observed with pure cultures of the genus *Shewanella* (Chapter 7 of this thesis; Jones et al., 2011), suggesting that these complexes are not direct intermediates in the microbial reduction of Fe(III) hydroxides. More importantly, SEC separations indicate that most Fe(II) is complexed by organic ligands in natural pore waters, implying that the $Fe(III)_d$ complexing ligand is

not recycled. These findings suggest that the organic-Fe(III) complexes formed in these sediments is not only composed of bacterially-generated ligands, but also DOM.

Instead, the high concentration of DOM in these sediments may play an important role in the generation of organic-Fe(III) complexes. DOM contains many oxygen-containing functional groups which are predicted to rapidly complex Fe(II) (Luther et al., 1992), and DOM-Fe(II) complexes are abundant in pore waters (Hakala et al., 2009). In fact, a correlation between DOC and $Fe(II)_d$ in sediments has been attributed to the release of adsorbed DOC from Fe(III) oxides under reducing conditions (Chin et al., 1998). In Satilla River sediments, the non-zero intercept of the correlation between absorbance at 254 nm and dissolved Fe(III) (Figure 4.7) indicates that organics are present in excess in these sediments. Combined with the existence of Fe(II) organic complexes in Satilla River sediments (Figure 4.6b), these findings suggest that the reductive dissolution of POM-Fe(III) aggregates, originating in the water column, releases DOM to complex Fe(II) and any eventual Fe(III) present in solution. Accordingly, solid Fe(III) minerals may rapidly oxidize DOM-Fe(II) complexes as chelating ligands may lower the reduction potential of the Fe(III)/Fe(II) couple by stabilizing Fe in the +III oxidation state (Boukhalfa and Crumbliss, 2002; Luther et al., 1992). Oxygen anions in the carboxylate functional groups abundant in DOM essentially push electron density towards the Fe(II), and π orbital overlap between the HOMO of the Fe(II) and the LUMO of Fe(III) allow for outer-sphere electron transfer to the solid Fe(III) (Eq. 4.4, where * indicates the same Fe atom, with DOM in excess; modified from Luther et al., 1992):

$$FeOOH + H^+ + {}^*Fe^{2+}(DOM) \xrightarrow{DOM} {}^*Fe^{3+}(DOM) + Fe^{2+}(DOM) + 2OH^- \qquad \text{(Eq. 4.4)}$$

As reactive Fe(III) minerals are abundant throughout the entire sediment column, this reaction is expected to proceed rapidly within the zone of Fe reduction. Indeed, pore water profiles of $Fe(III)_d$ in Satilla River sediments suggest that $Fe(III)_d$ is produced within the zone of reduction (e.g. Figure 4.2b) and diffuses upwards. This is consistent with eq. 4.4, in which Fe_d concentrations through the sediment column should increase while $Fe(II)_d$ concentrations should remain relatively constant (Luther et al, 1992), and possibly confined to a more localized depth increment. Additionally, $Fe(III)_d$ accumulated under Fe(III)-reducing conditions in sediment slurry incubations amended with a model Fe(III)-reducing microorganism, *S. putrefaciens*, but at higher concentrations in the presence of exogenous Fe(III) hydroxides (Figure 4.6), again consistent with the reaction in equation 4.4.

After removal of the solid phase, $Fe(III)_d$ was used as an electron acceptor alternative to Fe(III) (oxy)hydroxides in incubations with *S. putrefaciens*. As dissolved Fe(III) complexes are generally reduced faster than solid Fe(III) substrates by Fe(III)-reducing bacteria (Dollhopf et al., 2002; Haas and DiChristina, 2002), these complexes may be preferentially consumed, generating high concentrations of $Fe(II)_d$. Interestingly, $Fe(III)_{volt}$ correlates more closely with $Fe(II)_d$ than with $Fe(III)_d$ in both incubations (Figure 4.6) and sediments (Figure 4.2a). While this observation may seem counterintuitive, it can be explained if an endogenous ligand is secreted by Fe(III)-reducing microbes to displace the DOM from the DOM-Fe(III) complex and form a voltammetrically labile org-Fe(III) complex recognizable to the bacterium, analogous to pure culture incubations with *S. putrefaciens* and ferric citrate (Chapter 7 of this thesis). Ultimately, Fe(II) released from solid Fe(III) mineral aggregates may be efficiently

complexed by the excess DOM, thereby catalyzing a suboxic Fe cycle (Luther et al., 1992) that is illustrated in figure 4.8. Regardless of the production mechanism, these findings have important implications for biogeochemical processes in estuarine environments. Several studies have demonstrated that dissolved Fe(II) produced as a result of Fe(III)-reducing bacteria activity may flux from marine sediments (Elrod et al., 2004; Homoky et al., 2012) but usually precipitate immediately above the sediment water interface or adsorb to resuspended particles in the water column. Recently, however, org-Fe(III) complexes (Jones et al., 2011) and dissolved Fe with isotope signatures consistent with the non-reductive dissolution of Fe(III) oxides (Homoky et al., 2013) have been demonstrated to flux out of shelf sediments and remain stable in oxic seawater. These complexes may eventually be transported to continental shelves and provide a non-negligible source of Fe to phytoplankton.

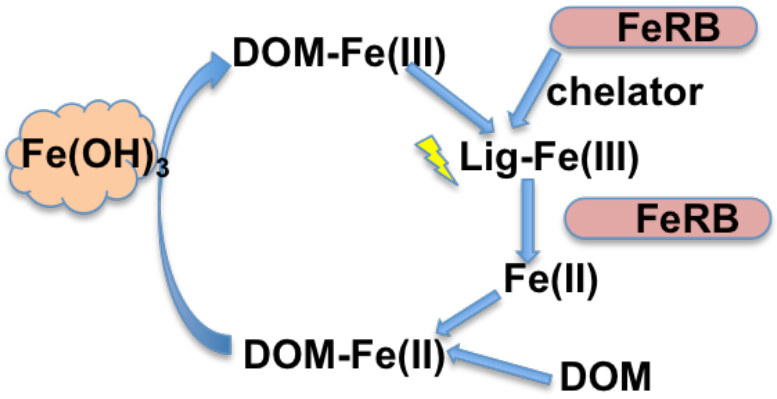

Figure 4.8 – Proposed mechanism for Fe(III) reduction in organic rich sediments: 1) DOM-Fe(II) is oxidized by Fe(III) (oxy)hydroxides; 2) FeRB secrete an endogenous chelator which displaces the DOM from the Fe(III), forming a voltammetrically labile org-Fe(III) complex; 3) the org-Fe(III) complex is reduced by the FeRB, recycling the biogenic ligand; 4) Excess DOM binds the Fe^{2+} and the cycle restarts.

4.5. Conclusions

In this study, the source and composition of dissolved Fe(III) (< 0.2 μm) produced in the sediments of an estuary fed by a blackwater river were investigated. Fe(III), likely under the form of terrestrially-derived DOM-Fe(III) complexes, flocculates in varying degrees during mixing with seawater and settles to the sediment-water interface to generate high concentrations of poorly-crystalline Fe(III) and some of the highest concentrations of dissolved Fe(III) ever reported in marine sediments. Overall concentrations Fe(III) hydroxides and dissolved Fe(III) in the sediments decrease towards the mouth of the estuary, likely by the combined decline in supply of Fe(III) hydroxides from the water column and increase in SO_4^{2-} reduction in these sediments. Both UV absorbance and voltammetric measurements provide evidence that a significant proportion of dissolved Fe(III) in these pore waters is truly dissolved (non-colloidal) under the form of organic-Fe(III) complexes. These complexes were simultaneously produced during microbial Fe(III) reduction in sediment incubations and used as electron acceptor in incubations conducted in the absence of solid phases. Finally, size exclusion chromatographic separations followed by the redox speciation of the separated fractions revealed that these organic-Fe(III) complexes are highly particle reactive and that Fe(II) produced in the pore waters is mainly in the form of organic complexes. As the endogenous production of organic ligands by Fe(III)-reducing microorganisms likely costs energy to the organisms, the ligands should be recycled efficiently to non-reductively dissolve more Fe(III) oxides rather than remain immobilized as Fe(II) complexes. These considerations suggest that the org-Fe(II) complexes are not produced during microbial Fe(III)-reduction and result instead from the complex interaction

between Fe(III) (oxy)hydroxides, DOM, and Fe(II). It is proposed that DOM-Fe(II) complexes, formed by complexation of DOM to Fe(II) produced by Fe(III)-reducing microorganisms in the freshwater end of the estuary, are oxidized by solid phase Fe(III) hydroxides, to generate soluble organic-Fe(III) complexes in the pore waters that may diffuse across the sediment-water interface and eventually reach the continental shelf. It is important to determine whether the production of such high concentrations of dissolved Fe(III) in pore waters is unique to blackwater rivers to evaluate their impact on a global scale.

4.6. Acknowledgements

The authors would like to thank Deidre Meiggs, Keaton Belli, Jason Peart, Wellington Merrit, and Patrick Wilson for help with sampling and analysis, as well as the Captain and crew of the R/V *Savannah* for their patience during the cruises.

CHAPTER 5

IMPORTANCE OF MICROBIAL IRON REDUCTION IN DEEP SEDIMENTS OF RIVER-DOMINATED CONTINENTAL-MARGINS

J.S. Beckler, N. Kiriazis, C. Rabouille, F.J. Stewart, M. Taillefert
To be submitted to Marine Chemistry

Abstract

Remineralization of organic carbon in deep-sea sediments is thought to proceed primarily via aerobic respiration and sulfate reduction because the supply of nitrate and metal oxides is not usually significant in deep-sea sediments. Dissimilatory metal reduction, on the other hand, may represent a dominant pathway in coastal and continental shelf sediments where delivery of terrigenous Fe and Mn oxides is sufficiently high or mixing processes near the sediment-water interface recycle these minerals efficiently. Passive continental margin sediments receiving outflow from large rivers are well-known deposition centers for organic carbon, but may also be hotspots for metal-reducing microbial activity considering the simultaneous high deposition rates of unconsolidated metal oxides of terrigenous origin. Metal reduction processes in these environments, however, are often neglected as aerobic and sulfate reduction are usually considered to be more important in these sediments. To investigate carbon remineralization processes in these environments, shallow sediment cores across various channels and levees in the Congo River fan (~5,000 m) and Louisiana slope (<1,800 m) were profiled for the main

redox species involved in early diagenesis. Interestingly, metal reduction dominated carbon remineralization processes in the top ~20 cm of sediment subject to high deposition, while evidence for sulfate reduction was lacking. These findings suggest that dissimilatory iron reduction may be more significant than previously thought in continental slope sediments which may have important implications on carbon cycling in marine environments, atmospheric oxygen levels over geological time, and the evolution of microbial life on Earth.

5.1. Introduction

The magnitude and lability of organic carbon (C_{org}) exported to marine sediments is generally inversely related with the depth of the overlying waters, due to increasing exposure time of marine and terrestrially derived C_{org} to degradation processes and decreasing terrestrial inputs further from shore (Hedges et al., 1997; Honjo et al., 2008). In deep-sea sediments, where the flux and lability of organic carbon are usually low, C_{org} oxidation is coupled almost entirely to the reduction of $O_{2(aq)}$ (the most thermodynamically favorable TEA) which may penetrate deeper than 1 meter into sediments (Bowles et al., 2014) Bender and Heggie, 1984; Cai and Reimers, 1995; Grundmanis and Murray, 1982; Rabouille and Gaillard, 1991), while anaerobic respiration processes such as dissimilatory NO_3^-, Fe(III), Mn(IV), or SO_4^{2-} reduction are relatively minimal or have little impact on carbon transformation (Jorgensen, 1982; Slomp et al., 1997). On the other hand, high C_{org} remineralization rates in coastal sediments with higher deposition rates result in $O_{2(aq)}$ being consumed faster than it can diffuse into sediments. C_{org} remineralization then proceeds primarily through SO_4^{2-}

reduction (Jorgensen, 1982) or through Fe(III) or Mn(IV) reduction (Meiggs and Taillefert, 2011; Thamdrup et al., 2000) if the areas receive significant terrigenous minerals (i.e. > 30 μmol cm^{-3} reactive Fe; Thamdrup et al., 2000) and their reduced products, Fe^{2+} and Mn(II), are reoxidized by advection or macrofaunal bioturbation (Aller and Blair, 2006; Canfield et al., 1993; Jensen et al., 2003; Taillefert et al., 2007b; Thamdrup et al., 2000). Relative to regions dominated by aerobic respiration, these regions may represent preservation centers (i.e. burial sites) for C_{org}, as C_{org} may be deposited faster than it may be processed by benthic microorganisms (Canfield, 1994), and it is hypothesized that anaerobic respiratory processes are less efficient at processing the more refractory, terrestrially derived C_{org} fraction (Hedges and Oades, 1997).

To better constrain global C budgets, total C_{org} remineralization rates and extents should be quantified in sediments from a variety of locations, depositional environments, and circulation regimes (Thullner et al., 2009). Interestingly, relatively high rates of C_{org} deposition have been observed in the deep-sea sediments in specific regions at the base of continental slopes (Haese et al., 2000; Law et al., 2009; Rabouille et al., 2009; Schulz et al., 1994), and in sediments underlying waters where local circulation features may stimulate C_{org} deposition, including upwelling regions (Ferdelman et al., 1999; Haeckel et al., 2001; Thamdrup and Canfield, 1996), semi-enclosed basins (Lee et al., 2008), and even in the deepest trench on earth (Glud et al., 2013), suggesting mineralization may proceed anaerobically and that these areas could represent significant C_{org} burial sites (Canfield, 1994). Interestingly, only a few studies have examined the role of microbial metal reduction in C_{org} remineralization in these environments (Haese et al., 2000; Law et al., 2009; Nedelec et al., 2007; Thamdrup and Canfield, 1996; van der Zee et al., 2002).

In river-dominated ocean margins (RiOMars), large rivers may discharge suspended sediment and C_{org} much further than in their deltas and, in turn, exert a dominant control on sediment biogeochemistry down continental slopes or even in deep-sea fans underlying slopes (McKee et al., 2004). Because of their proximity to land, these regions may also accumulate labile Fe(III) and Mn(IV) minerals, allowing C_{org} remineralization to proceed suboxically. For instance, the Louisiana slope (LAS) is subject to frequent mass slumping of spillover mud discharged from the Mississippi River (Bea et al., 1983; Bianchi et al., 2006) and produces unconsolidated clay and C_{org} rich deposits mid-slope at 1,000 m depth (Coleman et al., 1998; Dixon and Weimer, 1998; Konyukhov, 2008). On the other hand, the Congo River Fan (CRF) presents the unique geological feature that it is the only deep-sea fan in the world still directly connected to a large river through a submarine canyon (Babonneau et al. 2002). In this system, frequent turbidite flows deliver C_{org} rich mud and clay-sized particles to the abyssal plain at depths approaching 5,000 m water depth (Babonneau et al., 2002; Rabouille et al., 2009).

As SO_4^{2-} reduction is able to remineralize two carbons per mole of sulfate with acetate as an example of an electron donor (Eq. 5.3), while two moles of Mn(IV) and four moles of Fe(III) are required to remineralize one mole of carbon (Eq. 5.1 and 5.2), it is important to assess which of these anaerobic processes dominates in continental slope sediments:

$$CH_3COOH + 8Fe(OH)_3 + 14H^+ \rightarrow 8Fe^{2+} + 2HCO_3^- + 20H_2O \qquad \text{(Eq. 5.1)}$$

$$CH_3COOH + 4MnO_2 + 6H^+ \rightarrow 8Mn^{2+} + 2HCO_3^- + 4H_2O \qquad \text{(Eq. 5.2)}$$

$$CH_3COOH + SO_4^{2-} \rightarrow HS^- + 2HCO_3^- + H^+ \qquad \text{(Eq. 5.3)}$$

Unfortunately, measurement of the reduced products of anaerobic respiration cannot be used to quantify metal or SO_4^{2-} reduction, as metal oxides may also be reduced abiotically by ΣH_2S (Eq. 5.4 and 5.5) and ΣH_2S may also be removed from pore waters by precipitation with Fe^{2+} (Eq. 5.6):

$$2Fe(OH)_3 + HS^- + 5H^+ \rightarrow 2Fe^{2+} + S^0 + 6H_2O \quad \text{(Eq. 5.4)}$$

$$MnO_2 + HS^- + 3H^+ \rightarrow Mn^{2+} + S^0 + 2H_2O \quad \text{(Eq. 5.5)}$$

$$HS^- + Fe^{2+} \leftrightarrow FeS_{aq} + H^+ \rightarrow FeS_{am} \quad \text{(Eq. 5.6)}$$

In addition, changes in SO_4^{2-} concentrations may be too small to be detected in seawater. As a result, geochemical methods to determine whether reduction of metal oxides is microbial or abiotic have yet to be optimized. The development of gold/mercury (Au/Hg) voltammetric microelectrodes for the measurements of depth profiles of the main redox species in sediments (Brendel and Luther, 1995; Luther et al., 2008a; Taillefert et al., 2000b) may offer a unique advantage over more conventional methods with respect to the detection of SO_4^{2-} reduction by being able to detect both ΣH_2S as well as aqueous $FeS_{(aq)}$ clusters (Rickard et al., 1999). These clusters are in equilibrium with an amorphous FeS_{am} solid which eventually converts to mackinawite (FeS_s; Rickard and Morse, 2005; Theberge and Luther, 1997) and are also expected to be precursors to pyrite mineral formation (Rickard, 1997). In addition, Au/Hg voltammetric microelectrodes are able to detect organic complexes of Fe(III) (Taillefert et al., 2000a) which are pervasive in coastal sediments dominated by metal reduction (e.g. Jones et al., 2011; Meiggs and Taillefert, 2011; Taillefert et al., 2002a; Taillefert et al., 2007b; Taillefert et al., 2002b). As the reactivity of these complexes with ΣH_2S is extremely fast (Taillefert et al., 2000a),

their presence in pore waters should provide additional evidence that SO_4^{2-} reduction is not a dominant sediment process.

In this study, redox metabolites in both the dissolved and solid phases were profiled as a function of depth along a transect of 4 stations extending from the hypoxic shelf to the base of the slope outside the hypoxic zone in the LAS, and from 3 stations comprising a lateral transect from an extinct canyon of the CRF to the present day channel currently receiving massive terrigenous deposits. These data were used to determine whether SO_4^{2-} reduction is outcompeted by dissimilatory metal reduction in deep RiOMar sediments receiving significant C_{org} inputs.

5.2. Study sites

Sediment cores (9.6 cm ID x 70 cm) from the LAS were obtained using a multicorer (MC-800, Ocean Instruments) during a cruise on the R/V *Cape Hatteras* (University System of North Carolina, NC) in June 2012. Sediments were collected across a depth transect from the hypoxic continental shelf (stations GOM2, 65 m and GOM3, 128 m) to the middle of the continental slope outside the hypoxic zone (GOM12, 980 m), and finally at the base of the slope (GOM12, 1777 m) (Figure 5.5.1a). These stations were selected to represent areas where SO_4^{2-} reduction is active (hypoxic zone) in addition to slope sediments where metal reduction may dominate. Sediment cores (9.6 cm ID x 70 cm) from the Congo River fan (CRF) were obtained using a multicorer from 3 stations approaching 5,000 m depth and up to 800 km offshore (Figure 5.5.1b) during a cruise on the N/O *Pourquoi Pas?* (Ifremer, Brest, France) from December 2011 to January 2012. Stations are located along a transect from an extinct channel no longer

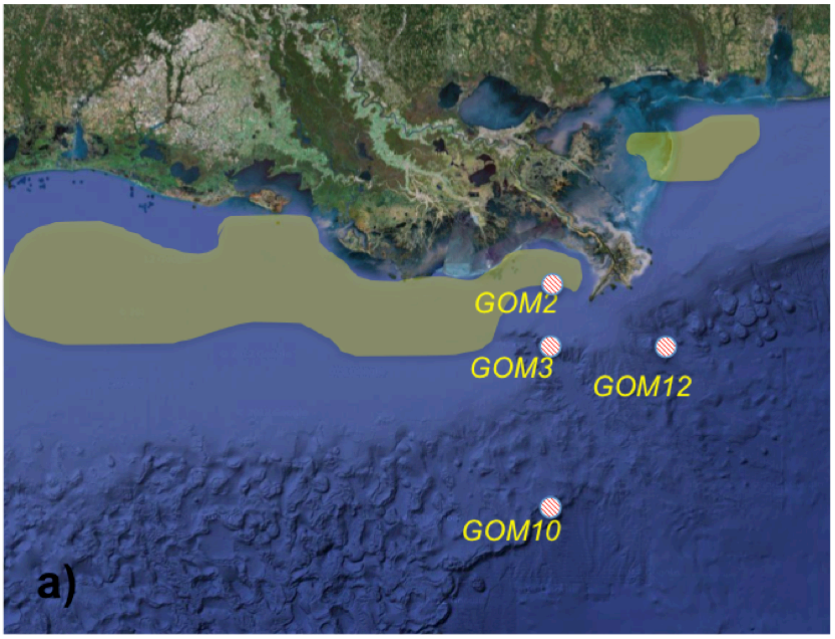

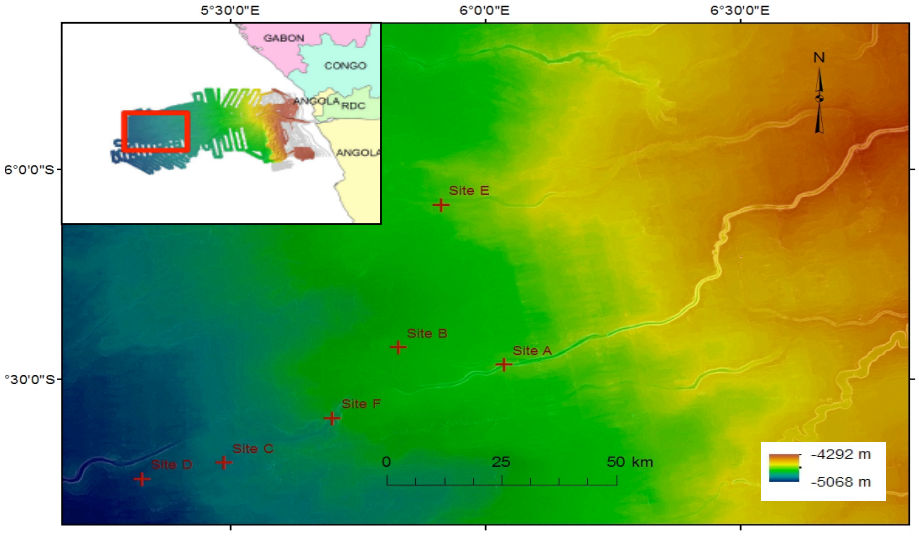

Figure 5.1 – Maps of sediment core locations on a) the Louisiana slope, with the typical hypoxic zone shaded yellow, and b) the Congo River Fan including the high resolution bathymetry obtained at the site during the same cruise (courtesy of Laurence Droz, ©Ifremer, Congolobe cruise).

receiving turbidite flows (CoLE, 4750 m), to a station ~10 km north from the active channel (CoLB, 4823 m), and to a station directly on the present channel levee (CoLA, 4759 m).

5.3. Methods

5.3.1. Analyses

Depth profiles of dissolved $O_{2(aq)}$, Fe^{2+}, organic-Fe(III) complexes, ΣH_2S ($=H_2S+HS^-+S(0)+S_x^{2-}$) , aqueous FeS clusters ($FeS_{(aq)}$), and pH were obtained using solid-state Au/Hg voltammetric microelectrodes (Luther et al., 2008b; Taillefert et al., 2000b) and needle combination pH microelectrodes immediately after retrieval of intact cores (Meiggs and Taillefert, 2011). Both measurements were conducted with an Analytical Instrument Systems, Inc. (AIS, Inc.) DLK-100 potentiostat. The pH microelectrode purchased for this application included a 10 cm long needle of 1.6 mm diameter beveled at the end to protect the bulb of the electrode (Microelectrodes, Inc.). The pH microelectrode was calibrated before each profile using TRIS buffer in synthetic seawater (Dickson, 1993). Voltammetry was conducted in a three-electrode configuration with an Ag/AgCl reference electrode and a Pt counter electrode. Working microelectrodes made of 100 μm gold wire (GoodFellow Corp.) soldered to the copper wire of a coaxial cable with BNC connector were encased in pyrex glass with a tip of 5 cm long and $\leq$ 1 mm diameter and sealed with marine epoxy (West Marine) as previously reported (Brendel and Luther, 1995; Luther et al., 1999). Reference and counter electrodes were made similarly by encasing 1 mm diameter Ag wire and 0.5 mm Pt wire in 3 mm diameter PEEK tubing sealed with marine epoxy, letting the wire protrude from the casing by

about 1 cm. The AgCl coating was formed on the Ag reference electrode by applying +9V between the Ag wire and the Pt electrode in a KCl saturated solution, and the AgCl coated wire was encased in a KCl solution with a porous glass frit (BioAnalytical Systems, Inc.) for contact with the outside solution (Brendel and Luther, 1995). The working voltammetric microelectrodes were plated with Hg by maintaining the electrode at -0.2 V for 4 minutes in a 0.1 M $Hg(NO_3)_2$ solution in 2% HNO_3. Au/Hg microlectrodes were then polarized at -9V for 90 seconds to ensure a better penetration of the mercury into the gold (Brendel and Luther 1995). They were then calibrated in a $MnCl_2$ solution (0 to 400 μM), and the pilot ion method was used to calculate concentrations of Fe^{2+} and ΣH_2S in the pore waters (Luther et al., 2008). Dissolved oxygen was calibrated *in situ* with the salinity and temperature of the overlying waters, assuming they were at saturation. As the voltammetric response of org-Fe(III) complexes and $FeS_{(aq)}$ cannot be quantified because their exact chemical composition is unknown, their response is directly reported in peak current intensities (Taillefert et al., 2000b). To compare the signal intensities of these species measured at different electrodes, each electrode's response to Mn^{2+} was normalized to a typical Mn^{2+} response, and this ratio was used to adjust the current response of the unquantifiable analytes.

Sediment cores were kept on ice while profiling to maintain *in situ* temperatures. The pH and Au/Hg voltammetric microelectrodes were affixed to a micromanipulator capable of sub-millimeter increments (AIS, Inc.), while Ag/AgCl reference and Pt counter electrodes were kept in the overlying waters. At each depth, $O_{2(aq)}$ was measured by linear sweep voltammetry (LSV) between -0.1 and -1.85 V with a conditioning period of 10 s at -0.1 V. All other species were measured by CSW voltammetry using a 200

mV/s scan rate and a preconditioning time of 10 s at -0.1 V. If dissolved sulfides or soluble org-Fe(III) signals were detected, an additional cleaning step at -0.9V for 10 s was added to clean the electrode surface between each measurement (Luther et al., 2008b; Taillefert et al., 2000b). At the end of each profile, the electrodes were returned to the overlying waters to ensure they provided the same $O_{2(aq)}$ and pH signals as before deployment. Peak heights and surface area were determined using a semi-automated VOLTINT software package (Bristow and Taillefert, 2008).

A few sediment samples from the surface ~20 cm of LAS cores were then frozen in ziplock bags (-80 °C) and shipped on dry ice to Georgia Tech for solid-phase Fe speciation. Sediment cores from the CRF, on the other hand, were sectioned onboard under N_2 atmosphere and at 4 °C in slices of approximately 7 mm, and each section was centrifuged under N_2 atmosphere for about 20 minutes at 3,000 RPM to extract pore waters. Pore waters were then immediately filtered onto 0.2 μm Whatman Puradisc syringe filters under N_2 atmosphere, and analyzed or preserved within 30 minutes. The leftover sediment was frozen (-20 °C) in 50 mL tubes and shipped on dry ice to Georgia Tech. Soluble orthophosphates (ΣPO_4^{3-}) were measured spectrophotometrically using the molybdate-blue technique (Murphy and Riley, 1962). Dissolved inorganic carbon (DIC) was measured by flow-injection analysis (Hall and Aller, 1992). Finally, poorly crystalline and crystalline Fe were determined in triplicate by ascorbate and dithionite extractions with Ferrozine analysis (Kostka and Luther, 1994) back at Georgia Tech. Prior analyses demonstrated that Fe in FeS minerals represented an insignificant portion of Fe extracted by dithionite (data not shown).

5.3.2. Thermodynamic calculations and modeling

The saturation state of $FeS_{(aq)}$ clusters was determined to provide insight into the relative roles of Fe and SO_4^{2-} reduction in the sediments. The solubility of $FeS_{(aq)}$ is related to Fe^{2+} and HS^- concentrations by:

$$K_{sp} = \frac{\{Fe^{2+}\}\{HS^-\}}{\{H^+\}} \quad \text{(Eq. 5.7)}$$

Assuming measurements with Au/Hg voltammetry provide concentrations of H_2S and HS^- mainly, the fraction of ΣH_2S in the form of HS^- as a function of pH can be calculated with the Henderson-Hasselbalch approximation equation:

$$\alpha_{HS^-} = \frac{[HS^-]}{[\Sigma H_2S]} \quad \text{(Eq. 5.8)}$$

$$\alpha_{HS^-} = \frac{\{H^+\}K_1}{\{H^+\}^2 + \{H^+\}K_1 + K_1K_2} \quad \text{(Eq. 5.9)}$$

Combining equations 5.7, 5.8, and 5.9, the equilibrium concentration of total dissolved sulfides can be calculated from the concentration of Fe^{2+} and the pH of the pore waters:

$$[\Sigma H_2S] = \frac{K_{sp}\{H^+\}}{\gamma_{Fe^{2+}}[Fe^{2+}]\cdot\gamma_{HS^-}\alpha_{HS^-}} \quad \text{(Eq. 5.10)}$$

Acid-base equilibrium constants (pK_{a1} and pK_{a2}) of 6.8 and 17.0 (Davison, 1991) and a dissociation constant ($\log K_{sp}$) of -2.2 (Rickard, 2006) were used for these calculations. Values of the activities of the free HS^- and Fe^{2+} ions, γ_{HS^-} and γ_{Fe2+}, were calculated using Pitzer parameters for Fe^{2+} (Millero and Schreiber, 1982) and HS^- (Millero, 1983).

The freely available program SUPCRT92 (Johnson et al., 1992) was used to compare reaction favorabilities by calculating the ΔG^0_{rxn} at various pressures and temperatures using an updated thermodynamic database (slop07.dat) and amended with

the ΔG^0 (-705.2 kJ mol^{-1}), ΔH^0 (-827.1 kJ mol^{-1}), and ΔS^0 (122.2 J K^{-1} mol^{-1}) for hydrated 2-line ferrihydrite ($Fe(OH)_3$; Snow et al., 2013). A ΔV^0 of 42.96 cm^3 mol^{-1} was calculated using a unit cell volume of 71.33 $Å^3$ (from www.mindat.org), and Maier-Kelley heat capacity coefficients of a = 0, b = 0.016 cal K^{-2} mol^{-1}, and c = 0 were obtained by reproducing C_p data from Snow et al., 2013, and solving for the slope of the line of best fit through the region of temperatures between 270 and 302 K, i.e. those temperature relevant in the ocean. All energies were converted to calorie units as required by SUPCRT92. Deviations of the Gibbs free energy from non-standard state conditions at each of the new references states obtained from the SUPCRT92 output were then calculated using the reaction quotient determined from the activities of the reactants and products obtained with seawater activity coefficients from the literature (Millero and Schreiber, 1982) or calculated using Pitzer parameters for Fe^{2+} (Millero and Schreiber, 1982) and HS^- (Millero, 1983).

5.4. Results

5.4.1. Louisiana slope transect sediment biogeochemistry

The biogeochemistry of the sediments across the LAS shelf and slope were highly variable (Figure 5.2). The continental shelf and shelf break sediments displayed evidence of SO_4^{2-} reduction, while respiration in the slope sediments proceeded primarily through aerobic and metal reduction (athough denitrification cannot be ruled out as it was not measured). $O_{2(aq)}$ penetration depths increased with the overlying waters column depth, from < 1 mm at GOM2 (65 m), to ~ 3 mm at GOM3 (128 m), ~6 mm at GOM12 (980 m) and 10 cm in the sediments of GOM10 (1778 m) (Figure 5.2a, c, e, and g). Interestingly,

the pH of the overlying waters was between 7.5 and 7.7 at GOM2 and GOM3, but much higher (>8.3) at the offshore stations GOM12 and GOM10 suggesting that respiration processes in the hypoxic zone were responsible for the decrease in pH of the overlying waters (Figure 5.2b and d). Accordingly, bottom water $O_{2(aq)}$ saturation ratios as measured by CTD ~1 m above the SWI were low (55% and 52% at GOM2 and GOM3), but not hypoxic by definition (< ~30%). The CTD, however, is not capable of measuring $O_{2(aq)}$ directly at the SWI, which could have had lower values. Indeed, pH profiles always decreased more drastically in the zone of aerobic respiration, and then gradually decreased throughout the sediment column, reaching ~ 7.0 at GOM2 and GOM3 (Figure 5.2a and c) and between 7.5 and 8 at GOM12 and GOM10 (Figure 5.2e and g). Although ΣH_2S was never detected in any of the cores (MDL < 0.2 μM), a voltammetric current for molecular clusters of FeS was detected below 6 cm at GOM2 and throughout the sediment column at GOM3 (Figure 5.2b and d) but not at the deeper stations (Figure 5.2f and h). Simultaneously, dissolved Mn^{2+} was detected immediately below the sediment-water interface (SWI) at GOM2 (Figure 5.2a) and reached relatively constant concentrations > 300 μM by 3 cm. In turn, dissolved Fe^{2+} remained below detection limit (~20 μM), and voltammetric signals for soluble org-Fe(III) complexes were just above detection limit (~ 1 nA) throughout the sediment. At GOM3, Mn^{2+} was not detected until 4.5 cm depth where it reached similar concentrations as at GOM2, but eventually declined slightly in concentration below 12 cm, when Fe^{2+} and soluble org-Fe(III) complexes appeared in pore waters at a maximum concentration of 100 μM and current intensities of 55 nA (Figure 5.2c and d). Dissolved Mn(II) was detected 3 cm below the SWI at GOM12 (Figure 5.2e), eventually increasing to maximum concentrations of 1.9

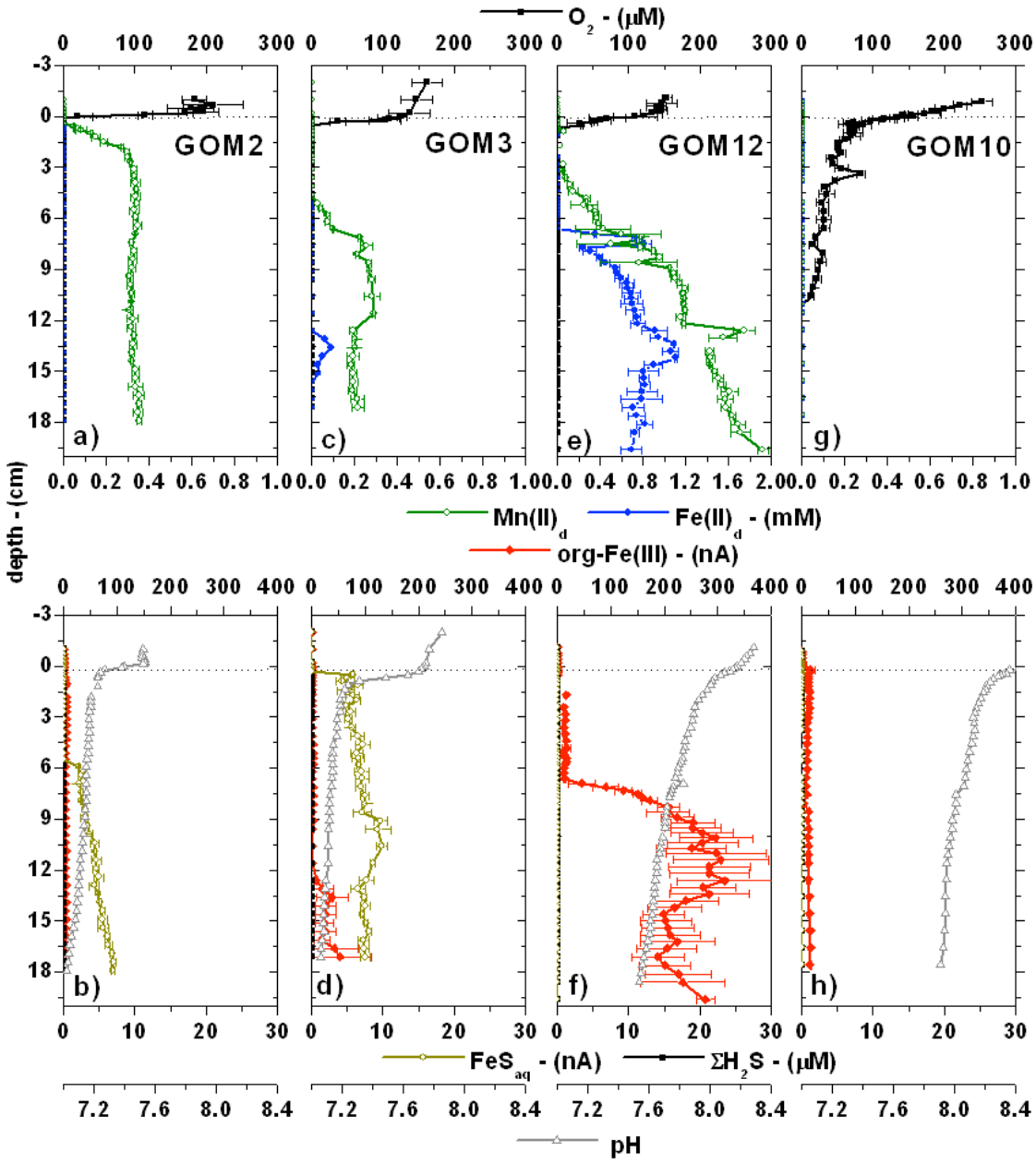

Figure 5.2 - Depth profiles of redox chemical species and pH in sediments collected during a transect from the shelf to the slope of the northern Gulf of Mexico from a) GOM2 (65 m); b) GOM3 (123 m); c) GOM12 (980 m); and d) GOM10 (1800 m). The transect reveals a transition from predominantly SO_4^{2-} reduction on the shelf (a - d), to metal reduction on the mid-slope (e - f), and finally to aerobic respiration at the base of the slope (g - h). Dissolved (NO_2^- + NO_3^-), ΣPO_4^{3-}, and DIC were not measured because the pore waters were not extracted from these sediments.

mM at 20 cm depth. In these sediments, dissolved Fe^{2+} and soluble org-Fe(III) complexes were produced below 6 cm and reached concentrations of ~1 mM and current intensities of ~300 nA within the first 20 cm depth (Figure 5.2e and f). Dissolved Mn(II) and Fe^{2+} were below detection limit (~15 and 20 μM) at GOM10, the deepest station of the LAS (Figure 5.2g), and small current Reactive Fe hydroxide (Fe_{reac}) concentrations, as determined by ascorbate-extraction, were 13.3 ± 3.8, 24.2 ± 4.0, and 11.5 ± 1.3 μmol/gdw in the top 10 cm at GOM2, GOM12, and GOM10, respectively (no data for GOM3), while crystalline Fe oxides (Fe_{crys}) concentrations, as determined by the difference between dithionite-extractable Fe and ascorbate-extractable Fe were 16.4 ± 9.8, 20.0 ± 14.1, 31.1 ± 7.1 μmol/gdw at the same stations.

5.4.2. Congo River fan sediments

Depth profiles of the main redox species, pH, DIC, and orthophosphate obtained at CoLA, CoLB, and CoLE in the CRF demonstrate the influence of canyon proximity on sediment biogeochemistry. CoLE is located in an extinct submarine canyon, no longer receiving turbidite deposits, and displays lower activity than CoLA, located at the base of the slope on the levee adjacent to the present day canyon, or CoLB, located between the two stations (Figure 5.1). While $O_{2(aq)}$ concentrations in the overlying waters were similar at each station (247 ± 12 μM at CoLE, 259 ± 7 μM at CoLB, and 261 ± 19 μM at CoLA), $O_{2(aq)}$ gradients were progressively sharper from CoLE, where the $O_{2(aq)}$ penetration depth reached 7 cm (Figure 5.3a), to CoLB with a penetration depth of 1.2 cm (Figure 5.3d), and finally to CoLA with a penetration depth of 8 mm (Figure 5.3g). Concentrations of NO_x (NO_3^- + NO_2^-) were also generally similar in the overlying waters of each station (21

μM at CoLE, 23.4 μM at CoLB, and 28 μM at CoLA), but their profiles in the sediment were completely different. At CoLE, NO_x concentrations increased slightly to 25.6 μM at a depth of 7.5 mm, but were below detection limit (< 1 μM) by 9 cm depth (Figure 5.3a). At CoLB, NO_x concentrations decreased to below detection limit by 1.3 cm before rebounding deeper to form a small peak centered at 5 cm with maximum concentrations of 28 μM. They remained below the detection limit deeper than 7 cm (Figure 5.3d). Finally, NO_x^- at CoLA was initially removed from the pore waters as at CoLB, but increased below 1.8 cm to as high as 100 μM at 4.5 cm depth, before decreasing to below detection limit at 7.5 cm (Figure 5.3g). Interestingly, Mn^{2+} was never detected in CRF sediments, suggesting that its involvement in early diagenesis is not significant. In turn, dissolved Fe^{2+} and org-Fe(III) complexes were pervasive in the active canyons (CoLA and CoLB) (Figure 5.3e and h) but not the extinct canyon (CoLE) where they were below detection limit throughout the profile (Figure 5.3b). Dissolved Fe^{2+} was produced just below the first NO_x^- minimum at CoLB (up to 116 μM at 1.8 cm), then slowly decreased down to below detection limit between 6 and 9 cm, before increasing progressively to concentrations as high as 240 μM at a depth of 14 cm (Figure 5.3e). In the same pore waters, currents for org-Fe(III) complexes were not observed until the zone of maximum Fe^{2+} production, where they were concomitantly produced in current intensities ranging between 126 and 186 nA (Figure 5.3e). Interestingly, the onset of Fe^{2+} production overlapped with the maximum zone of NO_x^- production at CoLA, and reached concentrations of ~700 μM by11 cm depth (Figure 5.3h). As at CoLB, organic-Fe(III) complexes at CoLA were also formed in the zone of Fe(III) reduction but about 1 cm below the onset of Fe^{2+} production only (~4 cm). Current intensities for these

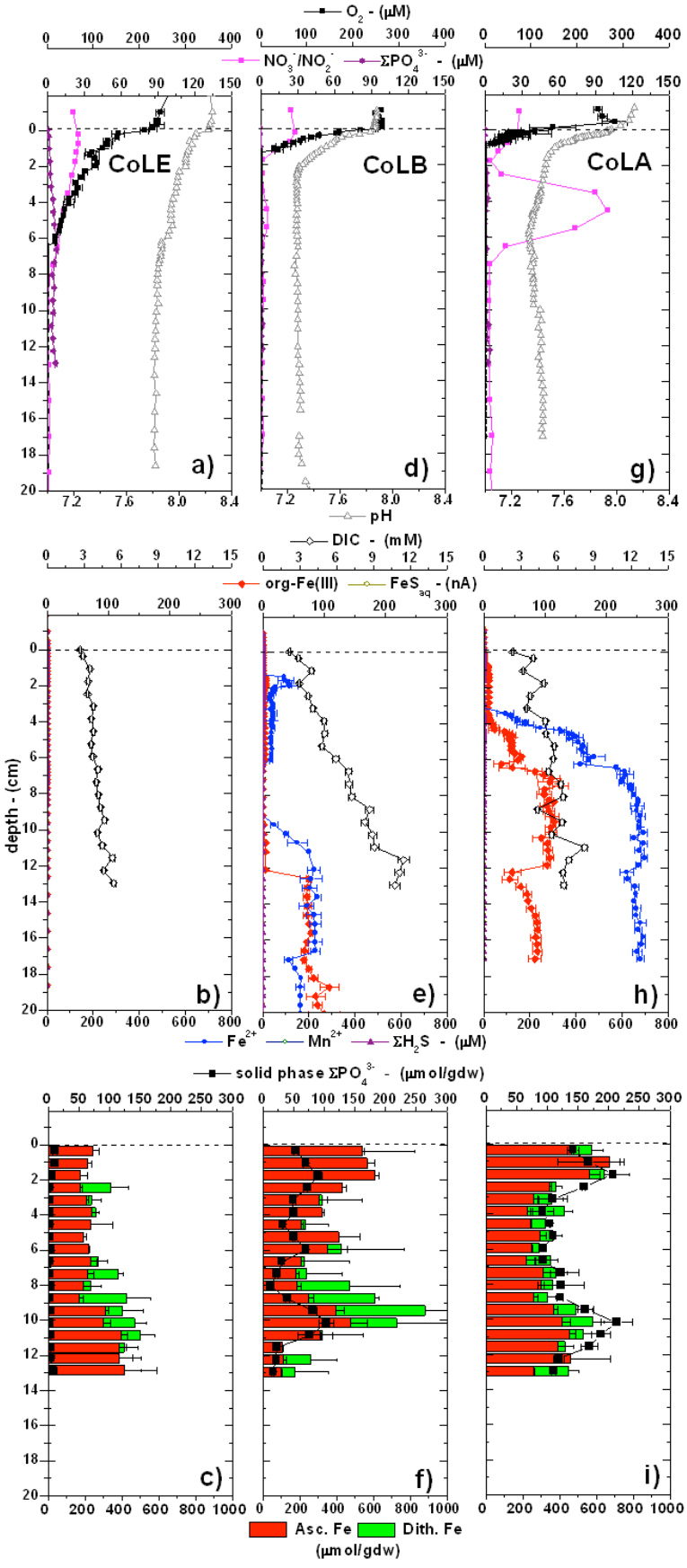
O2 - (µM)
NO3-/NO2- ΣPO4 3- - (µM)
CoLE
CoLB
CoLA
a)
d)
g)
pH
DIC - (mM)
org-Fe(III) FeSaq - (nA)
depth - (cm)
b)
e)
h)
Fe2+ Mn2+ ΣH2S - (µM)
solid phase ΣPO4 3- - (µmol/gdw)
c)
f)
i)
Asc. Fe
Dith. Fe
(µmol/gdw)

Figure 5.3 - Depth profiles of measured chemical species in Congo River fan sediments at the extinct channel, CoLE (a - c), a station intermediate to the extinct and active channels, CoLB (d – f), and from the active channel levee, CoLA (g – i). Both aerobic and anaerobic respiration processes are more intense closer to the active channel currently subject to turbidite flows.

complexes mirrored Fe^{2+} concentrations below that depth, and oscillated between 50 and 125 nA (Figure 5.3h). No evidence of SO_4^{2-} reduction was observed in CRF sediments, as neither ΣH_2S, nor $FeS_{(aq)}$ were observed at CoLE (Figure 5.3b), CoLB (Figure 5.3e), and CoLA (Figure 5.3h). The pH followed the expected behavior as a result of the intensity of aerobic respiration, NO_3^- reduction, and Fe(III) reduction in CRF sediments. The pH decreased less pronouncedly at CoLE from 8.26 in the overlying waters to ~ 7.92 at the bottom of the zone of aerobic and NO_3^- respiration, and then decreased more slowly deeper, finally reaching a value of 7.83 at a depth of 18 cm (Figure 5.3a). At CoLB, the pH was much lower in the overlying waters (~7.9), suggesting that respiration processes were more intense. It decreased more rapidly below the SWI to 7.3 by the bottom of the zone of NO_3^- reduction, and remained stable at 7.3 for the rest of the profile (Figure 5.3d). The pH profile of CoLA was particularly interesting, with three distinct regions (Figure 5.2c). Aerobic respiration and NO_3^- reduction decreased the pH drastically from ~ 8.14 in the overlying waters to ~ 7.6 at 7 mm, followed by a less rapid decrease to 7.3 at 5.6 cm, coinciding with the zone of NO_x production, and an increase back to 7.44, in the zone of intense Fe(III) reduction at 15 cm (Figure 5.3g). DIC generally increased steadily as a function of depth from 2.5 mM at the SWI to 5.4 mM at 13 cm at CoLE, the deepest depth where it was measured (Figure 5.3b), 11.5 mM at 11.5 cm in CoLB sediments (Figure 5.3e), and 8.2 mM at 11 cm (Figure 5.3h). Fe_{reac} concentrations extracted from the solid phase averaged 211 (±23) μmol/gdw in the top 8 cm of the sediment of CoLE,

but increased to 366 (±48) μmol/gdw deeper in the sediment column (Figure 5.3c). In the same sediments, Fe_{crys} concentrations were generally lower than Fe_{reac} in the top 6 cm (38 (±60)), but reached as high as 259 μmol/gdw below that depth (Figure 5.3c). Fe_{reac} concentrations were higher at CoLB than at CoLE, but quite variable (between 90 and 611 μmol/gdw) and with the highest concentrations in the top 2 cm (Figure 5.3f). Little Fe_{cryst} was observed at CoLB until below 6 cm, where concentrations reached 484 μmol/gdw; Figure 5.3f). Similar to CoLB, Fe_{reac} concentrations were highest in the top 2 cm of CoLA (672 μmol/gdw maximum), but were less variable, remaining above 225 μmol/gdw throughout the profile (Figure 5.3i). Fe_{crys} was observed throughout the profile at CoLA, albeit at low concentrations between 42 and 167 μmol/gdw (Figure 5.3i). Finally, $\sum PO_4^{3-}$ adsorbed onto reactive Fe hydroxides (P_s) was low at CoLE, at concentrations of only 11 μmol/gdw in the surface of sediment, and decreased to as low as 2 μmol/gdw deeper in the core (Figure 5.3c). Interestingly, solid phase ΣPO_4 (P_s) concentrations were much higher at CoLB (max concentration 103 μmol/gdw) and especially CoLA (between 92 and 214 μmol/gdw), and both profiles mirrored that of Fe_{reac} (Figure 5.3f and i).

5.5. Discussion

5.5.1. Absence of sulfate reduction and dominance of dissimilatory metal reduction

Both the LAS and CRF sediments are enriched in C_{org} relative to other deep areas of the ocean, suggesting SO_4^{2-} reduction may be an important respiration process in these sediments. In LAS sediments, the C_{org} content was reported to be 1.3% 25 km to the west of the slope station GOM12 at 574 m water depth compared to 0.8 - 1.0% near the shelf

and shelf-break stations GOM2 and GOM3 (Lin and Morse, 1991; Morse and Rowe, 1999). In CRF sediments, C_{org} content is >3% relative to Congo slope concentrations that are ≤ 2% (Rabouille et al., 2009). Interestingly, production of dissolved sulfides was not observed in any of the LAS or CRF sediment pore waters (Figure 5.2 and 3), indicating that SO_4^{2-} reduction was not intense or that sufficient reactive Mn and Fe minerals titrated ΣH_2S in these sediments. Voltammetric signals for $FeS_{(aq)}$, however, were consistently detected deeper than 6 cm at GOM2 (65 m water depth; Figure 5.2a) and immediately below the SWI at GOM3 (128 m water depth; Figure 5.2c), suggesting that SO_4^{2-} reduction was occuring in these sediments. Thermodynamic analysis can provide insight into the relative roles of microbial Fe(III) reduction and SO_4^{2-} reduction in the sediments, assuming that these sediments are near steady-state with respect to $FeS_{(s)}$. The concentration of ΣH_2S that should be in equilibrium with $FeS_{(aq)}$ at a particular pH can be determined by equation 5.11 as a function of pore water Fe^{2+} concentrations (Figure 5.4). Interestingly, Fe^{2+} (MDL < 20 μM) and ΣH_2S (MDL < 0.2 μM) remained below detection limits in GOM2 and most of GOM3 sediments, even though any theoretical equilibrium concentration of Fe^{2+} or ΣH_2S at pore water pH reflecting those of the pore waters of GOM2 and GOM3 (between 7.1 and 7.6) should be well above the detection limit of the Au/Hg microelectrodes (Figure 5.4). The $FeS_{(aq)}$ clusters may remain in solution either because they are more resilient to oxidation or because they are continuously generated from the dissolution of FeS solid phases. Accordingly, high concentrations of sediment total reducible sulfides (TRS, FeS_{am} + FeS_s + pyrite; 158 μmol/g) were previously observed in sediments near GOM2 (Morse and Rowe, 1999), suggesting these sediments could provide a constant source of $FeS_{(aq)}$ clusters. These findings suggest that these shelf

sediments are not at steady-state and that SO_4^{2-} reduction is controlled by a dynamic cycling between oxic and hypoxic conditions in the overlying waters (Morse and Eldridge, 2007).

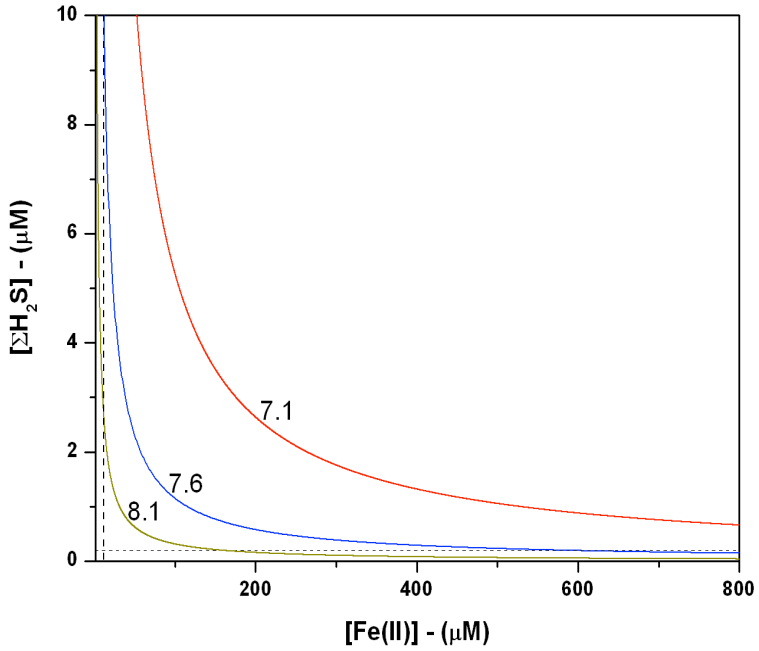

Figure 5.4 - Relationship between expected ΣH_2S and Fe^{2+} solution concentrations in equilibrium with $FeS_{(aq)}$ at several pH values. Detection limits for ΣH_2S and Fe^{2+} are indicated by dashed lines. LAS shelf and shelf-break stations GOM2 and GOM3 display $FeS_{(aq)}$ in pore waters in the absence of ΣH_2S and Fe^{2+}, suggesting the system is not at steady-state. The LAS slope station GOM12 and the CRF stations show high-concentrations of Fe^{2+} but no ΣH_2S, suggesting SO_4^{2-} reduction is not important in these sediments.

Simultaneously, the presence of Mn^{2+} but not Fe^{2+} in the pore waters at these two stations suggests either that Fe^{2+} was sequestered into sulfur minerals and Mn^{2+} was produced by reduction of Mn(III/IV) oxides by ΣH_2S, that microbial Mn but not Fe(III) reduction was ongoing at GOM2 and GOM3, that precipitation of carbonate minerals selectively removed Fe^{2+} from pore waters, or that Fe^{2+} was oxidized to Fe(III) during

excursion of overlying water $O_{2(aq)}$ into the pore waters. As microbial Mn reduction is likely not much more efficient than microbial Fe(III) reduction, as both siderite and rhodochrosite display similar solubilities and the kinetics of precipitation of rhodochrosite, though generally slow, is faster than that of siderite (Jensen et al., 2002), and as detection of dissolved $O_{2(aq)}$ as deep as 20 cm is highly unusual, it is likely that FeS precipitation selectively removes Fe^{2+} from the pore waters at GOM2 and GOM3. In the vicinity of GOM2 and GOM3, pyrite concentrations are generally high (73 μmol/g in sediments from 75 m water depth), but decrease when transitioning to sediments of 135 m water depth (11 μmol/g), demonstrating the decreasing influence of SO_4^{2-} reduction from the shelf to the slope (Lin and Morse, 1991), which is surprising given the high concentration of SO_4^{2-} in marine waters (28 mM).

At GOM12, midway down the slope (980 m water depth), neither ΣH_2S nor $FeS_{(aq)}$ were observed in the pore waters, while Fe^{2+} and Mn^{2+} concentrations reaching more than 1 mM were found deeper than 6 cm in the sediments (Figure 5.2c). Thermodynamic considerations indicate that in the presence of such high Fe^{2+} concentrations, only ~0.1 μM of ΣH_2S should be required to form $FeS_{(aq)}$ at pH 7.6 (Figure 5.4). The lack of ΣH_2S and $FeS_{(aq)}$ in the pore waters therefore suggests that SO_4^{2-} reduction is negligible in these sediments. The occurrence of soluble organic-Fe(III) complexes at the onset of Fe(III) reduction represents another piece of evidence that dissolved sulfides are not formed in these sediments. These complexes are well known to react rapidly with dissolved sulfides (Taillefert et al., 2000a) and are produced as intermediates in the reduction of Fe oxides by model iron-reducing bacteria (Jones et al., 2010; Taillefert et al., 2007a) and natural sediments amended with the same organism

(Chapter 4 of this thesis). Supporting this notion, SO_4^{2-} is not depleted to any great extent in the pore waters of sediments obtained 25 km to the west of GOM12 at 574 m water depth, and sediment pyrite never exceeds 5 μmol/g (Lin and Morse, 1991). These findings suggest that SO_4^{2-} reduction rates are low in these sediments and microbial metal reduction dominates anaerobic respiration processes. Although denititrification was not quantified and data is not available in the literature for the slope sites, the depth increment between $O_{2(aq)}$ penetration and Mn^{2+} production is only ~ 2.5 cm, leaving a limited zone for denitrification.

Similarly, several lines of evidence suggest the extremely high concentrations of Fe^{2+} at CoLA and CoLB are a product of dissimilatory metal reduction and not due to indirect reaction with ΣH_2S produced during SO_4^{2-} reduction. First, as discussed previously, ΣH_2S and $FeS_{(aq)}$ are not observed in the pore waters (Figure 5.3e and h). While it is possible that ΣH_2S could escape detection by immediate reaction with labile Fe(III) hydroxides, relatively high voltammetric signals for org-Fe(III) complexes and high aqueous Fe^{2+} concentrations (Figure 5.3e and h) would not be expected if SO_4^{2-} reduction was ongoing, as any excess ΣH_2S should more readily react with organic-Fe(III) complexes or aqueous Fe^{2+} instead of Fe(III) minerals (Rickard and Luther, 1997; Rickard et al., 1999; Taillefert et al., 2002a). Second, a good correlation ($R^2 = 0.70$) exists between org-Fe(III) current intensities and Fe^{2+} concentrations (Figure 5.5), suggesting these org-Fe(III) complexes are intermediates produced during Fe(III) reduction, but not Fe(II) oxidation given they are produced much deeper than $O_{2(aq)}$ penetration in these sediments (Figure 5.3). Third, in CRF sediments, ΣPO_4^{3-} associated with the solid phase mirrors Fe_{reac} at CoLB and CoLA. If the Fe_{reac} was reduced by ΣH_2S,

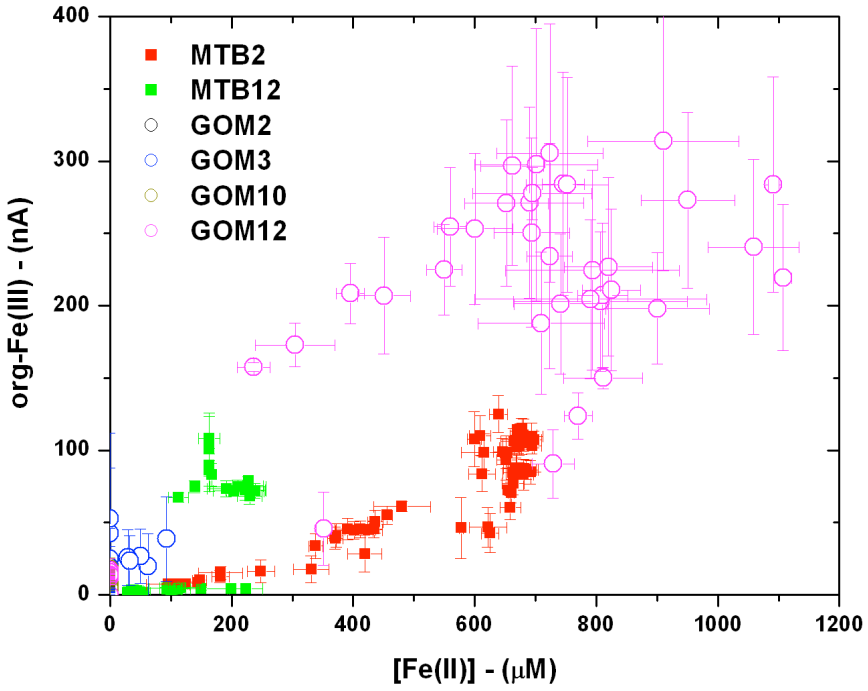

Figure 5.5 - Current intensities of org-Fe(III) complexes as a function of Fe^{2+} concentrations measured at each depth in the pore waters of the LAS and CRF continental slope stations. The positive correlation ($R^2 = 0.70$) between org-Fe(III) complexes and Fe^{2+} confirms that sulfate reduction is minimal in these sediments and suggests instead that dissimilatory Fe(III) reduction dominates anaerobic respiration.

FeS mineral precipitation should release adsorbed ΣPO_4^{3-} (Rozan et al., 2002) and result in pore water ΣPO_4^{3-} concentrations greater than the relatively low 10 μM maximum observed at these two stations (not shown). Finally, considering that denitrification or dissimilatory nitrate reduction to ammonium (DNRA) should have a negligible impact on DIC production given the NO_x concentrations in these sediments, between 1.5 and 4 mM of ΣH_2S should have been produced at CoLB and CoLA if SO_4^{2-} reduction dominated respiration processes and Fe(III) reduction was induced by ΣH_2S to account for the 3 to 8 mM DIC concentrations produced above background seawater concentrations in these sediments (Figure 5.3b, e, and h). In turn, the absence of dissolved Fe^{2+}, Mn^{2+}, and

dissolved sulfides at CoLE is not surprising given the depth of penetration of dissolved $O_{2(aq)}$ (~ 6 cm) at this station, indicating respiration is slowed in this extinct canyon no longer receiving high concentrations of C_{org} during turbidite flows.

5.5.2. The importance of riverine delivery

The sediment profiles across the LAS transect demonstrate a transition from SO_4^{2-} reduction on the shelf to a system dominated by Fe(III) and Mn(IV) reduction on the slope. In the CRF, an intensification of $O_{2(aq)}$, NO_3^-, and Fe(III) respiration is observed in the active channel relative to the extinct channel because of increased delivery of C_{org} and Fe(III) oxides, demonstrating the reliance of the benthic microbial community on the continued delivery of fresh terrigenous material. While these two environments are quite different from one another, it is clear that delivery of terrestrial C_{org} and oxidized Fe(III) and Mn(IV) minerals sets the stage for metal reduction-driven biogeochemistry in these sediments.

Major river-derived sediments may be deposited in delta regions (Type I system; e.g. Mississippi-Atchafalaya) or transported laterally alongshore on the shelf (Type II system, e.g. Amazon; Mckee et al., 2004). In such systems, C_{org} remineralization usually proceeds via anaerobic pathways, particularly in more tropical climates (Aller and Blair, 2006). The Mississippi RiOMar is a Type IIIa system (McKee et al., 2004), in which a significant proportion (> 10%) of the river plume is transported down-slope indirectly. Particles from the Mississippi, including C_{org} synthesized from within the Mississippi River plume (Bianchi et al., 2006; Sampere et al., 2011), accumulate on a prograding delta near the shelf-break (Coleman, 1988) and may spill-over in storms (Bea et al.,

1983), or more infrequently, during large-scale mass-slumping of rapidly deposited, over pressurized muds (Coleman et al., 1998; Dugan and Flemings, 2000; Dugan and Stigall, 2010; Fleming et al., 2008; Long et al., 2011; Stigall and Dugan, 2010). The net effect is an accumulation of terrigenous material much farther downslope than normal mixing processes would allow (Konyukhov, 2008), as has been demonstrated in the Ursa basin to the east of GOM12 (Long et al., 2011; Reece et al., 2012). Interestingly, Fe_{reac} concentrations in GOM12 sediments are close to the ~30 μmol cm gdw^{-1} threshold (converted from 30 μmol cm^{-3} assuming a 60% porosity and solid phase density of 2.6) at which the rate of microbial Fe(III) reduction is not limited by the concentration of Fe_{reac} (Thamdrup, 2000). However, a smectite-rich tongue, likely derived from the great-plain soils in the Missouri River drainage basin (Sionneau et al., 2008), extends from the Mississippi River delta to the Mississippi deep-sea fan (Balsam and Beeson, 2003), and Mississippi River delta sediments consist of 90% clays, mostly smectite and illite (Jaisi et al., 2008). While Fe silicate minerals should not be extracted significantly by the ascorbate and dithionite methods used in this study (Kostka and Luther, 1994), some may serve as TEAs for microbial Fe(III) reduction (Bishop et al., 2010; Jaisi et al., 2005; Kostka et al., 1999; O'Reilly et al., 2006) and thus provide a significant source of Fe^{2+} in these sediments.

In turn, most canyon systems were last active during the Pleistocene, when lower sea levels allowed rivers to be directly connected to their canyons and to deliver sediment directly across the continental shelf to the slope (Babonneau et al., 2002). Today, most deep-sea fans (e.g. Amazon and Indus) no longer directly receive fluvial deposits and are covered in pelagic calcareous ooze instead of mud (Damuth and Kumar, 1975; Prins et

al., 2000; Weimer, 1990). The Congo RiOMar is a Type IIIb system (McKee et al., 2004) because the river is still directly connected to its submarine canyon. Due to the low suspended sediment load in the Congo River, the active channel remains unfilled and thus extends 30 km up the estuary, such that during flood events, large-scale terrigenous deposits are funneled through the canyon to the abyssal plain. Flows remain confined in the deeply entrenched channel and are capable of traveling 800 km offshore. These processes explain how the Congo River, with such a low suspended sediment load, can produce such a large deep-sea fan (Babonneau et al., 2002). Accordingly, C/N ratios of organic matter in the CRF demonstrate the organic matter is largely terrestrially-derived (Rabouille et al., 2009). The CRF consists of a series of levees formed during the overflow of the finest-clay sized particles from these turbidite flows (Babonneau et al., 2002). The particles are rich in labile Fe(III) hydroxides extractable by ascorbate and concentrations exceed 600 μmol gdw^{-1} (Figure 5.3b and c), much greater than poorly crystalline Fe concentrations in coastal sediments dominated by Fe(III) reduction (e.g. (Jensen et al., 2003, Koretsky et al., 2003, Chapter 4 of this thesis). The extinct channel levee, on the other hand, harbors 65% less ascorbate-extractable iron in the top 2 cm of sediments than the active channel (Figure 5.3a), and Fe(III) reduction is barely detectable. While these Fe_{reac} concentrations are still relatively high compared to most sediments dominated by Fe(III) reduction (Thamdrup, 2000), both dissolved ΣPO_4^{3-} (not shown) and P_s (Figure 5.3c) remain low throughout the sediment, suggesting nutrient limitations may prevent significant Fe reduction.

The relative intensities of dissimilatory Fe and Mn reduction between the LAS and CRF and the resulting lack of dissolved Mn^{2+} in CRF fan sediments may be

controlled by the mineral composition of the input material. Elemental composition of the suspended loads indicates almost equivalent concentrations of Mn in either river (24 and 26 μmol Mn gdw^{-1} for the Mississippi and Congo, respectively), but 33% higher Fe in the Congo River (846 and 1268 μmol Fe gdw^{-1}; Martin and Meybeck, 1979). Further, the maximum concentration of Fe_{reac} measured (24 and 672 μmol Fe gdw^{-1}) indicate that up to 2.9% and 53% of the solid phase Fe may be under the form of Fe_{reac} in the Mississippi and Congo benthic sediments, assuming a similar composition between the riverine suspended sediment and offshore benthic sediment. Thus, the ratios of total Mn in the suspended load to the maximum measured Fe_{reac} content in the sediments are 26 times greater for the Mississippi than the Congo Rivers on a per mole basis (0.98 and 0.038), suggesting that Mn reduction may be more likely to occur in LAS sediments than CRF sediments. Additionally, bacteria may be specialized for Fe(III) reduction in the CRF given the significantly higher concentration Fe than Mn, as has been observed in other systems. For example, the addition of ferrihydrite to Black Sea surface sediments dominated by dissimilatory Mn reduction could not stimulate Fe reduction significantly (Thamdrup et al., 2000).

5.5.3. Thermodynamic considerations

While inputs of terrigenous organic and inorganic material may explain why iron reduction may be sustained in such environments, these considerations cannot explain why SO_4^{2-} reduction does not occur simultaneously in these sediments, as should be expected in such a C_{org}-rich environment (Thamdrup, 2000). Deep ocean sediments, however, may offer additional competitive advantages to metal-reducing bacteria,

including increases in the thermodynamic energy yields of respiration reactions and enhanced viabilities relative to other types of microbes at higher hydrostatic pressures and lower temperatures (Fang and Bazylinski, 2008). Several lines of experimental and theoretical evidence support the notion than Fe(III)-reducing organisms have an advantage in seawater at high pressures. *Shewanella* sp. are some of the most common and widely distributed bacteria isolated from the deep sea (Kato and Nogi, 2001), and many *Shewanella* sp. are piezophilic and psychrophilic (Fang et al., 2010). For example, the freshwater strain *S. oneidensis* MR-1 reduces Fe(III) oxides faster at high pressures than at surface pressures (Picard et al., 2012).

Thermodynamically, Fe(III) reduction becomes more favorable than SO_4^{2-} reduction in seawater at higher pressures, because Fe(III) reduction involves the dissolution of a solid phase (Fang and Bazylinski, 2008). Reactions resulting in a decrease in ΔV_{rxn} are favored under higher pressures (e.g. -167.1 cm^3 mol^{-1} for eq. 5.1 and +3.6 cm^3 mol^{-1} for eq. 5.3). Further, ion-pairing with seawater ions decreases the availability of SO_4^{2-} as TEA while the activity of Fe(III) oxides remain unchanged. Lastly, lower temperatures further decrease the potential energy of SO_4^{2-} reduction. Thermodynamic calculations for the anaerobic respiration of different Fe(III) oxides and SO_4^{2-} with acetate as electron donor (Equations 5.1 and 5.3) were conducted with SUPCRT92 to demonstrate these effects using relevant temperatures, pressures, and concentrations of a freshwater (25°C, 1 bar, I.S. = 0), coastal (25°C, 1 bar, I.S. = 0.7), and deep ocean (2°C, 500 bar, I.S. = 0.7) environment and correcting for ion-pairing and activities of all reactants and products (Figure 5.6). Gibbs free energy changes of each

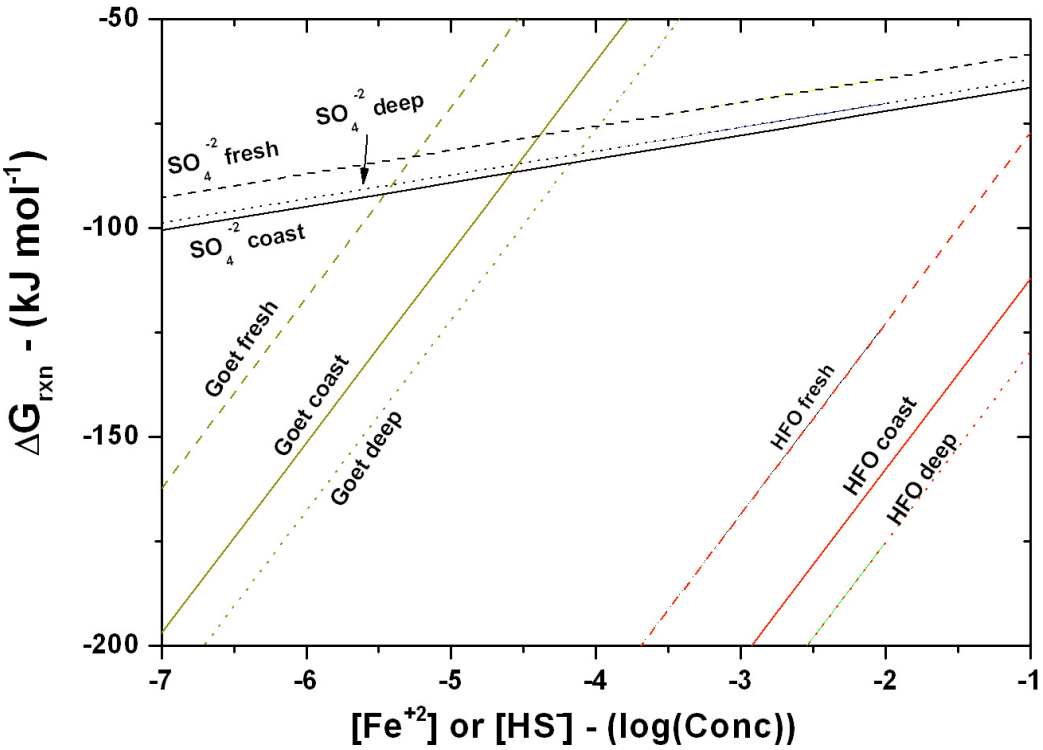

Figure 5.6 - ΔG_{rxn} for 2-line ferrihydrite, goethite, and SO_4^{2-} reduction coupled to acetate oxidation as a function of the reduced product for a fresh (25°C, 1 bar, I.S. = 0), coastal (25°C, 1 bar, I.S. = 0.7), and deep (2°C, 500 bar, I.S. = 0.7) water sediment. Fe(III) reduction becomes thermodynamically more favorable as depth increases, while SO_4^{2-} reduction becomes less favorable.

reaction (ΔG_{rxn}) were represented as a function of reduced substrate (i.e. Fe^{+2} or HS^-) accumulation assuming 100 μM CH_3COOH (Thurman, 1985), 1.93 mM HCO_3^- (Millero, 2005), and a pH of 7.4 (typical CRF sediment pH). Modeled results show that 2-line ferrihydrite reduction coupled to acetic acid oxidation is always favored relative to SO_4^{2-} reduction at any realistic Fe^{2+} concentrations (i.e. < 10 mM) (Figure 5.6). With more crystalline Fe (oxy)hydroxides, however, significant energy differences are observed, and the accumulation of reduced substrate must be considered. For example, at an assumed equilibrium pore water HS^- concentration of 10^{-12} M prior to the onset of SO_4^{2-} reduction

(although outside the range shown in figure 6) with 100 μM acetic acid, goethite reduction is still thermodynamically more favorable than SO_4^{2-} reduction in seawater at concentrations as high as 2.6 μM Fe^{+2} at 10 m depth and 25 °C, but at 5,000 m and at 2°C, this upper limit is tripled to 7.6 μM Fe^{+2}. These calculations therefore suggest that the supply of freshly formed iron oxides should allow Fe(III) reduction to dominate sulfate reduction in most marine environments provided sufficient electron donors are available. In environments dominated by more crystallized Fe(III) oxides, however, microbial Fe(III) reduction should only dominate if Fe^{2+} is removed from the pore waters via adsorption onto the solid phase, precipitation of siderite, or any other Fe^{2+} minerals.

5.5.4. Implications

The fact that C_{org} oxidation proceeds through dissimilatory metal reduction in river-dominated continental margin sediments such as the LAS and CRF has important implications for carbon cycling, atmospheric O_2 levels over geological time, and the evolution of microbial life on Earth. A previous study of the Congo fan suggested the CRF could be a C_{org} megaburial center. Although $O_{2(aq)}$ fluxes into sediments were high, C_{org} remineralization rates inferred from these measurements were only 1/3 of total C_{org} deposition rates (Rabouille et al., 2009). As dissimilatory Fe(III) reduction is the primary respiratory process in CRF sediments, however, estimates of C_{org} remineralization rates using $O_{2(aq)}$ flux measurements may be underestimated due to the formation of secondary minerals such as siderite or vivianite which prevent reoxidation of Fe^{2+} by dissolved $O_{2(aq)}$ (Glud, 2008). More importantly, even if dissimilatory Fe(III) reduction is much less efficient than SO_4^{2-} reduction in remineralizing carbon, the concentration of Fe(III) oxides

available to remineralize C_{org} in these sediments is about 3.3 times higher on a per mole C basis than SO_4^{2-} (752 mmol eq L^{-1} compared to 224 mmol eq L^{-1}, using an Fe_{reac} content of 684 μmol gdw^{-1}, a porosity of 0.6, and solid phase density of 2.65 g cm^{-3}), suggesting that dissimilatory Fe(III) reduction may in fact increase organic matter remineralization compared to SO_4^{2-} reduction in such environments. Additional evidence for the increase remineralization of carbon in iron-rich sediments include that the dissolution of Fe oxides releases otherwise protected natural organic matter that could promote microbial respiration (Lalonde et al., 2012). In a similar manner, Fe(III) oxides may catalyze hydrolytic reactions through both oxidative and non-oxidative pathways, forming smaller organic carbon compounds that may be more labile for microbial respiration (Mayer, 1995; Sunda and Kieber, 1994; Torrents and Stone, 1994). Finally, the production of O_2 radicals by Fe^{2+} oxidation may generate peroxide (Burns et al. 2010) which itself oxidizes some C_{org} (Burdige, 2007). On the other hand, SO_4^{2-} reducing conditions may actually promote C_{org} preservation, as vulcanization reactions between lignin and alkyl-rich substances may produce polymers more resistant to fermentation (Hedges and Oades, 1997). Ultimately, the extent of kerogen formation should thus depend on the exposure time to aerobic, metal-reducing, and SO_4^{2-}-reducing conditions, and kerogen formation may be overestimated in CRF or LAS slope sediments.

Over geologic timescales, atmospheric O_2 levels are controlled by pyrite weathering during exposure to the atmosphere (Berner, 2001; Berner and Canfield, 1988; Berner and Petsch, 1998). If erosion processes supply enough Fe(III) oxides in RiOMAR sediments, the findings of the present study suggest that SO_4^{2-} reduction, and thus pyritization, will be prevented at great depth. While the implications of such findings on

atmospheric O_2 levels on a geological timescale are difficult to evaluate, rises in temperature (Barnett et al., 2005; Levitus et al., 2001; Lyman et al., 2010), seawater levels (Wigley, 2005), and frequency of ENSO events (Khan et al., 2006) associated with climate changes may have an even larger negative impact on the potential for pyritization in these environments, as they may affect precipitation intensity and frequency and thus riverine discharge (Goudie, 2006; Hamilton, 2010), which should also increase the supply of Fe(III) oxide minerals to the oceans. Finally, these findings may have important implications on the changes in redox conditions on the Early Earth. If increases in riverine discharge associated with increases in temperatures provided enough Fe(III) oxides to RiOMAR sediments around the globe, dissolved sulfides present in the deep euxinic water column of the oceans during the Proterozoic may have been titrated during oxidation by Fe oxides and precipitation of $FeS_{(s)}$ (Arnold et al., 2004; Canfield et al., 2008; Lyons et al., 2009) which could have facilitated a shift in microbial processes from less energetically favorable SO_4^{2-} reduction to more energetically favored Fe(III) reduction in deep-sea sediments and favored the onset of oxygenic conditions on Earth.

5.6. Conclusions

Deep sediments of river-dominated ocean margins (RiOMars) are accumulation centers for C_{org} and terrigenous minerals, but relatively few studies have examined the pathways of anaerobic respiration in these sediments. In this study, two transects of the Congo River fan and Mississippi slope sediments were conducted using a combination of Au/Hg voltammetry and traditional wet chemistry techniques. In Mississippi slope and Congo fan sediments, Au/Hg voltammetry revealed C_{org} mineralization in the top ~20 cm

was dominated by dissimilatory Fe(III) and Mn reduction, as no evidence for SO_4^{2-} reduction was detected. The Congo fan provides evidence demonstrating that continued discharge of freshly weathered Fe minerals results in Fe(III)-reducing conditions in sediments and that shifts in turbidite flows may alter the intensity of the Fe(III) reduction. An intensification of aerobic, NO_3^-, and Fe(III) respiration is observed in the active channel because of increased delivery of C_{org} and Fe(III) oxides, demonstrating the reliance of benthic microorganisms on the continued delivery of fresh terrigenous material. The Mississippi slope, on the other hand, demonstrates a transition from SO_4^{2-} reduction on shelf sediments to a shift towards metal reduction in slope sediments subject to mass slumping or shelf-spillover of unconsolidated oxidized minerals.

It remains to be evaluated as to whether other RiOMars may be subject to similar processes by sediment transport through a canyon (Type IIIb, Indus; vonRad and Tahir, 1997) or transported alongshore into a canyon (Type IV; Ganges, (Kudrass et al., 1998)). Submarine landslides occur on every passive continental margin (e.g. Gales et al., 2014; Lee, 2009; Owen et al., 2007; Urgeles and Camerlenghi, 2013; Urlaub et al., 2013), the relative roles that riverine delivery and mass slumping play in promoting dissimilatory metal reduction remain to be evaluated. Climate-change induced effects in Fe depositional patterns may alter the pathways, rates, and extents of C_{org} remineralization in Fe-rich sediments (Meiggs and Taillefert, 2011), ultimately affecting global carbon inventories. On the geological timescale, pyrite precipitation may be prevented in these environments. Finally, delivery of Fe to depth at RiOMars may have titrated sulfides from the ocean, perhaps promoting the onset of oxygenic conditions on the early earth.

5.7. Acknowledgements

We would like to thank the captain and crew of the R/V *Cape Hatteras* and N/O *Pourquoi Pas?*, Laurence Droz for the Congo fan bathymetric data, and Panagiotis Michaelopoulos, Cécile Cathalot, and Rudolphe Corvoisier for their help in the sampling and analysis of some of these data. This research was partially funded by the National Science Foundation (OCE-0851156 to MT) and the Agence Nationale de la Recherche (ANR-11-BS56-0030 to CR).

CHAPTER 6

SHEWANELLA PUTREFACIENS PRODUCES AN FE(III) SOLUBILIZING ORGANIC LIGAND DURING ANAEROBIC RESPIRATION ON INSOLUBLE FE(III) OXIDES

This is a reprint of an article whose final and definitive form has been published in the *Journal of Inorganic Biochemistry*, authored by Martial Taillefert[1 #], Jordon S. Beckler[1], Elizabeth Carey[1], Justin L. Burns[2], Christine M. Fennessey[2], Thomas J. DiChristina[2] entitled "*Shewanella putrefaciens* Produces an Fe(III)-Solubilizing Organic Ligand during Anaerobic Respiration on Insoluble Fe(III) Oxides".

Abstract

The mechanism of Fe(III) reduction was investigated using voltammetric techniques in anaerobic incubations of *Shewanella putrefaciens* strain 200 supplemented with Fe(III) citrate or a suite of Fe(III) oxides as terminal electron acceptor. Results indicate that organic complexes of Fe(III) are produced during the reduction of Fe(III) at rates that correlate with the reactivity of the Fe(III) phase and bacterial cell density. Anaerobic Fe(III) solubilization activity is detected with either Fe(III) oxides or Fe(III) citrate, suggesting that the organic ligand produced is strong enough to destabilize Fe(III) from soluble or solid Fe(III) substrates. Results also demonstrate that Fe(III) oxide dissolution is not controlled by the intrinsic chemical reactivity of the Fe(III) oxides. Instead, the chemical reaction between the endogenous organic ligand is only affected by

the number of reactive surface sites available to *S. putrefaciens*. This report describes the first application of voltammetric techniques to demonstrate production of soluble organic-Fe(III) complexes by any Fe(III)-reducing microorganism and is the first report of a Fe(III)-solubilizing ligand generated by a metal-reducing member of the genus *Shewanella*.

6.1. Introduction

The ability to respire Fe(III) as an anaerobic terminal electron acceptor (TEA) is found throughout the prokaryotic world, from hyperthermophilic Archaea closely related to the last common ancestor to mesophilic Proteobacteria (Lovley et al., 1997; Vargas et al., 1998). Fe(III)-reducing proteobacteria include facultative anaerobes from the genus *Shewanella*. In addition to Fe(III), metal-reducing members of the genus *Shewanella* respire on a wide variety of alternate compounds as sole terminal electron acceptor, including oxygen ($O_{2(aq)}$), nitrate (NO_3^-), nitrite (NO_2^-), trimethylamine-N-oxide (TMAO), sulfite (SO_3^{2-}), thiosulfate ($S_2O_3^{2-}$), elemental sulfur ($S^{(0)}$), manganese oxides [Mn(IV)], uranyl carbonate [U(VI)], fumarate, anthraquinone 2,6-disulphonate (AQDS) and potentially several others (DiChristina, 2005; Nealson and Saffarini, 1994). The suite of TEAs respired by *Shewanella* spans nearly the entire range of redox potentials encountered in the environment (Dale et al., 2007; Nealson and Saffarini, 1994).

The molecular mechanism by which Fe(III)-reducing bacteria respire solid Fe(III) remains poorly understood. The paucity of mechanistic details on microbial Fe(III) reduction is due in part to a lack of analytical techniques to accurately determine the complex chemical speciation of Fe during the respiration process (DiChristina et al.,

2005; Hernandez and Newman, 2001). Fe(III)-reducing bacteria leave dissolution features on Fe(III) oxides (Grantham and Dove, 1996; Grantham et al., 1997) and reduce amorphous Fe(III) oxides and Fe(III)-containing clay minerals faster than crystalline Fe(III) oxides (Kostka et al., 1999a; Kostka et al., 1999b; Roden, 2003; Roden and Zachara, 1996; Royer et al., 2004). The differences in microbial Fe(III) reduction rates may be due to more efficient adsorption of biogenic Fe^{2+} on crystalline Fe(III) oxides, which leads to a masking of reactive Fe(III) sites and an inhibition of microbial reduction activity (Roden and Zachara, 1996), to a decrease in thermodynamic driving force during Fe(III) oxide reduction below the threshold required for microbial energy conservation (Royer et al., 2004), or to the lower surface area of crystalline Fe(III) oxides compared to amorphous Fe(III) oxides and clays (Kostka et al., 1999a; Roden, 2003; Roden and Zachara, 1996). In turn, the reduction of Fe(III)-containing clays, which seems to proceed through initial alteration of Fe(III) from the well-crystallized octahedral sheets (O'Reilly et al., 2005), may be accelerated in the presence of exogenous organic ligands (Kostka et al., 1999a) because these ligands complex Fe^{2+}, thereby preventing Fe^{2+} adsorption. Indeed, microbial Fe(III) reduction may be accelerated nearly two orders of magnitude by providing Fe(III) in a soluble organic form rather than amorphous ferrihydrite (Arnold et al., 1988; DiChristina, 1992; Dollhopf et al., 2000; Lovley and Woodward, 1996). Alternately, some Fe(III)-reducing bacteria generate relatively high concentrations of soluble Fe(III) in the absence of exogenous chelating compounds (Nevin and Lovley, 2002a), an indication that these bacteria synthesize and release endogenous chelators to solubilize Fe(III) during anaerobic Fe(III) respiration.

Respiration-linked terminal reductases are widely considered an integral part of or

associated with the cytoplasmic (inner) membrane of gram-negative bacteria (Madigan et al., 1997). This view is based on transfer of respiratory electrons to soluble TEAs such as dissolved $O_{2(aq)}$, NO_3^-, SO_4^{2-}, and CO_2 that diffuse passively into the cell or are taken up by transmembrane transport systems (Madigan et al., 1997). Fe(III), on the other hand, is largely found in a crystalline form or as amorphous oxyhydroxide particles at neutral pH. Neutrophilic Fe(III)-reducing bacteria are therefore required to generate energy via electron transfer to highly insoluble electron acceptors which are presumably unable to contact the inner membrane (Arnold et al., 1988; Lovley and Phillips, 1988). To overcome this physiological problem, Fe(III)-reducing bacteria may have developed several strategies, including the direct (enzymatic) reduction of solid Fe(III) or soluble Fe(III) complexes (formed by dissolution of solid Fe(III) with exogenous organic ligands (Arnold et al., 1988; Dichristina, 1992; Dollhopf et al., 2000; Lovley and Woodward, 1996)) by Fe(III) terminal reductases located in the periplasm (Pitts et al., 2003) or peripherally attached to the outside face of the cell outer membrane (DiChristina et al., 2002; Myers and Myers, 1993; Shi et al., 2006; Xiong et al., 2006) or other extracellular appendages (Gorby et al., 2006; Reguera et al., 2005). Alternately, Fe(III)-reducing bacteria may synthesize and release endogenous chelators to solubilize Fe(III) prior to reduction (Nevin and Lovley, 2002a). Fe(III)-reducing bacteria may also reduce exogenous quinone moieties found in humic substances, which then chemically reduce Fe(III) oxides extracellularly (Coates et al., 1998; Lovley et al., 1996; Nevin and Lovley, 2000; Newman and Kolter, 2000; Scott et al., 1998), or synthesize and release reduced menaquinones, although this mechanism has recently been brought into question (Lies et al., 2005).

Several metal-reducing members of the genus *Shewanella* (including *S. putrefaciens* strain 200) are able to respire Fe(III) by employing all of the strategies described above (DiChristina et al., 2002), however, the majority of previous studies on the mechanism of Fe(III) reduction by *Shewanella* has focused on the direct enzymatic reduction pathway (Shi et al., 2006; Xiong et al., 2006). Recently, laboratory investigations using voltammetric techniques have shown that Fe(III) is soluble at circumneutral pH in both low and high ionic strength solutions in the presence of organic chelators (Taillefert et al., 2000a; Taylor et al., 1994). In addition, soluble organic-Fe(III) complexes are found ubiquitously in marine and freshwater sediments (Taillefert et al., 2000a; Taillefert et al., 2002a; Taillefert et al., 2002b). These results suggest that voltammetric techniques can be used to investigate the mechanism by which Fe(III)-reducing bacteria solubilize Fe(III) during Fe(III) respiration. The two main objectives of the present study were to 1) determine if *S. putrefaciens* produces an Fe(III)-solubilizing chelator during anaerobic Fe(III) respiration and 2) examine the effects of crystallinity of the solid Fe(III) substrates on Fe(III) solubilization rates.

6.2. Experimental conditions

All solutions were prepared with ACS or trace metal grade chemicals in autoclaved 18 MΩ-water (Barnstedt). Amorphous Fe(III) oxides, 2L- and 6L-ferrihydrite, lepidocrocite, goethite, and hematite were prepared according to the methods of Cornell and Schwertmann, 1996. The purity of the different Fe(III) phases synthesized was determined by X-ray diffraction spectroscopy (XRD). Surface areas were either measured by Brunauer–Emmett–Teller isotherm (BET) or estimated from the recipes used (Cornell

and Schwertmann, 1996). Fe(III) citrate was prepared by dissolution of Fe(III) citrate salt at 80ºC in the presence of sodium hydroxide to maintain the pH around 7.5.

Single batch reactor experiments were performed in 100 mL reactors specially fabricated for these experiments. Single batch reactors are convenient to monitor the medium composition over time without removing significant amounts of samples. In contrast to flow-through systems, batch reactors also present the benefit of keeping by-products of microbial processes in the medium. These reactors consisted of polyethylenetherketone (PEEK™) that could be autoclaved and sealed with lids. Lids and reactors were threaded and contained O-rings to prevent contamination. Lids contained eight 3 mm diameter port holes to accommodate electrodes, gas lines, and a sampling septum. The port holes were threaded to the specifications of standard HPLC fittings, and the electrodes, gas lines, and the sampling septum were sealed in the lid using standard plastic wing nuts and ferrules (Upchurch Scientifics, Inc.). A stir bar was added to each reactor prior to autoclaving to mix the slurries. Reactors were stored in an anaerobic chamber under an anaerobic N_2/H_2 atmosphere and gently mixed to ensure that the cells or Fe oxides did not settle at the bottom of the reactors.

Reactor experiments consisted of incubating *S. putrefaciens* strain 200 in triplicate cultures in *Shewanella* basal growth medium (DiChristina and Delong, 1993; DiChristina et al., 2002) with 10 mM sodium lactate as carbon/energy source and 2 mM Fe(III) citrate or 0.4 g of the different forms of Fe(III) oxides as terminal electron acceptor. Inocula for the reactor experiments consisted of *S. putrefaciens* cultures grown aerobically to late log phase on identical *Shewanella* basal growth medium. Overnight cultures were washed twice with sterile growth medium prior to inoculation at pre-selected initial cell

concentrations. The changes in the chemical composition of the solution were measured over time with a combination of voltammetric and spectrophotometric techniques (see below). Before each experiment, the reactor contents were degassed for 2 h with ultra high purity (UHP) N_2 previously passed through a copper oxide column heated at 350ºC to remove traces of O_2. At time zero, the N_2 gas was turned off and the reactors were sealed. An aliquot of *S. putrefaciens* (10^6 - 10^8 cells/ml final concentration) was introduced into the reactor through a septum. Samples (0.1 to 0.3 mL) were collected over time with a clean polypropylene syringe (HSW Norm-Ject) and a needle using the septum sampling port. Samples were directly injected into 1 mL of a 0.1 M HCl and stored at 4ºC until analysis, generally within 24 h. Just before analysis, samples were filtered through a 0.2 µm polyethersulfone membrane (AS Puradisc filters, Whatman) and into a Ferrozine reagent mixture (see below). In control experiments, 90% of Fe^{2+} in solution at pH 7.5 was detected for over more than seven days. As a check for cell lysis, supernatants were collected from three anaerobic reactor experiments (via filtration through 0.2 ìm AS Puradisc filters) and subsequently analyzed for NADH oxidase activity and 2-keo-3-deoxyoctonate concentrations (DiChristina et al., 2002). Both measurements indicated that cell lysis products were below detectable levels (data not shown).

6.3. Analytical Techniques

Samples collected over time in the reactors were analyzed for Fe^{2+} using the ferrozine method (Stookey, 1970). Fe^{2+} measured by the Ferrozine technique represents total Fe^{2+}, including the dissolved fraction and the fraction adsorbed onto Fe(III) oxides. *In situ*

measurements were performed with 100 μm diameter gold-mercury (Au/Hg) voltammetric microelectrodes encased in 3 mm PEEK™ according to previously described design (Nuzzio et al., 2002). A platinum counter electrode and an Ag/AgCl reference electrode (also encased in PEEK™) completed the three-electrode circuit. The Au/Hg microelectrodes were prepared as previously described (Brendel and Luther, 1995) by first polishing the gold wire with 15, 6, 1, and 0.25 μm diamond pastes (Buehler), plating mercury at -0.1 V in a $Hg(NO_3)_2$ solution, and then polarizing at -9 V for 90 seconds to form an effective amalgam between the Au and Hg. Electrodes were calibrated for Mn^{2+} (Minimum Detection Limit, MDL ~ 5 μM) by cathodic square wave voltammetry (CSWV) in degassed medium. Voltammograms were obtained from -0.1 to -1.75 V with a scan rate of 200 mV s^{-1}. A preconditioning step at a potential of -0.1 V for 10 seconds was applied to clean the surface of the microelectrodes between measurements (Brendel and Luther, 1995).

Voltammetric measurements were carried out with a computer-operated DLK-100A potentiostat (Analytical Instrument Systems, Inc.). A benefit of voltammetry is the ability to analyze for multiple species simultaneously, including $O_{2(aq)}$, H_2O_2, Fe^{2+}, Mn^{2+}, $S_2O_3^{2-}$, ΣH_2S (= $H_2S + HS^- + S^{2-} + S^0 + S_x^{2-}$), soluble organic-Fe(III), and aqueous FeS, thiols, and disulfides (Heyrovsky et al., 1994; Taillefert et al., 2000a; Taillefert et al., 2000b; Theberge and Luther, 1997; White et al., 2002). Other benefits of voltammetry include low detection limits, fast analysis time, and high reproducibility (Brendel and Luther, 1995; Buffle and Horvai, 2000; Taillefert et al., 2000b). Ferrous iron (MDL ~ 10 μM in low ionic strength solutions) and soluble organic-Fe(III) were measured by CSWV under the same conditions used for Mn^{2+}, except that a cleaning step at -0.9 V for 10 seconds

was added to measure soluble organic-Fe(III). This step ensured that any soluble organic-Fe(III) adsorbed at the electrode surface was removed prior to the next measurement (Taillefert et al., 2000a). The Mn^{2+} calibration curves were used to elucidate the concentration of Fe^{2+} with the pilot ion method (Brendel and Luther, 1995). Soluble Fe(III) is only detected by voltammetry at circumneutral pH if it is complexed by an organic ligand (Taillefert et al., 2000a). According to what is known from the mobility and lability of complexes in solution, the contribution of species with sizes greater than a few nanometers should not react at the surface of voltammetric microelectrodes (Buffle and Horvai, 2000). In turn, several unknown organic-Fe(III) complexes may be detected simultaneously at the microelectrode. The sensitivities of these complexes have yet to be determined and their concentrations are therefore reported in current intensities (Taillefert et al., 2000a). To compare soluble organic-Fe(III) voltammetric currents from different incubations, it was necessary to consider that the sensitivity of electrodes varies according to the size of the deposited mercury film. The Mn^{2+} sensitivities of each electrode were normalized to that of a random electrode, and these sensitivity ratios multiplied by the organic-Fe(III) currents to calculate the normalized soluble organic-Fe(III) currents.

6.4. Results

To determine if *S. putrefaciens* produces chelators that solubilize Fe(III) during anaerobic Fe(III) reduction, the wild type strain was incubated in the presence of either Fe(III) citrate or a suite of Fe(III) oxides and the production of organic-Fe(III) complexes was monitored by voltammetry with Au/Hg microelectrodes. Results from incubations

with Fe(III) citrate and wild-type *S. putrefaciens* (Figure 6.1) indicate that soluble organic-Fe(III) complexes are produced over time and reach a steady-state simultaneously with Fe^{2+}. These data suggest that Fe(III) citrate, which does not produce a detectable voltammetric signal in abiotic or heat-killed biotic control experiments (data not shown), is transformed by *S. putrefaciens* to one or more electrochemically labile organic-Fe(III) complexes. These experiments were repeated with the same concentration of Fe(III) citrate but different initial cell concentrations to confirm that the production of these complexes is a function of bacterial cell density. Voltammetric current intensities for the soluble organic-Fe(III) complexes (Figure 6.1a and b) and Fe^{2+} concentrations (Figure 6.1c) increase proportionally with initial cell concentrations.

Anaerobic incubations conducted with goethite displayed similar results (Figure 6.2). Soluble organic-Fe(III) complexes were formed within 24 h after exposing *S. putrefaciens* to Fe(III) oxides, and their production reach a steady-state within 48 h (Figure 6.2b). Voltammetric peaks detected by CSWV are broad and shift towards more negative potentials over time, suggesting that soluble Fe(III) slowly aggregates to a larger complex (Taillefert et al., 2000a). Reduced Fe was produced concomitantly with soluble organic-Fe(III) for 48 h, but comparison with Fe^{2+} concentrations detected independently by the Ferrozine method revealed two distinct features. Initially, Fe^{2+} concentrations measured by voltammetry were higher than total Fe^{2+} quantified by the ferrozine method. After 48 h, however, voltammetric Fe^{2+} decreased linearly as a function of time, while total Fe^{2+} measured by the Ferrozine method increased asymptotically. These findings indicate that Fe^{2+} is initially complexed by an organic ligand that enhances its sensitivity

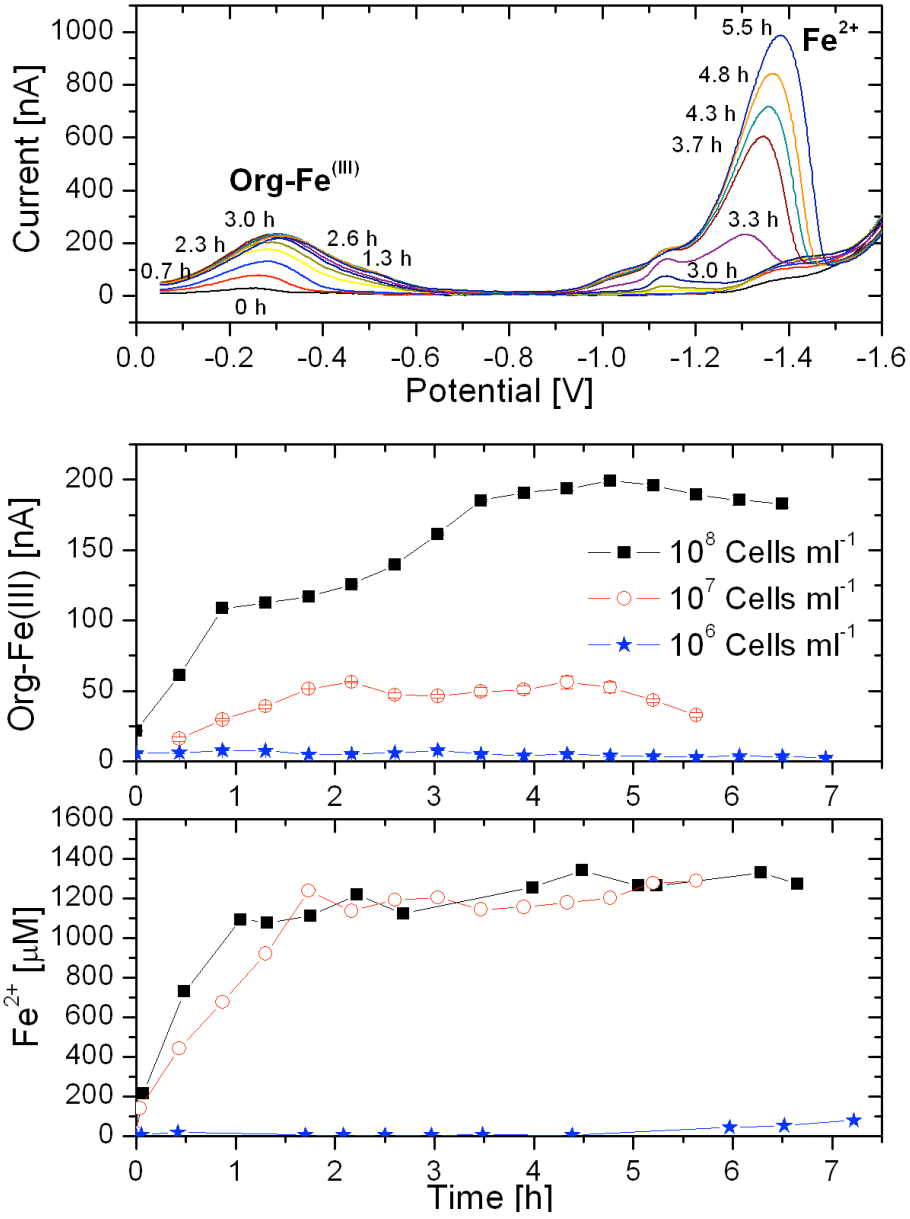

Figure 6.1 - Reduction kinetics of 2 mM Fe(III) citrate by 10^6, 10^7, and 10^8 cells ml^{-1} of *S. putrefaciens* strain 200R in Westlake medium. a. Selected cathodic square wave voltammograms showing the production of soluble organic-Fe(III) complexes (ca. -0.3 V) and Fe^{2+} (at -1.35 V) as a function of time. b. Change in current intensity of the organic-Fe(III) complexes as a function of time in each incubation; c. Change in Fe^{2+} concentration as a function of time in each incubation.

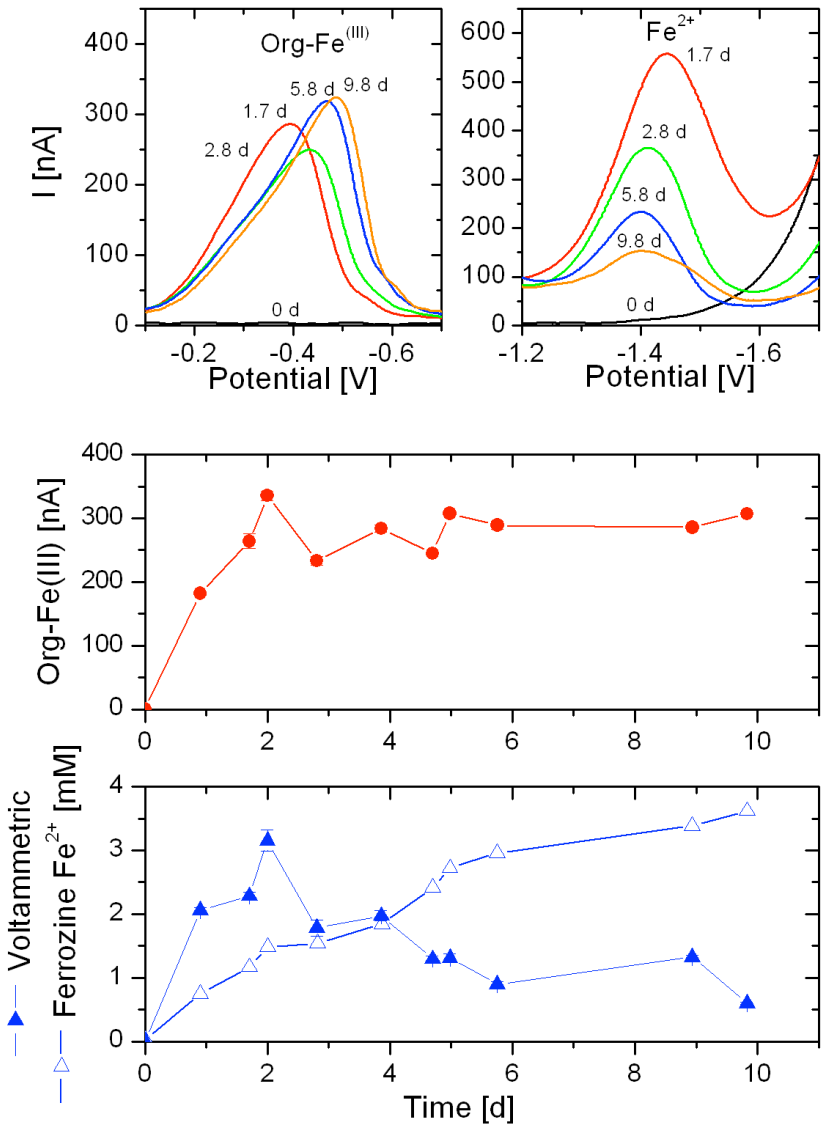

Figure 6.2 - Incubation of *S. putrefaciens* with goethite as function of time. a. Representative cathodic square wave voltammograms as a function of time. Voltammetric signals of soluble organic-Fe(III) complexes are produced at -0.4 V initially, then shift to more negative values over time. Voltammetric signals for Fe^{2+} are displayed near -1.4 V, depending on its concentration; b. Change in current intensity of soluble organic-Fe(III) as a function of time; c. Production of Fe^{2+} concentration as a function of time measured by the ferrozine method and voltammetry.

at the electrode surface. After 48 h, these Fe^{2+} complexes are removed by adsorption onto the Fe(III) oxides remaining in suspension.

Experiments conducted with 2L- and 6L-ferrihydrite, lepidocrocite, goethite, hematite and magnetite indicate that wild-type *S. putrefaciens* also produced soluble organic-Fe(III) complexes as intermediates in the reduction of Fe(III) oxides. The extent and rate of soluble organic-Fe(III) production was related to the crystallinity of the Fe(III) oxides (Figure 6.3a). Significantly larger soluble organic-Fe(III) currents were produced with Fe(III) oxides of more reactive crystal structure (i.e., 6L-ferrihydrite and lepidocrocite) than with well-crystalline Fe(III) oxides (e.g., goethite and hematite). In addition, incubations with more reactive Fe(III) oxides resulted in higher concentrations of total Fe^{2+} at steady-state compared to incubations with more crystalline Fe(III) oxides (Figure 6.3b). Both soluble organic-Fe(III) and total Fe^{2+} produced during the reduction of amorphous Fe(III) oxides (but not crystalline Fe(III) oxides) were removed after approximately six days, suggesting that secondary minerals are formed over time.

Initial rates of Fe(III) reduction were compared with initial rates of soluble organic-Fe(III) production to determine the relationship between Fe(III) reduction and solubilization (Figure 6.4). Initial rates were determined by linear regression of the change in total Fe^{2+} concentration and soluble organic-Fe(III) current intensity as a function of time within the first 40 h of the incubations. Initial rates measured in the incubations with Fe(III) citrate were normalized to initial cell counts (inset of Figure 6.4). Initial rates of soluble organic-Fe(III) production correlate with the initial rates of Fe(III) reduction, both for the Fe(III) citrate (inset of Figure 6.4) and the different Fe(III) oxides (Figure 6.4). Initial rates of Fe(III) reduction and Fe(III) solubilization are lower for

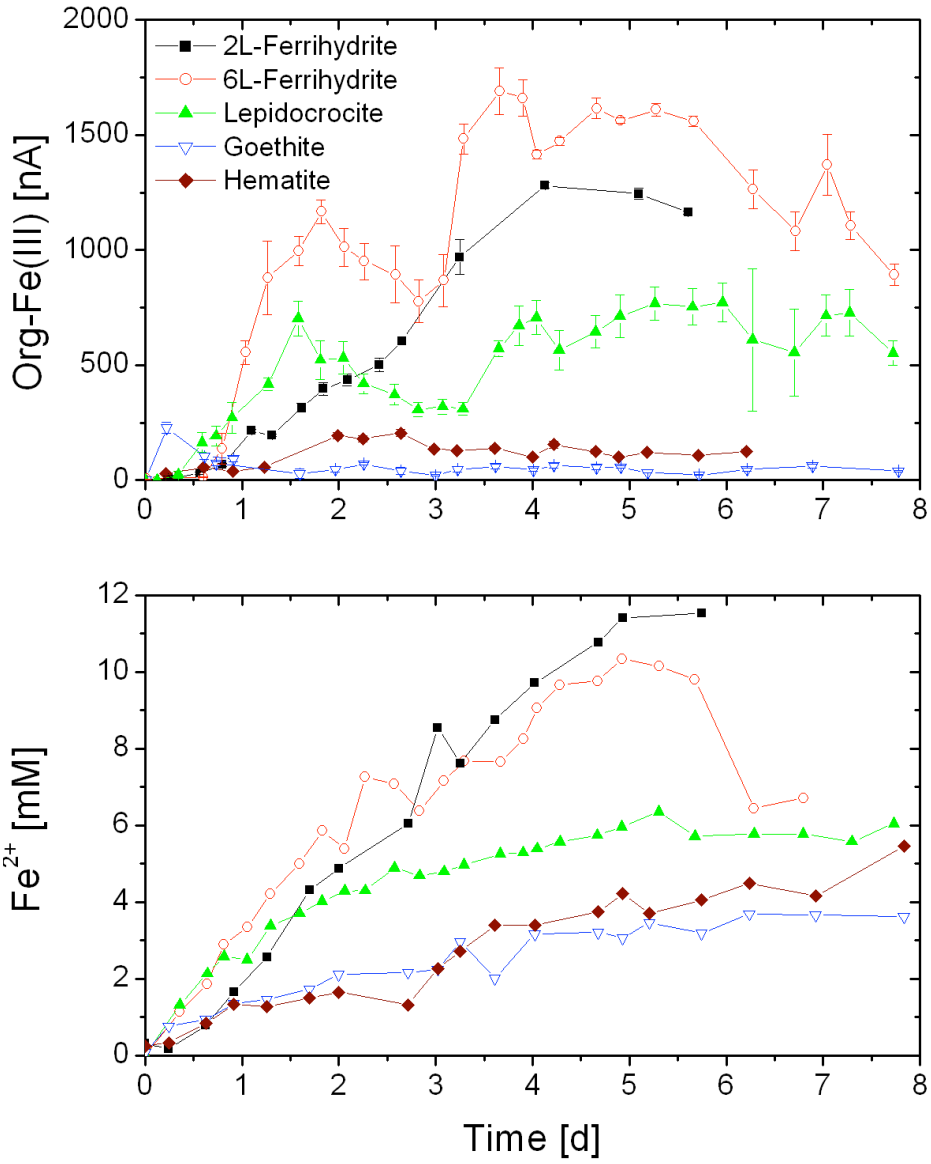

Figure 6.3 - Reduction of 6L-ferrihydrite, 2L-ferrihydrite, lepidocrocite, goethite, and hematite by *S. putrefaciens* strain 200R in Westlake medium as a function of time: a. Normalized organic-Fe(III) electrochemical signals; b. Ferrozine Fe^{2+} measurements.

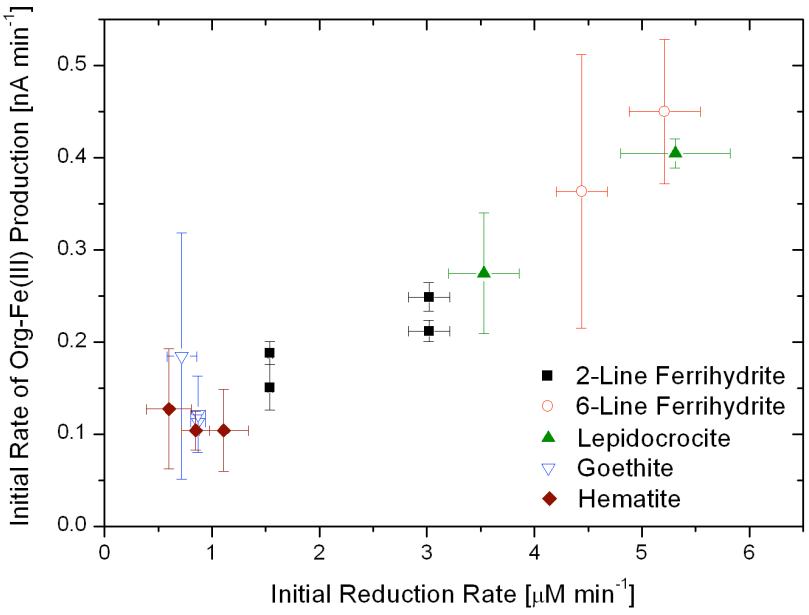

Figure 6.4 - Correlation between initial production rates of soluble organic-Fe(III) and Fe(III) reduction rates for incubations conducted with *S. putrefaciens* strain 200R and different forms of Fe(III) oxides (hematite, goethite, lepidocrocite, 6L-ferrihydrite, 2L-ferrihydrite). Inset shows correlation between initial production rates of soluble organic-Fe(III) and Fe(III) reduction rates normalized to the initial cell concentrations in the Fe(III) citrate incubations (Figure 6.1).

crystalline Fe(III) oxides (i.e., goethite and hematite) than for the more amorphous Fe(III) oxides (i.e, 6L-ferrihydrite and lepidocrocite), while solubilization and reduction rates for 2-L ferrihydrite are intermediate in magnitude (Figure 6.4).

6.5. Discussion

Results from the present study indicate that the chemical composition of Fe(III) is altered by *S. putrefaciens* during the anaerobic reduction process. An electrochemically reactive Fe(III) compound is rapidly produced during anaerobic incubations with either

soluble or solid Fe(III) substrates. The soluble Fe(III) compound is only detected with Au/Hg voltammetric microelectrodes at circumneutral pH if Fe(III) is complexed by organic ligands (Taillefert et al., 2000a) with sizes that should be smaller than a few nanometers (Buffle and Horvai, 2000). *Shewanella* growth medium used in the present study only contains lactate and inorganic salts, neither of which produce voltammetric signals, an indication that the organic ligands are produced and subsequently released by *S. putrefaciens*. These findings suggest that *S. putrefaciens* destabilizes Fe(III) from soluble or solid Fe(III) substrates during anaerobic Fe(III) respiration. In the case of Fe(III) citrate, *S. putrefaciens* produces organic ligands (L) that exchange for citrate. At circumneutral pH, Fe(III) citrate generally forms a mononuclear bidentate complex ($[Fe(OH)_2cit]^{2-}$) at 1:1 metal to ligand ratio (Francis and Dodge, 1993; Konigsberger et al., 2000) or a strong ternary dinuclear complex ($[Fe_2(OH)_2(cit)_2]^{2-}$) in excess ligand (Hamada et al., 2006). Tridentate complexes ($Fecit^0$) may exist but generally hydrolyze to the more stable bidentate complex at circumneutral pH (Francis and Dodge, 1993). Larger dinuclear complexes may also form, but only in the presence of pyridine-type counter ions to stabilize these molecules (Bino et al., 1998; Shweky et al., 1994). As a result, possible reactions for the ligand exchange of citrate include:

$$[Fe(OH)_2(cit)]^{2-} + yLH_n \overset{K}{\longleftrightarrow} FeL_y^{(3-ny)} \qquad \text{(Eq. 6.1)}$$

$$+cit^{3-} + (ny-2)H^+ + 2H_2O \qquad \text{(Eq. 6.2)}$$

$$[Fe_2(OH)_2(cit)_2]^{2-} + 2yLH_n \overset{K}{\longleftrightarrow} 2FeL_y^{(3-ny)} \qquad \text{(Eq 6.3)}$$

$$+2cit^{3-} + (2ny-2)H^+ + 2H_2O \qquad \text{(Eq 6.4)}$$

where y is a stoichiometric coefficient and n the maximum number of reactive sites on the chelator. As the concentration of citrate is in a 1:1 mole to mole ratio with that of

Fe(III), the reaction with the monobidentate complex (Eq. 6.1) is likely the ligand-exchange reaction occurring in the anaerobic incubations carried out in the present study.

The binding strength of Fe(III) complexes influences the rate of Fe(III) reduction by *S. putrefaciens*: Organic ligands forming Fe(III) complexes with formation constants (log K) greater than 20 are not reduced, while Fe(III) citrate is more bioavailable for dissimilatory Fe(III) respiration (Haas and DiChristina, 2002). Results from the present study indicate that the organic ligand secreted by *S. putrefaciens* forms Fe(III) complexes with formation constants greater than that of Fe(III) citrate. These results also suggest that the decrease in Fe(III) reduction rates observed with Fe(III) complexes of greater binding strength (Haas and DiChristina, 2002) is directly due to the competing effect between the organic chelator secreted by *S. putrefaciens* and exogenous organic ligands. Thus, *S. putrefaciens* produces an organic ligand that displaces the equilibrium between Fe(III) and exogenous ligands in solution toward another organic Fe(III) complex that is more readily reduced. Interestingly, initial rates of production of both soluble organic-Fe(III) and Fe^{2+}, when normalized to initial cell concentrations, increase proportionally with cell concentration (inset of Figure 6.4). These data indicate that the rates of organic-Fe(III) and Fe^{2+} production are not controlled by cell concentrations but rather by the organic ligand concentration generated in the incubations. As the overall concentration of organic ligand produced by the cells is most likely proportional to the cell concentration, these findings suggest that the produced organic ligand is recycled after reduction of Fe(III) to enhance the rate of organic-Fe(III) and Fe^{2+} production. Alternately, the *S. putrefaciens* cells are induced to produce increased levels of organic ligand via an as yet unidentified environmental cue.

The correlation between rates of Fe(III) reduction and Fe(III) dissolution in the presence of Fe(III) oxides with different crystal structures (Figure 6.4) indicates that Fe(III) solubilization is required during anaerobic Fe(III) respiration. In the case of Fe(III) oxides, *S. putrefaciens* may produce organic ligands that non-reductively dissolve and complex Fe(III) from Fe(III) oxides prior to reduction, according to:

$$(x+1)Fe(OH)_{3(s)} + yH_nL + (3-ny)H^+ \overset{K}{\longleftrightarrow} FeL_y^{(3-ny)} + xFe(OH)_{3(s)} + 3H_2O \quad \text{(Eq 6.5)}$$

where x and y are stoichiometric coefficients and n the maximum number of reactive sites on the chelator.

The non-reductive dissolution of Fe(III) oxides by organic ligands occurs abiotically at circumneutral pH (Bondietti et al., 1993; Luther et al., 1992; Zinder et al., 1986) and is generally facilitated with the π electron-donating ability of the coordinated ligand (Stumm, 1997) or with ligands forming mononuclear complexes with Fe(III) (Bondietti et al., 1993). Multidentate ligands generally increase the rate of dissolution because they weaken the strength of the remaining coordination with the mineral surface (Stumm, 1997; Zinder et al., 1986). The increase in Fe(III) dissolution rates when incubating *S. putrefaciens* in the presence of more amorphous Fe(III) oxides such as 6L-ferrihydrite or lepidocrocite compared to well crystalline minerals such as hematite and goethite (Figure 6.4) may be explained by the reactivity of the Fe(III) oxides. The ligand-promoted dissolution of Fe(III) oxides with greater number of active surface sites is accelerated, especially with high hydroxyl surface content (Deng and Stumm, 1994). Thus, amorphous Fe(III) oxides with larger surface areas and correspondingly higher number of reactive hydroxyl groups, dissolve much faster than well crystalline Fe(III) oxides with lower surface areas. Indeed, microbial reduction of amorphous Fe(III) oxides is faster

than that observed with well-crystallized minerals (Kostka et al., 1999b; Roden, 2003; Roden and Zachara, 1996) and even faster in the presence of soluble Fe(III) complexes (Arnold et al., 1988; Lovley and Woodward, 1996). However, initial Fe(III) reduction rates normalized to mineral surface area are similar for all Fe(III) oxide phases except 2L-ferrihydrite and lepidocrocite, which are respectively slightly less and about a 2-fold more reactive than the other forms of substrate (Figure 6.5b).

In previous studies, lower microbial reduction rates for 2L-ferrihydrite have been attributed to the tendency of 2L-ferrihydrite to aggregate when dehydrated during synthesis (Roden, 2003). Similarly, higher reduction rates for lepidocrocite have been reported (Roden, 2003; Schwertmann and Cornell, 2000) and may be related to the type of crystals formed during synthesis. Highly serrated lepidocrocite crystals usually display a higher reactivity than well crystallized lepidocrocite with smooth edges (Schwertmann and Cornell, 2000). Interestingly, rates of production of soluble organic-Fe(III), normalized to surface area, are nearly identical for all the types of Fe(III) oxide except 2L-ferrihydrite (Figure 6.5a). These findings, as previously proposed using Fe^{2+} measurements (Roden, 2003), indicate that Fe(III) oxide dissolution is not controlled by the intrinsic chemical reactivity of the Fe(III) oxides. Instead, the chemical reaction between the endogenous organic ligand is only affected by the number of reactive surface sites available to *S. putrefaciens*. Furthermore, these findings indicate that the secreted organic ligand is strong enough to destabilize Fe(III) from iron substrates.

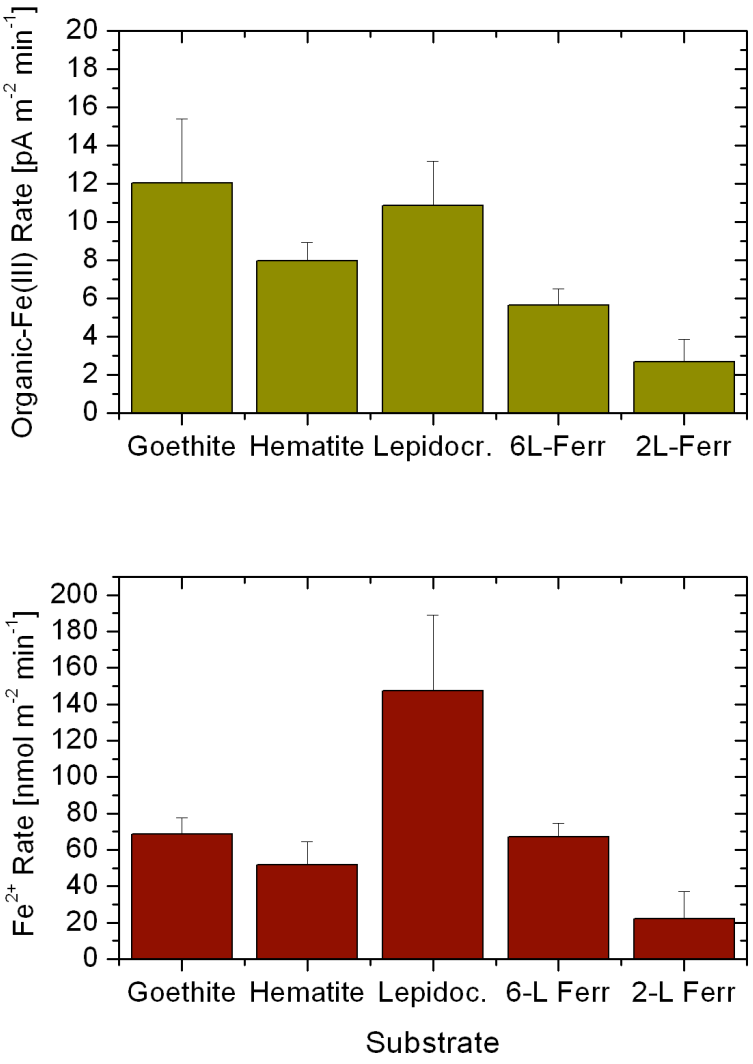

Figure 6.5 - a. Soluble organic-Fe(III) production and b. Fe(III) reduction rates by *S. putrefaciens* for goethite, hematite, lepidocrocite, 6L- and 2L-ferrihydrite normalized to the surface area of each individual Fe(III) oxides.

Direct quantification of soluble organic-Fe(III) is not possible, therefore, it is difficult to determine explicitly whether the solubilization step is rate limiting. However, soluble organic complexes reach steady-state after a few hours with Fe(III) citrate (Figure 6.1b) and after a few days with most Fe(III) minerals (Figure 6.3a), an indication that the organic chelator is recycled rapidly after reduction to solubilize additional Fe(III). These

findings suggest that the reduction of the TEA may be the rate limiting step in dissimilatory Fe(III) respiration, as previously proposed (Roden, 2003). Other mathematical models, that use first and second order kinetics or Michaelis-Menten kinetics to describe bacterial reduction of Fe(III) oxides, propose that the rate of reduction of Fe(III) oxide is proportional to the concentration of 'free' Fe(III) oxide surface sites (Bonneville et al., 2006; Liu et al., 2001; Roden, 2006). Results from the present study suggest that the rate of Fe(III) reduction is proportional to the concentration of soluble organic-Fe(III) complexes produced by *S. putrefaciens*. The proposed kinetic models do not currently account for ligand-promoted dissolution, although the mathematical formulation of Fe^{2+} production does not change conceptually from ligand-promoted dissolution. Therefore, the kinetic parameters derived from such models may not change, but the mechanistic interpretation of these models may be different.

This investigation demonstrates that the endogenous organic ligand produced by *S. putrefaciens* lowers the reduction potential of Fe(III) to form an electrochemically reactive complex in the analytical window of Hg electrodes (Figure 6.6). The decrease in the reduction potential of Fe(III) and corresponding increase in Gibbs free energy results in the formation of less stable complexes that increase the reduction rate, most likely due to the lower activation energy associated with the terminal Fe(III)-reductase complex and decrease in K_m (Figure 6.6). This model will be testable when the terminal Fe(III) reductase is isolated and purified. To our knowledge, this is the first report of a Fe(III)-solubilizing organic ligand produced by *S. putrefaciens*. *Geothrix fermentans* was previously shown to solubilize Fe(III) oxides prior to reduction, but the origin and composition of the solubilizing compound was not determined (Nevin and Lovley,

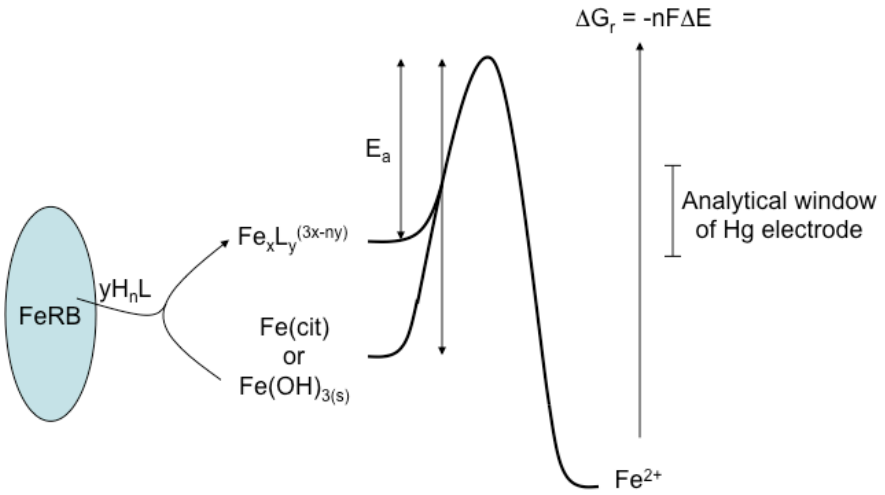

Figure 6.6 - Proposed mechanism of solubilization and reduction of Fe(III) by *S. putrefaciens*. *S. putrefaciens* produces an organic ligand to outcompete citrate- and oxyhydroxide-bound Fe(III). This ligand destabilizes Fe(III) by generating organic-Fe(III) complexes that are shifted towards more negative potentials (i.e., higher Gibbs free energy) and detected voltammetrically at mercury electrodes. As a result, the activation energy needed to produce the terminal Fe(III)- reductase complex is lowered, thus facilitating the formation of the intermediate complex (i.e., decrease in K_m). The production of higher concentrations of intermediate complex in turn increases the reduction rate.

2002b). Evidence for nonlocal reduction of Fe(III) oxides by *S. putrefaciens* strain CN-32 was found using atomic force microscopy and tentatively explained by the release of endogenous Fe(III)-solubilizing or -reducing compounds (Rosso et al., 2003). Siderophore-like ligands are also known to chelate and solubilize Fe(III) oxides (Hersman et al. 1995). *S. putrefaciens*, for example, produces hydroxamate-type siderophores during aerobic growth under iron-limited conditions (Gram 1994; Ledyard and Butler 1995). Such siderophores, however, display binding constants that are typically much higher than Fe(III) complexes reduced by *Shewanella* (Haas and DiChristina 2002). In addition, Fe(III) oxide solubilization experiments performed with commercially-available hydroxamate compounds did not reveal any electrochemical

Fe(III) signals (not shown). Thus it is unlikely that siderophores are responsible for the production of the soluble Fe(III) compounds detected by voltammetry. Current work is aimed at identifying the chemical characteristics of the Fe(III)-solubilizing ligand produced by *S. putrefaciens*.

6.6. Acknowledgements

This work was supported by the National Science Foundation Biocomplexity in the Environment and Biogeosciences programs and by the U. S. Department of Energy Environmental Remediation Sciences and Biogeochemistry Grand Challenge programs.

CHAPTER 7

CHARACTERIZATION OF IRON-BINDING ORGANIC LIGANDS IN MARINE SEDIMENT PORE WATERS

Abstract

Although organic-Fe(III) complexes that can provide a significant flux of Fe to the overlying waters appear to be pervasive in marine sediments, the origin of these complexes and their mechanism of formation remains unknown. In this work, a novel extraction scheme was developed to extract Fe-specific binding ligands from the bulk of pore water natural organic matter (NOM). The overall objective of this study was to attempt to identify the composition of the Fe-binding ligands to determine the source of these complexes. Fe-reactive ligands from the pore waters of a variety of sites across a coastal marsh in southern Georgia, US, were fractionated by an immobilized-metal affinity chromatography (IMAC) procedure that first eluted pore waters through Fe(III)-coated Chelex® resins to accumulate the ligands, then collected the ligands by rinsing the column with EDTA. The non-polar and moderately polar ligands were subsequently concentrated through hydrophilic-liphophilic balanced solid-phase extraction catridges (HLB-SPE) and eluted with methanol/H_2O. Finally, liquid chromatography / electrospray ionization mass spectrometry (LC/ESI-MS) was used to characterize the fractionated molecules. Results demonstrate the presence of at least seven low-molecular weight

ligands in significant concentration, of which three are common to pore waters from different sampling locations or collected at different times. Efforts were made to identify the ligands, but no ligands matching the inferred formula weights were found in literature or chemical databases. Interestingly, a series of N-containing ligands differing in mass by 14 Da (CH_2 group) was detected in multiple pore water samples. These ligands may correspond to a peptide-containing molecule with a fatty-acid side chain, similar to an amphiphilic siderophore. One ligand at mass 191 displayed a slight correlation with the original pore water dissolved Fe content under Fe-reducing conditions, suggesting this compound might be involved in Fe solubilization during dissimilatory Fe reduction.

7.1. Introduction

The importance of Fe to ocean primary productivity is well documented (reviewed in Breitbarth et al., 2010). Iron is a limiting nutrient in surface waters (e.g., (Boyd and Law, 2001; Coale et al., 1996; Martin and Fitzwater, 1988) because the low solubility of Fe(III) limits the concentration of dissolved Fe (< 0.4 μm) available for biological uptake (Millero, 1998). However, organic ligands, including fulvic and humic acids, siderophores, extracellular polymeric substances (EPS), and cell lysis products, increase its solubility in seawater by 3 to 17 fold (Hunter and Boyd, 2007) and may thus play an important role in the bioavailability of Fe in the oceans (Gledhill et al., 1998; Gledhill and Buck 2010; Hutchins et al., 1999; Rue and Bruland, 1995; Van Den Berg, 1995; Witter et al., 2000; Witter and Luther, 1998). In estuaries, the majority of dissolved riverine Fe is lost to sediments through flocculation and precipitation during mixing with seawater (Boyle et al., 1977). Dissolved Fe, however, may be stabilized by

organic ligands, including riverine (Gerringa et al., 2007; Perdue et al., 1976) and sedimentary (Burdige et al., 1992) dissolved organic matter (DOM), and 2 to 20% of dissolved riverine Fe may be exported to the continental shelf depending on the river DOM content (Boyle et al., 1977; Perdue et al., 1976). Likewise, significant concentrations of Fe produced from continental margin sediments seem to be transported laterally over long distances in deep waters (Lam and Bishop, 2008; Lam et al., 2006; Lohan and Bruland 2008' Nedelec et al., 2007; Noffke et al., 2012). Although the exact composition of dissolved Fe is often not measured, a fraction (< 20 nM) may be stabilized by organic ligands (e.g. Buck et al., 2007; Gledhill et al., 1998; Rue and Bruland, 1995; Van Den Berg, 1995; Witter et al., 2000; Witter and Luther, 1998) while a significant fraction may be found under the form of colloids or nanoparticles (Cullen et al., 2006; Guo and Santschi, 1997; Raiswell et al., 2006; Wu et al., 2001).

Soluble Fe(III) (< 0.2 μm) has been detected in significant concentrations (Table 4.3) and, in some cases, may represent a dominant oxidant in marine sediments (Jones et al., 2011; Koretsky et al., 2008; Luther et al., 1996). Electrochemical signals with gold amalgam (Au/Hg) voltammetric microelectrodes have demonstrated the presence of soluble Fe(III) complexed by organic ligands in anaerobic marine sediments after collection (Brendel and Luther, 1995; Bull and Taillefert, 2001; Carey and Taillefert, 2005; Huettel et al., 1998; Rickard et al., 1999; Taillefert et al., 2000; Taillefert et al., 2002a; Taillefert et al., 2007b; Taillefert et al., 2002b) or during *in situ* measurements (Meiggs and Taillefert, 2011; Tercier-Weber and Taillefert, 2008). *In situ* measurements have demonstrated that the formation of these complexes is not the result of artifacts upon sediment sampling (Meiggs and Taillefert, 2011; Taillefert et al., 2007b; Tercier-

Waeber and Taillefert, 2008), yet their chemical composition remains poorly defined. Voltammetric experiments demonstrated that several soluble organic-Fe(III) complexes that aggregate slowly in seawater may be detected simultaneously at the electrode surface during oxygenic oxidation of Fe^{2+}, while voltammetric signals for colloidal Fe(III) is only briefly observed in the absence of organic ligands as aggregation rapidly precipitates Fe(III) oxides at circumneutral pH (Taillefert et al., 2000). These findings imply that soluble Fe diffusing across the sediment-water interface (SWI) into oxygenated overlying waters must be oxidized and complexed by organic ligands to be a significant source of Fe to the water column. Sedimentary DOM is composed of a complex mixture of compounds ranging from relatively large macromolecules (> 3kDa), including humic substances and proteins, to smaller molecules such as amino acids or short-chain organic acids (Thurman, 1985). Interestingly, Fe(III) complexes with strong binding ligands and stability constants consistent with those of fulvic acids (Laglera and van den Berg, 2009) are routinely detected in estuaries (Perdue et al., 1976), and these complexes may play an important role in the transfer of Fe(III) to the oceans (Buck et al., 2007; Jones et al., 2011; Powell and Wilson-Finelli, 2003), as fulvic DOM is resistant to salt-induced flocculation (Powell and Wilson-Finelli, 2003). While Fe(III)-DOM complexes or colloids formed in estuarine waters are the precursors to the Fe eventually flocculating to the sediments (e.g. Boyle et al., 1977; Powell et al., 1996; Chapter 4 of this thesis), a strong correlation was found between absorbance at 254 nm, typically used as a proxy for DOC (Chin et al., 1994; Chin et al., 1998), and dissolved Fe(III) in the pore waters of the Satilla River Estuary (Chapter 4 of this thesis), suggesting that diagenetic processes disturb the established equilibrium between the mineral aggregates and the pore waters

and result in the accumulation of dissolved organic-Fe(III) complexes.

The existence of soluble organic-Fe(III) complexes is not limited to coastal environments, as continental slope and deep-sea sediments that receive significant inputs of Fe oxides also represent sources of these complexes (Chapter 5 of this thesis). *In situ* measurements on the shelf break of Cape Hatteras (250 m water depth) revealed consistent signals for soluble organic-Fe(III) deep in the sediments, with the highest currents recorded near the maximum $O_{2(aq)}$ penetration depth at the onset of Fe^{2+} production (Chapter 2 of this thesis). The production of these org-Fe(III) complexes correlated well with the onset of Fe(III) reduction, suggesting that these complexes are formed as intermediates during both Fe(III) reduction in anaerobic conditions and Fe(II) oxidation in aerobic conditions. Non-reductive dissolution of amorphous Fe(III) oxides by multidentate organic ligands forming mononuclear complexes with Fe(III) oxides (Huheey et al., 1993) may occur at circumneutral pH (Bondietti et al., 1993; Deng and Stumm, 1994; Luther et al., 1996; Nowack and Sigg, 1997; Zinder et al., 1986). These complexes are also intermediate products in the bacterial reduction of Fe(III) oxides (Taillefert et al., 2007a), and mutagenesis studies with model metal- reducing bacteria (*Shewanella* genus) demonstrate that the ligand is produced endogenically, is not a siderophore (Fennessey et al., 2010), and is directly involved in the respiration of iron oxides (Chapter 6 of this thesis; Jones et al., 2010).

The composition of the organic-Fe(III) complexes found below the maximum depth of $O_{2(aq)}$ penetration remains elusive, but findings that model iron- reducing bacteria produce such complexes as intermediates during the reduction of Fe(III) oxides (Chapter 6 of this thesis; Fennessey et al., 2010; Jones et al., 2010; Taillefert et al., 2007a) suggest

that these ligands may be of biogenic origin. Given the pervasiveness of soluble organic-Fe(III) complexes in suboxic sediments, confirmation of these findings would also have important ramifications on the understanding of the importance of iron-reducing bacteria in marine sediments. In this work, a novel, multi-step fractionation scheme using immobilized metal-affinity chromatography (IMAC) and hydrophilic-lipophilic balanced solid-phase extraction (HLB-SPE) was developed to isolate Fe(III)-reactive ligands from sediment pore waters for subsequent characterization by liquid chromatography electrospray ionization mass spectrometry (LC/ESI-MS).

7.2. Methods

7.2.1. Sediment profiling and pore water sampling

Sediment cores were taken from the Salt Marsh Ecosystem Research Facility (SERF) at the Skidaway Institute of Oceanography (Savannah, GA, USA) within three weeks in the Spring of 2014 (Figure 7.1) using a home-made sediment corer made of acrylic core barrels (8 x 50 cm). A major advantage of SERF is a 250 m long boardwalk which provides direct access to the marsh and spans a range of environments, from an inland meadow to tidal creeks. This site has been extensively studied by our group (Bull and Taillefert, 2001; Carey and Taillefert, 2005; Taillefert et al., 2007b; Tercier-Waeber and Taillefert, 2008), and a remotely controlled *in situ* electrochemical analyzer has been deployed in these sediments to remotely monitor the composition of the pore waters continuously from Georgia Tech (Meiggs, 2010; Tercier-Waeber and Taillefert, 2008). Previous work has demonstrated the dominance of microbial metal-reduction in creeks and creek banks, as compared to mud flats, where SO_4^{2-} dominates (Meiggs, 2010;

Taillefert et al., 2007b). Core A was collected from the center of the large creek at the end of the boardwalk at low tide, with only a few cm of water in the creek and no vegetation nearby. The sediment was a uniform brown color throughout the core, but became very dense and clay-like by 8 cm. Some plant debris were observed in the core at 4 cm depth. Core B was taken from the center of the small creek at high tide in an unvegetated location. The sediment was of uniform brown color, but became much denser by 8 cm depth. Core C was taken from the bank of a small adjacent creek at low

Figure 7.1 – A map of locations where the sediment cores were collected at SERF on Skidaway Island, Georgia (USA). A 250 m long boardwalk allows to access diverse regions of this intertidal coastal marsh.

tide, approximately 4 cm away from live *Spartina*. The mud was brown at the surface, but by 10 cm depth was partially black and contained plant debris. The cores were sectioned in slices of between 1.6 and 2.1 cm under an N_2 atmosphere to provide between 8 and 12 discrete samples. Each section was centrifuged under a N_2 atmosphere for 20 minutes at 3,000 RPM to extract pore waters. Pore waters were then immediately filtered onto 0.2 μm Whatman Puradisc syringe filters into 15 mL tubes under a N_2 atmosphere, and processed within 30 minutes for analyses. Iron speciation (i.e. dissolved Fe(II) and total dissolved Fe to calculate dissolved Fe(III) concentrations by difference) in each filtered sample was determined spectrophotometrically by the Ferrozine method (Stookey, 1970; Viollier et al., 2000). After taking note of the volumes of each pore water sample, between 2 to 4 pore water samples were then combined into 50 mL tubes under N_2 atmosphere to yield samples large enough for the separation procedure.

7.2.2. Metal affinity chromatography and electrospray ionization mass spectrometry

Well known Fe(III)-binding ligands (citrate, riboflavin, and desferrioxamine mesylate (DefB)) as controls and natural Fe(III)-binding ligands from sediment pore waters were extracted using IMAC according to the following strategy. Ligands presenting affinity for Fe(III) were first isolated on a Chelex®-100 resin pre-equilibrated with Fe^{3+} ions. The column retentate was then eluted and the natural ligands simultaneously decomplexed from Fe^{3+} using EDTA as competitive ligand. The samples were then loaded on a hydrophilic modified C-18 solid-phase extraction cartridge to

extract the natural organic ligands and eluted with methanol for Liquid Chromatography-Electron Spray Ionization-Mass Spectrometry LC/ESI-MS analysis.

All chemicals were purchased from Sigma-Aldrich and prepared with HPLC-grade deionized H_2O (Fisher Scientific). The Fe(III) solid sorbent was first prepared by packing 1 g of Chelex®-100 resin (Sigma, sodium form) in a low-pressure column (Kontes, Flex-column 0.7 mm ID x 4 mm). The resin was converted from sodium form to Fe form by flushing in sequence 4 mL HCl, 10 mL dionized H_2O, 4 mL 100 mM $FeCl_3$ adjusted to pH 2.2 with NaOH, and 10 mL dionized H_2O with a low speed peristaltic pump (Ismatec®) at a flow rate of 1 mL/min. The column was subsequently conditioned for natural saline samples with 4 mL of 0.54 M NaCl containing 2.3 mM $NaHCO_3$ (pH 7.5). Between 10 and 50 mL of pore water samples or 15 mL of standards were loaded onto the Fe(III)-Chelex®, and excess salts then rinsed with 4 mL deionized H_2O. Standards were prepared at 1 mM concentration in artificial seawater with 10 mM $NaHCO_3$ added. Artifical seawater consisted of the following salts: NaCl (0.428 M), Na_2SO_4 (29.27 mM), $MgCl_2.6H_2O$ (54.74 mM), KCl (10.58 mM), and $CaCl_2.2H_2O$ (10.75 mM). Ligands bound to the Fe(III)-Chelex® were then extracted with 4 mL of 20 mM EDTA adjusted to pH 8.5 with NaOH and allowed to equilibrate with the column overnight. Solid-phase extraction cartridges (Supelco, Select HLB SPE tube 60 mg) were conditioned with 2 mL of 80% methanol and then 2 mL of dionized water. The EDTA extracts were syringe-loaded onto the SPE tubes, and retained ligands were subsequently eluted with 2 mL of 80% methanol. These samples were then concentrated ~10 fold by evaporation under vacuum overnight in the presence of desiccant (Drierite).

Ligands were identified by LC-ESI-MS by introducing extracted samples into a triple quadropole mass spectrometer (Micromass Quattro LC) using electrospray after chromatographic separation on a reversed phase C-18 column (Phenomenex Gemeni C-18, 150 x 2 mm, 5 um). A linear gradient from 5% acetonitrile to 100% acetonitrile (both water and acetonitrile solutions contained 0.2% formic acid to promote the formation of positive ions) was provided by a binary HPLC system (Agilent 1100 Series). NaI and RbI cluster standards from 20 to 3,000 Da were used to calibrate the instrument, and data were collected in both positive and negative ionization modes.

7.3. Results

7.3.1. Separation and characterization of well-known Fe(III)-binding ligands

Solutions of synthetic Fe(III)-binding ligands were subjected to the IMAC procedure and LC-ESI-MS analysis to determine the efficiency of the technique in identifying Fe(III)-binding ligands (Figure 7.2 and 7.3). Total-ion chromatograms (TICs) revealed various degrees of recovery depending on the ionization mode used (Figure 7.2). In general, positive ionization mode yielded larger chromatographic peaks than negative ionization mode (Figure 7.2a and b). Riboflavin (MW = 376.36) produced strong peaks in positive ionization mode at 17.8, 18.4, and 21.9 minutes (Figure 7.2a) corresponding to m/z ratios of 377.3, 375.2, and 243.2 (Figure 7.3a-c). In turn, negative ionization mode for riboflavin revealed smaller peaks at 17.8 and 18.4 minutes (Figure 7.2b) corresponding to m/z ratios of 375.3 and 421.1 (Figure 7.3d). DefB (MW = 560.68) eluted earlier, producing a peak at 15.9 minutes (Figure 7.2a) with a m/z ratio of 561.5 and an additional doubled charged ion with a m/z ratio of 281.2 in the positive ionization

mode (Figure 7.3e) and a single peak in the negative mode (Figure 7.2b) with a m/z ratio of 559.4 (Figure 7.3f). On the other hand, citric acid (MW = 192.12) failed to produce any discernable peak, even after searching for $[m+H^+] = 193$ and $[m-H^+] = 191$ in both positive and negative single ion chromatograms (SICs) (Figure 7.2a and b). The peaks between 3 and 5 minutes in both ionization modes correspond to EDTA and Fe-EDTA (data not shown).

7.3.2. Separation and characterization of pore water Fe(III)-binding ligands

The concentration and depth distribution of dissolved Fe(II) and Fe(III) were dependent on the location of the sediment core with respect to marsh topography and vegetation (Figure 7.4). Sediment pore waters from the center of the creek (Figure 7.4a and b) on average contained less dissolved Fe(II) and Fe(III) (128 ± 74 and 127 ± 107 μM) than creek bank sediments (463 ± 255 μM), which were also closer to the vegetation (Figure 7.4c). Additionally, while all cores displayed a general decrease in concentration of Fe(II) with depth in the sediment, a subsurface maximum in Fe(II) was found in the vegetated creek bank sediment (Figure 7.4c). In contrast, concentrations of dissolved Fe(III), while slightly higher in the vegetated creek bank sediment, did not vary significantly across the sediment column. TICs of the extracted pore water sample from the first 9.3 cm of the vegetated creek bank in both the positive and negative ion modes are presented as examples, along with water blanks subjected to the same extraction

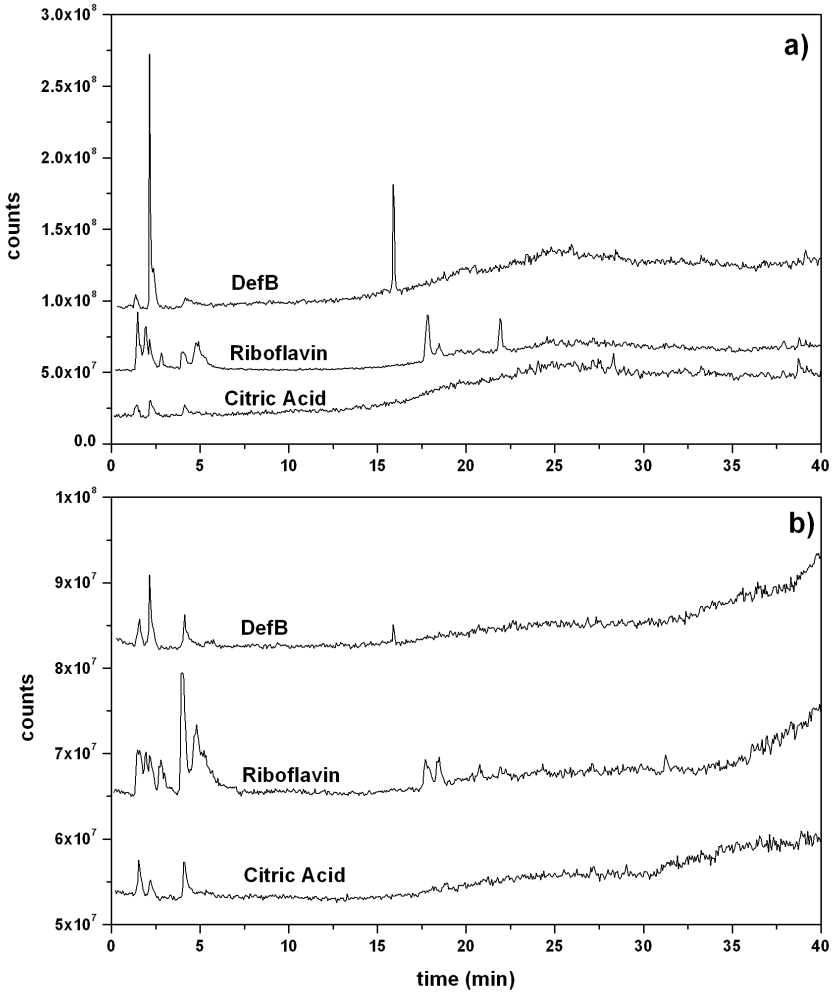

Figure 7.2 – Total Ion Chromatographs in the a) positive and b) negative ionization mode of DefB, riboflavin, and citric acid standards subjected to the Fe-IMACs procedure and LC-ESI-MS analysis using reverse phase chromatography.

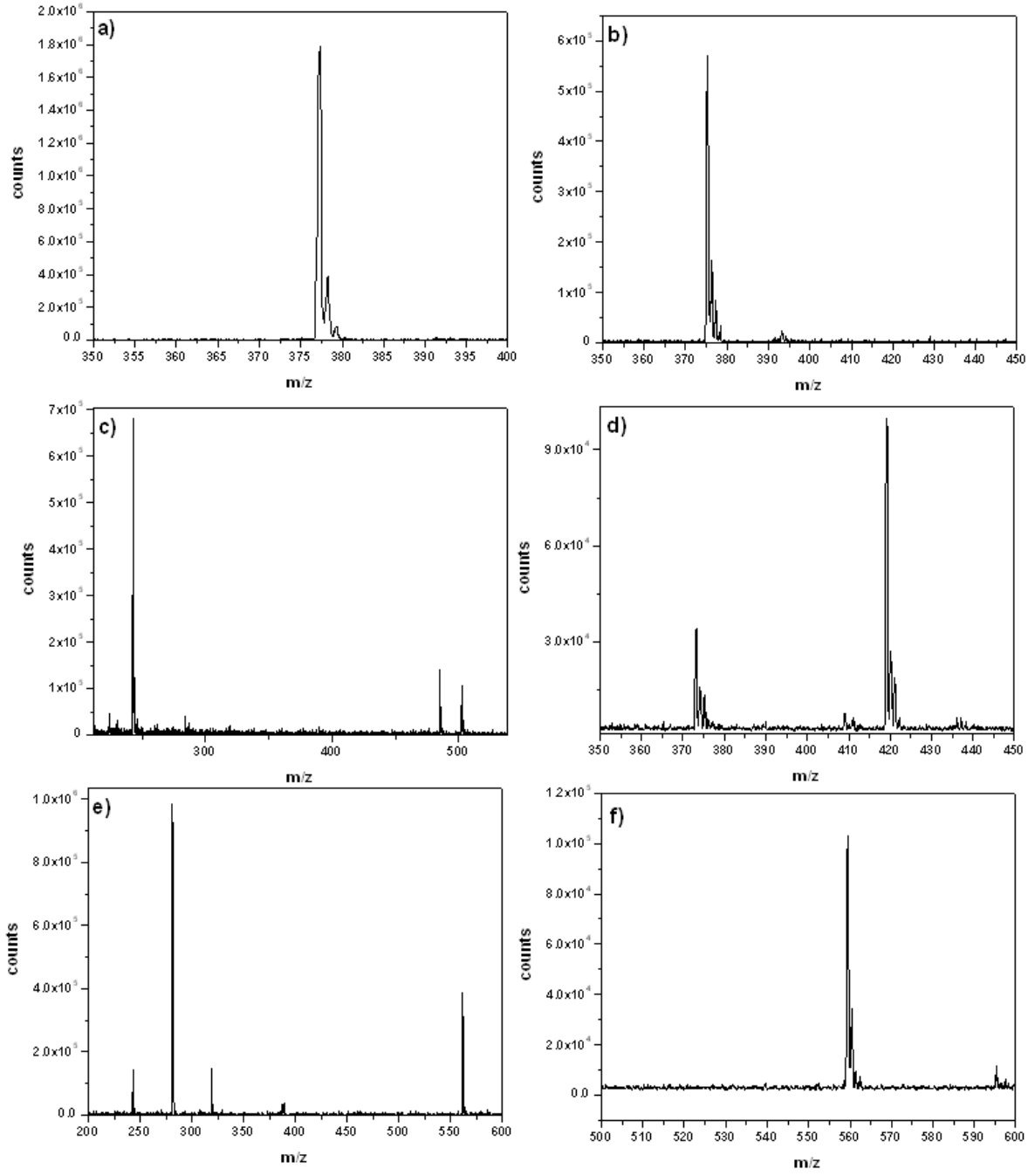

Figure 7.3 – Mass spectrometry results for dominant peaks for the chromatograms in figure 7.2 for riboflavin at minute a) 17.8 (+ mode), b) 18.4 (+ mode), c) 21.9 (+ mode), and d) 18.4 (- mode), as well as DefB at minute e) 15.9 (- mode), and f) 15.9 (- mode).

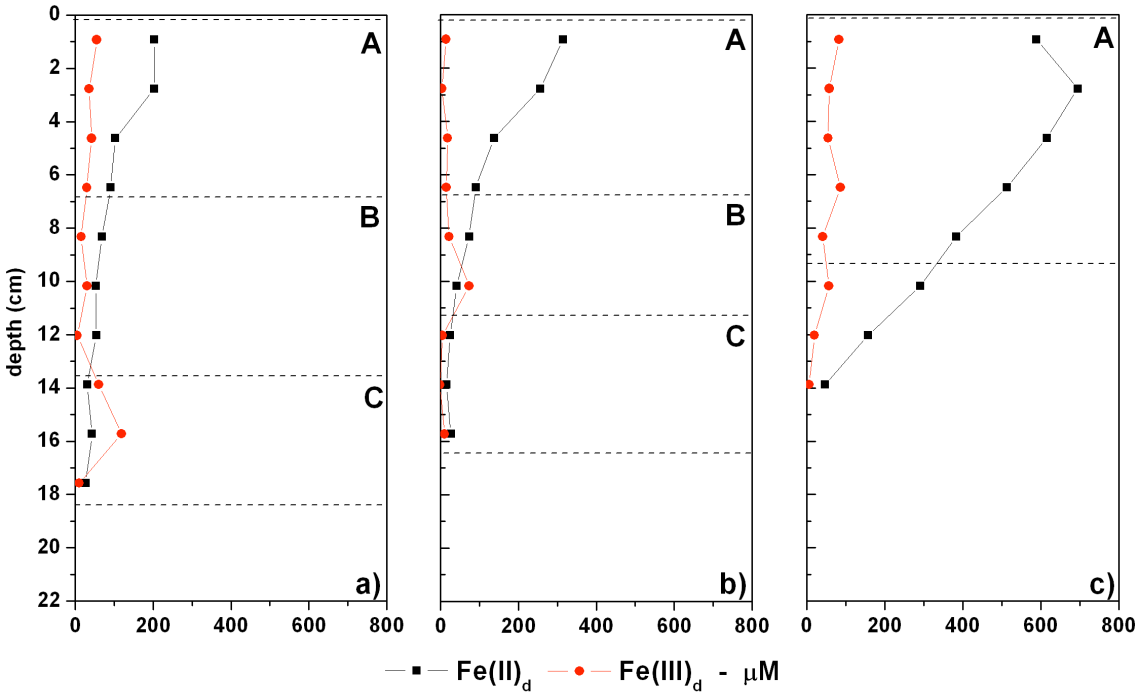

Figure 7.4 – Profiles of dissolved iron speciation from a) Core A collected in the center of the large creek (unvegetated); b) Core B collected in the center of a small adjacent creek (unvegetated); c) Core C collected from the bank of the same creek, ~4 cm from *Spartina*. Dashed lines delineate depth intervals combined and subjected to the Fe-IMACs procedure and LC-ESI-MS analysis.

procedure (Figure 7.5). Blanks generally did not display large peaks in both ionization modes, and variations in the baseline were due to solvent interactions. As for the synthetic ligands, the peaks between 3 and 5 minutes in both ionization modes correspond to EDTA and Fe-EDTA used to extract the organic ligands from the Chelex® column. Approximately seven ligands extracted from the pore waters generated peaks between 16 and 28 minutes in one or in both ionization modes (Figure 7.5, Table 7.1). The peaks most significantly larger than the blanks appeared at 16.0, 19.0, and 28.3 minutes in positive ionization mode (Figure 7.5a), and at 19.0, 19.8, and 22.3 minutes in

negative ionization mode (Figure 7.5b). Mass spectral analysis indicated that smaller peaks 1 and 2 m/z units larger than the base peaks were consistent with carbon-containing, singly-charged molecules. Therefore, peaks may be referred to subsequently in this chapter by their inferred formula masses (MW column, Table 7.1), to ease comparison of positive and negative ion spectra. Peaks were of relatively low molecular weight (MW) (Figure 7.6), and corresponded to compounds with MW of 173, 187, 173, 188, and 191 Da. Some similarities were observed between the seven extracted pore waters with respect to LC-MS peaks. The peaks at 19.0, 22.4, and 28.4 minutes (MW = 187, 188, and 191) were common to the other pore waters (Table 7.1). However, an additional peak at 21.4 minutes corresponding to a MW of 201 was observed in both positive and negative modes in the pore waters from the center of the creeks (core A and core B; Table 1).

7.4. Discussion

Soluble organic-Fe(III) complexes are pervasive in the pore waters of coastal and continental margin sediments. Resolving the nature of these Fe-binding ligands will provide insight into their formation mechanisms, reactivities, and stability. However, the composition of the Fe-complexing organic ligands remains unknown. In this work, a novel extraction scheme was developed to extract Fe(III)-binding ligands from pore waters and identify their molecular composition using LC-ESI-MS. Immobilized metal affinity chromatography (IMAC) has been used previously to analyze siderophores (Braich and Codd, 2008), humic substances (Burba et al., 2000; Ross et al., 2003), peptides (Li and Dass, 1999), and seawater ligands (Ross et al., 2003). To our

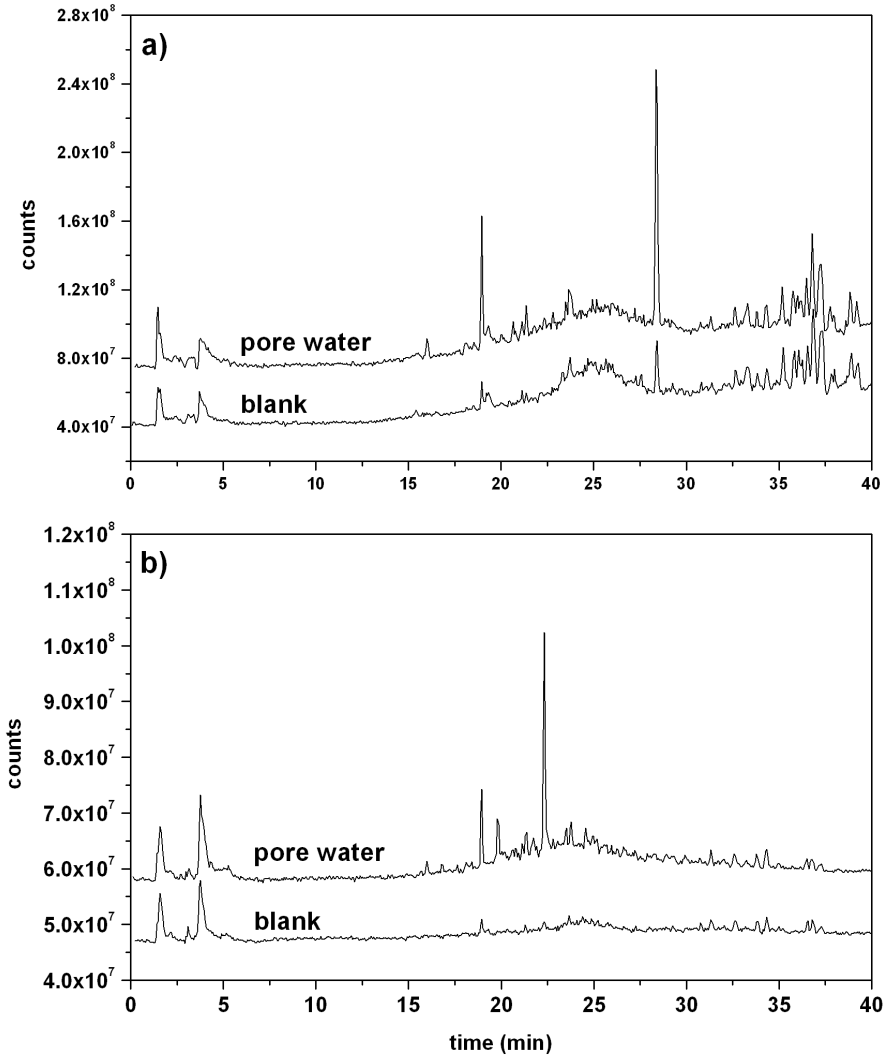

Figure 7.5 – Total Ion Chromatographs (TICs) of the extracted sample from the surface 9.3 cm core C (and a blank subjected to the same extraction procedure in a) positive and b) negative ion modes.

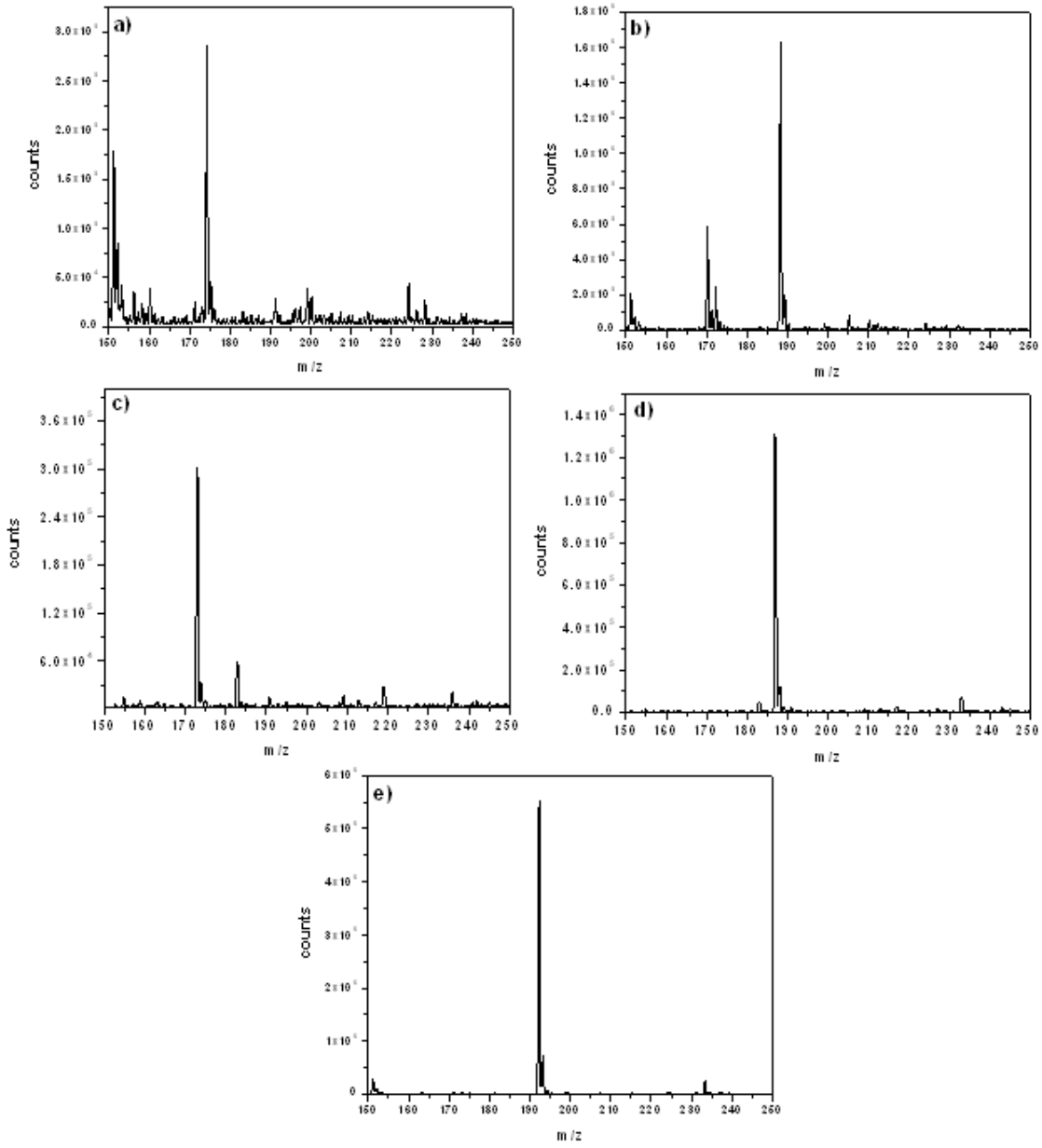

Figure 7.6 – Mass spectrometry results for dominant peaks for the chromatogram in figure 7.5 at a) 16 (+ mode), b) 19 (+ mode), c) 19.8 (- mode), d) 22.3 (- mode), e) 28.4 (+ mode) minutes.

Table 7.1 – Iron composition and LC-ESI-MS data for extracted pore water samples from the sediment layers shown in Figure 7.4. The sample iron concentrations represent the concentrations of Fe_T, Fe^{2+}, and Fe(III) by difference in the original pore waters of each sediment layer. The sample iron loaded on the Chelex® column was determined from the product of the concentration in the original sample and volume of sample loaded onto the column. EDTA rinse volumes eluted through the Chelex® to desorb Fe(III) and ligands, the volume of the EDTA rinse solutions loaded on the HLB-SPE cartridges (SPE loaded volumes), and the concentrate volume obtained after flushing the HLB-SPE cartridge with methanol / H_2O and evaporating the final solution under vacuum are provided for reference. The concentration of iron initially present in the samples can be normalized to the concentration injected into the LC/ESI-MS using equation 7.1

		Core A			Core B			Core C
		A	B	C	A	B	C	A
total vol.	(mL)	31.5	27	33.5	42.5	18.5	19.5	33.5
sample Fe_T	(μmol L^{-1})	221.5	94.0	90.3	323.8	200.8	152.4	645.8
sample Fe(II)	(μmol L^{-1})	175.6	68.7	39.4	308.2	164.0	77.8	579.2
sample Fe(III)	(μmol L^{-1})	45.9	25.3	50.9	15.7	36.8	74.6	66.6
Loaded Fe_T	(μmol)	6.98	2.54	3.02	13.76	3.72	2.97	21.63
Loaded Fe(II)	(μmol)	5.53	1.85	1.32	13.10	3.03	1.52	19.40
Loaded Fe(III)	(μmol)	1.45	0.68	1.71	0.67	0.68	1.46	2.23
EDTA rinse vol.	(mL)	5	5	5	5	5	5	5
SPE loaded vol.	(mL)	4	4	4	4	4	4	4
concentrate vol.	(mL)	0.44	0.41	0.40	0.44	0.40	0.49	0.40
concentrate Fe_T	(mmol L^{-1})	12.7	5.0	6.1	25.1	7.4	4.8	43.3
concentrate Fe(II)	(mmol L^{-1})	10.1	3.6	2.6	23.9	6.0	2.5	38.8
concentrate Fe(III)	(mmol L^{-1})	2.6	1.3	3.4	1.2	1.4	2.4	4.5

LC-MS Peak counts (x 10^5)			Core A (pos / neg)			Core B (pos / neg)			Core C (pos / neg)
time (min)	m/z (+)	m/z (-)	AA	AB	AC	BA	BB	BC	CA
16.0	174.3	172.1	0.0 / 0.0	0.0 / 0.0	0.0 / 0.0	0.0 / 0.0	0.0 / 0.0	0.0 / 0.0	9.6 / 2.1
19.0	188.2	185.9	49.5 / 11.3	62.2 / 13.7	47.8 / 9.5	110.1 / 36.0	52.1 / 14.2	71.5 / 19.0	51.6 / 111.7
19.8	nd	173.0	0.0 / 0.0	0.0 / 0.0	0.0 / 0.0	0.0 / 0.0	0.0 / 0.0	0.0 / 0.0	0.0 / 0.0
21.4	202.2	200.1	12.3 / 3.1	17.4 / 3.9	13.7 / 3.1	30.0 / 9.2	15.1 / 4.6	21.2 / 5.1	0.0 / 0.0
22.4	nd	186.9	0.0 / 4.7	0.0 / 7.3	0.0 / 6.1	0.0 / 25.7	0.0 / 13.7	0.0 / 17.4	0.0 / 25.8
23.7	216.3	nd	0.0 / 0.0	0.0 / 0.0	0.0 / 0.0	0.0 / 0.0	0.0 / 0.0	0.0 / 0.0	6.3 / 0.0
23.7	275.4	nd	0.0 / 0.0	0.0 / 0.0	0.0 / 0.0	0.0 / 0.0	0.0 / 0.0	0.0 / 0.0	3.2 / 0.0
28.4	192.2	nd	69.8 / 0.0	47.4 / 0.0	44.1 / 0.0	121.7 / 0.0	133.2 / 0.0	115.0 / 0.0	194.0 / 0.0

knowledge, however, this is the first study to examine Fe(III)-binding ligands in sediment pore waters. Additionally, a post IMACs step with C-18 SPE cartridges is usually used to concentrate non-polar compounds of interest via reverse phase and replace the seawater matrix by a mass spectrometry-compatible solvent. In this work, hydrophilic-modified solid phase extraction resins were used for the first time to extract both non-polar and polar molecules.

7.4.1. Evaluation of the extraction scheme

To test the effectiveness of the extraction scheme, a suite of well-defined Fe(III)-binding organic ligands representative of groups of ligands with varying denticities or structure backbones were subject to the exact same separation scheme as the pore water samples (Figure 7.2). DefB is a strong Fe(III)-binding, multiple bidentate ligand that is often used as a model siderophore in experiments (Kalinowski et al., 2000; McCormack et al., 2003). Riboflavin is a bidentate ligand with a phenolic backbone. Citrate is a tridentate ligand, similar to other multidentate ligands such as EDTA, TRIS, or NTA. Peaks corresponding to DefB and Riboflavin were visible on their respective TICs. While DefB eluted as a single peak at 15.9 minutes in both positive and negative mode with a MW of 560.5 (Figure 7.3e and f) close to its true mass (MW = 560.6), riboflavin (nominal MW = 376) eluted at 17.8 minutes, but two more peaks from the sample eluted later (MWs = 374 & 242; possibly decomposition or fragmentation products). The observed retention times of extracted riboflavin and DefB are consistent with riboflavin having a higher octanol-water partition coefficient (log K_{ow}) than DefB (Ihnat et al., 2000; Nahum and Horvath, 1980), and therefore being more lipophilic. Peaks in positive

ion mode were much larger, probably because compounds were more easily ionized after the addition of formic acid to the eluents. Unfortunately, citrate could not be characterized by LC-ESI-MS even when a 100 μM Na-citrate standard was injected directly into the mass spectrometer (data not shown), suggesting that citrate is not readily ionized in positive-ion mode, even with 2% formic acid added. These findings do not necessarily imply that citrate and similar compounds cannot be extracted by the IMAC procedure. More tests will have to be conducted to fine-tune this procedure.

7.4.2. Natural Fe(III)-binding ligands isolated from pore waters

Using the developed IMAC procedure, seven ligands were successfully extracted from pore waters that produced peaks significantly different from the blanks, and three were common to all pore waters. The natural Fe(III)-binding ligands eluted between 16 and 28.4 minutes, suggesting their hydrophobic character were at least the same or greater than that of DefB. Molecular weights between 173 and 274 were identified for these natural ligands, much lower than those of typical humic substances (e.g. Chin et al., 1994; Miles and Brezonik, 1983; Rausa et al., 1991; Chapter 2 of this thesis), which readily complex Fe in pore waters (Chin et al., 1998; Laglera and van den Berg, 2009; Perdue et al., 1976; Rose and Waite, 2003). Similar investigations conducted with Cu-binding ligands in sea water also identified low molecular weight compounds only (Ross et al. 2003). As humic acids must be present in the pore waters extracted, these findings suggest they are either not extracted by the IMAC procedure or are too variable with respect to composition (i.e. MW) to produce discrete peaks on the TICs. A slight brown color is observed, however, in both the Fe(III)-Chelex® column and the HLB-SPE

cartridge when a significant amount (>10 mL) of pore waters is extracted (not shown). In addition, the final methanol/water extract is slightly tinted brown suggesting that humics are in fact separated by the IMAC procedure as Fe(III)-binding ligands.

The ChemSpider database (www.chemspider.com) was searched for molecules or known complexes with a MW 56 ± 4 Da higher than the molecular weights of the ligands identified in Table 7.1 that contained at least one C, H, O, and Fe, while allowing the presence of N or S or ligands. The compounds identified by this procedure were further filtered by ensuring they formed a single complex, that Fe was in divalent or trivalent form, and that no C-C triple bonds were considered. Approximately 50 ligands matched the criteria for all seven unidentified ligands, but only one ligand, nitrilotriacetic acid (NTA), met the criteria for the mass at 191. NTA is synthetic and should not be present to a great extent in the relatively pristine SERF site sediments. Indeed, NTA (MW = 191) standards injected directly into the LC/ESI-MS eluted much earlier, with a retention time of 6.8 minutes (data not shown), than the pore water extracted by IMAC (Figure 7.5). It should be noted, however that the NTA peak on the TIC was of low intensity (as was citrate in the same multi-standard), suggesting the LC/ESI-MS procedure may not be optimized to detect ligands with acidic (carboxylic) functional groups.

However, using general principles, it is possible to provide insight into the molecular composition of some of the ligands. The even mass 188 could correspond to the dipeptides Ala-Val, Gly-Ile, Gly-Leu. The other even mass, 274, could correspond to quite a few dipeptides: Gly-Gly-Ala-Ala, Gln-Gln, Gly-Ala-Gln, Gly-Ala-Lys, Lys-Gln, Ala-Ala-Orn, and Lys-Lys. The series with the nomial mass of 274 could be further separated into three groups differing by 36.4 mDa, indicating the substitution of a CH_4

group in place of an O atom. Using the Nitrogen Rule, it can be concluded that the odd series of masses must contain an odd number of N atoms (McLafferty 1993). The series of 173, 187, 201, and 215 differ by a nominal mass of 14, consistent witho a methylene C-H_2 group. Further, these four ligands have increasing retention times, suggesting each additional methylene group makes the molecule more non-polar. Together, this data suggests this series may be an amine containing peptide or similar compound with a fatty-acid tail of differing chain length. Interestingly, similar amphiphilic peptidic siderophores, synechobactins, have been previously isolated from marine bacteria.

Although Fe initially present in the samples should not be retained on the Fe(III)-Chelex column or the SPE cartridge, the Fe content was normalized for concentration effects throughout the separation procedure (Table 7.1), with the idea that the Fe content and Fe-binding ligands initially in pore waters could be correlated. To generalize, the number of moles of any compound in the concentrated sample after the extraction/concentration procedure is:

$$C_{conc} = \frac{C_{pw} V_{pw} \left(\frac{V_{SPE}}{V_{EDTA}} \right)}{V_{final}} \qquad \text{(Eq. 7.1)}$$

where V_{pw} is the volume of pore water eluted through the Fe(III)-Chelex column, C_{pw} is the concentration of the species of interest in the pore water sample, V_{EDTA} is the volume of EDTA used to elute the Fe(III)-binding ligands from the Fe(III)-Chelex column during the extraction, V_{SPE} is the volume of the EDTA permeate loaded onto the HLB-SPE cartridge, and V_{final} is the final sample after concentration by evaporation. A slight correlation ($R^2 = 0.59$) was observed between the adjusted Fe_T concentration of the pore water samples corrected for the dilution and concentration steps used during the

extraction (Eq. 7.1) and the counts of m/z ratio [M+H$^+$] = 192.2 on the SIC (Figure 7.7). Although only seven data points are present, the correlation may indicate that in general, more ligand of mass 191 exists under Fe(III) reducing conditions. No other significant correlations between peak heights or normalized Fe content were observed.

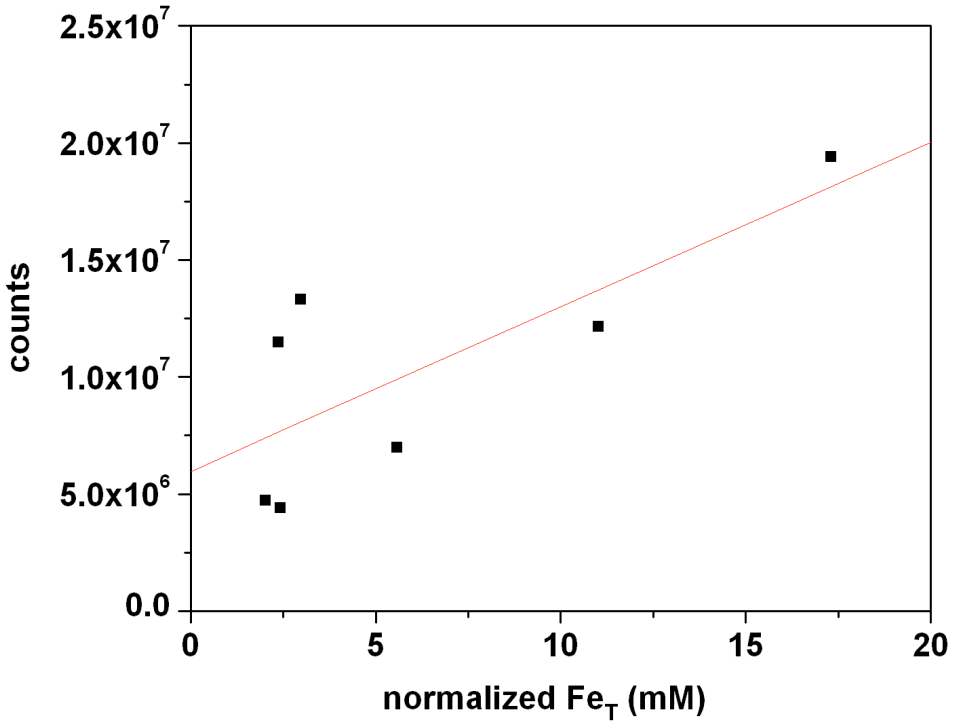

Figure 7.7 – Correlation ($R^2 = 0.59$) between Fe_T in original pore water samples normalized to the volume after the extraction and concentration procedure.

7.4.3 Recommendations for improvement

While this new procedure selecting for Fe(III)-binding ligands shows some exciting promises, several items should be addressed to improve the extraction procedure and the mass spectrometric characterization. First, the ESI-MS step was performed under the same conditions in both positive and negative ionization modes (i.e. with 2% formic

acid). While formic acid promotes the formation of $[M+H^+]$ ions in the positive ionization mode and enhance peak signals, it may hamper the formation of negative ions in the negative ionization mode, which may be more important as Fe-reactive ligands contain mostly acidic functional groups (e.g. carboxylics, phenolics, and thiols; Ross et al., 2003). NH_4-acetate (or no pH modifier) instead of formic acid is usually used to enhance counts when running mass spectrometric analyses in the negative ionization mode (Ross et al., 2000, 2003), and this approach may help characterize organic ligands carrying carboxylic acid groups. A multi-standard containing representative ligands and humic acid standards should also be separated by LC/ESI-MS under different chromatographic conditions to optimize the separation of the potentially numerous Fe(III)-binding ligands present in natural pore waters. Finally, an internal standard should also be added to pore water extracts prior to LC/ESI-MS analysis to better compare peak heights obtained by ESI-MS in different samples.

After optimizing the ESI-MS analysis, the HLB-SPE extraction process could be further improved. The manufacturer recommends adjusting sample pH to at least 2 pH units lower than the pK_a of the target compounds, likely to improve the binding between a less polar form of the compound with the lipophilic groups on the HLB-SPE cartridges. Considering that carboxylic moieties of NOM are probably the most abundant Fe(III)-binding functional groups in pore waters and have a pK_a of around 4.5 (Ritchie and Perdue, 2003), the sample pH should be adjusted to less than 3 with acetic acid. Again, a suite of representative NOM standards should be tested for recovery prior to continuing with pore water sample analyses.

Finally, the efficiency of the Fe(III)-Chelex column in extracting natural Fe(III)-binding ligands from samples should be confirmed. First, some natural ligands may be strong enough to strip Fe from the resin during the sample loading phase and, thus, lose potentially important ligands from the extraction procedure. Iron should therefore be measured in the effluent from the Chelex column after loading the sample to ensure that a tolerable amount of Fe(III) is released from the column. Additionally, the ligand binding capacity of a given amount of Chelex-100 resin is unknown, and DOC should also be measured in the effluent of control extractions conducted with synthetic Fe(III)-binding ligands to ensure that they are completely retained on the Fe(III)-Chelex column. Finally, the concentration and volume of EDTA required to strip all Fe from the Chelex column after loading the sample may have to be optimized depending on the type of natural ligands present in the sample investigated. For example, the strong ligand DefB when adsorbed to the Fe-Chelex® formed a bright red complex that was not easily eluted from the column even after equilibrating it for two days with 5 mL of 20 mM EDTA. Eventually, a stronger ligand, such diethylene triamine pentaacetic acid (DTPA) may be better suited to fully strip iron and strong Fe(III)-binding ligands from the Chelex column.

7.5 Conclusions

It is necessary to understand the chemical composition of Fe-reactive ligands in sediment pore waters in order to identify their sources and potential role in stabilizing Fe(III) in solution. It is often assumed that Fe in sediments is bound primarily to humic acids. However, under Fe(III) reducing conditions, it is possible that microbes may

secrete specific organic ligands designed to complex Fe, and that these ligands may in fact be more important than humics as they may stabilize Fe in a soluble form that may freely diffuse into the overlying waters or deeper in the sediments. In this work, a novel extraction scheme was used to isolate Fe-reactive ligands from marine pore waters. While more work needs to be completed, preliminary results demonstrate a few ligands are detected which may have properties that are consistent with lower molecular weight endogenous organic ligands that could be secreted by microorganisms.

7.5 Acknowledgements

We would like to thank Eryn Eitel and Mike Perdue for help with processing and interpreting LC/ESI-MS data, Bill Savidge for the opportunity to collect and process samples at Skidaway Oceanography Institute, as well as David Bosworth at the Bioanalytical Mass-Spectrometry Facility at Georgia Tech for conducting sample analyses.

CHAPTER 8

CONCLUSIONS

While Fe fluxes from the atmosphere are traditionally considered to represent the main inputs of Fe to the oceans, in the past decade icebergs, hydrothermal vents, and continental margin sediments have been demonstrated to contribute significantly to the overall flux of Fe to the oceans. Unlike dust depositions, which primarily consist of mineral particles with low solubility, Fe fluxing out from sediments is primarily contained in the dissolved fraction (<0.2 μm) and mainly considered to be in a reduced form. Dissolved Fe^{2+}, however, is expected to precipitate from solution upon reaching oxygenated ocean water given its high rate of oxidation. On the other hand, dissolved Fe(III) may be stable in seawater in the presence of $O_{2(aq)}$ if it is complexed by organic ligands, and an active flux of organic-Fe(III) complexes has recently been measured in estuarine sediments. Interestingly, the sources of these complexes are unknown. The main focus of this thesis has been to better constrain the biogeochemical conditions and type of sedimentary environments that result in the production of organic-Fe(III) complexes. To meet this goal, state-of-the-art geochemical techniques were developed and used in the field and laboratory.

Early studies hypothesized that organic-Fe(III) complexes were formed during early diagenesis from Fe(II) oxidation in the presence of organic ligands or tnon-reductive dissolution of Fe(III) minerals by dissolved organic matter or biomolecules.

Because of the coupling of the Fe cycle with other elements such as C, O, S, and N, a more complete understanding of diagenetic processes is needed to identify alternate biogeochemical processes eventually responsible for the production of these complexes. As the need for long-term monitoring of the exchange of components between the oceanic crust and the oceans became apparent, and as artifacts associated with traditional sampling techniques prevent the acquisition of high spatial resolution data, a shift towards *in situ* biogeochemical studies of the ocean floor spurred by recent technological advances has emerged. A portion of this work focused on the development of an HPLC instrument and methods suitable for *in situ* deployments on a benthic lander platform. By coupling this new *in situ* HPLC instrument to an existing *in situ* electrochemical analyzer, it is now possible to analyze the complete suite of redox chemical species involved in diagenetic processes, including $O_{2(aq)}$, NO_3^-, NO_2^-, SO_4^{2-}, Mn^{2+}, Fe^{2+}, and ΣH_2S, but also Cl^- and Br^-, which may offer insights into exchange processes, particularly in hydrothermal vent or sedimentary environments.

The three main challenges with the *in situ* HPLC project included designing an autonomous instrument with low power consumption, high sensitivity, and good reproducibility using relatively simple technology, developing a versatile HPLC method using simple liquid handling systems that provided high sensitivity to all the anions of interest, as well as designing a sample sipping probe to allow the collection of small volumes of pore water from sediments. In this dissertation, two methods were developed which relied on the UV absorbance properties of NO_3^-, NO_2^-, and Br^- and the suppression of the background absorbance of the eluent by Cl^- and SO_4^{2-} (not UV active) for their detection upon elution from the column. With the new methods, the suite of five anions

can be analyzed in a single step, without any interference from other anions potentially present. The method requires less than 100 μL of sample for analysis, which is collected directly from pore waters with a new sipping probe designed to simultaneously withdraw and filter pore waters from various depth increments. The combined *in situ* HPLC and electrochemical analyzer (ISEA-IV LC) was successfully used to obtain pore water profiles of anions and voltammetrically labile redox metabolites from estuarine sediments. To our knowledge, this data is the first time depth profiles of major and minor anions was obtained *in situ* in sediments. The ISEA-IV LC instrument can also be adapted to collect samples from benthic chambers, and deployments in this configuration provided the first *in situ* benthic flux measurements of NO_3^- and Br^-.

To determine the biogeochemical processes that control the production of organic-Fe(III) complexes, several types of benthic environments were studied, including coastal marsh (SERF facility on Skidaway Island, Georgia), a blackwater estuary (Satilla River, Georgia), continental slope sediments (Cape Hatteras, North Carolina, and Louisiana Shelf, Gulf of Mexico), and deep margin abyssal sediments (Congo River Fan). In each of these environments, the production of organic-Fe(III) complexes in the sediments was associated with microbial Fe(III)-reducing activity. A more comprehensive examination of the processes involved in the Fe cycle, including seasonal and salinity effects, was undertaken in the Satilla River estuary. Fe(III), likely in the form of terrestrially-derived DOM-Fe(III) complexes, flocculated to varying degrees during mixing with seawater and settled to the sediment-water interface to generate high concentrations of poorly-crystalline Fe(III) (oxy)hydroxides. Both UV absorbance and voltammetric measurements provided evidence that a significant proportion of dissolved

Fe(III) in these pore waters is truly dissolved (non-colloidal) in the form of organic-Fe(III) complexes. These complexes were simultaneously produced during microbial Fe(III) reduction in sediment incubations and used as electron acceptors in incubations conducted in the absence of solid phases. Finally, size exclusion chromatographic separations followed by the redox speciation of the fractions separated revealed that these organic-Fe(III) complexes are highly particle reactive and that Fe(II) produced in the pore waters is mainly in the form of organic complexes. Overall, these findings suggest that pore water DOM readily complexes Fe(II), which can be oxidized by Fe(III) hydroxides, forming DOM-Fe(III) complexes.

While the importance of dissimilatory metal reduction in coastal environments has been established through a number of field studies, few investigations have examined the potential for microbial metal reduction in deep-sea sediments (i.e. those underlying water columns deeper than 500 m). While most deep-sea sediments have low concentrations of organic matter, deep river-dominated ocean margin sediments (RiOMARs), i.e. continental slopes or deep-sea fans, are organic-rich environments traditionally assumed to be dominated by SO_4^{2-} reduction. As riverine delivery of terrigenous Fe hydroxides promoted microbial metal reduction in estuarine sediments, it was hypothesized that these deep sediments may in fact also host microbial metal reduction if metal oxides are delivered concomitantly with NOM. A subsequent transect of the Louisiana slope (i.e. from near the delta, down-slope, to pelagic sediments) revealed that terrigenous Fe(III) containing (oxy)hydroxides and clay minerals could accumulate deeper on the slope (~1,000 m) because of mass-slumping and shelf-spillover processes. While SO_4^{2-} reduction dominated in shelf and shelf-break sediments, the slope

sediments were dominated by dissimilatory Fe(III) reduction. To further test this hypothesis, the relative roles of Fe and SO_4^{2-} reduction were examined sediments from the Congo River deep-sea fan, which receives frequent turbidite flows directly through its submarine canyon. Results showed that the from levee sediments near the active channel contained some of the highest concentrations of reactive Fe hydroxides and were thus completely dominated by Fe(III) reduction. At a nearby extinct channel, aerobic respiration appeared to dominate C remineralization, further demonstrating the dependence of this system on riverine discharge. Finally, all of these field studies demonstrated that organic-Fe(III) complexes were produced in sediments depleted in dissolved $O_{2(aq)}$ and dominated by dissimilatory Fe(III) reduction, suggesting that these complexes may be directly produced by Fe(III)-reducing bacteria.

The mechanism by which dissimilatory Fe(III)-reducing microorganisms access an insoluble mineral for subsequent use as a TEA however, remains poorly understood, and several biochemical pathways have been proposed, including one that involves the non-reductive dissolution of Fe(III) minerals by multidentate organic ligands followed by intra- or extra-cellular reduction of the organic-Fe(III) complex intermediates. As this last pathways results in the accumulation of organic-Fe(III) complexes, a model Fe(III)-reducing microorganism, *Shewanella putrefaciens*, was incubated with pure Fe (oxy)hydroxides in the presence of voltammetric microelectrodes to determine whether these organisms represent and important source of these compounds. Not only were organic-Fe(III) complexes produced as a function of time, the intial rates of organic-Fe(III) production were correlated with Fe(II) production rates. Further, while rates of org-Fe(III) production depended on mineral composition, these rates were equivalent

(within error) when normalized to mineral surface area. Finally, org-Fe(III) complexes were also produced as intermediates during the reduction of exogenous soluble Fe(III) complexes. These findings suggest that *Shewanella* sp. secrete organic ligands to destabilize Fe(III) and reduce the activation energy required for the reduction step and simultaneously facilitate electron transfer. To ensure that this chelation pathway was viable in the environment, Satilla River estuarine sediments were incubated with the same microorganism. Organic-Fe(III) complexes were produced as a function of time during these incubations, but in much larger concentrations in the presence of both added Fe(III) hydroxides and microorganisms than in pure cultures, suggesting that pore water DOM may serve as additional Fe ligands. Perhaps more importantly, the organic-Fe(III) complexes produced during the reduction of Fe(III) hydroxides were used as TEAs when the solid mineral phase was removed, indicating that these complexes are bioavailable.

The final objective of this thesis was to characterize the organic-Fe(III) complexes present in sediment pore waters. During the series of Satilla River cruises, a size-exclusion chromatography technique was developed to fractionate dissolved organic matter and Fe as a function of size. Results showed that pore water dissolved Fe(II) eluted earlier than inorganic Fe(II) controls, indicating that the pore water Fe(II) was complexed by organics. In turn, pore water Fe(III) was retained on the column and only recoverable after rinsing with EDTA, suggesting that organic-Fe(III) complexes are highly charged and interact with the slightly negatively charged stationary phase. Overall, by demonstrating that Fe(II) is complexed by organic ligands, the results suggest that organic-Fe(II) complexes may be oxidized by Fe(III) minerals to produce organic-Fe(III) complexes, which may subsequently serve as TEAs and provide an additional

mechanism for the production of soluble organic-Fe(III) complexes in organic-rich sediments.

As this technique did not allow separation of the organic-Fe(III) complexes, an immobilized-metal affinity chromatography (IMAC) technique was developed to specifically isolate the Fe(III)-binding ligands from coastal marsh sediment pore waters. After collecting and concentrating the ligands via solid-phase extraction, liquid chromatography electrospray-ionization mass spectrometry was used to provide molecular weight information about the ligands. Although the technique developed probably excludes some organic ligands, preliminary data show that Fe(III) binding ligands are primarily of low molecular weight (< 250 Da) and in concentrations proportional to the concentration of dissolved Fe(III), consistent with expectations that they may consist of a chelating biomolecule excreted by Fe(III)-reducing microorganisms.

Overall, this work has revealed that sediments harboring dissimilatory Fe(III)-reducing organisms will be settings for org-Fe(III) production through complex interactions between microbes, minerals, and NOM. These complexes are stable in seawater and may flux from sediments to the water column. With eventual upwelling, these complexes could provide an underappreciated source of a limiting nutrient to surface waters, affecting C cycling. This work has also shown that in regions with sufficient reactive Fe deposition to sediments, Fe(III) reduction may actually outcompete SO_4^{2-} and dominate C remineralization. If erosion processes supply enough Fe(III) oxides in RiOMAR sediments, the SO_4^{2-} reduction, and thus pyritization, will be prevented at great depth. While the implications of these findings on atmospheric O_2

levels on a geological timescale are difficult to evaluate, climate changes may have an even larger negative impact on the potential for pyritization in these environments, as they affect precipitation intensity and frequency and thus riverine discharge, which should also increase the supply of Fe(III) oxide minerals to the oceans. Finally, these results may have important implications for the changes for redox conditions on the Early Earth. If increases in riverine discharge associated with increases in temperatures provided enough Fe(III) oxides to RiOMAR sediments around the globe, dissolved sulfides present in the deep euxinic water column of the oceans during the Proterozoic may have been titrated during oxidation by Fe(III) oxides and precipitation of $FeS_{(s)}$ which could have facilitated a shift in microbial processes from less energetically favorable SO_4^{2-} reduction to more energetically favored Fe reduction in deep-sea sediments and favored the onset of oxygenic conditions on Earth.

8.1. Recommendations for future work

While this research has made strides in the development of *in situ* techniques for measurements in sediment pore waters and techniques to study the origin of soluble organic-Fe(III) complexes, the work presented has raised several questions that will have to be addressed in future studies.

This work has progressed the ongoing movement towards the use of *in situ* technology in data collection in oceanography, and the possibilities for future implementations of the benthic landers and *in situ* HPLC are tremendous. While some potential applications are described in section 2.6, one of the most promising projects involves S cycling at hydrothermal vents. Conventionally, it has been assumed that

seawater SO_4^{2-} is almost entirely reduced to $\sum H_2S$ through abiotic reaction with basaltic rock at high temperature and pressure. For example, S complexes with intermediate oxidation states (i.e. S_x^{-2} or $S_2O_3^-$) have recently been detected *in situ* in diffuse flows (Gartman et al., 2011; Luther et al., 2001), suggesting $\sum H_2S$ may be partially reoxidized in the subsurface or immediately upon venting. In addition, $\sum H_2S$ oxidation intermediates (i.e. $S_2O_3^-$ and $S_4O_6^{-2}$) were detected at high concentrations (millimolar range) in samples retrieved from hydrothermal vents (Jones, 2011). Presently, it is unknown if these species are produced due to artifacts from temperature and pressure changes upon returning to atmospheric pressure, or if some subsurface process results in this oxidation. With some modification of the sample inlet probe and the inlet valve system (to handle high ambient pressures and temperatures), the *in situ* HPLC could be outfitted to sample directly from high temperature vents and may be able to minimize artifacts during sample retrieval, such that valuable insights into the processes responsible for the production of these intermediates may be gained.

The deep ocean is considered the final frontier in the exploration of earth. As extremophiles have developed numerous adaptations to survive the high pressures and cold temperatures, these environments are of interest not only for more traditional geochemistry topics such as carbon degradation pathways (i.e. Chapter 5 of this thesis), but also in paleobiology, exobiology, and even drug discovery (Fang and Bazylinski, 2008). River-dominated ocean margin sediments such as the Congo River Fan are essentially natural geochemical laboratories in which material transferred from coastal environments is subject to high pressures, and may therefore represent hot-beds for the discovery of new species that may have evolved in extreme pressure and temperature

conditions. Major difficulties arise in the study and cultivation of these microorganisms, particularly because samples may be depressurized during sampling, inducing artifacts and possibly killing these organisms. The voltammetric microelectrodes used in this research are stable at high pressures, could measure redox metabolites in situ in pressure vessels, and could therefore assist in deciphering deep ocean carbon remineralization mechanisms in a laboratory setting.

While this work has demonstrated one mechanism for org-Fe(III) production, other possibilities may exist. In turn, the chemical composition and stability of dissolved Fe(III) diffusing out of sediments are likely influenced by its mechanism of production, i.e. either the non-reductive solubilization of iron oxides by biogenically-produced organic ligands, oxidation of DOM-Fe(II) by $O_{2(aq)}$, NO_2^-, or Fe(III)/Mn(IV) minerals, or the non - reductive solubilization of iron oxides by allochthonous ligands. It is therefore expected that the flux of iron at the SWI is influenced by the type of organic ligands involved in the complexation of iron. Comparing the composition of Fe(II) and Fe(III) complexes in benthic chamber and pore water samples obtained in a variety of redox regimes will provide new insights into the relative importance of each of the mechanism of production of soluble organic - Fe(III) complexes on the benthic flux of iron. This information could be correlated to the conditional stability constants obtained in the samples using CLE-ASV analysis to assess the general biogeochemical conditions required to generate a benthic flux of stable iron complexes such that the key redox features of the sediments identified using conventional techniques in future studies may be extrapolated into relative flux intensities. The IMAC procedure presented in chapter 7 is in its early stages, and much work remains to optimize separation conditions to capture

and identify natural Fe(III)-binding ligands. To further expand this database of natural ligands, synthetic organic-Fe(III) complexes generated in the laboratory should be used, including biogenic ligands produced by model Fe(III)-reducing bacteria, to determine whether they have similar composition as those detected in pore waters. Additionally, HPLC could be coupled with carbon isotope ratio mass spectrometry in another effort to determine if ligands are of marine or terrigenous in origin.

REFERENCES

Adornato, L.R., Kaltenbacher, E.A., Greenhow, D.R., Byrne, R.H., 2007. High-resolution In situ analysis of nitrate and phosphate in the oligotrophic ocean. Environmental Science & Technology 41, 4045-4052.

Aller, R.C., Blair, N.E., 2006. Carbon remineralization in the Amazon-Guianas tropical mobile mudbelt: A sedimentary incinerator. Continental Shelf Research 26, 2241-2259.

Arnold, G.L., Anbar, A.D., Barling, J., Lyons, T.W., 2004. Molybdenum isotope evidence for widespread anoxia in mid-proterozoic oceans. Science 304, 87-90.

Arnold, R.G., Dichristina, T.J., Hoffmann, M.R., 1988. Reductive Dissolution of Fe(Iii) Oxides by Pseudomonas Sp 200. Biotechnology and Bioengineering 32, 1081-1096.

Arnold, R.G., Hoffmann, M.R., Dichristina, T.J., Picardal, F.W., 1990. regulation of dissimilatory Fe(III) reduction activity in *Shewanella-putrefaciens*. Applied and Environmental Microbiology 56, 2811-2817.

Babonneau, N., Savoye, B., Cremer, M., Klein, B., 2002. Morphology and architecture of the present canyon and channel system of the Zaire deep-sea fan. Marine and Petroleum Geology 19, 445-467.

Bak, F., Schuhmann, A., Jansen, K.-H., 1993. Determination of tetrathionate and thiosulfate in natural samples and microbial cultures by a new, fast and sensitive ion chromatographic technique. FEMS microbiology ecology 12, 257-264.

Balsam, W.L., Beeson, J.P., 2003. Sea-floor sediment distribution in the Gulf of Mexico. Deep-Sea Research Part I-Oceanographic Research Papers 50, 1421-1444.

Bannister, W.H., 1992. The biological chemistry of the elements: The inorganic chemistry of life: By J J R Fraústo da Silva and R J P Williams. pp 561. Clarendon Press, Oxford. 1991. Biochemical Education 20, 62-63.

Bard, A.J., Faulkner, L.R., 2000. Electrochemical Methods: Fundamentals and Applications. Wiley.

Barnett, T.P., Pierce, D.W., AchutaRao, K.M., Gleckler, P.J., Santer, B.D., Gregory, J.M., Washington, W.M., 2005. Penetration of human-induced warming into the world's oceans. Science 309, 284-287.

Bea, R.G., Wright, S.G., Sircar, P., Niedoroda, A.W., 1983. Wave-induced slides in south pass block 70, Mississippi Delta. J. Geotech. Eng.-ASCE 109, 619-644.

Beck, K.C., Reuter, J.H., Perdue, E.M., 1974. Organic and Inorganic Geochemistry of Some Coastal-Plain Rivers of Southeastern United-States. Geochimica Et Cosmochimica Acta 38, 341-364.

Beliaev, A.S., Saffarini, D.A., 1998. Shewanella putrefaciens mtrB encodes an outer membrane protein required for Fe(III) and Mn(IV) reduction. J. Bacteriol. 180, 6292-6297.

Bell, R.J., Savidge, W.B., Toler, S.K., Byrne, R.H., Short, R.T., 2012. In situ determination of porewater gases by underwater flow-through membrane inlet mass spectrometry. Limnology and Oceanography-Methods 10, 117-128.

Bender, M., Martin, W., Hess, J., Sayles, F., Ball, L., Lambert, C., 1987. A whole-core squeezer for interfacial pore-water sampling. Limnology and Oceanography 32, 1214-1225.

Bender, M.L., Heggie, D.T., 1984. Fate of organic-carbon reaching the deep-sea floor - a status-report. Geochimica Et Cosmochimica Acta 48, 977-986.

Bennett, S.A., Achterberg, E.P., Connelly, D.P., Statham, P.J., Fones, G.R., German, C.R., 2008. The distribution and stabilisation of dissolved Fe in deep-sea hydrothermal plumes. Earth and Planetary Science Letters 270, 157-167.

Berner, R.A., 1975. Diagenetic models of dissolved species in interstitial waters of compacting sediments. American Journal of Science 275, 88-96.

Berner, R.A., 2001. Modeling atmospheric O-2 over Phanerozoic time. Geochimica Et Cosmochimica Acta 65, 685-694.

Berner, R.A., Canfield, D.E., 1988. Sedimentation as a major control on the level of atmospheric oxygen. Chemical Geology 70, 114-114.

Berner, R.A., Petsch, S.T., 1998. PAleoclimate - The sulfur cycle and atmospheric oxygen. Science 282, 1426-1427.

Bianchi, T.S., Allison, M.A., Canuel, E.A., Corbett, D.R., McKee, B.A., Sampere, T.P., Wakeham, S.G., Waterson, E., 2006. Rapid export of organic matter to the Mississippi Canyon. Eos, Transactions American Geophysical Union 87, 565-573.

Biber, M.V., Afonso, M.D., Stumm, W., 1994. The Coordination Chemistry of Weathering .4. Inhibition of the Dissolution of Oxide Minerals. Geochimica Et Cosmochimica Acta 58, 1999-2010.

Bidigare, R.R., Van Heukelem, L., Trees, C.C., 2005. Analysis of algal pigments by high-performance liquid chromatography.

Bino, A., Shweky, I., Cohen, S., Bauminger, E.R., Lippard, S.J., 1998. A novel nonairon(III) citrate complex: A "ferric triple-decker". Inorg. Chem. 37, 5168-5172.

Bishop, M.E., Jaisi, D.P., Dong, H.L., Kukkadapu, R.K., Ji, J.F., 2010. Bioavailability of Fe(III) in loess sediments: an important source of electron acceptors. Clays and Clay Minerals 58, 542-557.

Bondietti, G., Sinniger, J., Stumm, W., 1993. The reactivity of Fe(III) (hydr)oxides - effects of ligands in inhibiting the dissolution. Colloids and Surfaces a-Physicochemical and Engineering Aspects 79, 157-167.

Bonneville, S., Behrends, T., Van Cappellen, P., Hyacinthe, C., Roling, W.F.M., 2006. Reduction of Fe(III) colloids by Shewanella putrefaciens: A kinetic model. Geochimica Et Cosmochimica Acta 70, 5842-5854.

Borch, T., Masue, Y., Kukkadapu, R.K., Fendorf, S., 2007. Phosphate imposed limitations on biological reduction and alteration of ferrihydrite. Environmental Science & Technology 41, 166-172.

Boudreau, B.P., 1997. Diagenetic models and their implementation: modelling transport and reactions in aquatic sediments. Berlin;, Springer;.

Boukhalfa, H., Crumbliss, A.L., 2002. Chemical aspects of siderophore mediated iron transport. Biometals 15, 325-339.

Bowles, M.W., Mogollón, J.M., Kasten, S., Zabel, M., Hinrichs, K.-U., 2014. Global Rates of Marine Sulfate Reduction and Implications for Sub–Sea-Floor Metabolic Activities. Science.

Boyd, P.W., Law, C.S., 2001. The Southern Ocean Iron RElease Experiment (SOIREE) - introduction and summary. Deep-Sea Res. Part II-Top. Stud. Oceanogr. 48, 2425-2438.

Boyd, P.W., Watson, A.J., Law, C.S., Abraham, E.R., Trull, T., Murdoch, R., Bakker, D.C.E., Bowie, A.R., Buesseler, K.O., Chang, H., Charette, M., Croot, P., Downing, K., Frew, R., Gall, M., Hadfield, M., Hall, J., Harvey, M., Jameson, G., LaRoche, J., Liddicoat, M., Ling, R., Maldonado, M.T., McKay, R.M., Nodder, S., Pickmere, S., Pridmore, R., Rintoul, S., Safi, K., Sutton, P., Strzepek, R., Tanneberger, K., Turner, S., Waite, A., Zeldis, J., 2000. A mesoscale phytoplankton bloom in the polar Southern Ocean stimulated by iron fertilization. Nature 407, 695-702.

Boyd, P.W., Ellwood, M.J., 2010. The biogeochemical cycle of iron in the ocean. Nat. Geosci. 3, 675-682.

Boyle, E.A., Edmond, J.M., Sholkovitz, E.R., 1977. Mechanism of iron removal in estuaries. Geochimica Et Cosmochimica Acta 41, 1313-1324.

Braich, N., Codd, R., 2008. Immobilised metal affinity chromatography for the capture of hydroxamate-containing siderophores and other Fe(III)-binding metabolites directly from bacterial culture supernatants. Analyst 133, 877-880.

Brandes, J.A., Devol, A.H., Deutsch, C., 2007. New developments in the marine nitrogen cycle. Chem. Rev. 107, 577-589.

Breitbarth, E., Achterberg, E.P., Ardelan, M.V., Baker, A.R., Bucciarelli, E., Chever, F., Croot, P.L., Duggen, S., Gledhill, M., Hassellov, M., Hassler, C., Hoffmann, L.J., Hunter, K.A., Hutchins, D.A., Ingri, J., Jickells, T., Lohan, M.C., Nielsdottir, M.C., Sarthou, G., Schoemann, V., Trapp, J.M., Turner, D.R., Ye, Y., 2010. Iron biogeochemistry across marine systems - progress from the past decade. Biogeosciences 7, 1075-1097.

Brendel, P.J., Luther, G.W., 1995. Development of a Gold Amalgam Voltammetric Microelectrode for the Determination of Dissolved Fe, Mn, O-2, and S(-Ii) in Porewaters of Marine and Fresh-Water Sediments. Environmental Science & Technology 29, 751-761.

Brickman, T.J., McIntosh, M.A., 1992. Overexpression and purification of ferric enterobactin esterase from escherichia-coli - demonstration of enzymatic-hydrolysis of enterobactin and its iron complex. J. Biol. Chem. 267, 12350-12355.

Bristow, G., Taillefert, M., 2008. VOLTINT: A Matlabg (R)-based program for semi-automated processing of geochemical data acquired by voltammetry. Computers & Geosciences 34, 153-162.

Brutinel, E.D., Gralnick, J.A., 2012. Shuttling happens: soluble flavin mediators of extracellular electron transfer in Shewanella. Appl. Microbiol. Biotechnol. 93, 41-48.

Buck, C.S., Landing, W.M., Resing, J.A., 2010. Particle size and aerosol iron solubility: A high-resolution analysis of Atlantic aerosols. Marine Chemistry 120, 14-24.

Buck, K.N., Bruland, K.W., 2007. The physicochemical speciation of dissolved iron in the Bering Sea, Alaska. Limnology and Oceanography 52, 1800-1808.

Buck, K.N., Lohan, M.C., Berger, C.J.M., Bruland, K.W., 2007. Dissolved iron speciation in two distinct river plumes and an estuary: Implications for riverine iron supply. Limnology and Oceanography 52, 843-855.

Buffle, J., Horvai, G., 2000. In situ Monitoring of Aquatic Systems: Chemical Analysis and Speciation. Wiley Chichester, New York.

Bull, D.C., Taillefert, M., 2001. Seasonal and topographic variations in porewaters of a southeastern USA salt marsh as revealed by voltammetric profilingdagger. Geochem Trans 2, 104.

Burba, P., Jakubowski, B., Kuckuk, R., Kullmer, K., Heumann, K.G., 2000. Characterization of aquatic humic substances and their metal complexes by immobilized metal-chelate affinity chromatography on iron(III)-loaded ion exchangers. Fresenius J. Anal. Chem. 368, 689-696.

Burdige, D.J., 2007. Preservation of organic matter in marine sediments: Controls, mechanisms, and an imbalance in sediment organic carbon budgets? Chem. Rev. 107, 467-485.

Burdige, D.J., Alperin, M.J., Homstead, J., Martens, C.S., 1992. The role of benthic fluxes of dissolved organic-carbon in oceanic and sedimentary carbon cycling. Geophys. Res. Lett. 19, 1851-1854.

Burns, J.M., Craig, P.S., Shaw, T.J., Ferry, J.L., 2010. Multivariate Examination of Fe(II)/Fe(III) Cycling and Consequent Hydroxyl Radical Generation. Environmental Science & Technology 44, 7226-7231.

Burns, J.L., Ginn, B.R., Bates, D.J., Dublin, S.N., Taylor, J.V., Apkarian, R.P., Amaro-Garcia, S., Neal, A.L., Dichristina, T.J., 2010. Outer Membrane-Associated Serine Protease Involved in Adhesion of Shewanella oneidensis to Fe(III) Oxides. Environmental Science & Technology 44, 68-73.

Butterfield, D.A., Massoth, G.J., 1994. Geochemistry of north cleft segment vent fluids - temporal changes in chlorinity and their possible relation to recent volcanism. Journal of Geophysical Research-Solid Earth 99, 4951-4968.

Cai, W.J., Reimers, C.E., 1995. Benthic oxygen flux, bottom water oxygen concentration and core top organic carbon content in the deep northeast Pacific Ocean. Deep-Sea Research Part I-Oceanographic Research Papers 42, 1681-1699.

Campana, P., Knox, J., Grundstein, A., Dowd, J., 2012. The 2007-2009 Drought in Athens, Georgia, United States: A Climatological Analysis and an Assessment of Future Water Availability. J. Am. Water Resour. Assoc. 48, 379-390.

Canfield, D.E., 1994. Factors influencing organic-carbon preservation in marine-sediments. Chemical Geology 114, 315-329.

Canfield, D.E., Jorgensen, B.B., Fossing, H., Glud, R., Gundersen, J., Ramsing, N.B., Thamdrup, B., Hansen, J.W., Nielsen, L.P., Hall, P.O.J., 1993. Pathways of organic-carbon oxidation in 3 continental-margin sediments. Elsevier Science Bv, pp. 27-40.

Canfield, D.E., Poulton, S.W., Knoll, A.H., Narbonne, G.M., Ross, G., Goldberg, T., Strauss, H., 2008. Ferruginous conditions dominated later neoproterozoic deep-water chemistry. Science 321, 949-952.

Canfield, D.E., Thamdrup, B., 1994. The production of s-34-depleted sulfide during bacterial disproportionation of elemental sulfur. Science 266, 1973-1975.

Carey, E., Taillefert, M., 2005. The role of soluble Fe(III) in the cycling of iron and sulfur in coastal marine sediments. Limnology and Oceanography 50, 1129-1141.

Castellini, D.G., Dickens, G.R., Snyder, G.T., Ruppel, C.D., 2006. Barium cycling in shallow sediment above active mud volcanoes in the Gulf of Mexico. Chemical Geology 226, 1-30.

Chapman, P., Truesdale, V.W., 2011. Preliminary Evidence for Iodate Reduction in Bottom Waters of the Gulf of Mexico During an Hypoxic Event. Aquatic Geochemistry 17, 671-695.

Chen, M., Wang, W.X., Guo, L.D., 2004. Phase partitioning and solubility of iron in natural seawater controlled by dissolved organic matter. Glob. Biogeochem. Cycle 18, 12.

Chin, Y.P., Aiken, G., Oloughlin, E., 1994. Molecular-Weight, Polydispersity, and Spectroscopic Properties of Aquatic Humic Substances. Environmental Science & Technology 28, 1853-1858.

Chin, Y.P., Traina, S.J., Swank, C.R., Backhus, D., 1998. Abundance and properties of dissolved organic matter in pore waters of a freshwater wetland. Limnology and Oceanography 43, 1287-1296.

Coale, K.H., Johnson, K.S., Fitzwater, S.E., Gordon, R.M., Tanner, S., Chavez, F.P., Ferioli, L., Sakamoto, C., Rogers, P., Millero, F., Steinberg, P., Nightingale, P., Cooper, D., Cochlan, W.P., Landry, M.R., Constantinou, J., Rollwagen, G., Trasvina, A., Kudela, R., 1996. A massive phytoplankton bloom induced by an ecosystem-scale iron fertilization experiment in the equatorial Pacific Ocean. Nature 383, 495-501.

Coates, J.D., Ellis, D.J., Blunt-Harris, E.L., Gaw, C.V., Roden, E.E., Lovley, D.R., 1998. Recovery of humic-reducing bacteria from a diversity of environments. Applied and Environmental Microbiology 64, 1504-1509.

Coleman, J.M., 1988. Dynamic changes and processes in the Mississippi River delta. Geol. Soc. Am. Bull. 100, 999-1015.

Coleman, J.M., Roberts, H.H., Stone, G.W., 1998. Mississippi River delta: an overview. Journal of Coastal Research 14, 698-716.

Connolly, D., Paull, B., 2002. Fast ion chromatography of common inorganic anions on a short ODS column permanently coated with didodecyldimethylammonium bromide. Journal of Chromatography A 953, 299-303.

Cornell, R., Schwertmann, U., 1996. The iron oxides: Structure, properties, reactions, occurrence, and uses. VCH (Weinheim and New York).

Cotton, F.A., 2007. Advanced Inorganic Chemistry, 6TH ED. Wiley India Pvt. Limited.

Cowen, J.P., Copson, D.A., Jolly, J., Hsieh, C.-C., Lin, H.-T., Glazer, B.T., Wheat, C.G., 2012. Advanced instrument system for real-time and time-series microbial geochemical sampling of the deep (basaltic) crustal biosphere. Deep Sea Research Part I: Oceanographic Research Papers 61, 43-56.

Cullen, J.T., Bergquist, B.A., Moffett, J.W., 2006. Thermodynamic characterization of the partitioning of iron between soluble and colloidal species in the Atlantic Ocean. Marine Chemistry 98, 295-303.

Dale, J.R., Wade, R., DiChristina, T.J., 2007. A conserved histidine in cytochrome c maturation permease CcmB of Shewanella putrefaciens is required for anaerobic growth below a threshold standard redox potential. J. Bacteriol. 189, 1036-1043.

Damuth, J.E., Kumar, N., 1975. Amazon cone - morphology, sediments, age, and growth-pattern. Geol. Soc. Am. Bull. 86, 863-878.

Davison, W., Seed, G., 1983. The kinetics of the oxidation of ferrous iron in synthetic and natural-waters. Geochimica Et Cosmochimica Acta 47, 67-79.

Davison, W., Zhang, H., Grime, G.W., 1994. Performance-characteristics of gel probes used for measuring the chemistry of pore waters. Environmental Science & Technology 28, 1623-1632.

deBeer, D., Schramm, A., Santegoeds, C.M., Kuhl, M., 1997. A nitrite microsensor for profiling environmental biofilms. Applied and Environmental Microbiology 63, 973-977.

Debeer, D., Sweerts, J.P.R., 1989. Measurement of nitrate gradients with an ion-selective microelectrode. Analytica Chimica Acta 219, 351-356.

Delaney, J.R., Chave, A.D., 2000. NEPTUNE: A fiber-optic 'telescope' to inner space. Oceanus 42, 10-11.

Deng, Y.W., Stumm, W., 1994. Reactivity of aquatic iron(III) oxyhydroxides implications for redox cycling of iron in natural-waters. Appl. Geochem. 9, 23-36.

Desiderio, R.A., Moore, C., Lantz, C., Cowles, T.J., 1997. Multiple excitation fluorometer for in situ oceanographic applications. Applied Optics 36, 1289-1296.

Dichristina, T.J., 1992. Effects of nitrate and nitrite on dissimilatory iron reduction by Shewanella-Putrefaciens-200. J. Bacteriol. 174, 1891-1896.

Dichristina, T.J., Delong, E.F., 1993. Design and application of ribosomal-rna-targeted oligonucleotide probes for the dissimilatory iron-reducing and manganese-reducing bacterium Shewanella-Putrefaciens. Applied and Environmental Microbiology 59, 4152-4160.

Dichristina, T.J., Delong, E.F., 1994. Isolation of Anaerobic Respiratory Mutants of Shewanella-Putrefaciens and Genetic-Analysis of Mutants Deficient in Anaerobic Growth on Fe3+. J. Bacteriol. 176, 1468-1474.

DiChristina, T.J., Fredrickson, J.K., Zachara, J.M., 2005. Enzymology of electron transport: Energy generation with geochemical consequences, Molecular Geomicrobiology. Mineralogical Soc America, Chantilly, pp. 27-52.

DiChristina, T.J., Moore, C.M., Haller, C.A., 2002. Dissimilatory Fe(III) and Mn(IV) reduction by Shewanella putrefaciens requires ferE, a homolog of the pulE (gspE) type II protein secretion gene. J. Bacteriol. 184, 142-151.

Dickey, T.D., Bidigare, R.R., 2005. Interdisciplinary oceanographic observations: the wave of the future. Scientia Marina 69, 23-42.

Dickson, A.G., 1993. pH buffers for sea-water media based on the total hydrogen-ion concentration scale. Deep-Sea Research Part I-Oceanographic Research Papers 40, 107-118.

Dixit, S., Van Cappellen, P., van Bennekom, A.J., 2001. Processes controlling solubility of biogenic silica and pore water build-up of silicic acid in marine sediments. Marine Chemistry 73, 333-352.

Dixon, B.T., Weimer, P., 1998. Sequence stratigraphy and depositional history of the eastern Mississippi Fan (Pleistocene), northeastern deep Gulf of Mexico. AAPG Bull.-Am. Assoc. Petr. Geol. 82, 1207-1232.

Dollhopf, M.E., Nealson, K.H., Simon, D.M., Luther, G.W., 2000. Kinetics of Fe(III) and Mn(IV) reduction by the Black Sea strain of Shewanella putrefaciens using in situ solid state voltammetric Au/Hg electrodes. Marine Chemistry 70, 171-180.

Druschel, G.K., Emerson, D., Sutka, R., Suchecki, P., Luther, G.W., 2008. Low-oxygen and chemical kinetic constraints on the geochemical niche of neutrophilic iron(II) oxidizing microorganisms. Geochimica Et Cosmochimica Acta 72, 3358-3370.

Dugan, B., Flemings, P.B., 2000. Overpressure and fluid flow in the New Jersey continental slope: Implications for slope failure and cold seeps. Science 289, 288-291.

Dugan, B., Stigall, J., 2010. Origin of Overpressure and Slope Failure in the Ursa Region, Northern Gulf of Mexico. Springer, Dordrecht.

Edwards, M.J., Fredrickson, J.K., Zachara, J.M., Richardson, D.J., Clarke, T.A., 2012. Analysis of structural MtrC models based on homology with the crystal structure of MtrF. Biochem. Soc. Trans. 40, 1181-1185.

El-Naggar, M.Y., Gorby, Y.A., Xia, W., Nealson, K.H., 2008. The molecular density of states in bacterial nanowires. Biophysical Journal 95, L10-L12.

Elrod, V.A., Berelson, W.M., Coale, K.H., Johnson, K.S., 2004. The flux of iron from continental shelf sediments: A missing source for global budgets. Geophys. Res. Lett. 31, 4.

Evenhuis, C.J., Buchberger, W., Hilder, E.F., Flook, K.J., Pohl, C.A., Nesterenko, P.N., Haddad, P.R., 2008. Separation of inorganic anions on a high capacity porous polymeric monolithic column and application to direct determination of anions in seawater. Journal of Separation Science 31, 2598-2604.

Fang, J., Bazylinski, D.A., 2008. Deep-sea geomicrobiology and biogeochemistry., High-Pressure Microbiology. American Society for Microbiology, pp. 237-264.

Fang, J.S., Zhang, L., Bazylinski, D.A., 2010. Deep-sea piezosphere and piezophiles: geomicrobiology and biogeochemistry. Trends in Microbiology 18, 413-422.

Fennessey, C.M., Jones, M.E., Taillefert, M., DiChristina, T.J., 2010. Siderophores Are Not Involved in Fe(III) Solubilization during Anaerobic Fe(III) Respiration by Shewanella oneidensis MR-1. Applied and Environmental Microbiology 76, 2425-2432.

Ferdelman, T.G., Fossing, H., Neumann, K., Schulz, H.D., 1999. Sulfate reduction in surface sediments of the southeast Atlantic continental margin between 15 degrees 38'S and 27 degrees 57'S (Angola and Namibia). Limnology and Oceanography 44, 650-661.

Firer-Sherwood, M., Pulcu, G.S., Elliott, S.J., 2008. Electrochemical interrogations of the Mtr cytochromes from Shewanella: opening a potential window. Journal of Biological Inorganic Chemistry 13, 849-854.

Firer-Sherwood, M.A., Ando, N., Drennan, C.L., Elliott, S.J., 2011. Solution-Based Structural Analysis of the Decaheme Cytochrome, MtrA, by Small-Angle X-ray Scattering and Analytical Ultracentrifugation. J. Phys. Chem. B 115, 11208-11214.

Fleming, P.B., Long, H., Dugan, B., Germaine, J., John, C., Behrmann, J.H., Sawyer, D., Scientists, I.E., 2008. Pore pressure penetrometers document high overpressure

near the seafloor where multiple submarine landslides have occurred on the continental slope, offshore Louisiana, Gulf of Mexico. Earth and Planetary Science Letters 269, 309-324.

Francis, A.J., Dodge, C.J., 1993. Influence of Complex Structure on the Biodegradation of Iron-Citrate Complexes. Applied and Environmental Microbiology 59, 109-113.

Froelich, P.N., Bender, M.L., Luedtke, N.A., Heath, G.R., Devries, T., 1982. The marine phosphorus cycle. American Journal of Science 282, 474-511.

Froelich, P.N., Klinkhammer, G.P., Bender, M.L., Luedtke, N.A., Heath, G.R., Cullen, D., Dauphin, P., Hammond, D., Hartman, B., Maynard, V., 1979. Early oxidation of organic-matter in pelagic sediments of the eastern equatorial Atlantic - suboxic diagenesis. Geochimica Et Cosmochimica Acta 43, 1075-1090.

Furukawa, Y., Reed, A.H., Zhang, G.P., 2014. Effect of organic matter on estuarine flocculation: a laboratory study using montmorillonite, humic acid, xanthan gum, guar gum and natural estuarine flocs. Geochem. Trans. 15, 9.

Gales, J.A., Leat, P.T., Larter, R.D., Kuhn, G., Hillenbrand, C.D., Graham, A.G.C., Mitchell, N.C., Tate, A.J., Buys, G.B., Jokat, W., 2014. Large-scale submarine landslides, channel and gully systems on the southern Weddell Sea margin, Antarctica. Marine Geology 348, 73-87.

Galloway, J.N., Dentener, F.J., Capone, D.G., Boyer, E.W., Howarth, R.W., Seitzinger, S.P., Asner, G.P., Cleveland, C.C., Green, P.A., Holland, E.A., Karl, D.M., Michaels, A.F., Porter, J.H., Townsend, A.R., Vorosmarty, C.J., 2004. Nitrogen cycles: past, present, and future. Biogeochemistry 70, 153-226.

Gartman, A., Findlay, A.J., Luther, G.W., 2014. Nanoparticulate pyrite and other nanoparticles are a widespread component of hydrothermal vent black smoker emissions. Chemical Geology 366, 32-41.

Gartman, A., Yucel, M., Madison, A.S., Chu, D.W., Ma, S.F., Janzen, C.P., Becker, E.L., Beinart, R.A., Girguis, P.R., Luther, G.W., 2011. Sulfide Oxidation across Diffuse Flow Zones of Hydrothermal Vents. Aquatic Geochemistry 17, 583-601.

Gerringa, L.J.A., Rijkenberg, M.J.A., Wolterbeek, H.T., Verburg, T.G., Boye, M., de Baar, H.J.W., 2007. Kinetic study reveals weak Fe-binding ligand, which affects the solubility of Fe in the Scheldt estuary. Marine Chemistry 103, 30-45.

Gjerde, D.T., Fritz, J.S., Schmuckler, G., 1979. Anion chromatography with low-conductivity eluents. Journal of Chromatography 186, 509-519.

Gjerde, D.T., Schmuckler, G., Fritz, J.S., 1980. Anion chromatography with low-conductivity eluents .2. Journal of Chromatography 187, 35-45.

Glazer, B.T., Luther Iii, G.W., Konovalov, S.K., Friederich, G.E., Nuzzio, D.B., Trouwborst, R.E., Tebo, B.M., Clement, B., Murray, K., Romanov, A.S., 2006. Documenting the suboxic zone of the Black Sea via high-resolution real-time redox profiling. Deep Sea Research Part II: Topical Studies in Oceanography 53, 1740-1755.

Glazer, B.T., Rouxel, O.J., 2009. Redox speciation and distribution within diverse iron-dominated microbial habitats at Loihi Seamount. Geomicrobiology Journal 26, 606-622.

Gledhill, M., Buck, K.N., 2012. The organic complexation of iron in the marine environment: a review. Front. Microbiol. 3, 17.

Gledhill, M., van den Berg, C.M.G., Nolting, R.F., Timmermans, K.R., 1998. Variability in the speciation of iron in the northern North Sea. Marine Chemistry 59, 283-300.

Glud, R.N., 2008. Oxygen dynamics of marine sediments. Marine Biology Research 4, 243-289.

Glud, R.N., Wenzhofer, F., Middelboe, M., Oguri, K., Turnewitsch, R., Canfield, D.E., Kitazato, H., 2013. High rates of microbial carbon turnover in sediments in the deepest oceanic trench on Earth. Nat. Geosci. 6, 284-288.

Gong, W.D., Mowlem, M., Kraft, M., Morgan, H., 2009. A Simple, Low-Cost Double Beam Spectrophotometer for Colorimetric Detection of Nitrite in Seawater. IEEE Sens. J. 9, 862-869.

Gorby, Y.A., Yanina, S., McLean, J.S., Rosso, K.M., Moyles, D., Dohnalkova, A., Beveridge, T.J., Chang, I.S., Kim, B.H., Kim, K.S., Culley, D.E., Reed, S.B., Romine, M.F., Saffarini, D.A., Hill, E.A., Shi, L., Elias, D.A., Kennedy, D.W., Pinchuk, G., Watanabe, K., Ishii, S., Logan, B., Nealson, K.H., Fredrickson, J.K., 2006. Electrically conductive bacterial nanowires produced by Shewanella oneidensis strain MR-1 and other microorganisms. Proc. Natl. Acad. Sci. U. S. A. 103, 11358-11363.

Goudie, A.S., 2006. Global warming and fluvial geomorphology. Geomorphology 79, 384-394.

Grace, V.B., Mas-Pla, J., Novais, T.O., Sacchi, E., Zuppi, G.M., 2008. Hydrological mixing and geochemical processes characterization in an estuarine/mangrove system using environmental tracers in Babitonga Bay (Santa Catarina, Brazil). Continental Shelf Research 28, 682-695.

Grantham, M.C., Dove, P.M., 1996. Investigation of bacterial-mineral interactions using fluid tapping mode(TM) atomic force microscopy. Geochimica Et Cosmochimica Acta 60, 2473-2480.

Grantham, M.C., Dove, P.M., DiChristina, T.J., 1997. Microbially catalyzed dissolution of iron and aluminum oxyhydroxide mineral surface coatings. Geochimica Et Cosmochimica Acta 61, 4467-4477.

Gremm, T.J., Kaplan, L.A., 1997. Dissolved carbohydrates in streamwater determined by HPLC and pulsed amperometric detection. Limnology and Oceanography 42, 385-393.

Gros, N., Camoes, M.F., Oliveira, C., Silva, M.C., 2008a. Ionic composition of seawaters and derived saline solutions determined by ion chromatography and its relation to other water quality parameters. J Chromatogr A 1210, 92-98.

Grundmanis, V., Murray, J.W., 1982. Aerobic respiration in pelagic marine-sediments. Geochimica Et Cosmochimica Acta 46, 1101-1120.

Guo, L.D., Santschi, P.H., 1997. Composition and cycling of colloids in marine environments. Rev. Geophys. 35, 17-40.

Haas, J.R., Dichristina, T.J., 2002. Effects of Fe(III) chemical speciation on dissimilatory Fe(III) reduction by Shewanella putrefaciens. Environmental Science & Technology 36, 373-380.

Haeckel, M., Konig, I., Reich, V., Weber, M.E., Suess, E., 2001. Pore water profiles and numerical modelling of biogeochemical processes in Peru Basin deep-sea sediments. Deep-Sea Res. Part II-Top. Stud. Oceanogr. 48, 3713-3736.

Haese, R.R., Schramm, J., van der Loeff, M.M.R., Schulz, H.D., 2000. A comparative study of iron and manganese diagenesis in continental slope and deep sea basin sediments off Uruguay (SW Atlantic). Int. J. Earth Sci. 88, 619-629.

Hakala, J.A., Fimmen, R.L., Chin, Y.P., Agrawal, S.G., Ward, C.P., 2009. Assessment of the geochemical reactivity of Fe-DOM complexes in wetland sediment pore waters using a nitroaromatic probe compound. Geochimica Et Cosmochimica Acta 73, 1382-1393.

Hall, P.O., Aller, R.C., 1992. Rapid, small-volume, flow-injection analysis for CO_2 and $NH4^+$ in marine and fresh-waters. Limnology and Oceanography 37, 1113-1119.

Hamada, Y.Z., Bayakly, N., Peipho, A., Carlson, B., 2006. Accurate potentiometric studies of chromium-citrate and ferric-citrate complexes in aqueous solutions at physiological and alkaline pH values. Synth. React. Inorg. Met.-Org. Nano-Metal Chem. 36, 469-476.

Hamilton, S.K., 2010. Biogeochemical implications of climate change for tropical rivers and floodplains. Hydrobiologia 657, 19-35.

Hartshorne, R.S., Reardon, C.L., Ross, D., Nuester, J., Clarke, T.A., Gates, A.J., Mills, P.C., Fredrickson, J.K., Zachara, J.M., Shi, L., Beliaev, A.S., Marshall, M.J., Tien, M., Brantley, S., Butt, J.N., Richardson, D.J., 2009. Characterization of an electron conduit between bacteria and the extracellular environment. Proc. Natl. Acad. Sci. U. S. A. 106, 22169-22174.

Hawkings, J.R., Wadham, J.L., Tranter, M., Raiswell, R., Benning, L.G., Statham, P.J., Tedstone, A., Nienow, P., Lee, K., Telling, J., 2014. Ice sheets as a significant source of highly reactive nanoparticulate iron to the oceans. Nat. Commun. 5, 8.

Hedges, J.I., Keil, R.G., Benner, R., 1997. What happens to terrestrial organic matter in the ocean? Organic Geochemistry 27, 195-212.

Hedges, J.I., Oades, J.M., 1997. Comparative organic geochemistries of soils and marine sediments. Organic Geochemistry 27, 319-361.

Her, N., Amy, G., Foss, D., Cho, J.W., 2002. Variations of molecular weight estimation by HP-size exclusion chromatography with UVA versus online DOC detection. Environmental Science & Technology 36, 3393-3399.

Hernandez, M.E., Kappler, A., Newman, D.K., 2004. Phenazines and other redox-active antibiotics promote microbial mineral reduction. Applied and Environmental Microbiology 70, 921-928.

Hernandez, M.E., Newman, D.K., 2001. Extracellular electron transfer. Cellular and Molecular Life Sciences 58, 1562-1571.

Hesslein, R., 1976. In situ sampler for close interval pore water studies. Limnology and Oceanography 21, 912-914.

Heyrovsky, M., Mader, P., Vesela, V., Fedurco, M., 1994. The reactions of cystine at mercury-electrodes. J. Electroanal. Chem. 369, 53-70.

Hoehler, T.M., Alperin, M.J., Albert, D.B., Martens, C.S., 2001. Apparent minimum free energy requirements for methanogenic Archaea and sulfate-reducing bacteria in an anoxic marine sediment. Fems Microbiology Ecology 38, 33-41.

Homoky, W.B., John, S.G., Conway, T.M., Mills, R.A., 2013. Distinct iron isotopic signatures and supply from marine sediment dissolution. Nat. Commun. 4, 10.

Homoky, W.B., Severmann, S., McManus, J., Berelson, W.M., Riedel, T.E., Statham, P.J., Mills, R.A., 2012. Dissolved oxygen and suspended particles regulate the benthic flux of iron from continental margins. Marine Chemistry 134, 59-70.

Homoky, W.B., Severmann, S., Mills, R.A., Statham, P.J., Fones, G.R., 2009. Pore-fluid Fe isotopes reflect the extent of benthic Fe redox recycling: Evidence from continental shelf and deep-sea sediments. Geology 37, 751-754.

Honjo, S., Manganini, S.J., Krishfield, R.A., Francois, R., 2008. Particulate organic carbon fluxes to the ocean interior and factors controlling the biological pump: A synthesis of global sediment trap programs since 1983. Progress in Oceanography 76, 217-285.

Hopkinson, C.S., Buffam, I., Hobbie, J., Vallino, J., Perdue, M., Eversmeyer, B., Prahl, F., Covert, J., Hodson, R., Moran, M.A., Smith, E., Baross, J., Crump, B., Findlay, S., Foreman, K., 1998. Terrestrial inputs of organic matter to coastal ecosystems: An intercomparison of chemical characteristics and bioavailability. Biogeochemistry 43, 211-234.

Hu, W.Z., Haddad, P.R., Hasebe, K., Tanaka, K., Tong, P., Khoo, C., 1999. Direct determination of bromide, nitrate, and iodide in saline matrixes using electrostatic ion chromatography with an electrolyte as eluent. Analytical Chemistry 71, 1617-1620.

Huettel, M., Ziebis, W., Forster, S., Luther, G.W., 1998. Advective transport affecting metal and nutrient distributions and interfacial fluxes in permeable sediments. Geochimica Et Cosmochimica Acta 62, 613-631.

Huheey, J.E., Keiter, E.A., Keiter, R.L., 1993. Inorganic Chemistry: Principals of structure and reactivity,, 4th ed. Harper Collins College Publishers, New York, New York.

Hunter, K.A., Boyd, P.W., 2007. Iron-binding ligands and their role in the ocean biogeochemistry of iron. Environ. Chem. 4, 221-232.

Hunter, K.S., Wang, Y.F., Van Cappellen, P., 1998. Kinetic modeling of microbially-driven redox chemistry of subsurface environments: coupling transport, microbial metabolism and geochemistry. Journal of Hydrology 209, 53-80.

Hutchins, D.A., Witter, A.E., Butler, A., Luther, G.W., 1999. Competition among marine phytoplankton for different chelated iron species. Nature 400, 858-861.

Hyacinthe, C., Bonneville, S., Van Cappellen, P., 2006. Reactive iron(III) in sediments: Chemical versus microbial extractions. Geochimica Et Cosmochimica Acta 70, 4166-4180.

Ihnat, P.M., Vennerstrom, J.L., Robinson, D.H., 2000. Synthesis and solution properties of deferoxamine amides. J. Pharm. Sci. 89, 1525-1536.

Illes, E., Tombacz, E., 2006. The effect of humic acid adsorption on pH-dependent surface charging and aggregation of magnetite nanoparticles. Journal of Colloid and Interface Science 295, 115-123.

Ingri, J., Malinovsky, D., Rodushkin, I., Baxter, D.C., Widerlund, A., Andersson, P., Gustafsson, O., Forsling, W., Ohlander, B., 2006. Iron isotope fractionation in river colloidal matter. Earth and Planetary Science Letters 245, 792-798.

Ito, K., Nomura, R., Fujii, T., Tanaka, M., Tsumura, T., Shibata, H., Hirokawa, T., 2012. Determination of nitrite, nitrate, bromide, and iodide in seawater by ion chromatography with UV detection using dilauryldimethylammonium-coated monolithic ODS columns and sodium chloride as an eluent. Analytical and Bioanalytical Chemistry 404, 2513-2517.

Ito, K., Takayama, Y., Makabe, N., Mitsui, R., Hirokawa, T., 2005. Ion chromatography for determination of nitrite and nitrate in seawater using monolithic ODS columns. Journal of Chromatography A 1083, 63-67.

Jahnke, R.A., Alexander, C.R., Kostka, J.E., 2003. Advective pore water input of nutrients to the Satilla River Estuary, Georgia, USA. Estuarine Coastal and Shelf Science 56, 641-653.

Jahnke, R.A., Christiansen, M.B., 1989. A free-vehicle benthic chamber instrument for sea-floor studies. Deep-Sea Research Part a-Oceanographic Research Papers 36, 625-637.

Jahnke, R.A., Jahnke, D.B., 2000. Rates of C, N, P and Si recycling and denitrification at the US Mid-Atlantic continental slope depocenter. Deep-Sea Research Part I-Oceanographic Research Papers 47, 1405-1428.

Jahnke, R.A., Nelson, J.R., Marinelli, R.L., Eckman, J.E., 2000. Benthic flux of biogenic elements on the Southeastern US continental shelf: influence of pore water advective transport and benthic microalgae. Continental Shelf Research 20, 109-127.

Jaisi, D.P., Ji, S.S., Dong, H.L., Blake, R.E., Eberl, D.D., Kim, J.W., 2008. Role of microbial Fe(III) reduction and solution chemistry in aggregation and settling of suspended particles in the Mississippi River delta plain, Louisiana, USA. Clays and Clay Minerals 56, 416-428.

Jaisi, D.P., Kukkadapu, R.K., Eberl, D.D., Dong, H.L., 2005. Control of Fe(III) site occupancy on the rate and extent of microbial reduction of Fe(III) in nontronite. Geochimica Et Cosmochimica Acta 69, 5429-5440.

Janecky, D.R., Seyfried, W.E., 1984. Formation of massive sulfide deposits on oceanic ridge crests - incremental reaction models for mixing between hydrothermal solutions and seawater. Geochimica Et Cosmochimica Acta 48, 2723-2738.

Jensen, D.L., Boddum, J.K., Tjell, J.C., Christensen, T.H., 2002. The solubility of rhodochrosite (MnCO3) and siderite (FeCO3) in anaerobic aquatic environments. Appl. Geochem. 17, 503-511.

Jensen, M.M., Thamdrup, B., Rysgaard, S., Holmer, M., Fossing, H., 2003. Rates and regulation of microbial iron reduction in sediments of the Baltic-North Sea transition. Biogeochemistry 65, 295-317.

Jickells, T.D., An, Z.S., Andersen, K.K., Baker, A.R., Bergametti, G., Brooks, N., Cao, J.J., Boyd, P.W., Duce, R.A., Hunter, K.A., Kawahata, H., Kubilay, N., laRoche, J., Liss, P.S., Mahowald, N., Prospero, J.M., Ridgwell, A.J., Tegen, I., Torres, R., 2005. Global iron connections between desert dust, ocean biogeochemistry, and climate. Science 308, 67-71.

Johansen, A.M., Siefert, R.L., Hoffmann, M.R., 2000. Chemical composition of aerosols collected over the tropical North Atlantic Ocean. Journal of Geophysical Research-Atmospheres 105, 15277-15312.

Johnson, J.W., Oelkers, E.H., Helgeson, H.C., 1992. SUPCRT92 - A software package for calculating the standard molal thermodynamic properties of minerals, gases, aqueous species, and reactions from 1-bar to 5000-bar and 0-degrees-C to 1000-degrees-C. Computers & Geosciences 18, 899-947.

Johnson, K.S., Coletti, L.J., 2002. In situ ultraviolet spectrophotometry for high resolution and long-term monitoring of nitrate, bromide and bisulfide in the ocean. Deep-Sea Research Part I-Oceanographic Research Papers 49, 1291-1305.

Jones, M., 2011. Soluble Organic-Fe(III) complexes: rethinking iron solubility and bioavailability, School of Earth and Atmospheric Sciences. Georgia Institute of Technology, Atlanta, GA.

Jones, M.E., Beckler, J.S., Taillefert, M., 2011. The flux of soluble organic-iron(III) complexes from sediments represents a source of stable iron(III) to estuarine waters and to the continental shelf. Limnology and Oceanography 56, 1811-1823.

Jones, M.E., Fennessey, C.M., DiChristina, T.J., Taillefert, M., 2010. Shewanella oneidensis MR-1 mutants selected for their inability to produce soluble organic-Fe(III) complexes are unable to respire Fe(III) as anaerobic electron acceptor. Environ. Microbiol. 12, 938-950.

Jorgensen, B.B., 1982. Mineralization of organic-matter in the sea bed - the role of sulfate reduction. Nature 296, 643-645.

Jorgensen, B.B., Bak, F., 1991. Pathways and microbiology of thiosulfate transformations and sulfate reduction in a marine sediment (kattegat, denmark). Applied and Environmental Microbiology 57, 847-856.

Kalinowski, B.E., Liermann, L.J., Givens, S., Brantley, S.L., 2000. Rates of bacteria-promoted solubilization of Fe from minerals: a review of problems and approaches. Chemical Geology 169, 357-370.

Kappler, A., Benz, M., Schink, B., Brune, A., 2004. Electron shuttling via humic acids in microbial iron(III) reduction in a freshwater sediment. Fems Microbiology Ecology 47, 85-92.

Kato, C., Nogi, Y., 2001. Correlation between phylogenetic structure and function: examples from deep-sea Shewanella. Fems Microbiology Ecology 35, 223-230.

Khan, S., Ganguly, A.R., Bandyopadhyay, S., Saigal, S., Erickson, D.J., Protopopescu, V., Ostrouchov, G., 2006. Nonlinear statistics reveals stronger ties between ENSO and the tropical hydrological cycle. Geophys. Res. Lett. 33, 6.

King, D.W., Lounsbury, H.A., Millero, F.J., 1995. Rates and mechanism of Fe(II) oxidation at nanomolar total iron concentrations. Environmental Science & Technology 29, 818-824.

Konigsberger, L.C., Konigsberger, E., May, P.M., Hefter, G.T., 2000. Complexation of iron(III) and iron(II) by citrate. Implications for iron speciation in blood plasma. Journal of Inorganic Biochemistry 78, 175-184.

Konyukhov, A.I., 2008. Sedimentary basins of passive margins filled with sediments of river deltas and submarine fans. Lithology and Mineral Resources 43, 507-519.

Koretsky, C.M., Haveman, M., Cuellar, A., Beuving, L., Shattuck, T., Wagner, M., 2008. Influence of Spartina and Juncus on Saltmarsh Sediments. I. Pore Water Geochemistry. Chemical Geology 255, 87-99.

Kostka, J.E., Haefele, E., Viehweger, R., Stucki, J.W., 1999. Respiration and dissolution of iron(III) containing clay minerals by bacteria. Environmental Science & Technology 33, 3127-3133.

Kostka, J.E., Luther, G.W., 1994. Partitioning and speciation of solid-phase iron in salt-marsh sediments. Geochimica Et Cosmochimica Acta 58, 1701-1710.

Kostka, J.E., Wu, J., Nealson, K.H., Stucki, J.W., 1999b. The impact of structural Fe(III) reduction by bacteria on the surface chemistry of smectite clay minerals. Geochimica Et Cosmochimica Acta 63, 3705-3713.

Kotloski, N.J., Gralnick, J.A., 2013. Flavin Electron Shuttles Dominate Extracellular Electron Transfer by Shewanella oneidensis. mBio 4, 4.

Krachler, R., Krachler, R.F., von der Kammer, F., Suephandag, A., Jirsa, F., Ayromlou, S., Hofmann, T., Keppler, B.K., 2010. Relevance of peat-draining rivers for the riverine input of dissolved iron into the ocean. Science of the Total Environment 408, 2402-2408.

Krachler, R., von der Kammer, F., Jirsa, F., Suphandag, A., Krachler, R.F., Plessl, C., Vogt, M., Keppler, B.K., Hofmann, T., 2012. Nanoscale lignin particles as sources of dissolved iron to the ocean. Glob. Biogeochem. Cycle 26.

Kraemer, S.M., 2004. Iron oxide dissolution and solubility in the presence of siderophores. Aquatic sciences 66, 3-18.

Kristensen, E., 2000. Organic matter diagenesis at the oxic/anoxic interface in coastal marine sediments, with emphasis on the role of burrowing animals. Hydrobiologia 426, 1-24.

Kudrass, H.R., Michels, K.H., Wiedicke, M., Suckow, A., 1998. Cyclones and tides as feeders of a submarine canyon off Bangladesh. Geology 26, 715-718.

Laglera, L.M., van den Berg, C.M.G., 2009. Evidence for geochemical control of iron by humic substances in seawater. Limnology and Oceanography 54, 610-619.

Lalonde, K., Mucci, A., Ouellet, A., Gelinas, Y., 2012. Preservation of organic matter in sediments promoted by iron. Nature 483, 198-200.

Lam, P.J., Bishop, J.K.B., 2008. The continental margin is a key source of iron to the HNLC North Pacific Ocean. Geophys. Res. Lett. 35.

Lam, P.J., Bishop, J.K.B., Henning, C.C., Marcus, M.A., Waychunas, G.A., Fung, I.Y., 2006. Wintertime phytoplankton bloom in the subarctic Pacific supported by continental margin iron. Glob. Biogeochem. Cycle 20, 12.

Lapham, L.L., Alperin, M., Chanton, J., Martens, C., 2008. Upward advection rates and methane fluxes, oxidation, and sources at two Gulf of Mexico brine seeps. Marine Chemistry 112, 65-71.

Larsen, M., Thamdrup, B., Shimmield, T., Glud, R.N., 2013. Benthic mineralization and solute exchange on a Celtic Sea sand-bank (Jones Bank). Progress in Oceanography.

Law, G.T.W., Shimmield, T.M., Shimmield, G.B., Cowie, G.L., Breuer, E.R., Harvey, S.M., 2009. Manganese, iron, and sulphur cycling on the Pakistan margin. Deep-Sea Res. Part II-Top. Stud. Oceanogr. 56, 305-323.

Lee, H.J., 2009. Timing of occurrence of large submarine landslides on the Atlantic Ocean margin. Marine Geology 264, 53-64.

Lee, T., Hyun, J.H., Mok, J.S., Kim, D., 2008. Organic carbon accumulation and sulfate reduction rates in slope and basin sediments of the Ulleung Basin, East/Japan Sea. Geo-Mar. Lett. 28, 153-159.

Levitus, S., Antonov, J.I., Wang, J.L., Delworth, T.L., Dixon, K.W., Broccoli, A.J., 2001. Anthropogenic warming of Earth's climate system. Science 292, 267-270.

Lewis, B.L., Glazer, B.T., Montbriand, P.J., Luther III, G.W., Nuzzio, D.B., Deering, T., Ma, S., Theberge, S., 2007. Short-term and interannual variability of redox-sensitive chemical parameters in hypoxic/anoxic bottom waters of the Chesapeake Bay. Marine chemistry 105, 296-308.

Li, S.H., Dass, C., 1999. Iron(lll)-immobilized metal ion affinity chromatography and mass spectrometry for the purification and characterization of synthetic phosphopeptides. Anal. Biochem. 270, 9-14.

Liang, L., McCarthy, J.F., Jolley, L.W., McNabb, J.A., Mehlhorn, T.L., 1993. Iron dynamics: Transformation of Fe(II)/Fe(III) during injection of natural organic matter in a sandy aquifer. Geochimica Et Cosmochimica Acta 57, 1987-1999.

Lies, D.P., Hernandez, M.E., Kappler, A., Mielke, R.E., Gralnick, J.A., Newman, D.K., 2005. Shewanella oneidensis MR-1 uses overlapping pathways for iron reduction at a distance and by direct contact under conditions relevant for biofilms. Applied and Environmental Microbiology 71, 4414-4426.

Lin, H., Szeinbaum, N.H., DiChristina, T.J., Taillefert, M., 2012. Microbial Mn(IV) reduction requires an initial one-electron reductive solubilization step. Geochimica Et Cosmochimica Acta 99, 179-192.

Lin, S., Morse, J.W., 1991. Sulfate reduction and iron sulfide mineral formation in Gulf of Mexico anoxic sediments. American Journal of Science 291, 55-89.

Liu, C.G., Zachara, J.M., Gorby, Y.A., Szecsody, J.E., Brown, C.F., 2001. Microbial reduction of Fe(III) and sorption/precipitation of Fe(II) on Shewanella putrefaciens strain CN32. Environmental Science & Technology 35, 1385-1393.

Liu, C.X., Gorby, Y.A., Zachara, J.M., Fredrickson, J.K., Brown, C.F., 2002. Reduction kinetics of Fe(III), Co(III), U(VI) Cr(VI) and Tc(VII) in cultures of dissimilatory metal-reducing bacteria. Biotechnology and Bioengineering 80, 637-649.

Liu, X.W., Millero, F.J., 2002. The solubility of iron in seawater. Marine Chemistry 77, 43-54.

Lohan, M.C., Bruland, K.W., 2008. Elevated Fe(II) and dissolved Fe in hypoxic shelf waters off Oregon and Washington: An enhanced source of iron to coastal upwelling regimes. Environmental Science & Technology 42, 6462-6468.

Long, H., Flemings, P.B., Germaine, J.T., Saffer, D.M., 2011. Consolidation and overpressure near the seafloor in the Ursa Basin, Deepwater Gulf of Mexico. Earth and Planetary Science Letters 305, 11-20.

Lovley, D.R., 1993. Dissimilatory metal reduction. Annu. Rev. Microbiol. 47, 263-290.

Lovley, D.R., Baedecker, M.J., Lonergan, D.J., Cozzarelli, I.M., Phillips, E.J.P., Siegel, D.I., 1989. Oxidation of Aromatic Contaminants Coupled to Microbial Iron Reduction. Nature 339, 297-300.

Lovley, D.R., Coates, J.D., BluntHarris, E.L., Phillips, E.J.P., Woodward, J.C., 1996. Humic substances as electron acceptors for microbial respiration. Nature 382, 445-448.

Lovley, D.R., Coates, J.D., Saffarini, D.A., Lonergan, D.J., 1997. Dissimilatory Fe(III) reduction, in: Winkelman, G., Carrano, C.J. (Eds.), Transition metals in microbial metabolism. Harwood Academic Publishers, Amsteldjik, Netherlands, pp. 187-219.

Lovley, D.R., Fraga, J.L., Coates, J.D., Blunt-Harris, E.L., 1999. Humics as an electron donor for anaerobic respiration. Environ. Microbiol. 1, 89-98.

Lovley, D.R., Phillips, E.J.P., 1988. Novel Mode of Microbial Energy-Metabolism - Organic-Carbon Oxidation Coupled to Dissimilatory Reduction of Iron or Manganese. Applied and Environmental Microbiology 54, 1472-1480.

Lovley, D.R., Phillips, E.J.P., Gorby, Y.A., Landa, E.R., 1991. Microbial reduction of uranium. Nature 350, 413-416.

Lovley, D.R., Stolz, J.F., Nord, G.L., Phillips, E.J.P., 1987. Anaerobic Production of Magnetite by a Dissimilatory Iron-Reducing Microorganism. Nature 330, 252-254.

Lovley, D.R., Woodward, J.C., 1996. Mechanisms for chelator stimulation of microbial Fe(III)-oxide reduction. Chemical Geology 132, 19-24.

Luther, G.W., Ferdelman, T.G., Kostka, J.E., Tsamakis, E.J., Church, T.M., 1991. Temporal and spatial variability of reduced sulfur species (FeS_2,$S_2O_3^{2-}$) and porewater parameters in salt-marsh sediments. Biogeochemistry 14, 57-88.

Luther, G.W., Glazer, B.T., Ma, S.F., Trouwborst, R.E., Moore, T.S., Metzger, E., Kraiya, C., Waite, T.J., Druschel, G., Sundby, B., Taillefert, M., Nuzzio, D.B., Shank, T.M., Lewis, B.L., Brendel, P.J., 2008b. Use of voltammetric solid-state (micro)electrodes for studying biogeochemical processes: Laboratory measurements to real time measurements with an in situ electrochemical analyzer (ISEA). Marine Chemistry 108, 221-235.

Luther, G.W., Kostka, J.E., Church, T.M., Sulzberger, B., Stumm, W., 1992. Seasonal iron cycling in the salt-marsh sedimentary environment - the importance of ligand complexes with Fe(II) and Fe(III) in the dissolution of Fe(III) minerals and pyrite, respectively. Elsevier Science Bv, pp. 81-103.

Luther, G.W., Reimers, C.E., Nuzzio, D.B., Lovalvo, D., 1999. In situ deployment of voltammetric, potentiometric. and amperometric microelectrodes from a ROV to determine dissolved O-2, Mn, Fe, S(-2), and pH in porewaters. Environmental Science & Technology 33, 4352-4356.

Luther, G.W., Rozan, T.F., Taillefert, M., Nuzzio, D.B., Di Meo, C., Shank, T.M., Lutz, R.A., Cary, S.C., 2001. Chemical speciation drives hydrothermal vent ecology. Nature 410, 813-816.

Luther, G.W., Shellenbarger, P.A., Brendel, P.J., 1996. Dissolved organic Fe(III) and Fe(II) complexes in salt marsh porewaters. Geochimica Et Cosmochimica Acta 60, 951-960.

Lyman, J.M., Good, S.A., Gouretski, V.V., Ishii, M., Johnson, G.C., Palmer, M.D., Smith, D.M., Willis, J.K., 2010. Robust warming of the global upper ocean. Nature 465, 334-337.

Lyons, T.W., Anbar, A.D., Severmann, S., Scott, C., Gill, B.C., 2009. Tracking Euxinia in the Ancient Ocean: A Multiproxy Perspective and Proterozoic Case Study, Annual Review of Earth and Planetary Sciences. Annual Reviews, Palo Alto, pp. 507-534.

Madigan, M.T., Martinko, J.M., Parker, J., 1997. Biology of microorganisms. Prentice-Hall, Upper Saddle River, NJ.

Madison, A.S., Tebo, B.M., Mucci, A., Sundby, B., Luther, G.W., 2013. Abundant Porewater Mn(III) Is a Major Component of the Sedimentary Redox System. Science 341, 875-878.

Marinelli, R.L., Jahnke, R.A., Craven, D.B., Nelson, J.R., Eckman, J.E., 1998. Sediment nutrient dynamics on the South Atlantic Bight continental shelf. Limnology and Oceanography 43, 1305-1320.

Marritt, S.J., McMillan, D.G.G., Shi, L., Fredrickson, J.K., Zachara, J.M., Richardson, D.J., Jeuken, L.J.C., Butt, J.N., 2012. The roles of CymA in support of the respiratory flexibility of Shewanella oneidensis MR-1. Biochem. Soc. Trans. 40, 1217-1221.

Marsili, E., Baron, D.B., Shikhare, I.D., Coursolle, D., Gralnick, J.A., Bond, D.R., 2008. Shewanella Secretes flavins that mediate extracellular electron transfer. Proc. Natl. Acad. Sci. U. S. A. 105, 3968-3973.

Martin, J.H., Fitzwater, S.E., 1988. Iron-deficiency limits phytoplankton growth in the northeast Pacific subarctic. Nature 331, 341-343.

Martin, J.M., Meybeck, M., 1979. Elemental mass-balance of material carried by major world rivers. Marine Chemistry 7, 173-206.

Mayer, L.M., 1995. Sedimentary organic-matter preservation - an assessment and speculative synthesis - a comment. Marine Chemistry 49, 123-126.

McBeth, J.M., Fleming, E.J., Emerson, D., 2013. The transition from freshwater to marine iron-oxidizing bacterial lineages along a salinity gradient on the Sheepscot River, Maine, USA. Environ. Microbiol. Rep. 5, 453-463.

McCormack, P., Worsfold, P.J., Gledhill, M., 2003. Separation and detection of siderophores produced by marine bacterioplankton using high-performance liquid chromatography with electrospray ionization mass spectrometry. Analytical Chemistry 75, 2647-2652.

McKee, B.A., Aller, R.C., Allison, M.A., Bianchi, T.S., Kineke, G.C., 2004. Transport and transformation of dissolved and particulate materials on continental margins influenced by major rivers: benthic boundary layer and seabed processes. Continental Shelf Research 24, 899-926.

McLafferty, F.W., Tureček, F., 1993. Interpretation of Mass Spectra. University Science Books.

Meiggs, D., 2010. Development of autonomous in situ techniques to examine the impacts of dynamic forcings on sediment biogeochemistry in highly productive estuarine ecosystems, School of Earth and Atmospheric Sciences. Georgia Institute of Technology, Atlanta, GA.

Meiggs, D., Taillefert, M., 2011. The effect of riverine discharge on biogeochemical processes in estuarine sediments. Limnology and Oceanography 56, 1797-1810.

Metzger, E., Simonucci, C., Viollier, E., Sarazin, G., Prevot, F., Jezequel, D., 2007. Benthic response to shellfish farming in Thau lagoon: Pore water signature. Estuarine Coastal and Shelf Science 72, 406-419.

Meyer, J.L., 1986. Dissolved organic-carbon dynamics in 2 subtropical blackwater rivers. Archiv Fur Hydrobiologie 108, 119-134.

Middelburg, J.J., Soetaert, K., Herman, P.M.J., 1997. Empirical relationships for use in global diagenetic models. Deep-Sea Research Part I-Oceanographic Research Papers 44, 327-344.

Miethke, M., Hou, J., Marahiel, M.A., 2011. The Siderophore-Interacting Protein YqjH Acts as a Ferric Reductase in Different Iron Assimilation Pathways of Escherichia coli. Biochemistry 50, 10951-10964.

Miles, C.J., Brezonik, P.L., 1983. High-Performance Size Exclusion Chromatography of Aquatic Humic Substances. Journal of Chromatography 259, 499-503.

Millero, F.J., 1983. The estimation of the pKa of acids in seawater using the Pitzer equations. Geochimica Et Cosmochimica Acta 47, 2121-2129.

Millero, F.J., 1998. Solubility of Fe(III) in seawater. Earth and Planetary Science Letters 154, 323-329.

Millero, F.J., Schreiber, D.R., 1982. Use of the ion-pairing model to estimate activity-coefficients of the ionic components of natural-waters. American Journal of Science 282, 1508-1540.

Miot, J., Benzerara, K., Obst, M., Kappler, A., Hegler, F., Schadler, S., Bouchez, C., Guyot, F., Morin, G., 2009. Extracellular Iron Biomineralization by Photoautotrophic Iron-Oxidizing Bacteria. Applied and Environmental Microbiology 75, 5586-5591.

Moore, T.S., Nuzzio, D.B., Deering, T.W., Taillefert, M., Luther, G.W., 2007. Use of voltammetry to monitor O-2 using Au/Hg electrodes and to control physical sensors on an unattended observatory in the Delaware bay. Electroanalysis 19, 2110-2116.

Mopper, K., Lindroth, P., 1982. Diel and depth variations in dissolved free amino acids and ammonium in the Baltic Sea determined by shipboard HPLC analysis. Limnology and Oceanography, 336-347.

Morse, J.W., Eldridge, P.M., 2007. A non-steady state diagenetic model for changes in sediment biogeochemistry in response to seasonally hypoxic/anoxic conditions in the "dead zone" of the Louisiana shelf. Marine Chemistry 106, 239-255.

Morse, J.W., Rowe, G.T., 1999. Benthic biogeochemistry beneath the Mississippi River plume. Estuaries 22, 206-214.

Muller, B., Buis, K., Stierli, R., Wehrli, B., 1998. High spatial resolution measurements in lake sediments with PVC based liquid membrane ion-selective electrodes. Limnology and Oceanography 43, 1728-1733.

Murphy, J., Riley, J.P., 1962. A modified single solution method for determination of phosphate in natural waters. Analytica Chimica Acta 26, 31-&.

Myers, C.R., Myers, J.M., 1992. Localization of Cytochromes to the Outer-Membrane of Anaerobically Grown Shewanella-Putrefaciens Mr-1. J. Bacteriol. 174, 3429-3438.

Myers, C.R., Myers, J.M., 1993. Ferric reductase is associated with the membranes of anaerobically grown Shewanella-putrefaciens MR-1. FEMS Microbiol. Lett. 108, 15-22.

Myers, C.R., Myers, J.M., 2003. Cell surface exposure of the outer membrane cytochromes of Shewanella oneidensis MR-1. Letters in Applied Microbiology 37, 254-258.

Myers, C.R., Nealson, K.H., 1988. Microbial reduction of manganese oxides - interactions with iron and sulfur. Geochimica Et Cosmochimica Acta 52, 2727-2732.

Mylon, S.E., Chen, K.L., Elimelech, M., 2004. Influence of natural organic matter and ionic composition on the kinetics and structure of hematite colloid aggregation: Implications to iron depletion in estuaries. Langmuir 20, 9000-9006.

Nahum, A., Horvath, C., 1980. Evaluation of octanol-water partition-coefficients by using high-performance liquid-chromatography. Journal of Chromatography 192, 315-322.

Nealson, K.H., Saffarini, D., 1994. Iron and manganese in anaerobic respiration - environmental significance, physiology, and regulation. Annu. Rev. Microbiol. 48, 311-343.

Nedelec, F., Statham, P.J., Mowlem, M., 2007. Processes influencing dissolved iron distributions below the surface at the Atlantic Ocean-Celtic Sea shelf edge. Marine Chemistry 104, 156-170.

Nevin, K.P., Lovley, D.R., 2000. Potential for nonenzymatic reduction of Fe(III) via electron shuttling in subsurface sediments. Environmental Science & Technology 34, 2472-2478.

Nevin, K.P., Lovley, D.R., 2002. Mechanisms for accessing insoluble Fe(III) oxide during dissimilatory Fe(III) reduction by Geothrix fermentans. Applied and Environmental Microbiology 68, 2294-2299.

Nevin, K.P., Lovley, D.R., 2002b. Mechanisms for Fe(III) oxide reduction in sedimentary environments. Geomicrobiology Journal 19, 141-159.

Newman, D.K., Kolter, R., 2000. A role for excreted quinones in extracellular electron transfer. Nature 405, 94-97.

Noffke, A., Hensen, C., Sommer, S., Scholz, F., Bohlen, L., Mosch, T., Graco, M., Wallmann, K., 2012. Benthic iron and phosphorus fluxes across the Peruvian oxygen minimum zone. Limnology and Oceanography 57, 851-867.

Nowack, B., Sigg, L., 1997. Dissolution of Fe(III)(hydr)oxides by metal-EDTA complexes. Geochimica Et Cosmochimica Acta 61, 951-963.

Nuzzio, D.B., Taillefert, M., Cary, S.C., Reysenbach, A.L., III, G.W.L., 2002. In situ Voltammetry at Deep-Sea Hydrothermal vents, in: Taillefert, M., Rozan, T.F. (Eds.), Environmental Electrochemistry: Analyses of Trace Element Biogeochemistry. American Chemical Society, Washington, D.C, pp. 40-53.

O'Reilly, S.E., Furukawa, Y., Newell, S., 2006. Dissolution and microbial Fe(III) reduction of nontronite (NAu-1). Chemical Geology 235, 1-11.

O'Reilly, S.E., Watkins, J., Furukawa, Y., 2005. Secondary mineral formation associated with respiration of nontronite, NAu-1 by iron reducing bacteria. Geochem. Trans. 6, 67-76.

Obuekwe, C.O., Westlake, D.W.S., Cook, F.D., Costerton, J.W., 1981. Surface changes in mild-steel coupons from the action of corrosion-causing bacteria. Applied and Environmental Microbiology 41, 766-774.

Ohta, K., Tanaka, K., Fritz, J.S., 1996. Non-suppressed ion chromatography of inorganic anions, magnesium and calcium ions using a pyromellitate eluent and its application in evaluating environmental water quality. Journal of Chromatography A 731, 179-186.

Okamoto, A., Hashimoto, K., Nakamura, R., 2012. Long-range electron conduction of Shewanella biofilms mediated by outer membrane C-type cytochromes. Bioelectrochemistry 85, 61-65.

Okamoto, A., Hashimoto, K., Nealson, K.H., Nakamura, R., 2013. Rate enhancement of bacterial extracellular electron transport involves bound flavin semiquinones. Proc. Natl. Acad. Sci. U. S. A. 110, 7856-7861.

O'Loughlin, E., and Chin, Y.P., 2001. Effect of detector wavelength on the determination of the molecular weight of humic substances by high-pressure size exclusion chromatography. Water Res. 35, 333-338.

Otero, E., Culp, R., Noakes, J.E., Hodson, R.E., 2000. Allocation of particulate organic carbon from different sources in two contrasting estuaries of southeastern USA. Limnology and Oceanography 45, 1753-1763.

Owen, M., Day, S., Maslin, M., 2007. Late Pleistocene submarine mass movements: occurrence and causes. Quat. Sci. Rev. 26, 958-978.

Perdue, E.M., Beck, K.C., Reuter, J.H., 1976. Organic complexes of iron and aluminum in natural-waters. Nature 260, 418-420.

Pester, N.J., Rough, M., Ding, K., Seyfried, W.E., 2011. A new Fe/Mn geothermometer for hydrothermal systems: Implications for high-salinity fluids at 13 degrees N on the East Pacific Rise. Geochimica Et Cosmochimica Acta 75, 7881-7892.

Picard, A., Testemale, D., Hazemann, J.L., Daniel, I., 2012. The influence of high hydrostatic pressure on bacterial dissimilatory iron reduction. Geochimica Et Cosmochimica Acta 88, 120-129.

Pitts, K.E., Dobbin, P.S., Reyes-Ramirez, F., Thomson, A.J., Richardson, D.J., Seward, H.E., 2003. Characterization of the Shewanella oneidensis MR-1 decaheme cytochrome MtrA: expression in Escherichia coli confers the ability to reduce soluble Fe(III) chelates. The Journal of biological chemistry 278, 27758-27765.

Postma, D., 1985. Concentration of Mn and separation from Fe in sediments .1. Kinetics and stoichiometry of the reaction between birnessite and dissolved Fe(II) at 10-degrees-C. Geochimica Et Cosmochimica Acta 49, 1023-1033.

Postma, D., Appelo, C.A.J., 2000. Reduction of Mn-oxides by ferrous iron in a flow system: Column experiment and reactive transport modeling. Geochimica Et Cosmochimica Acta 64, 1237-1247.

Powell, R.T., Landing, W.M., Bauer, J.E., 1996. Colloidal trace metals, organic carbon and nitrogen in a southeastern US estuary. Marine Chemistry 55, 165-176.

Powell, R.T., Wilson-Finelli, A., 2003. Importance of organic Fe complexing ligands in the Mississippi River plume. Estuarine Coastal and Shelf Science 58, 757-763.

Precht, E., Franke, U., Polerecky, L., Huettel, M., 2004. Oxygen dynamics in permeable sediments with wave-driven pore water exchange. Limnology and Oceanography 49, 693-705.

Prins, M.A., Postma, G., Cleveringa, J., Cramp, A., Kenyon, N.H., 2000. Controls on terrigenous sediment supply to the Arabian Sea during the late Quaternary: the Indus Fan. Marine Geology 169, 327-349.

Pullin, M.J., Cabaniss, S.E., 2001. Colorimetric flow-injection analysis of dissolved iron in high DOC waters. Water Research 35, 363-372.

Rabouille, C., Caprais, J.C., Lansard, B., Crassous, P., Dedieu, K., Reyss, J.L., Khripounoff, A., 2009. Organic matter budget in the Southeast Atlantic continental margin close to the Congo Canyon: In situ measurements of sediment oxygen consumption. Deep Sea Research Part II: Topical Studies in Oceanography 56, 2223-2238.

Rabouille, C., Gaillard, J.F., 1991. A coupled model representing the deep-sea organic-carbon mineralization and oxygen-consumption in surficial sediments. Journal of Geophysical Research-Oceans 96, 2761-2776.

Radic, A., Lacan, F., Murray, J.W., 2011. Iron isotopes in the seawater of the equatorial Pacific Ocean: New constraints for the oceanic iron cycle. Earth and Planetary Science Letters 306, 1-10.

Raiswell, R., Benning, L.G., Tranter, M., Tulaczyk, S., 2008. Bioavailable iron in the Southern Ocean: the significance of the iceberg conveyor belt. Geochem. Trans. 9.

Raiswell, R., Tranter, M., Benning, L.G., Siegert, M., De'ath, R., Huybrechts, P., Payne, T., 2006. Contributions from glacially derived sediment to the global iron (oxyhydr)oxide cycle: Implications for iron delivery to the oceans. Geochimica Et Cosmochimica Acta 70, 2765-2780.

Rausa, R., Mazzolari, E., Calemma, V., 1991. Determination of Molecular-Size Distributions of Humic Acids by High-Performance Size-Exclusion Chromatography. Journal of Chromatography 541, 419-429.

Reece, J.S., Flemings, P.B., Dugan, B., Long, H., Germaine, J.T., 2012. Permeability-porosity relationships of shallow mudstones in the Ursa Basin, northern deepwater Gulf of Mexico. Journal of Geophysical Research-Solid Earth 117, 13.

Reguera, G., McCarthy, K.D., Mehta, T., Nicoll, J.S., Tuominen, M.T., Lovley, D.R., 2005. Extracellular electron transfer via microbial nanowires. Nature 435, 1098-1101.

Reimers, C.E., 2007. Applications of microelectrodes to problems in chemical oceanography. Chem. Rev. 107, 590-600.

Rickard, D., Luther, G.W., 1997. Kinetics of pyrite formation by the H2S oxidation of iron(II) monosulfide in aqueous solutions between 25 and 125 degrees C: The mechanism. Geochimica Et Cosmochimica Acta 61, 135-147.

Rickard, D., Morse, J.W., 2005. Acid volatile sulfide (AVS). Marine Chemistry 97, 141-197.

Rickard, D., Oldroyd, A., Cramp, A., 1999. Voltammetric evidence for soluble FeS complexes in anoxic estuarine muds. Estuaries 22, 693-701.

Ritchie, J.D., Perdue, E.M., 2003. Proton-binding study of standard and reference fulvic acids, humic acids, and natural organic matter. Geochimica Et Cosmochimica Acta 67, 85-96.

Roden, E.E., 2003. Fe(III) oxide reactivity toward biological versus chemical reduction. Environmental Science & Technology 37, 1319-1324.

Roden, E.E., 2006. Geochemical and microbiological controls on dissimilatory iron reduction. Comptes Rendus Geoscience 338, 456-467.

Roden, E.E., Sobolev, D., Glazer, B., Luther, G.W., 2004. Potential for microscale bacterial Fe redox cycling at the aerobic-anaerobic interface. Geomicrobiology Journal 21, 379-391.

Roden, E.E., Zachara, J.M., 1996. Microbial reduction of crystalline iron(III) oxides: Influence of oxide surface area and potential for cell growth. Environmental Science & Technology 30, 1618-1628.

Rose, A.L., Waite, T.D., 2003. Kinetics of iron complexation by dissolved natural organic matter in coastal waters. Marine Chemistry 84, 85-103.

Ross, A.R.S., Ikonomou, M.G., Orians, K.J., 2000. Characterization of dissolved tannins and their metal-ion complexes by electrospray ionization mass spectrometry. Analytica Chimica Acta 411, 91-102.

Ross, A.R.S., Ikonomou, M.G., Orians, K.J., 2003. Characterization of copper-complexing ligands in seawater using immobilized copper(Il)-ion affinity chromatography and electrospray ionization mass spectrometry. Marine Chemistry 83, 47-58.

Ross, D.E., Ruebush, S.S., Brantley, S.L., Hartshorne, R.S., Clarke, T.A., Richardson, D.J., Tien, M., 2007. Characterization of protein-protein interactions involved in iron reduction by Shewanella oneidensis MR-1. Applied and Environmental Microbiology 73, 5797-5808.

Rosso, K.M., Zachara, J.M., Fredrickson, J.K., Gorby, Y.A., Smith, S.C., 2003. Nonlocal bacterial electron transfer to hematite surfaces. Geochimica Et Cosmochimica Acta 67, 1081-1087.

Royer, R.A., Dempsey, B.A., Jeon, B.H., Burgos, W.D., 2004. Inhibition of biological reductive dissolution of hematite by ferrous iron. Environmental Science & Technology 38, 187-193.

Rozan, T.F., Luther, G.W., 2002. An anion chromatography/ultraviolet detection method to determine nitrite, nitrate, and sulfide concentrations in saline (pore) waters. Marine Chemistry 77, 1-6.

Rozan, T.F., Taillefert, M., Trouwborst, R.E., Glazer, B.T., Ma, S.F., Herszage, J., Valdes, L.M., Price, K.S., Luther, G.W., 2002. Iron-sulfur-phosphorus cycling in the sediments of a shallow coastal bay: Implications for sediment nutrient release and benthic macroalgal blooms. Limnology and Oceanography 47, 1346-1354.

Rue, E.L., Bruland, K.W., 1995. Complexation of Iron(Iii) by Natural Organic-Ligands in the Central North Pacific as Determined by a New Competitive Ligand Equilibration Adsorptive Cathodic Stripping Voltammetric Method. Marine Chemistry 50, 117-138.

Saini, G., Chan, C.S., 2013. Near-neutral surface charge and hydrophilicity prevent mineral encrustation of Fe-oxidizing micro-organisms. Geobiology 11, 191-200.

Saito, M.A., Noble, A.E., Tagliabue, A., Goepfert, T.J., Lamborg, C.H., Jenkins, W.J., 2013. Slow-spreading submarine ridges in the South Atlantic as a significant oceanic iron source. Nat. Geosci. 6, 775-779.

Sampere, T.P., Bianchi, T.S., Allison, M.A., McKee, B.A., 2011. Burial and degradation of organic carbon in Louisiana shelf/slope sediments. Estuarine, Coastal and Shelf Science 95, 232-244.

Santana-Casiano, J.M., Gonzalez-Davila, M., Rodriguez, M.J., Millero, F.J., 2000. The effect of organic compounds in the oxidation kinetics of Fe(II). Marine Chemistry 70, 211-222.

Sarmiento, J.L., Gruber, N., 2006. Ocean Biogeochemical Dynamics. Princeton University Press, Princeton, NJ.

Schicklberger, M., Sturm, G., Gescher, J., 2013. Genomic Plasticity Enables a Secondary Electron Transport Pathway in Shewanella oneidensis. Applied and Environmental Microbiology 79, 1150-1159.

Schmidt, M., Hensen, C., Morz, T., Muller, C., Grevemeyer, I., Wallmann, K., Mau, S., Kaul, N., 2005. Methane hydrate accumulation in "Mound 11" mud volcano, Costa Rica forearc. Marine Geology 216, 83-100.

Schulz, H.D., Dahmke, A., Schinzel, U., Wallmann, K., Zabel, M., 1994. EARLY DIAGENETIC PROCESSES, FLUXES, AND REACTION-RATES IN SEDIMENTS OF THE SOUTH-ATLANTIC. Geochimica Et Cosmochimica Acta 58, 2041-2060.

Schwehr, K.A., Santschi, P.H., 2003. Sensitive determination of iodine species, including organo-iodine, for freshwater and seawater samples using high performance liquid chromatography and spectrophotometric detection. Analytica Chimica Acta 482, 59-71.

Schwertmann, U., Cornell, R.M., 2000. Iron oxides in the Laboratory: Preparation and Characterization. Wiley-VCH, Weinheim.

Scott, D.T., McKnight, D.M., Blunt-Harris, E.L., Kolesar, S.E., Lovley, D.R., 1998. Quinone moieties act as electron acceptors in the reduction of humic substances by humics-reducing microorganisms. Environmental Science & Technology 32, 2984-2989.

Severmann, S., McManus, J., Berelson, W.M., Hammond, D.E., 2010. The continental shelf benthic iron flux and its isotope composition. Geochimica Et Cosmochimica Acta 74, 3984-4004.

Shi, L., Chen, B.W., Wang, Z.M., Elias, D.A., Mayer, M.U., Gorby, Y.A., Ni, S., Lower, B.H., Kennedy, D.W., Wunschel, D.S., Mottaz, H.M., Marshall, M.J., Hill, E.A.,

Beliaev, A.S., Zachara, J.M., Fredrickson, J.K., Squier, T.C., 2006. Isolation of a high-affinity functional protein complex between OmcA and MtrC: Two outer membrane decaheme c-type cytochromes of Shewanella oneidensis MR-1. J. Bacteriol. 188, 4705-4714.

Shi, L., Deng, S., Marshall, M.J., Wang, Z.M., Kennedy, D.W., Dohnalkova, A.C., Mottaz, H.M., Hill, E.A., Gorby, Y.A., Beliaev, A.S., Richardson, D.J., Zachara, J.M., Fredrickson, J.K., 2008. Direct involvement of type II secretion system in extracellular translocation of Shewanella oneidensis outer membrane cytochromes MtrC and OmcA. J. Bacteriol. 190, 5512-5516.

Sholkovitz, E.R., 1976. Flocculation of dissolved organic and inorganic matter during mixing of river water and seawater. Geochimica Et Cosmochimica Acta 40, 831-845.

Shweky, I., Bino, A., Goldberg, D.P., Lippard, S.J., 1994. Syntheses, structures, and magnetic-properties of 2 dinuclear Iron(III) citrate complexes. Inorg. Chem. 33, 5161-5162.

Shyu, J.B.H., Lies, D.P., Newman, D.K., 2002. Protective Role of tolC in Efflux of the Electron Shuttle Anthraquinone-2,6-Disulfonate. J. Bacteriol. 184, 1806-1810.

Sionneau, T., Bout-Roumazeilles, V., Biscaye, P.E., Van Vliet-Lanoe, B., Bory, A., 2008. Clay mineral distributions in and around the Mississippi River watershed and Northern Gulf of Mexico: sources and transport patterns. Quat. Sci. Rev. 27, 1740-1751.

Sleep, N.H., 1991. Hydrothermal circulation, anhydrite precipitation, and thermal structure at ridge axes. Journal of Geophysical Research-Solid Earth and Planets 96, 2375-2387.

Slomp, C.P., Malschaert, J.F.P., Lohse, L., VanRaaphorst, W., 1997. Iron and manganese cycling in different sedimentary environments on the North Sea continental margin. Continental Shelf Research 17, 1083-1117.

Small, H., Stevens, T.S., Bauman, W.C., 1975. Novel ion-exchange chromatographic method using conductimetric detection. Analytical Chemistry 47, 1801-1809.

Smee, B.W., Hall, G.E.M., Koop, D.J., 1978. Analysis of fluoride, chloride, nitrate and sulfate in natural-waters using ion chromatography. Journal of Geochemical Exploration 10, 245-258.

Snow, C.L., Lilova, K.I., Radha, A.V., Shi, Q., Smith, S., Navrotsky, A., Boerio-Goates, J., Woodfield, B.F., 2013. Heat capacity and thermodynamics of a synthetic two-line ferrihydrite, FeOOH center dot 0.027H(2)O. Journal of Chemical Thermodynamics 58, 307-314.

Sobolev, D., Roden, E.E., 2001. Suboxic deposition of ferric iron by bacteria in opposing gradients of Fe(II) and oxygen at circumneutral pH. Applied and Environmental Microbiology 67, 1328-1334.

Sorokina, A.Y., Chernousova, E.Y., Dubinina, G.A., 2012. Hoeflea siderophila sp nov., a New Neutrophilic Iron-Oxidizing Bacterium. Microbiology 81, 59-66.

Stigall, J., Dugan, B., 2010. Overpressure and earthquake initiated slope failure in the Ursa region, northern Gulf of Mexico. Journal of Geophysical Research-Solid Earth 115, 11.

Stolpe, B., Guo, L., Shiller, A.M., Hassellöv, M., 2010. Size and composition of colloidal organic matter and trace elements in the Mississippi River, Pearl River and the northern Gulf of Mexico, as characterized by flow field-flow fractionation. Marine Chemistry 118, 119-128.

Stolpe, B., Guo, L.D., Shiller, A.M., 2013. Binding and transport of rare earth elements by organic and iron-rich nanocolloids in Alaskan rivers, as revealed by field-flow fractionation and ICP-MS. Geochimica Et Cosmochimica Acta 106, 446-462.

Stolpe, B., Hassellov, M., 2007. Changes in size distribution of fresh water nanoscale colloidal matter and associated elements on mixing with seawater. Geochimica Et Cosmochimica Acta 71, 3292-3301.

Stookey, L.L., 1970. Ferrozine - a new spectrophotometric reagent for iron. Analytical Chemistry 42, 779-&.

Straub, K.L., Benz, M., Schink, B., Widdel, F., 1996. Anaerobic, nitrate-dependent microbial oxidation of ferrous iron. Applied and Environmental Microbiology 62, 1458-1460.

Stumm, W., 1997. Reactivity at the mineral-water interface: dissolution and inhibition.

Stumm, W., Morgan, J.J., 1996. Aquatic chemistry: chemical equilibria and rates in natural waters. Wiley.

Sugawara, K., Terada, K., 1958. Oxidized iodine in sea water. Nature 182, 250-251.

Sunda, W.G., Kieber, D.J., 1994. Oxidation of humic substances by manganese oxides yields low-molecular-weight organic substrates. Nature 367, 62-64.

Sung, W., Morgan, J.J., 1980. Kinetics and product of ferrous iron oxygenation in aqueous systems. Environmental Science & Technology 14, 561-568.

Tabatabai, M.A., Dick, W.A., 1983. Simultaneous determination of nitrate, chloride, sulfate, and phosphate in natural-waters by ion chromatography. Journal of Environmental Quality 12, 209-213.

Taillefert, M., Beckler, J.S., Carey, E., Burns, J.L., Fennessey, C.M., DiChristina, T.J., 2007a. Shewanella putrefaciens produces an Fe(III)-solubilizing organic ligand during anaerobic respiration on insoluble Fe(III) oxides. Journal of Inorganic Biochemistry 101, 1760-1767.

Taillefert, M., Bono, A.B., Luther, G.W., 2000. Reactivity of freshly formed Fe(III) in synthetic solutions and (pore)waters: Voltammetric evidence of an aging process. Environmental Science & Technology 34, 2169-2177.

Taillefert, M., Hover, V.C., Rozan, T.F., Theberge, S.M., Luther, G.W., 2002a. The influence of sulfides on soluble organic-Fe(III) in anoxic sediment porewaters. Estuaries 25, 1088-1096.

Taillefert, M., Luther, G.W., Nuzzio, D.B., 2000b. The application of electrochemical tools for in situ measurements in aquatic systems. Electroanalysis 12, 401-412.

Taillefert, M., Neuhuber, S., Bristow, G., 2007b. The effect of tidal forcing on biogeochemical processes in intertidal salt marsh sediments. Geochem. Trans. 8.

Taillefert, M., Rozan, T.F., Glazer, B.T., Herszage, J., Trouwborst, R.E., Luther, G.W., , 2002b. Seasonal Variations of Soluble Organic-Fe(III) in Sediment Porewaters as Revealed by Voltammetric Microelectrodes, in: Taillefert, M., Rozan, T.F. (Eds.), Environmental Electrochemistry: Analyses of Trace Element Biogeochemistry. American Chemical Society Press, pp. 247-264.

Takeda, K., Takedoi, H., Yamaji, S., Ohta, K., Sakugawa, H., 2004. Determination of hydroxyl radical photoproduction rates in natural waters. Anal. Sci. 20, 153-158.

Taylor, S.W., Luther, G.W., Waite, J.H., 1994. Polarographic and spectrophotometric investigation of iron(III) complexation to 3,4-dihydroxyphenylalanine-containing peptides and proteins from mytilus-edulis. Inorg. Chem. 33, 5819-5824.

Tercier-Waeber, M.L., Taillefert, M., 2008. Remote in situ voltammetric techniques to characterize the biogeochemical cycling of trace metals in aquatic systems. Journal of Environmental Monitoring 10, 30-54.

Thamdrup, B., 2000. Bacterial manganese and iron reduction in aquatic sediments, Advances in Microbial Ecology, Vol 16. Kluwer Academic / Plenum Publ, New York, pp. 41-84.

Thamdrup, B., Canfield, D.E., 1996. Pathways of carbon oxidation in continental margin sediments off central Chile. Limnology and Oceanography 41, 1629-1650.

Thamdrup, B., Rossello-Mora, R., Amann, R., 2000. Microbial manganese and sulfate reduction in Black Sea shelf sediments. Applied and Environmental Microbiology 66, 2888-2897.

Theberge, S.M., Luther, G.W., 1997. Determination of the Electrochemical Properties of a Soluble Aqueous FeS Species Present in Sulfidic Solutions. Aquatic Geochemistry 3, 191-211.

Thullner, M., Dale, A.W., Regnier, P., 2009. Global-scale quantification of mineralization pathways in marine sediments: A reaction-transport modeling approach. Geochemistry Geophysics Geosystems 10, 24.

Thurman, M., 1985. Organic geochemistry of natural waters. M. Nijhoff.

Tirumalesh, K., 2008. Simultaneous determination of bromide and nitrate in contaminated waters by ion chromatography using amperometry and absorbance detectors. Talanta 74, 1428-1434.

Torrents, A., Stone, A.T., 1994. Oxide surface-catalyzed hydrolysis of carboxylate esters and phosphorothioate esters. Soil Sci. Soc. Am. J. 58, 738-745.

Treguer, P., Nelson, D.M., Vanbennekom, A.J., Demaster, D.J., Leynaert, A., Queguiner, B., 1995. The silica balance in the world ocean - a reestimate. Science 268, 375-379.

Urgeles, R., Camerlenghi, A., 2013. Submarine landslides of the Mediterranean Sea: Trigger mechanisms, dynamics, and frequency-magnitude distribution. J. Geophys. Res.-Earth Surf. 118, 2600-2618.

Urlaub, M., Talling, P.J., Masson, D.G., 2013. Timing and frequency of large submarine landslides: implications for understanding triggers and future geohazard. Quat. Sci. Rev. 72, 63-82.

Van Den Berg, C.M.G., 1995. Evidence for organic complexation of iron in seawater. Marine Chemistry 50, 139-157.

van der Zee, C., van Raaphorst, W., Helder, W., 2002. Fe redox cycling in Iberian continental margin sediments (NE Atlantic). J. Mar. Res. 60, 855-886.

Vargas, M., Kashefi, K., Blunt-Harris, E.L., Lovley, D.R., 1998. Microbiological evidence for Fe(III) reduction on early Earth. Nature 395, 65-67.

Viollier, E., Inglett, P.W., Hunter, K., Roychoudhury, A.N., Van Cappellen, P., 2000. The ferrozine method revisited: Fe(II)/Fe(III) determination in natural waters. Appl. Geochem. 15, 785-790.

von Canstein, H., Ogawa, J., Shimizu, S., Lloyd, J.R., 2008. Secretion of flavins by Shewanella species and their role in extracellular electron transfer. Applied and Environmental Microbiology 74, 615-623.

vonRad, U., Tahir, M., 1997. Late Quaternary sedimentation on the outer Indus shelf and slope (Pakistan): Evidence from high-resolution seismic data and coring. Marine Geology 138, 193-236.

Vraspir, J.M., Butler, A., 2009. Chemistry of Marine Ligands and Siderophores. Annual Review of Marine Science 1, 43-63.

Wallmann, K., Drews, M., Aloisi, G., Bohrmann, G., 2006. Methane discharge into the Black Sea and the global ocean via fluid flow through submarine mud volcanoes. Earth and Planetary Science Letters 248, 545-560.

Wang, R.Q., Wang, N.N., Ye, M.L., Zhu, Y., 2012. Determination of low-level anions in seawater by ion chromatography with cycling-column-switching. Journal of Chromatography A 1265, 186-190.

Wang, Y.F., VanCappellen, P., 1996. A multicomponent reactive transport model of early diagenesis: Application to redox cycling in coastal marine sediments. Geochimica Et Cosmochimica Acta 60, 2993-3014.

Wankel, S.D., Huang, Y.W., Gupta, M., Provencal, R., Leen, J.B., Fahrland, A., Vidoudez, C., Girguis, P.R., 2013. Characterizing the Distribution of Methane Sources and Cycling in the Deep Sea via in Situ Stable Isotope Analysis. Environmental Science & Technology 47, 1478-1486.

Weimer, P., 1990. Sequence stratigraphy, facies geometries, and depositional history of the Mississippi fan, gulf of mexico. AAPG Bull.-Am. Assoc. Petr. Geol. 74, 425-453.

Weston, N.B., Porubsky, W.P., Samarkin, V.A., Erickson, M., Macavoy, S.E., Joye, S.B., 2006. Porewater Stoichiometry of Terminal Metabolic Products, Sulfate, and Dissolved Organic Carbon and Nitrogen in Estuarine Intertidal Creek-bank Sediments. Biogeochemistry 77, 375-408.

White, G.F., Shi, Z., Shi, L., Wang, Z.M., Dohnalkova, A.C., Marshall, M.J., Fredrickson, J.K., Zachara, J.M., Butt, J.N., Richardson, D.J., Clarke, T.A., 2013. Rapid electron exchange between surface-exposed bacterial cytochromes and Fe(III) minerals. Proc. Natl. Acad. Sci. U. S. A. 110, 6346-6351.

White, P.C., Lawrence, N.S., Davis, J., Compton, R.G., 2002. Electrochemical determination of thiols: A perspective. Electroanalysis 14, 89-98.

White, S.N., Dunk, R.M., Peltzer, E.T., Freeman, J.J., Brewer, P.G., 2006. In situ Raman analyses of deep-sea hydrothermal and cold seep systems (Gorda Ridge and Hydrate Ridge). Geochemistry Geophysics Geosystems 7.

Wigley, T.M.L., 2005. The climate change commitment. Science 307, 1766-1769.

Witter, A.E., Lewis, B.L., Luther, G.W., 2000. Iron speciation in the Arabian Sea. Deep-Sea Res. Part II-Top. Stud. Oceanogr. 47, 1517-1539.

Witter, A.E., Luther, G.W., 1998. Variation in Fe-organic complexation with depth in the Northwestern Atlantic Ocean as determined using a kinetic approach. Marine Chemistry 62, 241-258.

Wu, J., Boyle, E., Sunda, W., Wen, L.S., 2001. Soluble and colloidal iron in the oligotrophic North Atlantic and North Pacific. Science 293, 847-849.

Wu, J.F., Luther, G.W., 1995. Complexation of Fe(III) by Natural Organic-Ligands in the Northwest Atlantic-Ocean by a Competitive Ligand Equilibration Method and a Kinetic Approach. Marine Chemistry 50, 159-177.

Xiong, Y.J., Shi, L., Chen, B.W., Mayer, M.U., Lower, B.H., Londer, Y., Bose, S., Hochella, M.F., Fredrickson, J.K., Squier, T.C., 2006. High-affinity binding and direct electron transfer to solid metals by the Shewanella oneidensis MR-1 outer membrane c-type cytochrome OmcA. J. Am. Chem. Soc. 128, 13978-13979.

Yucel, M., Gartman, A., Chan, C.S., Luther, G.W., 2011. Hydrothermal vents as a kinetically stable source of iron-sulphide-bearing nanoparticles to the ocean. Nat. Geosci. 4, 367-371.

Zachara, J.M., Fredrickson, J.K., Li, S.M., Kennedy, D.W., Smith, S.C., Gassman, P.L., 1998. Bacterial reduction of crystalline Fe3+ oxides in single phase suspensions and subsurface materials. American Mineralogist 83, 1426-1443.

Zinder, B., Furrer, G., Stumm, W., 1986. The coordination chemistry of weathering .2. dissolution of Fe(III) oxides. Geochimica Et Cosmochimica Acta 50, 1861-1869.